DOCTORAL THESIS - ΔΙΔΑΚΤΟΡΙΚΗ ΔΙΑΤΡΙΒΗ

A tale of two proteins:

S. cerevisiae Rad9 DNA damage checkpoint protein and Aft1 transcription factor on the surveillance of DNA damage-prone chromatin under non DNA damage-induced conditions.
Insights from genome-wide analyses.

Μια ιστορία δύο πρωτεϊνών:

Η πρωτεΐνη ελέγχου καταστροφής DNA ScRad9 και ο μεταγραφικός παράγοντας Aft1 στην επιτήρηση της ευαίσθητης σε καταστροφή DNA χρωματίνης υπό φυσιολογικές συνθήκες.
Μελέτη με γονιδιωματικής κλίμακας αναλύσεις.

CHRISTOS ANDREADIS / ΧΡΗΣΤΟΣ ΑΝΔΡΕΑΔΗΣ

Supervisor: **Prof. Despina Alexandraki**
Υπεύθυνη καθηγήτρια: **Δέσποινα Αλεξανδράκη**

OCTOBER / ΟΚΤΩΒΡΙΟΣ 2012

To my parents.
Στους γονείς μου.

ACKNOWLEDGEMENTS

A special thank you goes to my supervisor Prof. Despina Alexandraki for all the help, support and advice that she provided me with during my doctoral studies. Her group set the foundation for my career as a researcher, which is something I am truly grateful for.

Thank you to my PhD advisors, Prof. Georges Chalepakis and Dr Dimitris Kafetzopoulos, for their constant support throughout the progression of my research, and to all my examiners for their insightful comments. Many thanks to Prof. Dimitris Tzamarias, Prof. Charalampos Spilianakis, Prof. George Garinis and Dr Ioannis Iliopoulos.

Many thanks go to my friends and lab collaborators Dr George Fragiadakis and Dr Kalliopi Gkouskou for all the support during my years in Heraklion.

Thank you to George Papagiannakis for the technical assistance he was constantly offering.

None of what I accomplished would materialise without the company, love and strong support of my partner Dr Ioannis Polychronakis, and my friends Dr Rena Chiotaki, Dr Niki Panagiotaki and Dr Kiriaki Kanakousaki, who all hold a very special place in my heart.

The constant love and guidance of my parents and sister made all this possible and I want to thank them from the bottom of my heart.

Thank you also to all the people of the first floor of IMMB for their support and friendly company during all the years of my studies at the University of Crete.

TABLE OF CONTENTS

1.1.1—Περίληψη και σκοπός εργασίας

Το γονίδιο της ζύμης *RAD9[1]* ήταν το πρώτο γονίδιο ελέγχου καταστροφής DNA το οποίο ταυτοποιήθηκε στη ζύμη περίπου 25 χρόνια πριν (Weinert and Hartwell, 1988). Παρά το γεγονός αυτό, ο ακριβής ρόλος της κωδικεύουσας πρωτεΐνης, η ρύθμιση και η λειτουργικότητά της δεν είναι πλήρως κατανοητά. Στον κλασικό της ρόλο, η Rad9 δρα ως μεταγωγέας του σήματος μεταξύ upstream και downstream κινασών στο μονοπάτι απόκρισης σε καταστροφή DNA (DNA Damage Response, DDR). Βλάβες σε αυτό το συντηρημένο μονοπάτι μπορεί να οδηγήσουν σε αυξημένη γονιδιωματική αστάθεια, ευαισθησία σε καρκίνους, γήρανση και αρκετά ανθρώπινα σύνδρομα. Τα κύτταρα αποκρίνονται στην καταστροφή του DNA με το να την αντιλαμβάνονται και να μετάγουν το σήμα μέσω ενός καταρράκτη φωσφορυλιώσεων σε downstream στόχους, μέλη των οποίων είναι εξελικτικά συντηρημένα. Παρόλο που δεν υπάρχει ακριβές ομόλογο της Rad9 στα θηλαστικά, υπάρχουν τουλάχιστον δύο πρωτεΐνες, η 53BP1 (p53 binding protein) και η BRCA1 (Breast CAncer) που έχουν λειτουργικά ομόλογες περιοχές με τη Rad9. Οι δύο πρωτεΐνες των θηλαστικών εμπλέκονται στην απόκριση σε καταστροφή DNA, όπως επίσης και σε άλλα κυτταρικά μονοπάτια, ενώ μεταλλαγές τους οδηγούν σε καρκίνο.

Παρά το ότι πολλά είναι γνωστά σχετικά με τη λειτουργία της Rad9 στο μονοπάτι απόκρισης σε καταστροφή DNA, η γνώση σχετικά με το ρόλο της σε συνθήκες μη επαγόμενης καταστροφής DNA, αν υπάρχει, είναι πολύ περιορισμένη. Οι μέχρι σήμερα μελέτες της Rad9 στη βιβλιογραφία έχουν εστιαστεί κυρίως στο ρόλο της ως μεταγωγέα του σήματος 'καταστροφή DNA' σε downstream πρωτεΐνες του DDR μονοπατιού, έχοντας ως τελικό αποτέλεσμα το σταμάτημα του κυτταρικού κύκλου και την επιδιόρθωση της βλάβης, εξασφαλίζοντας την ακεραιότητα του γονιδιώματος. Η συστηματική ανάλυση της Rad9 στην παρούσα εργασία αποκαλύπτει νέες πτυχές για τη δράση της σε συνθήκες μη επαγόμενης καταστροφής DNA.

Οι γονιδιωματικές αναλύσεις της Rad9 που αφορούν στο πρότυπο πρόσδεσης της σε διάφορες συνθήκες ανάπτυξης, καθώς και η μελέτη του μεταγραφικού προφίλ υπό την απουσία της, βρίσκονται στους κεντρικούς άξονες της παρούσας εργασίας. Ένας άλλος στόχος είναι να μελετηθούν περαιτέρω ο βιολογικός ρόλος της Rad9 και

---

[1] Να μη συγχέεται με το γονίδιο rad9 του *S.pombe* και το γονίδιο RAD9 του ανθρώπου.

η λειτουργική ανάλυση νέων πρωτεϊνών που αλληλεπιδρούν με αυτήν, όπως έχουν ταυτοποιηθεί από την ομάδα μας βιοχημικά με το σύστημα των δύο υβριδίων (Y2H) και επιβεβαιωθεί τόσο με *in vitro* δικιμασίες, όσο και με πειράματα συνανοσοκατακρήμνισης (co-IP) σε πρωτεϊνικά εκχυλίσματα ζύμης (Gkouskou et al. Voutsina et al., unpublished).

Οι συγκεκριμένες άμεσες αλληλεπιδράσεις (επιβεβαιωμένες *in vivo* και *in vitro*) συσχετίζουν τη Rad9 με τον χαλκορυθμιζόμενο Mac1 και τον σιδηρορυθμιζόμενο Aft1 μεταγραφικούς παράγοντες. Ξεκινώντας με αυτές τις αλληλεπιδράσεις, βρήκαμε με μικρής κλίμακας αναλύσεις ότι η Rad9 στρατολογείται στη χρωματίνη, σε γονίδια που ρυθμίζονται από αυτούς τους μεταγραφικούς παράγοντες. Βρέθηκε ότι η στρατολόγηση της Rad9 επηρεάζει άμεσα σε μικρό βαθμό τη μεταγραφή των μεταλλορυθμιζόμενων γονιδίων που εξετάστηκαν, υπό συνθήκες μη επαγόμενης καταστροφής DNA. *In silico* ανάλυση σε γονιδιωματικής κλίμακας πειράματα έδειξε ότι η Rad9 δε φαίνεται να αναγνωρίζει συγκεκριμένες αλληλουχίες DNA.

Πραγματοποιώντας δοκιμασίες ανάπτυξης σε 6-αζαουρακίλη, καθώς και μικρής κλίμακας πειράματα ανοσοκατακρήμνισης χρωματίνης (ChIP), καταλήξαμε σε ενδείξεις συσχέτισης των Rad9-Aft1 και της επιμήκυνσης της μεταγραφής. Ένα από τα επόμενα ερωτήματα προς απάντηση ήταν το εάν η Rad9 εμπλέκεται στη μεταγραφική ρύθμιση των γονιδίων της ζύμης γενικώς ή εάν επηρεάζει τη μεταγραφή συγκεκριμένων ομάδων γονιδίων. Προκειμένου να απαντήσουμε αυτό το ερώτημα πραγματοποιήσαμε μεγάλης κλίμακας ανάλυση έκφρασης σε *rad9Δ* κύτταρα, ώστε να μελετήσουμε εάν/πώς μεταβάλλεται το μεταγραφικό προφίλ της ζύμης. Παρόλο που βρήκαμε ότι υπήρχε μεταβολή ενός μικρού μόνο ποσοστού γονιδίων (~2%), το πείραμα είχε υψηλή επαναληψιμότητα. Πρόκειται για την πρώτη φορά που το μεταγραφικό προφίλ της ζύμης μελετάται υπό την απουσία του *RAD9* γονιδίου. Θεωρούμε ότι τα αποτελέσματα από την παραπάνω μελέτη είναι πολύ σημαντικά, διότι αποκαλύπτουν νέες πτυχές της διασύνδεσης μεταξύ μεταγραφής και πρωτεϊνών γονιδιωματικής ακεραιότητας στη ζύμη. Λειτουργική ανάλυση των αποτελεσμάτων μας έδειξε εμπλοκή της Rad9 στη μεταγραφή συγκεκριμένων ομάδων γονιδίων που ανήκουν σε συγκεκριμένες GO (Gene Ontology) κατηγορίες (όπως του μεταβολισμού).

Ο επόμενος στόχος μας ήταν να εξετάσουμε εάν η εμπλοκή της Rad9 στη μεταγραφή γονιδίων που κωδικεύουν για πρωτεΐνες με συγκεκριμένες βιολογικές

λειτουργίες είναι άμεση ή έμμεση. Για να απαντήσουμε σε αυτό το ερώτημα πραγματοποιήσαμε μια σειρά αναλύσεων στρατολόγησης σε επίπεδο γονιδιώματος (υποκινητές, κωδικεύουσες και μη κωδικεύουσες περιοχές, κεντρομερή, τελομερή) χρησιμοποιώντας μικροσυστοιχίες DNA για τη συγκεκριμένη ανάλυση (Tiling Arrays, ανοσοκατακρήμνιση χρωματίνης σε πλακάκι-ChIP on chip). Αυτή η *in vivo* ανάλυση πρωτεϊνών-DNA πραγματοποιήθηκε υπό διάφορες συνθήκες ανάπτυξης των κυττάρων, ώστε τα αποτελέσματα να είναι περισσότερο αξιόπιστα.

Στη συνέχεια εστιάσαμε στη σχέση Rad9-Aft1 παρά στη σχέση Rad9-Mac1, διότι ο Aft1 έχει από άλλες μελέτες συνδεθεί με κυτταρικές διαδικασίες και μονοπάτια διαφορετικά από το κλασικό μονοπάτι της σιδηρορύθμισης [όπως η σταθερότητα των χρωμοσωμάτων και του κυτταρικού τοιχώματος, η ακεραιότητα του γονιδιώματος, η καταστροφή DNA και η μεταφορά πρωτεϊνών (Berthelet et al., 2010; Hamza and Baetz, 2011; Measday et al., 2005; Shakoury-Elizeh et al., 2004)], επομένως η σχέση Rad9-Aft1 ήταν πιο ενδιαφέρουσα να μελετηθεί. Επιπλέον, δόθηκε έμφαση στην πιθανή αλληλεξάρτηση μεταξύ Rad9 και Aft1 πραγματοποιώντας ChIP on chip αναλύσεις σε στελέχη όπου το ένα από τα δύο γονίδια είχε απαλοιφθεί (*rad9Δ* Aft1-9Myc και *aft1Δ* Rad9-13Myc).

Μετά από εκτενή ανάλυση των αποτελεσμάτων από τα παραπάνω πειράματα γονιδιωματικής κλίμακας βρήκαμε τη Rad9 παρούσα σε ένα μεγάλο αριθμό περιοχών του γονιδιώματος, παρά το γεγονός ότι ο μέσος όρος του αριθμού των μορίων της έχει αναφερθεί ότι είναι της τάξης των 400 μορίων ανά κύτταρο σε πλούσιες συνθήκες καλλιέργειας. Λόγω του ότι η Rad9 ήταν παρούσα σε περισσότερες περιοχές στο γονιδίωμα (800-1600 γονίδια ανάλογα με τις συνθήκες ανάπτυξης και το κατώφλι που θέτουμε), κάποιος θα μπορούσε να σκεφτεί ότι εάν η Rad9 υπήρχε σε περισσότερα μόρια ανά κύτταρο, θα μπορούσε να εντοπίζεται σε ακόμα περισσότερες περιοχές. Για να απαντήσουμε σε αυτό το ερώτημα, εξετάσαμε το πρότυπο εντοπισμού της Rad9 στο γονιδίωμα αφού την υπερεκφράσαμε σε πλασμίδιο (τα μόρια της Rad9 ήταν 10-20 φορές περισσότερα από το φυσιολογικό). Δείξαμε ότι η Rad9 εντοπίζεται σε ένα συγκρίσιμο αριθμό γονιδίων, το οποίο δείχνει ότι υπάρχει εξειδίκευση στον εντοπισμό της στο γονιδίωμα.

Είναι αξιοσημείωτο ότι, παρόλο που η Rad9 εντοπίζεται σε ~16% του συνόλου των γονιδίων της ζύμης, βρήκαμε ότι εντοπίζεται σε μόνο ~25% των γονιδίων που ανιχνεύσαμε ότι επηρεάζει μεταγραφικά, τα οποία σχετίζονται κυρίως με μονοπάτια μεταβολισμού. Βασιζόμενοι σε όλα τα μεγάλης κλίμακας πειράματα,

βρήκαμε ότι η Rad9 είναι παρούσα κυρίως στις κωδικεύουσες παρά στις μη κωδικεύουσες περιοχές γονιδίων, παρουσιάζοντας μια τάση προς την 3' περιοχή του ORF, ενός γονιδίου που αντιπροσωπεύει το πρότυπο πρόσδεσης της Rad9 σε όλα τα γονίδια (average gene analysis). Η Rad9 παρουσιάζει μια προτίμηση πρόσδεσης σε περιοχές πλούσιες σε νουκλεοτίδια GC. Τέτοιες περιοχές είναι και τα hotspots μειωτικού ανασυνδυασμού (Gerton et al., 2000) και βρήκαμε ότι η Rad9 (όπως επίσης και ο Aft1) εντοπίζονται σε αυτές τις ευαίσθητες σε καταστροφή DNA περιοχές με υψηλή πιθανότητα. Η Rad9 έχει την τάση να εντοπίζεται σε γονίδια μεγαλύτερου μήκους (>1800bp) από το μέσο όρο κατανομής όλων των γονιδίων και σε ακόμα μεγαλύτερου μήκους γονίδια όταν ο Aft1 απουσιάζει. Η Rad9 είναι επίσης παρούσα σε κεντρομερή όπου εντοπίζεται επίσης και ο Aft1, όπως και σε τελομερή και άλλα μη-ORF στοιχεία. Επιπλέον, εφαρμόζοντας average gene ανάλυση βρήκαμε ότι ο εντοπισμός της Rad9 είχε παρόμοιο πρότυπο με αυτό επιγενετικών τροποποιήσεων όπως H3K36me3 και H3K79me3 που συνδέονται με μεταγραφή και καταστροφή DNA αντίστοιχα.

Από τα πιο σημαντικά ευρήματα ήταν η ισχυρή αντιπροσώπευση της Rad9 σε μεταγραφικά ενεργές περιοχές με Aft1-εξαρτώμενο τρόπο. Η Rad9 χάνει σε σημαντικό βαθμό την προτίμηση να προσδένεται σε γονίδια με υψηλή μεταγραφική ενεργότητα όταν ο Aft1 απουσιάζει, πράγμα που τονίζει την εξάρτηση της Rad9 από τον Aft1 για τον εντοπισμό της σε συγκεκριμένες χρωματινικές περιοχές. Οι περιοχές με υψηλή μεταγραφική ενεργότητα σχετίζονται με υψηλότερο από το μέσο όρο ρυθμό μεταλλαγών (Kim et al., 2007). Προκειμένου να εξετάσουμε εάν το πρότυπο εντοπισμού της Rad9 είναι τυχαίο και εάν εξαρτάται ή όχι από την ενεργότητα των γονιδίων, πραγματοποιήσαμε ένα πείραμα ChIP on chip όπου το στέλεχος είχε αναπτυχθεί σε μέσο που περιείχε γαλακτόζη αντί για γλυκόζη, όπου είναι γνωστό ότι συγκεκριμένες ομάδες γονιδίων ενεργοποιούνται μεταγραφικά. Εάν η Rad9 σχετιζόταν ισχυρά με τον εντοπισμό σε μεταγραφικά ενεργές περιοχές, θα περιμέναμε να τη βρούμε σε γονίδια που είναι μεταγραφικώς ενεργά παρουσία γαλακτόζης. Πράγματι, η Rad9 βρέθηκε στα περισσότερα από αυτά, το οποίο αποτελεί ισχυρή ένδειξη της σχέσης της Rad9 με μεταγραφικώς ενεργές περιοχές του γονιδιώματος. Λειτουργική ανάλυση των αποτελεσμάτων των μεγάλης κλίμακας πειραμάτων εντοπισμού έδειξαν ένα δυναμικό εμπλοκής της Rad9 σε μονοπάτια με τα οποία δεν είχε συνδεθεί στο παρελθόν. Οι υπεραντιπροσωπευμένες ομάδες γονιδίων στις οποίες η Rad9 εντοπίστηκε περιελάμβαναν ορισμένες από τις πιο

υψηλώς ενεργές όπως τις σχετιζόμενες με μεταβολισμό γλυκόζης και αμινοξέων ή τις σχετιζόμενες με την κυτταρική ανάπτυξη. Η τάση της Rad9 να προσδένεται σε υψηλώς ενεργά γονίδια υποστηρίζεται επίσης και από το ότι σε γονιδιωματικής κλίμακας πειράματα εντοπισμού της Rad9 σε συνθήκες όπου σιδηρο- και χαλκορυθμιζόμενα γονίδια επάγονταν μεταγραφικά (SC BCS BPS), δείξαμε ότι η Rad9 προσδενόταν ισχυρά σε αυτούς τους στόχους.

Τα παραπάνω αποτελέσματα σχετικά με τη Rad9 και τον Aft1, δείχνουν υψηλή πιθανότητα να δρουν μαζί ως τμήμα ενός μεγαλύτερου συμπλόκου που μπορεί να δράσει κατά τη μεταγραφή άλλων γονιδίων γενικώς και συγκεκριμένων GO ομάδων γονιδίων ειδικώς.

Παράλληλα, η παρούσα εργασία μελετά τον εντοπισμό του Aft1 μεταγραφικού παράγοντα στο γονιδίωμα (μονο του και σε συσχετισμό με τη Rad9). Είναι εντυπωσιακό το γεγονός οτι βρήκαμε τον Aft1 παρόντα κυρίως σε κωδικεύουσες παρά σε μη κωδικεύουσες περιοχές. Επιπλέον, η λειτουργική ανάλυση αποκάλυψε ότι εντοπίζεται σε πολύ περισσότερα γονίδια επιπλέον των σιδηρορυθμιζόμενων. Τα παραπάνω αποτελέσματα είναι νέα για τον μεταγραφικό παράγοντα Aft1.

Τι κάνει η Rad9 σε τόσα πολλά γονίδια; Ποιο ρόλο έχει σε συνθήκες μη επαγόμενης καταστροφής DNA; Πώς ο Aft1 βοηθά στον εντοπισμό της Rad9 σε υψηλώς μεταγραφικές και ευαίσθητες σε καταστροφή DNA περιοχές και για ποιο σκοπό; Μια λογική εξήγηση θα μπορούσε να είναι ότι το σύμπλοκο είναι εκεί για να επιτελέσει ένα ρόλο επιτήρησης της χρωματίνης, να εξασφαλίσει την ακεραιότητα του γονιδιώματος σε οποιοδήποτε σημείο του κυτταρικού κύκλου ακόμα και χωρίς την επαγωγή καταστροφής DNA. Με αυτόν τον τρόπο, ειδικά στα γονίδια με υψηλή μεταγραφική ενεργότητα, όπου ο ρυθμός καταστροφής του DNA είναι υψηλότερος, η Rad9 θα είναι έτοιμη να δράσει άμεσα όταν χρειαστεί, εξασφαλίζοντας ότι η κυτταρική απόκριση θα είναι όσο το δυνατόν γρηγορότερη.

Η παρούσα διατριβή παρέχει μια περιεκτική ανάλυση του εντοπισμού της Rad9 στο γονιδίωμα υπό συνθήκες μη επαγόμενης καταστροφής DNA και αποκαλύπτει τη συνεργασία της με τον Aft1 στην ευαίσθητη χρωματίνη, εικάζοντας ένα μηχανισμό που εξασφαλίζει γρήγορη και αποτελεσματική απόκριση στην καταστροφή. Οι γονιδιωματικοί χάρτες εντοπισμού των Rad9 και Aft1 που παρουσιάζονται σε αυτή την εργασία παρέχουν στους ερευνητές πληροφορίες για ανάλυση σε περισσότερο βάθος της τοπολογίας και της λειτουργίας του μηχανισμού

επιδιόρθωσης σε σχέση με τη μεταγραφική ενεργότητα, υπό συνθήκες μη επαγόμενης καταστροφής DNA. Φαίνεται ότι το κύτταρο έχει αναπτύξει απλούς, ωστόσο εξελιγμένους, μηχανισμούς για να παράσχει επιπλέον προστασία στις πολύ ευαίσθητες σε καταστροφή DNA περιοχές του γονιδιώματος. Διατηρώντας τις πρωτεΐνες του μηχανισμού επιδιόρθωσης DNA στη γειτονία τέτοιων ευαίσθητων περιοχών, στρατολογούμενες μεταξύ άλλων και από μεταγραφικούς ενεργοποιητές, έχει αναπτύξει ένα καλά ενορχηστρωμένο σύστημα προστασίας.

Η βασική έρευνα πάνω στην πρωτεΐνη Rad9, σε συνδυασμό με αποτελέσματα που προκύπτουν από πειράματα με Rad9-αλληλεπιδρώσες πρωτεΐνες ουσιώδεις για την εξασφάλιση της ακεραιότητας του γονιδιώματος, μπορεί να ενισχύσει σημαντικά τη γνώση σχετικά με εφαρμογές που στοχεύουν μηχανισμούς γήρανσης και καρκινογένεσης.

*Berthelet, S., Usher, J., Shulist, K., Hamza, A., Maltez, N., Johnston, A., Fong, Y., Harris, L. J., and Baetz, K. (2010). Functional genomics analysis of the Saccharomyces cerevisiae iron responsive transcription factor Aft1 reveals iron-independent functions. Genetics *185*, 1111-1128.
*Gerton, J. L., DeRisi, J., Shroff, R., Lichten, M., Brown, P. O., and Petes, T. D. (2000). Global mapping of meiotic recombination hotspots and coldspots in the yeast Saccharomyces cerevisiae. Proc Natl Acad Sci U S A *97*, 11383-11390.
*Hamza, A., and Baetz, K. (2011). The iron-responsive transcription factor Aft1 interacts with the kinetochore protein Iml3 and promotes pericentromeric cohesin. J Biol Chem.
*Kim, N., Abdulovic, A. L., Gealy, R., Lippert, M. J., and Jinks-Robertson, S. (2007). Transcription-associated mutagenesis in yeast is directly proportional to the level of gene expression and influenced by the direction of DNA replication. DNA Repair (Amst) *6*, 1285-1296.
Measday, V., Baetz, K., Guzzo, J., Yuen, K., Kwok, T., Sheikh, B., Ding, H., Ueta, R., Hoac, T., Cheng, B., et al.* (2005). Systematic yeast synthetic lethal and synthetic dosage lethal screens identify genes required for chromosome segregation. Proc Natl Acad Sci U S A *102*, 13956-13961.
*Shakoury-Elizeh, M., Tiedeman, J., Rashford, J., Ferea, T., Demeter, J., Garcia, E., Rolfes, R., Brown, P. O., Botstein, D., and Philpott, C. C. (2004). Transcriptional remodeling in response to iron deprivation in Saccharomyces cerevisiae. Mol Biol Cell *15*, 1233-1243.
*Weinert, T. A., and Hartwell, L. H. (1988). The RAD9 gene controls the cell cycle response to DNA damage in Saccharomyces cerevisiae. Science *241*, 317-322.

CHAPTER 1

INTRODUCTION

1.1.1---Abstract and Purpose of the Study

Saccharomyces cerevisiae RAD9[2] was the first DNA damage checkpoint gene identified in yeast almost 25 years ago (Weinert and Hartwell, 1988). In spite of that, the precise role of the encoding protein, its regulation and functionality are not completely understood. In its classic role, Rad9 acts as the signal mediator between upstream and downstream essential kinases in the DNA Damage Response pathway (DDR). Defects in this conserved pathway can lead to elevated genomic instability, cancer susceptibility, ageing and several human disorders. Cells respond after DNA damage by sensing the lesions and transducing the signal to downstream targets in a phosphorylation cascade, members of which are evolutionary conserved. Although there is not an exact homolog of Rad9 in mammals, there are at least two proteins, 53BP1 (p53 Binding Protein) and BRCA1 (BReast CAncer) that have functional homologous domains with Rad9. Both mammalian proteins are implicated in the response to DNA damage, as well as in other cellular pathways and when they are mutated can lead to cancer.

Although much is established about Rad9 function in DDR, the knowledge about its role under non DNA damage induced conditions, if any, is quite limited. The up-to-date studies of Rad9 in bibliography were focused on its role as the mediator of the signal "DNA damage" to downstream members of the DDR protein cascade, having as an ultimate result cell cycle arrest and repair of the damage, ensuring genome integrity. Our systematic analysis of Rad9 role reveals new aspects about its action under non DNA damage inducing conditions.

The genome-wide analyses of Rad9, regarding both its global binding pattern under multiple growth conditions and the global transcriptional profile in its absence, are on the central axes of my work. Another aim of this study is to get further insight into the biological role of Rad9 and the functional analysis of new Rad9-interacting proteins identified by our group biochemically by the Yeast Two Hybrid system and

---

[2] Not to be confused with *S.pombe* rad9 and human RAD9 genes.

confirmed both by *in vitro* tests and by co-immunoprecipitation (co-IP) experiments in yeast protein extracts (Gkouskou et al., Voutsina et al., unpublished).

The particular direct interactions (confirmed *in vivo* and *in vitro*) implicate Rad9 in copper-regulated Mac1 and iron-regulated Aft1 transcription factors. Starting with these interactions we were able to find by small scale analyses that Rad9 is recruited to chromatin, on genes which are regulated by the above transcription factors. Rad9 recruitment was found to mildly affect the transcription of the metal-regulated genes tested, in non DNA damage inducing conditions, in a direct way. Rad9 itself does not seem to recognize specific DNA sequences, as examined by *in silico* analyses.

By performing 6-azauracil growth assays and small scale ChIP experiments, we ended up with indications of a connection between Rad9-Aft1 and transcription elongation. One of the following tasks was to answer whether Rad9 is implicated in the transcriptional regulation of yeast genes in general or if it affects the transcription of only particular gene groups. To address this question we performed genome-wide expression analysis of *rad9Δ* cells, in order to study if/how the transcriptional profile of yeast is altered. Although we found only a small percentage of yeast genes to be transcriptionally altered (~2%), the experiment was highly reproducible. This is the first time where the yeast transcriptional profile is studied in the absence of *RAD9*. We consider these results to be of great importance because they reveal new aspects of interconnection between transcription and genome integrity proteins in yeast. Functional analyses of our results showed Rad9 implication in transcription of specific gene groups belonging to particular gene ontology (GO) categories (such as metabolism).

Our next goal was to test whether Rad9 implication in transcription of genes encoding proteins with particular biological functions was direct or indirect. To answer that question, we performed a series of genome-wide recruitment analyses of Rad9 on the yeast genome (promoters, coding regions, non coding regions, centromeres, telomeres) using DNA tiling arrays (Chromatin ImmunoPrecipitation on chip -ChIP on chip). This *in vivo* protein-DNA analysis was performed under multiple growth conditions in order to have a more reliable follow up of the procedure.

Subsequently, we focused on the Rad9-Aft1 relation rather than the Rad9-Mac1 because Aft1 has been previously connected to cellular procedures and

pathways other than the classic iron regulation one [such as chromosome stability, genome integrity, DNA damage, cell wall stability, protein transport (Berthelet et al., 2010; Hamza and Baetz, 2011; Measday et al., 2005; Shakoury-Elizeh et al., 2004)] and was thus more intriguing to study. Furthermore, we emphasized on the possible interdependency between Rad9 and Aft1 by performing ChIP on chip analyses in strains where one gene was each time deleted (*rad9Δ* Aft1-9Myc and *aft1Δ* Rad9-13Myc).

After thorough analysis of the output data of the above large scale experiments we have found Rad9 to be present to a large number of genomic regions, in spite of the fact that the average number of Rad9 molecules has been previously reported to be only 400 molecules per cell in rich growth conditions. Because of Rad9 was present on multiple loci in the genome (800-1600 genes depending on the growth condition and the threshold set) one could have thought that if Rad9 existed in more molecules per cell it could localise to even more loci. To decipher that, we examined Rad9 genome-wide localisation pattern after overexpressing it in a plasmid (Rad9 molecules were 10-20 times more than normal). We have shown that Rad9 was localized to a comparable number of genes, indicating that it does not localise unselectively to the genome.

It is worth noting that even though Rad9 is localised to ~16% of all yeast genes, it is localised to only 25% of the ones whose transcription affects, which are mostly related to metabolic pathways. Based on all the large scale experiments we found Rad9 present mainly on coding regions of genes rather than non-coding, showing a binding bias towards the 3' region of the ORF in an average gene analysis. It has a binding preference to regions rich in G+C nucleotides. GC rich are also the hotspots of meiotic recombination (Gerton et al., 2000) and we found that Rad9 (as well as Aft1) localise to these DNA damage-prone areas with high probability. Rad9 tends to localize to genes longer (>1800bp) than the average overall distribution of all yeast genes and to even longer ones when *AFT1* is absent. Rad9 is also present on centromeres where Aft1 also localises, as well as on telomeres and other non-ORF elements. Moreover, Rad9 localisation exhibited similar pattern on an average gene with specific epigenetic marks such as H3K36me3 and H3K79me3 which are connected to transcription and DNA damage respectively.

Of the most important findings was the strong and overrepresented presence of Rad9 to transcriptionally active regions in an Aft1-dependent manner. Rad9 loses

significantly the preference to bind on highly active genes when *AFT1* is absent, a fact that highlights the Rad9 dependency on Aft1 for its localization to the specific chromatinic loci. The highly transcriptionally active regions correlate to higher than the average mutation rate (Kim et al., 2007). In order to examine if Rad9 localisation pattern was random and depended or not on the activity state of the genes, we conducted a ChIP on chip experiment with the strain grown in medium with galactose instead of glucose, where it is known that particular gene groups are transcriptionally activated. If Rad9 had a strong correlation to localisation to transcriptionally active regions, we would expect to find it onto genes transcriptionally active in galactose. We indeed found Rad9 present to most of them, which was a strong indication of Rad9 relation to transcriptionally active regions. Functional analyses of the results of genome-wide localization experiments showed a potential of Rad9 involvement in pathways to which it has never been connected before. The overrepresented gene groups to which Rad9 was localised included some of the most highly active such as the ones related to glucose and aminoacid metabolism or related to cell growth. The binding bias of Rad9 to highly active genes is also supported by the fact that in the genome-wide localisation experiment performed in SC BCS BPS growth conditions (where iron- and copper-regulated genes are up-regulated) we observed strong binding of Rad9 to these targets.

The above data about Rad9 and Aft1, raise the possibility of them acting together as part of a larger complex which can influence the transcription of other genes in general and specific GO gene groups in particular.

In parallel, this study examines the genome-wide localisation of Aft1 transcription factor (in relation to Rad9 and on its own). It is striking that we found Aft1 present mostly on coding rather than non-coding regions. Furthermore, the functional analysis revealed that it is localised to a lot more genes than the ones included in the iron-regulon. The above data are novel for the Aft1 transcription factor.

What does Rad9 do on so many genes? What role does it have in non-DNA damage inducing conditions? How does Aft1 assist Rad9 localization to highly active, prone to DNA damage loci and for which purpose? A logical explanation could be that the protein complex is there to accomplish a surveillance role on chromatin, to ensure genome integrity at any point of cell cycle (even without the experimentally induced DNA damage). In this way, especially on highly transcribed genes, where the

DNA damage rate is higher, Rad9 will be ready to act rapidly when needed, ensuring that cell response will be as quick as possible.

The present thesis provides a comprehensive analysis of Rad9 genome-wide localisation under no DNA damage induced conditions and establishes its cooperation with Aft1 in fragile chromatin speculating a mechanism that ensures a rapid and effective response to damage. The genome-wide maps of Rad9 and Aft1 occupancy presented in this work should provide investigators information for a more in depth analysis of the topology and function of the DNA repair machinery in relation to transcriptional activity, under no DNA damage induced conditions. It seems that cell has developed simple, yet sophisticated, mechanisms to provide its fairly sensitive loci with additional protection. By maintaining DDR proteins in the neighborhood of fragile sites, possibly recruited by transcriptional activators, it establishes a well orchestrated safeguarding system.

Basic research on Rad9 protein, in combination with results deduced by experiments with Rad9-interacting proteins which are vital to ensure genome integrity, can offer an important input to the knowledge about applications targeting carcinogenic and aging mechanisms of the cell.

1.1.2.--- Significance of the study

i) A novel way of protection of fairly sensitive genomic loci is described in this study. This is characterized by the presence of Rad9 protein, under non DNA damage-induced conditions, in a non-random way, to specific regions of the genome. These regions are highly transcriptionally active, have high content in GC and are DNA damage prone. The localisation to such regions is driven by the Aft1 transcription factor, since Rad9 loses this preference in *aft1Δ* cells. Aft1 TF is also identified as a new Rad9-interacting protein. The present study provides information on the cell's protective mechanisms against the DNA damage before the actual damage occurs. It is complementary to other studies which relate high transcriptional activity to high proportion of mutagenic events (Kim et al., 2007; Kim and Jinks-Robertson, 2009).

ii) The genome-wide localization map of Rad9 DNA damage checkpoint protein and Aft1 transcription factor under non DNA damage-induced conditions is

described for the first time. This is important since Rad9 has been studied so far mainly for its role in the DDR. Biochemical studies have shown Rad9 presence to chromatin fraction under unperturbed conditions; however little is known about its function there (Gilbert et al., 2001; Granata et al., 2010; Hammet et al., 2007). Analyses in the present study give insights to Rad9 role on chromatin under unperturbed conditions.

iii) A novel way of Rad9 recruitment to chromatin through Aft1 TF and possibly through epigenetic marks is provided in this study. Rad9 recruitment to chromatin has been studied by others primarily after the activation of DDR and the mechanism by which it is localised to chromatinic regions under non DNA damage-induced conditions has not been the focus of previous studies (Granata et al., 2010; Hammet et al., 2007; Huyen et al., 2004; Nnakwe et al., 2009; Soulier and Lowndes, 1999).

iv) Data from functional as well as ChIP assays indicate implication of Rad9 protein and Aft1 transcription factor in transcription elongation to which they have not been connected before. This not only is novel for Rad9 protein but is also remarkable for a transcription factor. A synthetic phenotype between the two proteins also exists in 6-AU growth assays (indicative of a direct or indirect implication to transcription elongation).

v) Aft1 genome-wide localisation analysis in relation to Rad9 as well as on its own is of special importance, since Aft1 –apart from its classic role as the regulator of iron homeostasis- has been connected genetically to genome integrity, chromosome and cell wall stability and is turning out to be a multifunctional transcription factor of high significance for the cell (Berthelet et al., 2010; Hamza and Baetz, 2011; Measday et al., 2005; Shakoury-Elizeh et al., 2004).

1.2.--- Yeast as a Model Organism

The yeast *Saccharomyces cerevisiae* is a model organism which represents a simple eukaryote with a genome that is easy to manipulate (Sherman, 2002). Yeast is slightly more complex than bacteria, and they have many technical advantages in common. Yeast is suitable for biological studies because they grow rapidly, have dispersed cells, it is easy to do replica plating and isolate mutants, and they have a

very effective system to transform their DNA (Woods and Gietz, 2001). Yeast is non pathogenic and does not require a vast amount of precautions and it is quite cheap source for biochemical studies.

Strains of *S. cerevisiae* have both a stable haploid and diploid state, and can live with a lot of incorporated markers. In this way, recessive mutations are manifested in haploid strains, and tests that require complementation are easily to be done with diploid strains.

DNA transformation technique has made gene cloning and other genetic engineering applications in yeast very effective. Plasmids are easily introduced into yeast cells as replicating molecules and they can also be integrated into the genome. In contrast to most other organisms, transformation of DNA which is integrated into the genome is accomplished with homologous recombination. Sequences of yeast genome which may also have other sequences from plasmids can be cloned in a directed way to specific genomic locations. It is also relatively feasible to replace wild type genes with altered ones. The phenotypes resulting from the disruption of yeast genes have contributed considerably to the understanding of the function of certain proteins *in vivo*. Transformation in yeast can be done directly with the use of short synthetic primers, which permits the production of possible altered forms of proteins. These techniques have been used to a great extend in the analysis of gene regulation, and to answer other general questions regarding the biology of the cell.

S. cerevisiae was the first eukaryote to have its genome sequenced (Goffeau et al., 1996). Subsequently, yeast was extensively used in genome-wide research applications, including DNA expression microarray experiments, in order to study the genome-wide alteration of the transcription profile in strains in which a gene (or combination of genes) was disrupted or in strains grown in different conditions. Furthermore, yeast system was and is extensively used to study interactions between proteins with the use of two-hybrid analysis and mass spectrometry of TAP-tagged proteins and also to perform functional analysis of synthetic lethality. Moreover, mammalian genes are easily introduced into yeast and this can be extremely valuable in order to study the encoding proteins.

There exist a lot of human genes which are connected to disease and have orthologues in yeast. This lead to the use of yeast as a model to study the molecular basis of human diseases.

1.3.1---Rad9: Introduction to the gene and protein product

RAD9 was the first DNA damage checkpoint gene identified in yeast more than 20 years ago (Weinert and Hartwell, 1988). Nevertheless, the exact role of the gene's product, its regulation and function remains not fully understood.

Saccharomyces cerevisiae Rad9 is a well conserved nuclear phosphoprotein, a DNA damage checkpoint protein required for the DNA damage response pathway throughout the cell cycle and has been shown to function at G1/S, intra-S and G2/M checkpoints (Paulovich et al., 1997; Siede et al., 1993; Weinert and Hartwell, 1988).

Rad9 is phosphorylated during the normal progression of a cell cycle but becomes overphosphorylated by Mec1 and Tel1 kinases in response to DNA damage (Emili, 1998; Vialard et al., 1998). Rad9 protein can be purified in two complexes, a large one that is hypophosphorylated of unknown function (850 kDa) and a small hyperphosphorylated one (560kDa) which participates in the DNA Damage Response (DDR) (see below). Both complexes contain the chaperone proteins Ssa1 and Ssa2 and the smaller complex also includes Rad53 kinase (van den Bosch and Lowndes, 2004).

Rad9 is a large multidomain protein of 148kDa. It contains **1)** a tandem repeat of the BRCT motif (BRCA-1 C-terminus) which is required for Rad9 oligomerization after DNA damage (Hammet et al., 2007; Nnakwe et al., 2009; Soulier and Lowndes, 1999), **2)** a TUDOR domain which recognizes H3K79 methylated histones [reviewed in (Lydall and Whitehall, 2005)] –part of TUDOR is also implicated in potential Rad9 binding on naked DNA (Lancelot et al., 2007)-, **3)** an ST-cluster domain (SCD) rich in S and T residues which are phosphorylated after DNA damage (Emili, 1998; Toh and Lowndes, 2003; Vialard et al., 1998) and **4)** a Chk1 activation domain which activates the downstream Chk1 kinase in the DDR pathway (Figure 1.1). Recent data confirmed that the Rad9 BRCT domains mediate Rad9 oligomerization and these interactions are also modulated by the Mec1/Tel1-dependent phosphorylation of the SCD cluster domain. Rad9 oligomerization is required in order to maintain checkpoint signaling through a feedback loop involving Rad53-dependent phosphorylation of the Rad9 BRCT domains which attenuates BRCT-SCD interactions (Usui et al., 2009). In Figure 1.1, the domains of Rad9 are shown schematically.
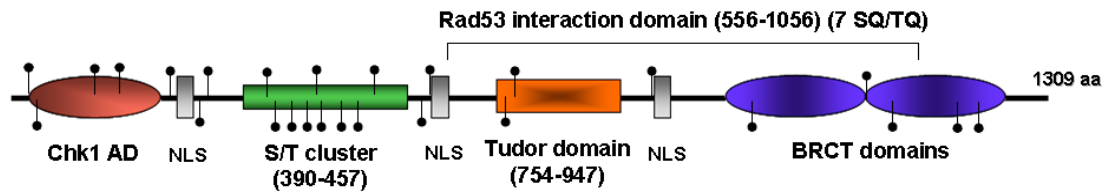
FIGURE 1.1: Rad9 protein structure
Rad9 is a multidomain protein including four main domains as described in the text. Bulleted lines represent phosphorylation sites.

1.3.2.--Rad9 Molecular Role

Rad9 is the signal mediator between essential upstream and downstream kinases in the DNA damage checkpoint pathway. More specifically, upon DNA damage, the first biochemical event following the checkpoint activation is the Mec1-dependent phosphorylation of its interacting subunit Ddc2 (Paciotti et al., 2000; Rouse and Jackson, 2000; Wakayama et al., 2001). Continuing downstream to the checkpoint pathway, Rad9 is being overphoshorylated by Mec1/Tel1 and it oligomerizes through its BRCT domains. Rad9 overphosphorylation is a prerequisite for its association to Rad53 effector kinase, and is mediated by the two forkhead associated (FHA) domains in Rad53 and specific Rad9 residues that are modified in the overphosphorylated form (Durocher et al., 1999; Emili, 1998; Schwartz et al., 2002; Sun et al., 1998; Sweeney et al., 2005; Usui et al., 2009; Vialard et al., 1998). In that activated form, Rad9 mediates the signal to Rad53, the main effector kinase, which is autophosphorylated. As (Gilbert et al., 2001) showed on purified Rad9 complexes from undamaged and UV-treated cells, Rad9 recruits and catalyses the activation of Rad53 by acting as a scaffold protein bringing Rad53 in close proximity, thus facilitating the Rad53 autophosphorylation reaction (and further phosphorylation of Rad53 by Mec1). In addition to Rad53 phosphorylation, activated Rad9 also stimulates Mec1 dependent phosphorylation of Chk1 effector kinase. Phosphorylation and activation of these effector kinases leads to various processes associated to cell cycle arrest (Figure 1.2) (Downs et al., 2000; Emili, 1998; Gilbert et al., 2001; Paciotti et al., 1998; Schwartz et al., 2002; Toh and Lowndes, 2003; Vialard et al., 1998). Such processes include trancriptional upregulation of DNA damage repair genes, transcriptional repression of cyclins and stabilization of replication forks reviewed in (Chen and Sanchez, 2004; Weinert, 1998).
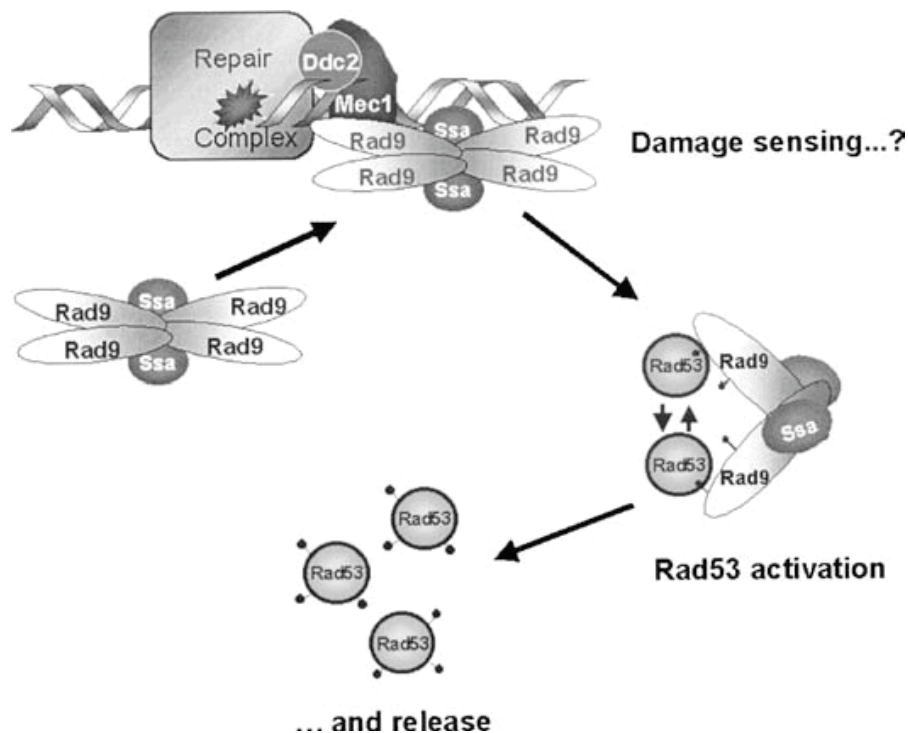
FIGURE 1.2: Biochemical model for Rad9 function (Toh and Lowndes, 2003)

DNA damage induces Mec1/Tel1 dependent Rad9 phosphorylation which leads to Rad9 oligomerization (through its BRCT domains) and to its overphosphorylated form. Chaperones like Ssa1 and/or Ssa2 are possibly required for this conformational change. Binding of hypophosphorylated Rad53 (through its FHA domains) on Rad9 phosphoresidues created by Mec1 increases local concentration of Rad53 to levels that allow its *in trans* autophosphorylation. Rad9 acts as Mec1 adaptor to allow Rad53 activation. Efficient Rad53 phosphorylation allows its release from Rad9 complex and this activated form of Rad53 effector kinase targets substrates required for the checkpoint pathway-regulated cell cycle arrest and efficient DNA repair.

The position of Rad9 protein in the DNA damage response pathway in *Saccharomyces cerevisie* is depicted in Figure 1.3.
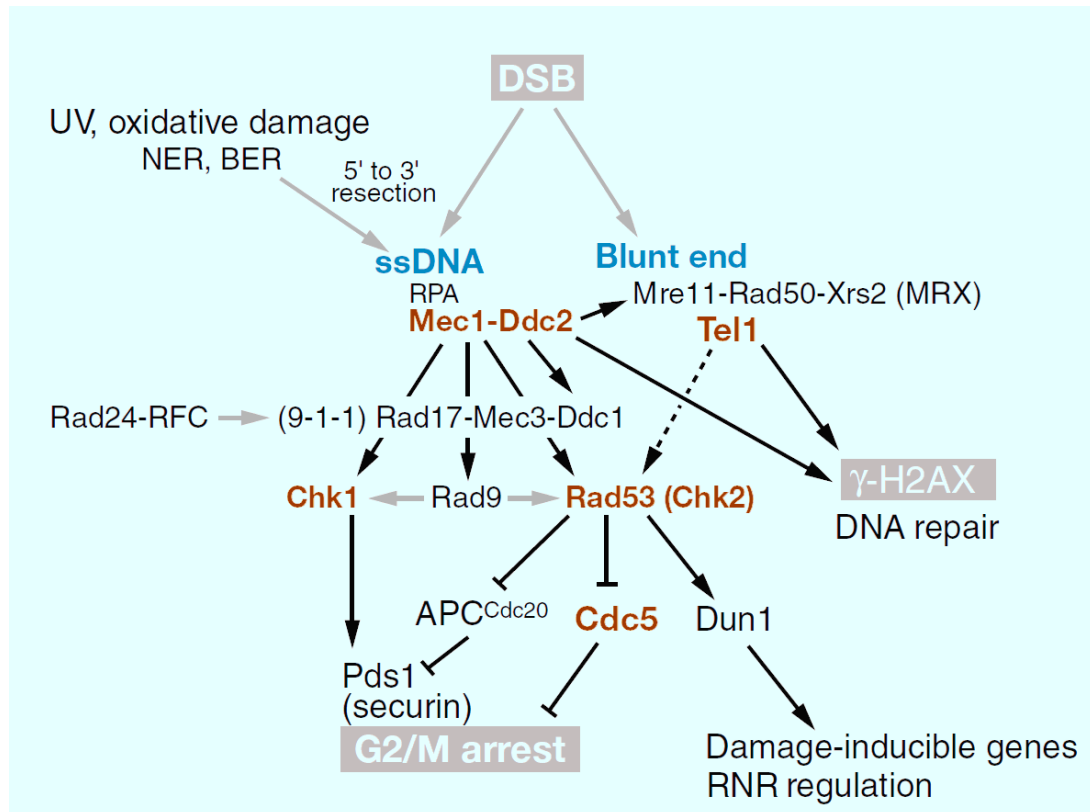
FIGURE 1.3: The *Saccharomyces cerevisiae* DNA damage checkpoint (Harrison and Haber, 2006)

Resection of the DSB end yields long 3'-ended **ssDNA** tails that trigger the **Mec1-Ddc2**-dependent DNA damage checkpoint kinase cascade. **Mec1** is also activated by ssDNA gaps encountered by nucleotide excision repair (**NER**) or base excision repair (**BER**). Unresected, blunt-ended DNA also activates a DNA damage response, primarily through the **Tel1** protein kinase and its associated **MRX** complex. Kinases in the cascade are indicated in red. Under some circumstances where Mec1 is absent, Tel1 can activate the S-phase checkpoint through Rad53 and other kinases, as indicated by a dotted line. Characteristics of DNA damage signalling are phosphorylation of histone **H2AX (γ-H2AX)** and increased in DSB repair events, arrest of the cell cycle prior to anaphase (G2/M arrest) and induction of damage-inducible genes as well as posttranslational regulation of ribonucleotide reductase (**RNR**). Black arrows indicate protein kinase phosophorylations of several target proteins that activate downstream events, whereas a black terminated line indicates an inhibitory modification. Gray arrows indicate protein interactions that facilitate checkpoint activation.

Rad9 is an adaptor protein required for *Saccharomyces cerevisiae* cell cycle checkpoint function. It mediates the phosphorylation of important effector kinases and facilitates the amplification of initial signals in response to DNA damage. Because of the ability of Rad9 to associate with double stranded breaks (DSBs), it is speculated that Rad9 acts as a DNA damage sensor by initiating these checkpoint signal transduction cascades (Naiki et al., 2004).

RAD9 null mutants, although viable, exhibit increased sensitivity to X-ray and UV irradiation, fail to arrest in response to DNA damage and are prone to chromosomal instability (Fasullo et al., 1998; Paulovich et al., 1997; Weinert and Hartwell, 1990).

1.3.3.--Rad9 and Homologues

Despite the fundamental nature of cell's response to DNA damage, it is surprising that *RAD9* is not a highly conserved protein among organisms. The *RAD9* ortholog in *Saccharomyces pombe* is *crb2* (Willson et al., 1997). There is no single metazoan ortholog of *RAD9* but there exists a family of proteins that contain BRCT domains (Alpha-Bazin et al., 2005; Bork et al., 1997) such as *BRCA1* and *53BP1. S. pombe's* crb2 and metazoan's *53BP1,* like *S. cerevisiae's* Rad9, contain a Tudor domain. Dimerization through BRCT domains had been shown to be essential for the biological function of both Rad9 and crb2, but in the metazoan 53BP1 this happens in a BRCT-independent manner (Ward et al., 2006; Zgheib et al., 2009). Structural studies showed that p53 has a conserved binding site for 53BP. This shows that the oligomerization of a checkpoint mediator may have been conserved through evolution, although in metazoan it is facilitated via a second protein rather than homotypic interactions (Kilkenny et al., 2008). In Figure 1.4.A the domain homologies between yeast's Rad9 and its human homologs 53BP1 and BRCA1 are visualized. In Figure 1.4.B the aligned sequences of human 53BP1, *Saccharomyces pombe* Crb2 and *Saccharomyces cerevisiae* Rad9 are compared.
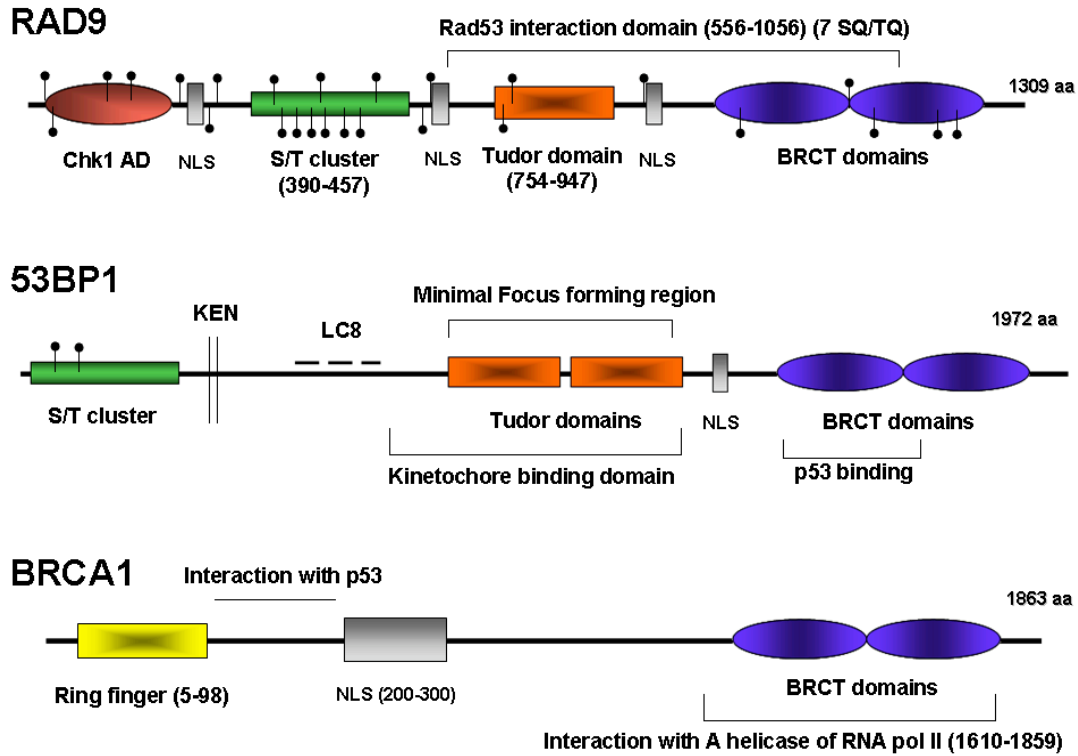
FIGURE 1.4.A: *Saccharomyces cerevisiae* **Rad9 and its human functional homologues**

Rad9 protein has 2 BRCT domains in its structure as both 53BP1 and BRCA1 have. It also has the Tudor domain as 53BP1. Thus, the closest functional homologue of Rad9 in humans is 53BP1 protein.

FIGURE 1.4.B: Amino acid sequence alignment of BRCT2 domains from Crb2, human 53BP1, and *S. cerevisiae* Rad9 (Kilkenny et al., 2008)

The major functional blocks are highlighted in yellow, Crb2 residues implicated in dimerization are shown in green bold letters, residues implicated in polar interactions with the phosphopeptide are shown in red bold, and residues involved in hydrophobic interaction with the C-terminal leucine of histone H2A are shown in blue bold letters. Topologically equivalent residues conserved in 53BP1 and Rad9 are colored accordingly. Arg1858 in 53BP1, which would prevent dimerization of the 53BP1–BRCT2 domain, is bold and underlined.

1.3.4.--Rad9 in Non DNA Damage-Induced Conditions

Rad9 is recruited to chromatin/DNA upon DNA damage but it has been shown that a significant proportion of Rad9 is already bound to chromatin in unperturbed conditions throughout the cell cycle (Gilbert et al., 2001; Hammet et al., 2007). In detail, after UV irradiation, Rad9 is redistributed from the soluble protein pool to the fraction which is enriched in chromatin. Mutations that lead to dysfunctional Tudor domain have as a result the detachment of Rad9 from chromatin in unperturbed cells and no further recruitment to chromatin upon DNA damage. This shows that the binding of Rad9 protein to chromatin is required for its hyperphosphorylation and subsequent enrichment in chromatin after the DNA damage event (Hammet et al., 2007). When $BRCT_2$ domains are mutated, Rad9 localisation to chromatin in undamaged cells is unperturbed, but Rad9 fails again to enrich chromatin upon DNA damage. The logical explanation given for these data is that Rad9 Tudor domain is important for the association of Rad9 with chromatin in undamaged cells, which is required for the enrichment in the neighborhood of the DNA damage (which is $BRCT_2$-dependent) (Hammet et al., 2007). This is in agreement with our results from large scale chromatin immunoprecitation experiments in non DNA damage-induced growth conditions in which we find Rad9 localised to ~18% of yeast genes. Based on the fact that Rad9 is consitutively localised to chromatin, one can speculate that the Rad9 Tudor domain can recognize histone methylation marks which drives its association with chromatin. Indeed, in budding yeast, there are particular histone lysine methylases which are required for the respone in G1 checkpoint (Giannattasio et al., 2005; Wysocki et al., 2005). Furthermore, the Tudor domain of 53BP1 recognizes at least three histone methylation marks *in vitro* (Botuyan et al., 2006).

It has been proposed that the constitutive Rad9 recruitment to chromatin may assist the efficiency and speed of the Rad9 dependent response to genotoxins (Granata et al., 2010) leading to a faster and more effective DNA-damage response. Following DNA damage, H2A phosphorylation may assist Rad9 recruitment near sites of damage through the $BRCT_2$ domain allowing efficient Rad9 phosphorylation and signaling. Rad9 is phosphorylated in normal post G1-cells and cyclin-dependent kinase (CDK) phosphorylation of Crb2 (the Rad9 orthologue in *S.pombe*) is required for the efficient repair of ionizing radiation induced lesions (Caspari et al., 2002) as

well as for ionizing induced focus formation in the absence of ligands for the Tudor and BRCT$_2$ domains (Du et al., 2006).

1.3.5.--Rad9, DNA Damage and Histone Modifications

The constitutive as well as the DNA-damage dependent binding of Rad9 to chromatin require the BRCT domains. Furthermore, this interaction appears to require the recognition of H3K79 methylated histones by Tudor domain of Rad9. This latter interaction modulates Rad9 function after DNA damage (Giannattasio et al., 2005; Grenon et al., 2006; Hammet et al., 2007; Huyen et al., 2004; Nnakwe et al., 2009). However, the Crb2 and 53BP1 orthologues of Rad9 both recognize H4 methylated at lysine 20 (H4K20me), although human 53BP1 may also be recruited to chromating through interactions with H3K79me (Botuyan et al., 2006; Du et al., 2006; Huyen et al., 2004; Sanders et al., 2004; Schotta et al., 2003). Further molecular interactions are required for the recruitment of the Rad9, Crb2 and 53BP1 mediator proteins. Rad9 and Crb2 use their BRCT domains to interact with H2A phosphorylated at serine 129 (γH2A) at sites of DNA damage (Du et al., 2006; Hammet et al., 2007; Javaheri et al., 2006; Kilkenny et al., 2008; Nakamura et al., 2004; Toh et al., 2006). 53BP1 binding to DSBs is facilitated by phosphorylation of serine 139 of the histone variant H2AX (γH2AX) (Iwabuchi et al., 2003; Pryde et al., 2005; Ward et al., 2006; Ward et al., 2003). A range of oligomerization domains in 53BP1 facilitate its recruitment to loci where DNA damage occurred (Zgheib et al., 2009). Moreover, ubiquitination of H2A and H2AX by RNF8 facilitate the localization of 53BP1 to chromatin (Huen et al., 2007; Kolas et al., 2007; Mailand et al., 2007).

The relation between Rad9 and Dot1 histone methyltransferase has been also studied (Conde et al., 2009; Lazzaro et al., 2008). Lazzaro et al (2008) propose potential mechanisms for the role of Rad9 in resection inhibition in response to DSBs and uncapped telomeres: Rad9, while bound to the methylated by Dot1 (histone methyl-transferase) H3K79, it interferes with the action of the nuclease(s) or generates a non permissive chromatin configuration, thus inhibiting exonucleolytic processing of DNA. Rad9-H3K79me interaction may be responsible for that, but some other interactions may also contribute: for example BRCT domains of Rad9 may interact with phosphorylated checkpoint proteins or histones at sites of DNA damage and inhibit nuclease activity (Du et al., 2006; Hammet et al., 2007). Dot1 and

Rad9 also contribute to cohesin-dependent DSB repair by sister chromatid recombination (SCR). SCR is a key mechanism for the repair of DSBs generated during replication and it is vital for the maintenance of the genomic stability. Conde et al. (2009) showed that Dot1, Rad9 and phosphorylation of histone H2A (γH2A) are prerequisites for effective SCR. They also showed that loading of cohesin onto chromatin after DNA damage is promoted by Dot1 and Rad9. The model proposed was that the localisation of Rad9 to DSB loci which is mediated by γH2A and H3K79 methylation can help the repair of the damaged site via SCR by regulating cohesion binding to damaged sites. Moreover, 53BP1 (the closest Rad9 homolog in metazoan systems) has been shown to change the dynamic behaviour of chromatin in order to promote DNA repair (Dimitrova et al., 2008).

In another study (Dotiwala et al., 2010), it was shown that *dot1Δ* H2A-S129A double mutant had a significantly longer cell-cycle delay than a *rad9Δ* mutation. Also, by using co-localisation studies in live cells and fixed chromatin (Cook et al., 2009) showed that Slx5 (of Slx5/Slx8 SUMO-targeted ubiquitin ligase) co-localises to DNA damaged induced foci of Rad9.

1.3.6.--Rad9 and Dpb11 Replication Initiation Protein

It has recently been shown that Dpb11 in *S. cerevisiae* and its *S.pombe* and metazoan orthologs, Rad4/Cut5 and TopBP1 respectively, are required for full PIKK-dependend (phosphoinositide 3-kinase-like kinase dependent) checkpoint activation in response to DNA damage (Furuya et al., 2004; Puddu et al., 2008). Dpb11 is a replication initiation protein that loads DNA polymerase epsilon onto pre-replication complexes at origins. It is a checkpoint sensor which is recruited to stalled replication forks by the checkpoint clamp complex and there it activates Mec1 kinase. It has been suggested that Dpb11 orthologs may modulate checkpoint activation through interaction with mediator/adaptor proteins (Du et al., 2006; Liu et al., 2006).

(Granata et al., 2010) proposed a model of the dynamics of Rad9 chromatin binding and its interaction with Dpb11 to modulate checkpoint activation in M phase. According to that model, under untreated conditions, Rad9 is chromatin bound through the interaction of its Tudor domain with H3K79me and its BRCT-mediated dimerization. After DNA damage, activated Rad9 may change its conformation,

becoming able to interact with γ-H2A. In M-phase, an alternative means of Rad9 recruitment near DNA lesions involves its interaction with Dpb11. This factor is brought near the Mec1-Ddc2 complex via its interaction with the 9-1-1 clamp, and it binds the phosphorylated N-terminal portion of Rad9 leading to full checkpoint activation (Figure 1.5).
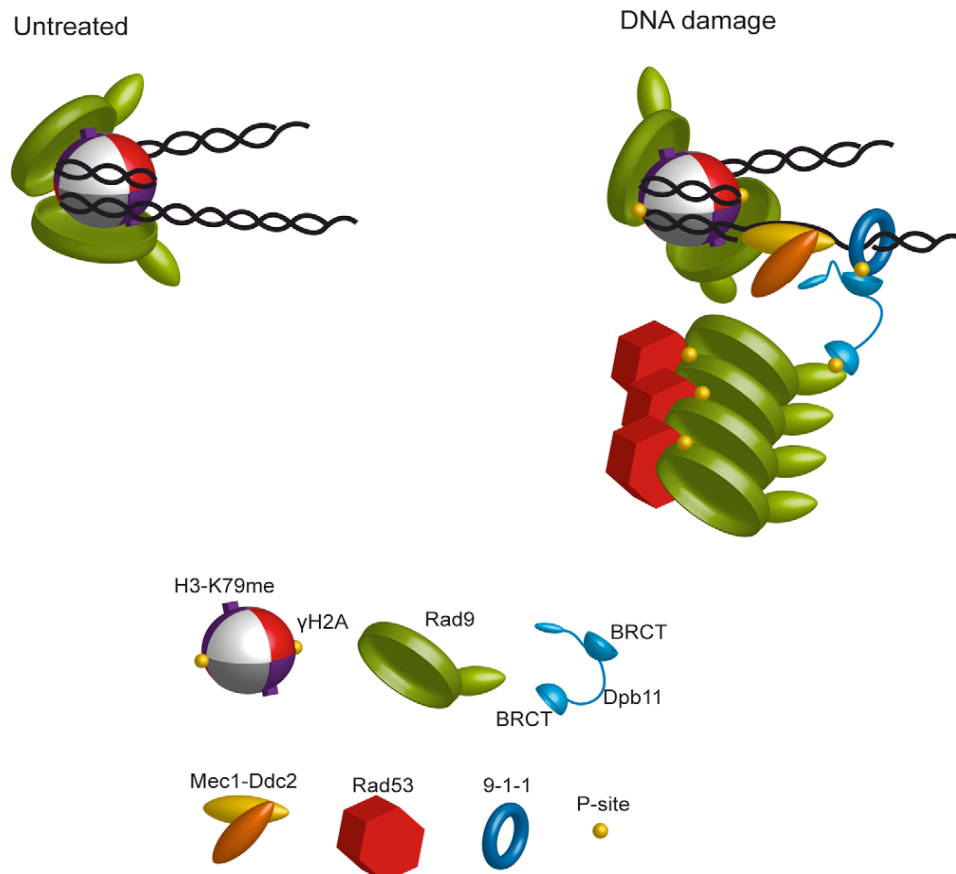
FIGURE 1.5: Possible model of the dynamics of Rad9 chromatin binding and its interaction with Dpb11 to modulate checkpoint activation in M phase (Granata et al., 2010).
See text for details.

1.3.7.--Rad9 and Transcription

The preferential repair of the transcribed strand of genes (Mellon et al., 1987) as well as promoter surrounding sequences (Tu et al., 1996) has established a functional link between transcription and DNA repair. At this point it is worth pointing out that in mammalian systems transcriptional activators are shown to stimulate DNA repair. Using chromatin templates and purified NER factors, Frit et al.

(2002) showed that Gal4-VP16 and RAR factors activators of transcription can stimulate the removal of DNA damage in promoter regions (and the surroundings of their binding site) as a result of a specific function of activators in local chromatin remodeling. They accomplish that by attracting cofactors which give access to the DNA repair factors. The way transcriptional activators stimulate the removal of DNA damage can be more direct: by interacting with DNA repair factors and recruiting them to the damage site. Gal4-VP16 and RAR are shown to interact with RPA and TFIIH essential NER factors respectively (He et al., 1993; Li and Botchan, 1993; Rochette-Egly et al., 1997), which are recruited once XPC/HR23B is bound to the damaged DNA to initiate the GGR subpathway of NER (Volker et al., 2001).

Frit et al (2002) also showed that transcriptional activators stimulate the removal of DNA lesions on both DNA strands and in the vicinity of their DNA binding sites, which usually includes the transcription initiation site. In that way they are ready to act fast there and in the surrounding areas when they are needed. Following DNA damage, activators can derepress chromatin in order to facilitate the repair process and to further allow accurate transcription initiation. This hypothesis is also supported by other studies which show that DNA repair was much faster and without strand selectivity near the transcription start site of the human JUN gene which has up to five activator DNA binding sites in the vicinity (Tu et al., 1996). This, along with the fact that the formation of the transcription complex requires both strands (coding and non coding) (Kim et al., 2000; Robert et al., 1998), highlights how important is this transcription initiation associated (TIAR) mode of repair which operates without strand bias. The transcribed strand exhibit a preferential repair, which may mean that once RNA synthesis is initiated, the elongating RNA pol II and its accompanying factors would play the role previously assumed to be executed by the activator in order to inspect the integrity of the gene to be transcribed (Frit et al., 2002). This transcription elongation coupled repair (TECR) targets distinctively the transcribed strand. There are data that are in agreement with the above model, such as the fact that RNA pol II is associated both with transcription factors and DNA repair factors such as RPA, XPG and XPF (Maldonado et al., 1996; Tantin et al., 1997).

By performing Yeast Two Hybrid Screening using Mac1 transcription factor as bait, our group has found Rad9 as one of the interactants (Voutsina et al., unpublished). This was also confirmed by co-immunoprecipitation experiments (co-IP) (Gkouskou et al., unpublished). Rad9 was found to associate directly with Mac1

TF via its BRCT domain which may interfere with Mac1 functionality (Gkouskou et al., unpublished). Mac1 is a copper repressed TF and activates genes such as *CTR1* and *FRE1* which are responsible for copper uptake in yeast cells.

Under no DNA damage-induced conditions[3], we found that Rad9 negatively regulates Mac1 DNA binding and transactivation function, it is recruited via Mac1 to the *CTR1* and *FRE1* promoters under induction conditions and it associates with *CTR1* coding region following elongating RNA polymerase II (Gkouskou et al., unpublished). Moreover, Rad9 physically interacts and partially affects localisation of Hir1 histone chaperone on *CTR1* promoter and coding region (Gkouskou et al., unpublished). It is recruited via Mac1 initiation complex to a heterologous coding region from the upstream fused *CTR1* promoter and it also recruits Rad53 on *CTR1* gene (Gkouskou et al., unpublished). Conclusively, we found a new way for Rad9 recruitment to chromatin under unperturbed conditions in an RNA polymerase II transcription context.

The studies in mammalian systems show a potential for a similar model in *Saccharomyces cerevisiae* and Rad9 DNA damage checkpoint protein which is indirectly involved in NER (Al-Moghrabi et al., 2009) and furthermore found to interact with Aft1 and Mac1 transcription factors (this study and Gkouskou et al., unpublished). We found Aft1 and Mac1 TFs localised to more targets than the ones already known to belong to their regulons. The fact that Rad9 is present on more genes than these TFs are localised to and also that their localization patterns are only partially overlapping, is indicative of a more complex regulation of Rad9 distribution to the genome.

1.4.--DNA Damage

Taking into account the Rad9-Mac1 interaction that we found in our laboratory (Gkouskou et al., unpublished) and also the fact that NER factors were found to be recruited to active promoters in order to facilitate chromatin modification for transcription in the absence of exogenous genotoxic attack (Le May et al., 2010b),

---

[3] There was no use of external DNA damage-inducing conditions/agents. Rad9 is overphosphorylated during DNA damage response and the overphosphorylated form is clearly detectable in a Western blot. In the conditions under which the experiments of this study were performed, Rad9 was in its hypophosphorylated form.

we wondered what was the connection between our analysis of Rad9 under non DNA damage-induced conditions with what Rad9 does upon DNA damage. Is Rad9 localisation pattern different and in which way? Is Rad9 present to more or less genes? Is there a specific overrepresentation of particular gene ontology (GO) groups in the one or the other case?

To address these questions we performed genome-wide analysis of Rad9 localisation pattern upon DNA damage using the drug zeocin.

We will first get an insight to some basic aspects of the DNA damage checkpoint pathway in yeast in order to examine the role of Rad9; reviewed in (Harrison and Haber, 2006; Longhese et al., 2006; Putnam et al., 2009; Reed, 2011).

1.4.1.--The Central DNA Damage Checkpoint in *Saccharomyces cerevisiae*

1.4.1.1.—Vegetative cycle

The molecular events of the checkpoint can be divided into activation (cell cycle arrest), maintenance (of the arrest) and inactivation (recovery/re-entry into the cell cycle). When a DNA damage event occurs in the form of a DSB, a resection of the damage occurs (5'$\rightarrow$3' nucleolytic degradation of one DNA strand at a DSB end which results in a long region of ssDNA with a 3' end) which triggers the Mec1-Ddc2-dependent DNA damage checkpoint kinase cascade. Mec1 is also activated by ssDNA gaps arising by nucleotide excision repair (NER) or base excision repair (BER). Unresected, blunt ended DNA also activates a DNA damage response, primarily through the Tel1 protein kinase and its associated MRX complex (Mre11-Rad50-Xrs2) (Figure 1.3). Recruitment of these checkpoint kinases (of the PIKK family) is considered the most upstream event that triggers the pathway activation and cell cycle arrest. Mec1 interacts with Ddc2 which recognizes ssDNA bound by replication protein A (RPA), while Tel1 binds to the DNA end-binding MRX complex (partly responsible for the creation of ssDNA through its nucleolytic action) and recruited mostly to blunt or minimally processed DSB ends. 9-1-1 complex (Rad17, Mec3, Ddc1) is also required for checkpoint activation and cell cycle arrest and is loaded onto DNA with the help of Rad24 (Figure 1.6).
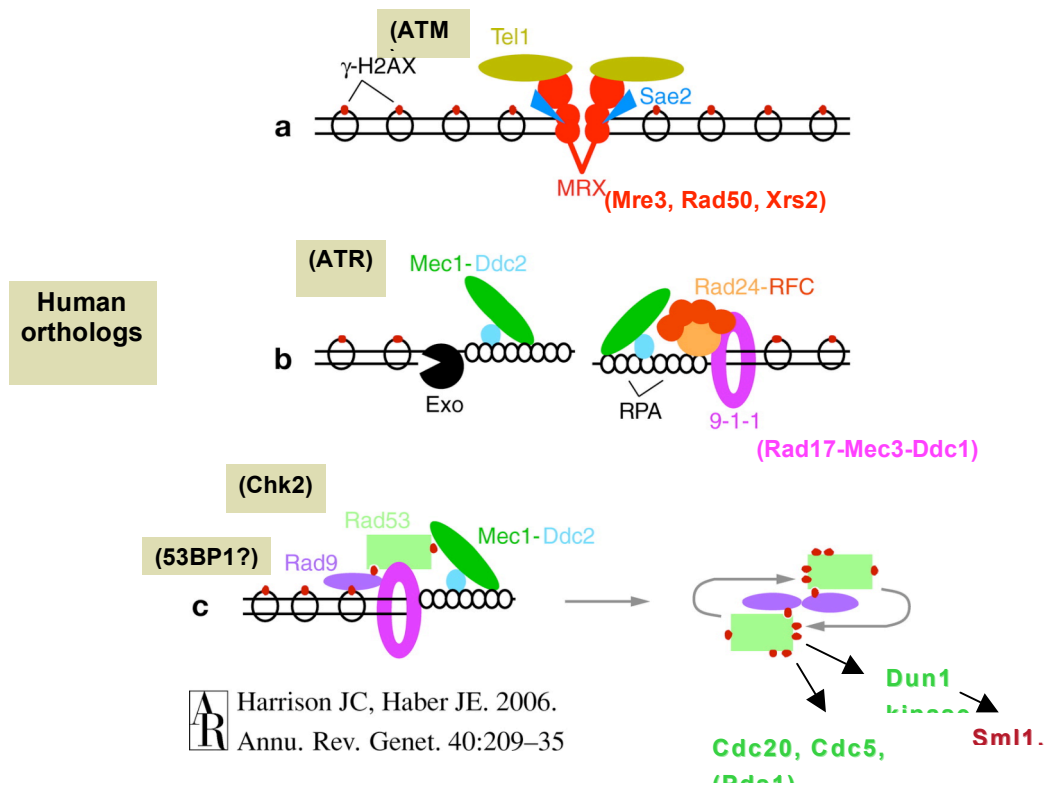
FIGURE 1.6: Checkpoint protein association with DSB (adapted from Harrison and Haber, 2006)

(a) The first important checkpoint proteins interacting with DSB ends are Mre11, Rad50, and Xrs2 (the MRX complex, red). MRX recruits the PIKK Tel1 (dark yellow) which can phosphorylate histone H2A in chromatin to create a region of γ-H2AX (red spot on nucleosome). Sae2 (blue wedge) stimulates the nuclease activity of the MRX complex and also promotes the removal of MRX and Tel1 from DNA thus limiting their signaling potential.

(b) DNA resection at a DSB is carried out by MRX, Exo1, and an unknown nuclease (collectively indicated in black). Resection leaves a region of 3'-ended ssDNA which is rapidly coated by the RPA heterotrimer (represented as white circles). Rad24 (orange), in complex with Rfc2-5 (dark orange), binds at the ssDNA/dsDNA junction and loads the 9-1-1 clamp (magenta). This clamp can slide over dsDNA but not over RPA-coated ssDNA. RPA-coated ssDNA also recruits the Mec1-Ddc2 heterodimer (green and light blue), which activates the checkpoint cascade. Like Tel1, Mec1 can generate a region of γ-H2AX around the DSB.

(c) Activation of the checkpoint cascade. Rad9 (purple) is recruited to DNA via its interactions with the modified histones including γ-H2AX. Rad9 is then phosphorylated (red dot) by Mec1 (green). Phosphorylated Rad9 recruits Rad53 (avocado) for phosphorylation (red dot) by Mec1. Both of these events are facilitated by the 9-1-1 complex, though the precise interactions have not been elucidated. A complex of Rad9 and phosphorylated Rad53 then dissociates from Mec1 and multimerizes in order to allow further trans-autophosphorylation and full activation of Rad53. Chk1 is activated by Mec1 and Rad9 via a similar but molecularly distinct mechanism.

After damage detection by upstream sensors, a kinase cascade amplifies and transmits the signal to checkpoint targets, notably the cell cycle machinery. In *Saccharomyces cerevisiae* the primary effector is the Chk2-family kinase Rad53 whose activation requires Mec1 and Rad9 "adaptor" protein. More specifically, Rad53's phosphothreonine-binding FHA domains interact with PIKK-phosphorylated Rad9 (cluster of 7 SQ/TQ motifs in its central region) leading to catalytic activation of Rad53 and extensive Rad53 autophosphorylation. Rad9 is also required for the Chk1

kinase activation. The biochemical aspect of Rad9 function as a mediator of the DNA damage signal has been proposed almost a decade ago (Toh and Lowndes, 2003) (Figure 1.2). The task for the cell cycle arrest and the beginning of DNA damage repair is performed by the effector kinases, mainly Rad53 and Chk1. Chk1 regulates the stability of Pds1, a securin which is required for normal cell cycle arrest in response to DNA damage after its overphosphorylation and subsequent stabilization (it is ubiquitinated and degraded at the entry in mitosis in normal conditions). Rad53 also regulates Pds1 stability by blocking its interaction with Cdc20 (a common regulatory target to prevent anaphase). Furthermore, Rad53 inhibits mitotic exit through inhibiting Cdc5. The proteins that participate in the DNA damage response pathway in *Saccharomyces cerevisiae* along with their counterparts in other organisms are presented in Table 1.

Class	*S. cerevisiae*	*S. pombe*	*H. sapiens*
PIKK	Mec1	Rad3	ATR
PIKK	Tel1	Tel1	ATM
Rfc1 homolog	Rad24	Rad17	Rad17
9-1-1 clamp	Rad17	Rad9	Rad9
9-1-1 clamp	Mec3	Hus1	Hus1
9-1-1 clamp	Ddc1	Rad1	Rad1
MRX complex	Mre11	Mre11	Mre11
MRX complex	Rad50	Rad50	Rad50
MRX complex	Xrs2	Nbs1	Nbs1
	Ddc2	Rad26	ATRIP
BRCT domain adaptor	Dpb11	Cut5/Rad4	TopBP1
			DNA-PKcs
Adaptor	Rad9	Crb2	53BP1, Mdc1, Brca1?
Adaptor	Mrc1	Mrc1	Clspn
Effector kinase	Rad53	Cds1	Chk2
Effector kinase	Chk1	Chk1	Chk1
Polo kinase	Cdc5	Plo1	Plk1
Securin	Pds1	Cut2	Securin
Separase	Esp1	Cut1	Separase

APC targeting subunit	Cdc20	Slp1	p55^{CDC}/CDC20

TABLE 1: DNA damage checkpoint proteins I n *S. cerevisiae* **and their homologues**
Colour code: Green-Sensors, Orange-Adaptors, Red-Effector kinases, Blue-Final targets.

In addition to regulating the signaling proteins, DNA damage also leads to Mec1- and Tel1-dependent phosphorylation at serine 129 of the histone variant H2AX. Phosphorylated H2AX (γ-H2AX) is found flanking 50-100kb around the DSB in yeast. As mentioned above, Rad9 interacts with γ-H2AX and change its conformation. The major role for γ-H2AX is the recruitment of chromatin remodelers, including the Ino80, Rvb1, NuA4 and Swr1 complexes to the DSB. γ-H2AX also recruits cohesin and the Smc5/6 complex to DSB.

Another modification following the DNA damage is the methylation of Lys79 of histone H3 (H3K79me) by Dot1 methyltransferase which is recognised by the Tudor domain of Rad9 protein.

After the DDR pathway is activated leading to cell cycle arrest, the actual repair begins in order to maintain genome integrity. DNA repair can be made in a variety of ways depending on the type of damage. Single strand lesions can be repaired by base excision repair (BER), nucleotide excision repair (NER) or mismatch repair using the non-altered strand as a template (Figure 1.7.A). Double strand breaks are repaired through two major pathways: non-homologous end joining (NHEJ) and homologous recombination (HR) (Figure 1.7.B); reviewed in (Longhese et al., 2006). Whereas HR uses the genetic information stored in the sister chromatid or in the homologous chromosome to repair DSBs with high fidelity, NHEJ is able to join two chromosomal ends with no, or minimal base pairing at the junction. However, while its ability to ligate essentially any pair of DNA ends makes NHEJ a very effective mechanism for DSB repair, it also makes it intrinsically mutagenic, because ligation of DNA ends with partially or fully non-complementary overhangs might require some end processing.

As far as Nucleotide Excision Repair (NER) is concerned there are two major repair pathways: Transcription Coupled NER (TCNER) and Global Genomic NER (GGNER). TCNER is utilized for the repair of the transcribed strand (TS) of active genes, while GGNER is implicated in correcting DNA lesions throughout the genome

(Fousteri and Mullenders, 2008; Hanawalt, 2002; Hanawalt and Spivak, 2008). In mammalian systems, it was found that RNA polymerase II transcription machinery (including TFIIH); reviewed by (Egly and Coin, 2011; Le May et al., 2010a) assembles sequentially with NER factors at the promoter (Le May et al., 2010b). This recruitment occurs in absence of exogenous genotoxic attack, is sensitive to transcription inhibitors, and depends on the XPC protein. The presence of these repair genes at the promoters of activated genes is necessary in order to achieve optimal DNA demethylation and histone post-transcriptional modifications (H3K4/H3K9 methylation, H3K9/14 acetylation) and thus efficient RNA synthesis. The data from Le May et al. (2010b) suggest that there is a functional difference between the presence of the NER factors at the promoters and the NER factors at the distal regions of the gene.
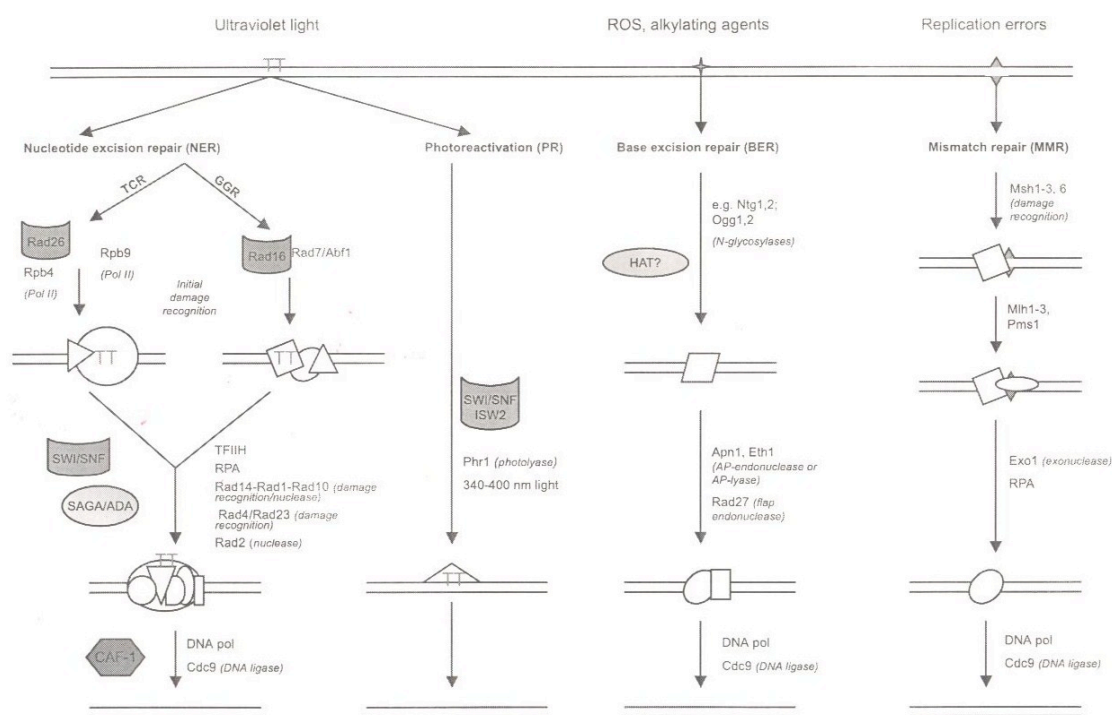
FIGURE 1.7.A: Excision repair pathways in the context of chromatin (Ataian and Krebs, 2006)

Illustrated are the three major excision repair pathways in yeast: Nucleotide Excision Repair (NER), Base Excision Repair (BER) and Mismatch Repair (MMR). In each pathway, depicted are the ATP-dependent remodelers, the histone modifying enzymes and the chromatin assembly factors. In the NER pathway, the ATP-dependent remodeling enzymes provide damage recognition and increased accessibility to the damaged site, as well as recruitment of modifying enzymes. Chromatin assembly is required for chromatin structure restoration.
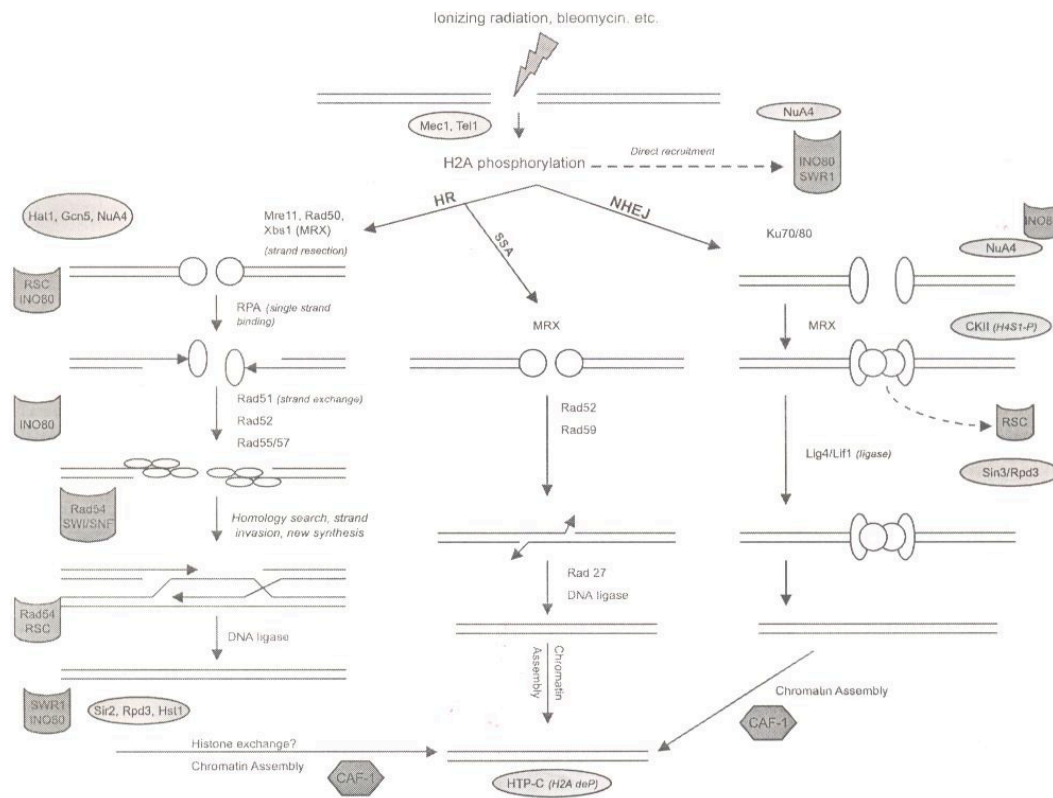
FIGURE 1.7.B: Double strand break repair pathways in the context of chromatin (Ataian and Krebs, 2006)
Illustrated are the major double strand break (DSB) repair pathways in yeast: Homologous Recombination (HR, left), the HR subpathway Single Strand Annealing (SSA, center), and Non Homologous End Joining (NHEJ, right). Key repair factors of each pathway are indicated along with the ATP-dependent remodelers, the histone modifying enzymes and the chromatin assembly factors. Phosphorylation of H2A surrounding a DSB allows binding of several chromatin remodeling and modifying enzymes, as well as recruitment of DNA repair factors.

These data are important and relevant to our work, since Rad9 protein is indirectly involved in NER (Al-Moghrabi et al., 2009), interacts with two transcription factors (Aft1, Mac1) (this sudy and Gkouskou et al., unpublished) and is found on the mostly active genes.

1.4.1.2.--DNA damage repair, Rad9 and transcription

It was shown that Rad9 is required for the repair of the TS and Non TS (NTS) of active genes but not for the repair of transcriptionally inactive sequences (Al-Moghrabi et al., 2009). This seems not to be related to chromatin compaction, since it was shown that *RAD9* is not required for the repair of two different non-transcribed

DNA sequences, one nucleosome free (*URA3*) and one with high compacted nucleosomes (*GAL10*). It was also shown that UV-dependent *de novo* protein synthesis is required for efficient repair of NTS of active genes but not for repair of non-transcribed DNA (Al-Moghrabi et al., 2003). This fact highlights a connection of Rad9 protein and transcriptionally active sequences as we show in our work. Furtheremore, Al-Moghrabi et al. have shown that the inhibition of UV-mediated *de novo* protein synthesis, which is required for efficient NER, does not have any effect on the efficiency of excision repair in the *rad9*Δ cells. This suggests that *RAD9* and *de novo* protein synthesis may act through the same pathway/mechanism. Therefore it is logical to attribute the role of Rad9 in NER to its UV-dependent trans-activator role which leads to the up-regulation of genes involved in this repair process after UV-exposure such as *RAD2, RAD7, RAD16* and *RAD23* which are in fact part of the *RAD9* regulon (Friedberg et al., 1995). Based on the work of Al-Moghrabi et al (2009), it can be pointed out that in the absence of the coupling between transcription and NER, UV-dependent *de novo* protein synthesis become dispensable for NER, despite the fact that the target gene is actively transcribed (Lee et al., 2001, 2002a). This suggests that UV-dependent gene trans-activation is required for NER only when the repair process is coupled to transcription, a process that cells have evolved to allow prompt removal of DNA damage by favoring repair of the TS to the detriment of the complementary NTS.

It has recently been found in embryonic stem cells that a DNA repair complex, namely the trimeric XPC nucleotide excision repair complex, is selectively required for the synergistic activation of the *Nanog* gene by Oct4 and Sox2 (Fong et al., 2011). This study identified a transcriptional coactivator with diversified functions in maintaining ES cell pluripotency and safeguarding genome integrity. Although, Rad9 protein cannot be considered a transcriptional regulator *per se*, the 2 systems are comparable, since Rad9 is involved in the DNA damage repair and interacts with two transcription factors (Mac1 and Aft1) (Gkouskou et al., unpublished and this study).

1.4.2.-- Meiotic cycle and DNA damage

Although our experiments were performed in vegetative cells, it is worth introducing some aspects of DNA damage in meiosis because of similarities that we found between the genome-wide binding pattern of Rad9 and the areas considered as hot spots of meiotic recombination as mapped by others (Blitzblau et al., 2007; Buhler et al., 2007; Gerton et al., 2000).

A critical step in meiosis is the recombination between homologous chromosomes. Crossovers resulting from recombination are essential for the physical links between homologs that mediate their segregation to opposite poles at the first meiotic division. Recombination is initiated by the introduction of DNA double strand breaks catalyzed by Spo11, a meiosis-specific transesterase which is highly conserved through evolution (Bergerat et al., 1997; Keeney, 2001; Keeney et al., 1997). DSBs occur preferentially in clusters of sites called ''hotspots'' in which, in yeast, the probability of DSB formation is 100–1000 times higher than at other sites (Baudat and Nicolas, 1997; Blitzblau et al., 2007; Buhler et al., 2007; Gerton et al., 2000; Pan et al., 2011). Hotspot activity is primarily determined by local features of chromatin structure, notably absence of nucleosomes (Lichten, 2008; Pan et al., 2011). Indeed, certain histone modifications are required to achieve wild-type levels of DSB formation and their patterns correlate to the DSB landscape (Borde et al., 2009; Mieczkowski et al., 2007; Yamashita et al., 2004). However, in addition to chromatin modifications, other factors are required to explain long-range effects, such as the fact that the activation of a hotspot can interfere with that of a neighboring one over distances of many kb (Keeney, 2001; Wu and Lichten, 1995; Xu and Kleckner, 1995). Furthermore, accessory proteins are required to link DSB sites to the chromosome axis in early meiotic recombination (Panizza et al., 2011).

Hot spots and hot ORFs are mapped mainly in regions rich in G+C nucleotides and there is also a gene ontology enrichment for genes implicated in metabolism and catabolism and also for genes encoding aminoacids and sugars (Gerton et al., 2000). The same observations are true for Rad9 binding pattern on the yeast genome, as shown by our results from Tiling Array genome-wide experiments.

Briefly, the steps of recombination during meiosis are described in Figure 1.8.
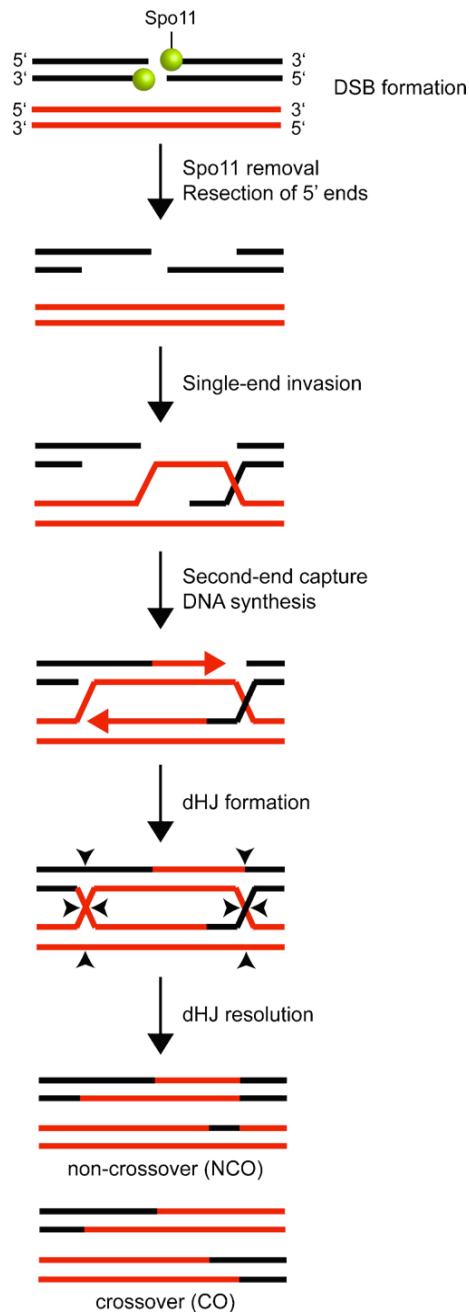
FIGURE 1.8: The double-strand break repair model of meiotic recombination (Longhese et al., 2009).

Homologs are indicated in black (paternal) and red (maternal). Spo11 generates a DSB in one of the parental chromatids. After Spo11 removal, DSB ends are resected to generate 3'-ended ssDNA tails and one 3'-ended ssDNA tail invades the duplex homologous DNA sequence (red lines). Capture of the second ssDNA end and DNA synthesis create a double Holliday junction (dHJ), whose resolution can occur in either plane at both junctions (triangles) to generate crossover or non-crossover products. Red arrows indicate the 3' ends of the newly synthesized strands.

The protein players in meiotic recombination DSB as well as their way of action are

presented in Figure 1.9.
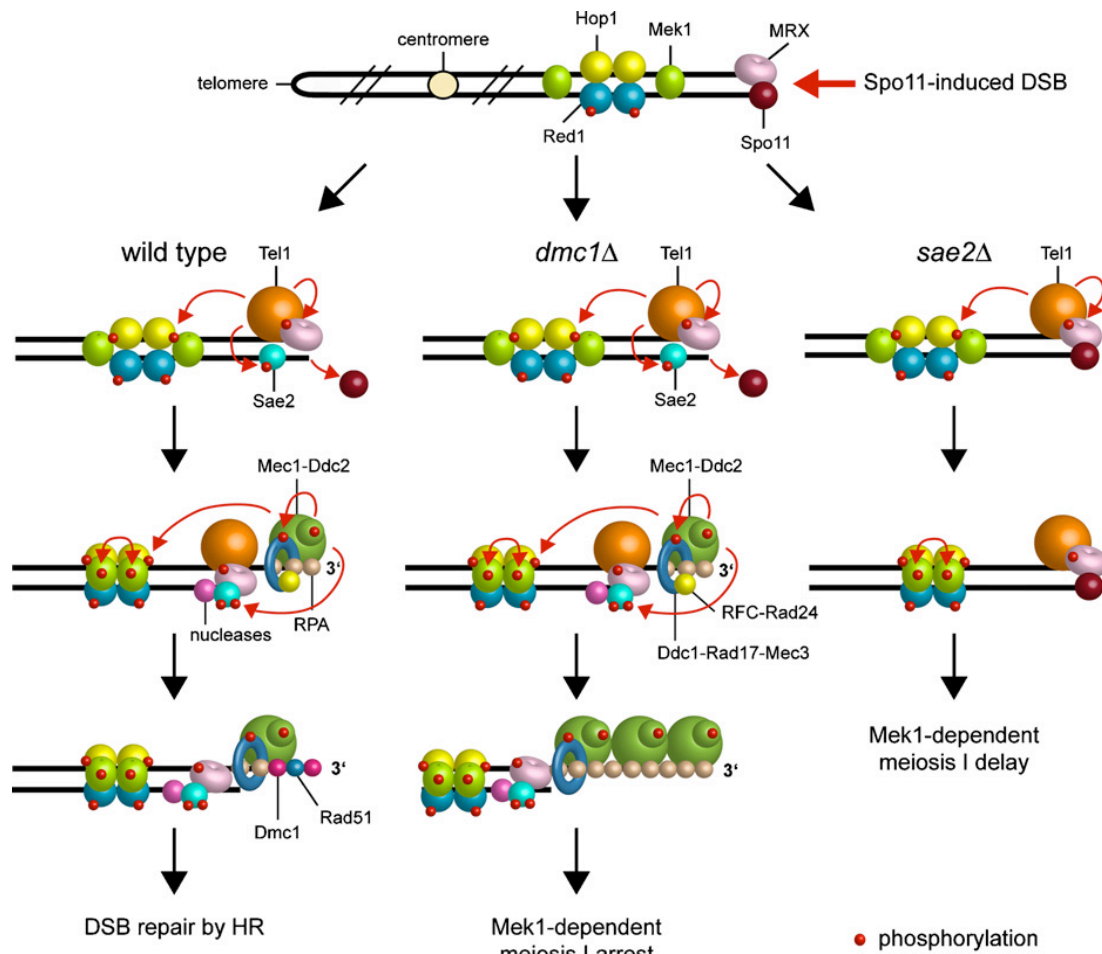
FIGURE 1.9 : The meiotic recombination checkpoint (Longhese et al., 2009)
Spo11, MRX and other proteins catalyze the formation of a DSB on the right arm of a yeast chromosome (top). Only one side of the DSB is shown. Hop1, Mek1 and phospho-Red1 are assembled onto DNA prior to DSB formation. In wild type cells (left panel) MRX allows checkpoint activation by recruiting Tel1, which in turn phosphorylates Sae2 endonuclease and MRX. When Spo11 is removed from the DSB end, DSB resection by MRX, Sae2 and other nucleases generates 3'-ended ssDNA tails coated by RPA, Rad51 and/or Dmc1 (required for repair of double-strand breaks and pairing between homologous chromosomes), which allow the loading of Mec1-Ddc2. Mec1 activation is also supported by independent loading of the Ddc1-Rad17-Mec3 complex by Rad24-RFC. Once loaded onto DNA, Mec1 and Tel1 trigger checkpoint activation by phosphorylating Hop1, which promotes Mek1 in trans autophosphorylation and activation. The absence of Dmc1 (middle panel) leads to accumulation of hyperesected meiotic DSBs, which trigger a Mec1-and Mek1-dependent meiosis I arrest. The absence of Sae2 (right panel) leads to accumulation of unprocessed meiotic DSBs, which trigger a Mek1-dependent slowing down of meiosis I that is primarily dependent of Tel1.

Much less is known about mitotic recombination hotspots (Lee et al., 2009). Most mitotic recombination occurs during interphase. It is believed that some sites are hotter for DSB formation than others. Common fragile sites, regions of the genome prone to chromosomal DSBs, are a normal feature of mammalian chromosomes, and analogous regions have been identified in yeast (Lemoine et al., 2005). Nevertheless, the up to date data about mitotic recombination hotspots do not allow us to make a comparison between them and Rad9 genome-wide localisation pattern.

1.5.--Aft1, Mac1 and Rad9: Actions and Interactions

As mentioned in Chapter 1.3.7, Rad9 was found to interact with Mac1 transcription factor *in vivo* and *in* vitro (Voutsina et al., Gkouskou et al., unpublished) by performing Yeast Two Hybrid Screening and co-IP experiments. Rad9 was also found to negatively regulate Mac1 DNA binding and transactivation function and that it is recruited to promoter and coding regions of genes regulated by Mac1 following the pattern of elongating RNA polymerase II. Moreover, we have established that Rad9 physically interacts and partially affects localisation of Hir1 histone chaperone on *CTR1* promoter and coding region.

Furthmore, Rad9 was found by co-IP experiments to interact with Aft1 transcription factor which is responsible for the iron ion metabolism. Rad9 was also present on promoters and coding regions of genes regulated by Aft1 like *FTR1*.

Subsequent experiments in our lab showed localisation of Aft1 to promoter and coding region of *CTR1* gene (which is regulated by Mac1 transcription factor) under inducing growth conditions (this study). Mac1 was also recruited to promoter and coding region of *FTR1* gene (which is regulated by Aft1 transcription factor) under inducing growth conditions.

The findings mentioned above indicate a possible functional relation between Rad9, Aft1 and Mac1 transcription factors. This led us to examine the relationship between these proteins in more depth. In this study we will focus on the Rad9-Aft1 interaction. We performed both small and large scale Chromatin Immunoprecipitation experiments for all three proteins, especially for Rad9 and Aft1.

1.5.1.--*Saccharomyces cerevisiae* and Fe/Cu Metabolism

Iron and copper are two metals necessary for life because they participate as vital cofactors in proteins that catalyse oxidizing and reducing reactions, thus playing a vital role in processes like respiration and photosynthesis.

Nevertheless, these metals can be toxic for the cell if their levels and distribution are not well regulated, leading for example in the release of toxic free

radicals. Organisms should keep the cytoplasmic metal concentration at levels non toxic for the cells but in the ideal quantity for a normal growth.

For the preservation of this homeostasis, complicated regulating mechanisms have been developed which are evolutionary conserved. In *Saccharomyces cerevisiae* there are metal-regulated transcription factors capable of sensing the changes in metal concentration and of regulating the expression of genes that relate to uptake, distribution and use of metals.

1.5.1.1.--Iron Metabolism

Budding yeast contain a variety of genes whose transcription is induced by Aft1 transcription factor as a result of low iron concentration. These genes encode for proteins related to iron uptake from the cell's surface. Free iron uptake is being done by high and low affinity transporting systems (Dix et al., 1994; Stearman et al., 1996).

The high affinity complex includes ferroxidase Fet3 which needs copper as cofactor to be functional. Thus, Fet3 is considered the protein which connects iron and copper uptake pathways. In this context, the genes implicated in copper transfer to this protein (*ATX1* and *CCC2*) are transcriptionally regulated by iron. For the high affinity iron uptake, it is necessary to have iron reducing action on the cell surface (Dancis et al., 1990; Dancis et al., 1992), a role played mainly by the two flavocytochromes Fre1 and Fre2, which reduce iron, so that it will be introduced to the cell in the reduced form (Fe^{+2} reduced to Fe^{+3}) (Georgatsou and Alexandraki, 1994; Georgatsou et al., 1997). Reduced iron is trapped by Fet3/Ftr1 complex and is oxidized again by Fet3 oxidase and transported through Ftr1 permease to the cell surface (Stearman et al., 1996).

Iron uptake by yeast can be further performed by siderophores, low molecular weight organic molecules that specifically bind iron. Siderophores are not yeast produced but they are introduced by a transporter family (Arn1-Arn4) which recycles between cell surface and endosome (Yun et al., 2000). Siderophores' iron can be reduced by the cell surface reductases (Fre1-Fre4) and in that form it is a substrate for the Fet3/Ftr1 complex (Yun et al., 2000). Fit1-Fit3 mannoproteins facilitate siderophores uptake by recruiting them to the cell wall.

Other genes transcriptionally induced in low iron concentration include *FET5, FTH1, SMF3* and encode for proteins of the vacuolar transporting systems. Further

induced proteins are the mitochondrial transporter Mrs4 as well as Isu1 and Isu2 proteins which are implicated in Fe-S clusters biosynthesis.

The response to iron deprivation in *Saccharomyces cerevisiae* is shown in Figure 1.10.
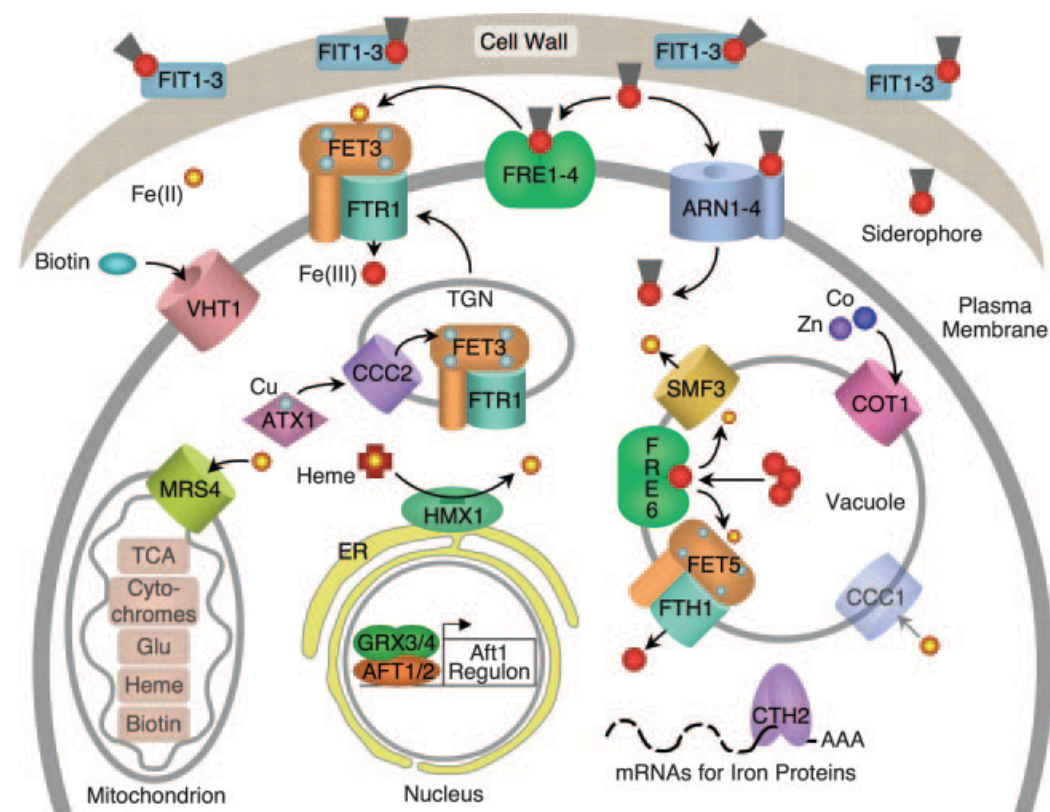
FIGURE 1.10: Iron homeostasis in *Saccharomyces cerevisiae* (Philpott and Protchenko, 2008)
See text for description.

1.5.1.2.‐‐Aft1 Transcription Factor

For the iron homeostasis, *Saccharomyces cerevisiae* has two paralog genes which encode for the iron responsive transcriptional activators Aft1 and Aft2 (Activator of Ferrous Transport). Upon iron deprivation they induce the expression of genes related to iron transport and subcellular distribution and utilization (Rutherford and Bird, 2004). Aft1 is a 98kDa protein rich in histidines in its N-terminal end and in gloutamine residues in the C-terminal end. In Figure 1.11 a map of the protein is illustrated.
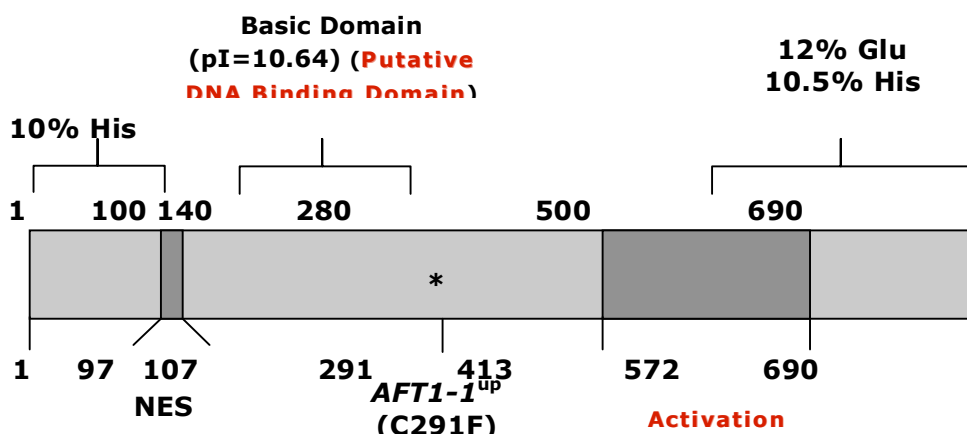
FIGURE 1.11: Aft1 transcription factor structure (Phd George Fragiadakis)
See text for description.

     Aft1 is constitutively expressed, and when intracellular iron is abundant, it is localised to the cytosol and does not activate transcription (Yamaguchi-Iwai et al., 2002). When iron levels are low, Aft1 accumulates in the nucleus, where it regulates the transcription of specific genes. Aft1 appears to sense intracellular iron levels, but it does not seem to bind iron. Aft1 is thought to continuously cycle in and out of the nucleus. Transport of Aft1 into the nucleus is dependent on the karyopherin Pse1 and occurs through the interaction of Pse1 with two nonclassical nuclear localisation sequences within Aft1 (Ueta et al., 2003). The binding of Pse1 to these sequences is not regulated by iron, and the effects of iron on Aft1 localisation do not appear to be exerted through nuclear import. More information on the iron dependent transcriptional regulation in *Saccharomyces cerevisiae* by Aft1 is given in Figure 1.12.
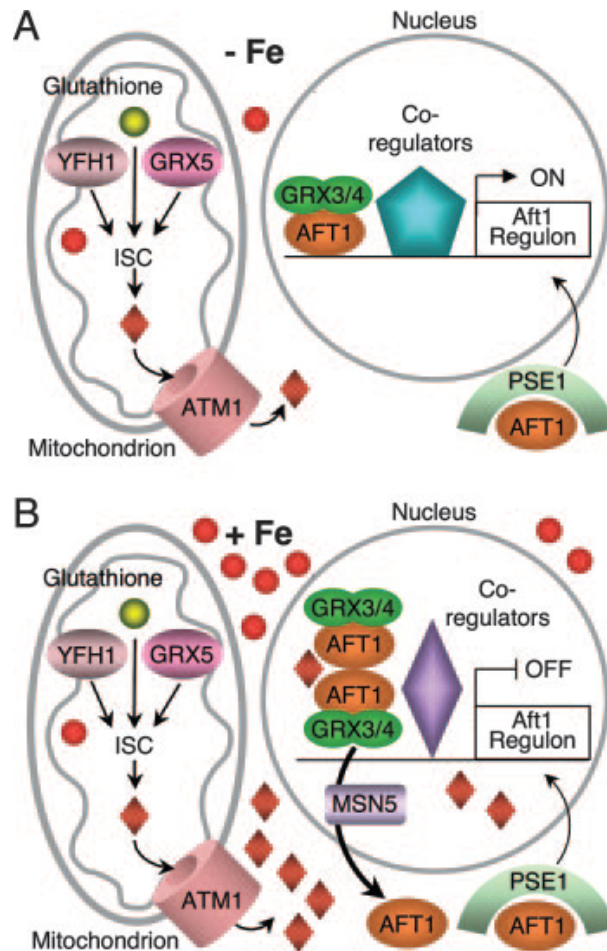
FIGURE 1.12: Iron-dependent transcriptional regulation in *Saccharomyces cerevisiae* (Philpott and Protchenko, 2008).
(A) **Activation of Aft1 under conditions of iron deprivation**. The nuclear importin Pse1 mediates Aft1 translocation into the nucleus. Aft1 forms a complex with Grx3 and Grx4, binds to DNA, and activates transcription. Although complex formation is not regulated by iron, it is not known whether complex formation occurs exclusively in the nucleus or also in the cytosol. "Coregulators" represent the numerous coactivators and corepressors that contribute to the regulation of the Aft1 regulon. These include the mediator complex, Snf1/Snf4, Ssn6, Nhp6, Tup1, Hda1, Cti6, and heme.
(B) **Regulation of Aft1 activity under iron-replete conditions**. Yfh1, Grx5, and glutathione are required for the production of Iron-Sulfur Cluster (ISC) and the formation of an unknown compound that is a substrate for Atm1. This compound is exported from mitochondria and may possibly be targeted to the nucleus. Under iron-replete conditions, Aft1 forms dimers that are recognized by the nuclear exportin Msn5 and lead to the accumulation of Aft1 in the cytosol. In a hypothetical model for the regulation of Aft1, the production of the substrate for Atm1 is proportional to cellular iron levels. This substrate accumulates in the nucleus and leads to the dimerization of Aft1p, perhaps through the formation of a mixed disulfide bridge, and the complex is exported from the nucleus.

Nuclear Aft1 recognizes and binds to consensus sequences (PyPuCACCC) (FeRE, Ferric Response Elements) in the upstream regions of target genes. Such genes are the ones which encode for Fet3 ferroxidase, Ftr1 iron permease, Ccc2 (P-type ATPase responsible for copper transport Fet3), the metal reductases Fre1-Fre4 of the plasma membrane, the siderophore transporters Arn1-Arn4 and the cell wall

mannoproteins Fit1-Fit3 which facilitate iron uptake by the siderophores. Aft1 is also implicated in the induction of other genes which encode for proteins such as the vacuolar iron transporter Fth1 and also other FRE family proteins (Fre5, Fre6) and Cth2 which is implicated in mRNA degradation in iron depletion (Puig et al., 2005). A list of Aft1 targets (iron regulon) is presented on the Table 2. See also Chapter 1.5.1.3 for further Aft1 targets. We have also found that Aft1 binding is facilitated by Nhp6 high mobility group (HMG) protein and Ssn6 co-regulator in specific promoter context (Fragiadakis et al., 2004).

Functional category and open reading frame	Gene name	Location	Function
Uptake of iron at the cell surface			
YDR534C	*FIT1*	Cell wall	Siderophore binding/uptake
YOR382W	*FIT2*	Cell wall	Siderophore binding/uptake
YOR383C	*FIT3*	Cell wall	Siderophore binding/uptake
YLR214W	*FRE1*	Plasma membrane	Metalloreductase
YKL220C	*FRE2*	Plasma membrane	Metalloreductase
YOR381W	*FRE3*	Plasma membrane	Siderophore reductase
YNR060W	*FRE4*	Unknown	Unknown reductase
YOR384W	*FRE5*	Unknown	Unknown reductase
YMR058W	*FET3*	Plasma membrane	Multicopper oxidase, Fe(II) uptake
YER145C	*FTR1*	Plasma membrane	Permease, Fe(II) uptake
YNL259C	*ATX1*	Cytosol	Cu chaperone, delivers Cu to Ccc2p
YDR270W	*CCC2*	Post-Golgi vesicle	Cu transport into vesicles
YHL040C	*ARN1*	Endosome, plasma membrane	Ferrichrome transport
YHL047C	*ARN2/TAF1*	Unknown	TAFC transport[b]
YEL065W	*ARN3/SIT1*	Endosome, plasma membrane	Hydroxamate siderophore transport
YOL158C	*ARN4/ENB1*	Plasma membrane	Enterobactin transport
Efflux of iron from vacuole to cytosol			
YLL051C	*FRE6*	Vacuole	Metalloreductase
YLR034C	*SMF3*[a]	Vacuole	Fe(II) transport
YFL041W	*FET5*	Vacuole	Multicopper oxidase, Fe(II) transport
YBR207W	*FTH1*	Vacuole	Permease, Fe(II) transport
Other transporters			
YGR065C	*VHT1*	Plasma membrane	Biotin transporter
YOR316C	*COT1*	Vacuole	Zn and Co storage/detoxification
YKR052C	*MRS4*[a]	Mitochondria	Mitochondrial iron import
Metabolic adaptation to low iron			
YLR205C	*HMX1*	Endoplasmic reticulum	Heme oxygenase
YLR136C	*CTH2/TIS11*	Cytosol	mRNA degradation

[a] Predominantly regulated by Aft2p. All others are predominantly regulated by Aft1p.
[b] TAFC, triacetylfusarinine C.

TABLE 2: Iron regulon (Philpott and Protchenko, 2008)

Aft1 paralog, Aft2, is 39% identical to Aft1, encodes for a 47kDa protein, recognizes similar consensus sequences, and can activate transcription of a partially overlapping set of target genes (Blaiseau et al., 2001; Courel et al., 2005; Rutherford et al., 2001; Rutherford et al., 2003). However, the role of Aft2 in the response to iron depletion is much less clear, as the transcriptional effects of Aft2 are not evident unless strains are deleted for Aft1. Similar to Aft1, Aft2 is activated under iron depletion and directs the transcription of many Aft1 target genes as well as two genes,

SMF3 and *MRS4*, which are not targets of Aft1. Aft2 appears to recognize a slightly different target sequence from that recognized by Aft1. While Aft1 exhibits its strongest activation when the target has the consesus TGCACCC, Aft2 can recognize the sequences GGCACCC (present in *MRS4*) and CGCACCC (present in *SMF3*) (Courel et al., 2005; Rutherford et al., 2003). The role of these genes in vacuolar and mitochondrial iron transport, respectively, have led some investigators to suggest that Aft2 preferentially influences intracellular iron utilization (Courel et al., 2005). It has also been shown that absence of either of the paralogs Aft1 or Aft2 leads to transcriptional induction of the other which is iron-dependent (Courel et al., 2005). This shows that there exists a partial overlap of their function. *aft1Δaft2Δ* double mutants are more sensitive in growth upon iron depletion (Rutherford et al., 2001) as well as in oxidative environment (Blaiseau et al., 2001). DNA expression microarray experiments have been performed to distinguish the genes regulated by the one or the other factor (Rutherford et al., 2003).

1.5.1.3.--Aft1 Beyond Iron Regulation

Aft1 turns out to be a special case of transcription factor, as it was shown to have potential roles beyond iron metabolism. More specifically, Aft1 was found to genetically and physically interact with Cbf1 inner kinetochore protein, to co-localise to chromatin with Ndc10 inner kinetochore protein and also that in *aft1Δ* mutants chromosome maintenance is defective (Measday et al., 2005).

Furthermore, in a recent study it is demonstrated that Aft1 associates with the kinetochore complex through Iml3 protein member of Ctf19 complex (Hamza and Baetz, 2011). The latter group showed that Aft1 is required for the increased association of cohesin with pericentric chromatin, which is required to resist microtubule tension, and also that *aft1Δ* cells display chromosome segregation defects in meiosis.

In our study, we further examine this Aft1 function in centromeres along with Rad9, in order to examine protein interactions with a role in chromosome segragation. It is worth mentioning here that it was shown that DNA damage induces epigenetic changes at the centromere, including the γ-H2AX modification, that appear to alter

kinetochore function, thus triggering the spindle assembly checkpoint (Dotiwala et al., 2010).

Shakoury-Elizeh et al. (2004) studied the transcriptional response to iron deprivation and identified new Aft1 target genes. They showed that when yeast is subjected to iron deprivation, it undergoes a transcriptional remodeling, resulting in a shift from iron-dependent to parallel, but iron-independent, metabolic pathways. It was found that other metabolic pathways are also regulated by iron: biotin uptake and biosynthesis, nitrogen assimilation, and purine biosynthesis. Furthermore, multiple genes involved in nitrogen assimilation and amino acid metabolism were induced by iron deprivation, whereas glutamate synthase, a key enzyme in nitrogen assimilation, was repressed.

In addition, (Berthelet et al., 2010), have performed genome-wide synthetic lethal and synthetic dosage lethal screens and have identified >70 deletion mutants that are sensitive to perturbations in *AFT1* levels. Their genetic network revealed that Aft1 affects a diverse range of cellular processes, including the *RIM101* pH pathway, cell wall stability, DNA damage, protein transport, chromosome stability and mitochondrial function. They demonstrated that Aft1 works in parallel with the *RIM101* pH pathway and the role of Aft1 in DNA damage repair is mediated by iron. Furthermore, through both genetic studies and microarray transcriptional profiling, they showed that the role of Aft1 in chromosome maintenance and benomyl resistance is independent of its iron regulatory role, and it is done potentially through a non transcriptional mechanism.

In the present study we take into account these new findings and we study if Aft1 regulates directly these new targets and whether Rad9 also has a role. We also examine a possible implication of Rad9 and Aft1 to transcription elongation.

1.5.2. -- Copper Metabolism and Mac1

As far as copper metabolism is concerned, there are factors that are induced as a response to copper ion deprivation or repletion and regulate the expression of genes encoding for proteins implicated in copper uptake and/or protection from its toxicity when it is in excess, respectively. Copper uptake is performed by the high affinity

system of copper transport and it requires reduction of Cu^{+2} to Cu^{+1}. The reduction is being done by the Fre1 and Fre2 flavocytochromes (also used in the iron regulation system), followed by the transport of reduced copper by the Ctr1 and Ctr3 transporters across the plasma membrane inside the cell. Ctr1 is transcriptionally induced under copper depletion and is degraded under copper repletion. Ctr1 and Ctr3 are functionally overlapping.

Once copper is inserted into the cell, it is bound by small cytoplasmic proteins which transmit copper to particular molecules or subcellular compartments. The copper transport system is visualized in Figure 1.13.
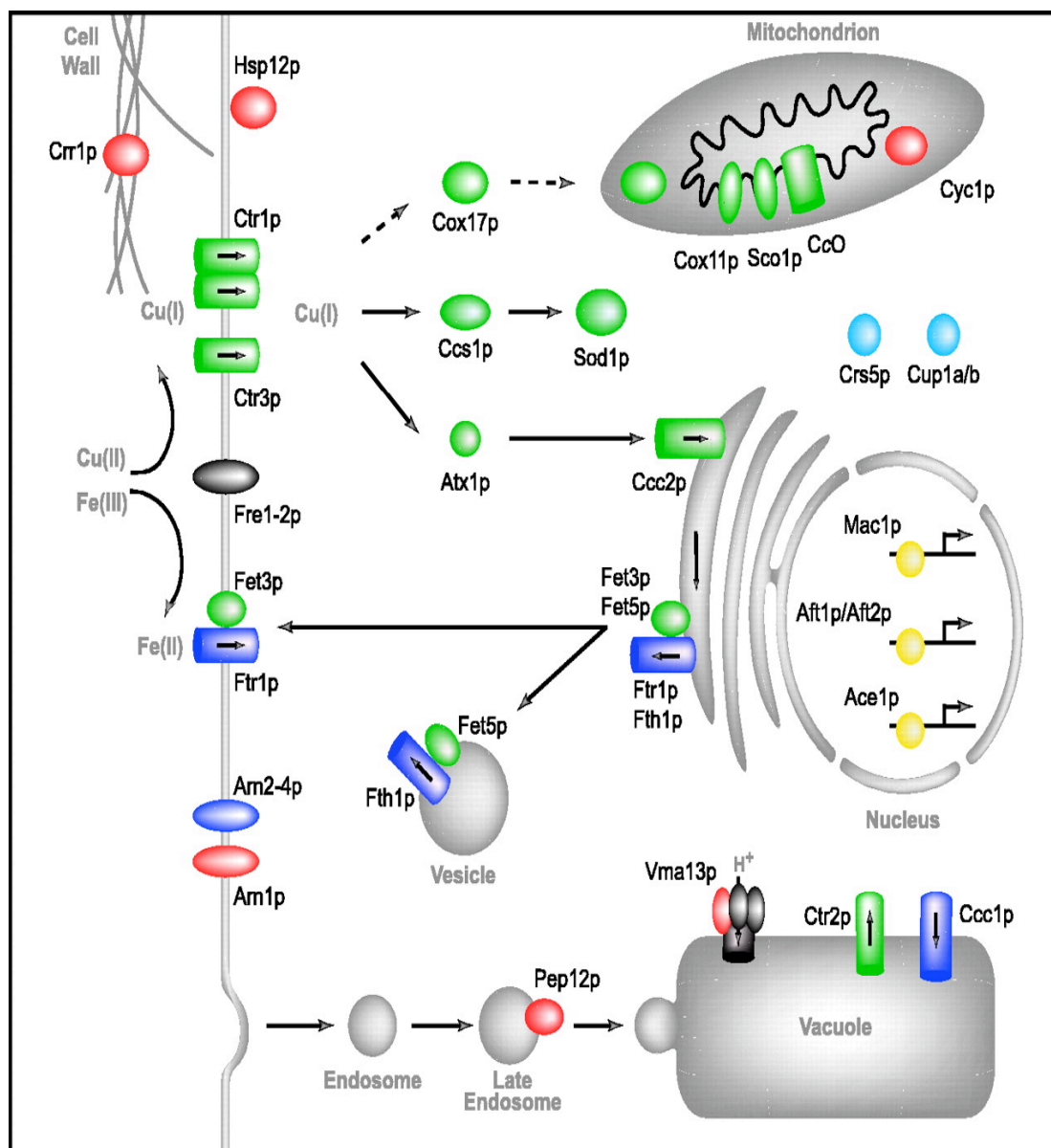
FIGURE 1.13: Copper and iron transport pathways in *Saccharomyces cerevisiae* (van Bakel et al., 2005)

After copper induction by Fre1 and Fre2, Cu^{+1} is inserted through Ctr1 and Ctr3 in the cell. Once inside, copper is bound by small molecules which escort the ions to particular subcellular compartments. Atx1 produces copper to the secretive pathway interacting firstly with Ccc2 ATPase of trans-Golgi network, followed by copper integration to Fet3 oxidase with the help of Gef1 which acts as ion channel providing Cl ions, thus making feasible the copper ion transport to trans-Golgi network where the pH is acidic. Ccs protein produces copper to Cu/Zn Super Oxide Dismutase (SOD1) using its N-terminal metal binding domain. Cox17 contributes to copper ion transport to mitochondria and especially to cytochrome oxidase. It moves between cytoplasm and intramemberane space of mitochondrion, while Sco1 assists probably the copper transport from Cox17 to the cytochrome oxidase through a copper binding motif that it possesses. The main defensive mechanism against copper repletion toxicity inside the cell is performed by Cup1 and Crs5 metallotheionins that binds free cytoplasmic copper. Another detoxification mechanism is provided by copper storage in the vacuole in order to be used in a future occasion of copper depletion (probably with the assistance of Ctr2 protein). Proteins whose expression is regulated by Mac1 are depicted in green, whereas the ones regulated by Aft1 are depicted in blue.

The regulation of copper metabolism at the transcriptional level is performed mainly by two transcription factors: Mac1 which is activated when copper is depleted and induces the transcription of genes related to copper uptake and Ace1 (Cup2) which is activated under copper replete conditions and induces the transcription of genes related to copper storage or removal.

Based on the Rad9-Mac1 interaction that we established in our group (Gkouskou et al., unpublished) as well as the Rad9 binding onto promoter and coding region of *CTR1* gene (regulated by Mac1) (Gkouskou et al., unpublished), it is useful to provide some more information about this transcription factor.

In contrast to Aft1, Mac1 is located in the nucleus at all times, regardless the copper ion concentration in the cell.

When copper is scarce, Mac1 induces the expression of genes encoding for proteins related to copper uptake such as Ctr1 and Ctr3 plasma membrane Cu^{+1} transporters. Mac1 also regulates (along with Aft1) the expression of the Fre1 Fe^{3+}/Cu^{2+} plasma membrane reductase as well as the Fre7 reductase (Georgatsou et al., 1997; Martins et al., 1998). Moreover, the post-translational Ctr1 degradation when copper is replete, requires Mac1 transcription factor (Yonkovich et al., 2002). DNA microarray experiments have been performed in *mac1Δ* strains to identify the genes whose transcription is altered (De Freitas et al., 2004), as well as experiments for the identification of genes regulated by copper levels (Gross et al., 2000).

Mac1 regulates the response to copper depletion by binding on particular *cis* elements of its targets (CuREs, copper responsive *cis*-acting elements) (Jamison McDaniels et al., 1999; Joshi et al., 1999; Labbe et al., 1997; Serpe et al., 1999;

Yamaguchi-Iwai et al., 1997). Expression microarray experiments have also been performed for the identification of copper regulon (Gross et al., 2000). Mac1 acts as a homodimer (Heredia et al., 2001; Joshi et al., 1999; Serpe et al., 1999) but it is also active as a monomer (Voutsina et al., 2001). Itself, Mac1 is regulated through phosphorylation (for optimum CuRE binding), whereas in copper repletion it becomes inactivated due to a change of its configuration in which its activation and binding domains interact with each other and both lose their functionality (closed configuration) (Figure 1.14). Upon copper repletion, Mac1 is degraded (Zhu et al., 1998).
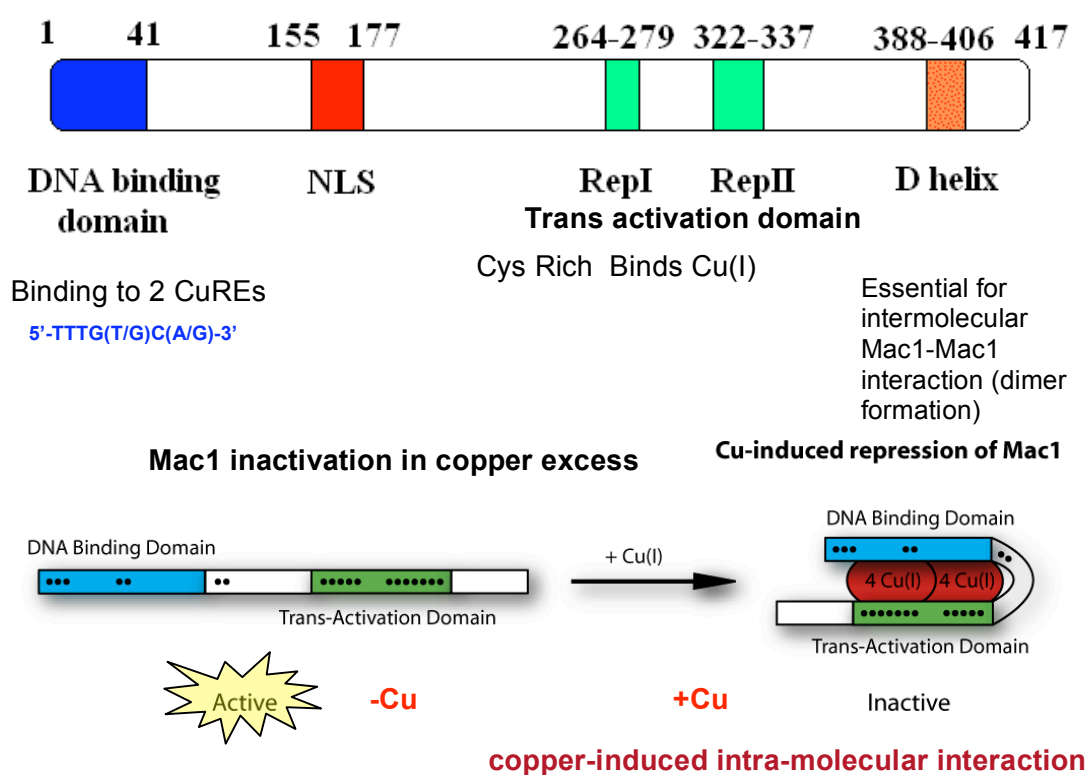
FIGURE 1.14: Mac1 transcription factor domains and regulation
Mac1 is a multidomain protein icluding a N-terminal DNA binding domain and a C-terminal trans activation domain consisting of Cys rich domains RepI and RepII. It also has a Nuclear Localisation Signal (NLS) sequence. Mac1 acts as a dimer. It is active in copper scarcity and is inactived via copper-induced intra-molecular interaction between DNA-binding domain and primarily the REPI trans-activation domain when copper is replete (Jensen and Winge 1998). Mac1 binds to two CuRE elements 5'-TTTG(T/G)C(A/G)-3' and binding to both elements is necessary for activation. Its action is facilitated by copper-independent Mac1 homodimerization (Joshi et al., 1999).

In our group we have found, as previously mentioned, that Rad9 protein interacts through its BRCT domains with Mac1 and may interferes with its functionality (Gkouskou et al., unpublished).

Finally, Ace1 transcription factor is activated under copper repletion conditions and activates the expression of genes related to storage or removal of copper such as *CUP1* and *CRS5* metallotheionins and *SOD1* superoxide dismutase (also Figure 1.13).

1.6. -- TRANSCRIPTION

Taking into account the relation we have found between Rad9 and transcription as described in Chapter 1.3.7, wefurther examined the details of this relation. For that reason, we performed small scale Chromatin Immunoprecipitation experiments as well as large scale analysis of the global transcription pattern of yeast genome in the absence of Rad9 in inducing growth conditions. Furthermore, we examined whether Rad9 has a role in transcription elongation and if there is a synthetic *aft1Δaft2Δ* phenotype.

By performing large scale analysis, we aimed to examine the localisation pattern of Rad9 in multiple growth conditions. We showed that Rad9 exhibits an Aft1-dependent localization bias to highly active genes. Rad9 was mostly localised to coding regions of genes which lead us to further examine the possible implication of Rad9 in transcription elongation (and in transcription in general).

Based on the above, and taking also into account the role of Rad9 in TCNER (See Chapter 1.4.1.2) it is worth making a brief introduction to transcription, focusing on aspects related to our work.

1.6.1. -- Basics of the Transcription Mechanism

During the RNA polymerase II (RNAPII) transcription cycle there are distinct stages during its progression:

i) Pre-initiation, where RNAPII is recognizing the core promoter sequence (usually the canonical TATA box sequence) of the gene to be transcribed. A series of events begin leading eventually to the formation of the pre-initiation complex (pre-IC). TATA-binding protein (TBP) which is part of the Transcription Factor II D (TFIID) recognizes and binds to TATA box.

After TFIID binding, more transcription factors as well as RNAPII combine around the TATA box to form the pre-IC. DNA helicase, as part of pre-IC, is involved in the separating of opposing strands of dsDNA to provide access to a single stranded DNA template.

ii) Initiation, in which RNAPII is bound on the promoter of the gene to be transcribed after the recruitment of the transcription machinery and it subsequently leaves the promoter in a process termed promoter clearance. Promoter clearance coincides with phosphorylation of Ser5 on the C-terminal domain of RNAPII, which is phosphorylated by TFIIH [reviewed by (Buratowski, 2009; Margaritis and Holstege, 2008)]. The general transcription factors are released and this may serve to reveal interaction surfaces on RNAPII which can be utilised by other components during transcription elongation (Luse, 2012).

iii) Elongation, during which the non coding strand of the gene is used as a template for RNA synthesis in a 5'→3' direction following base complementarity. Transcript elongation occurs in the context of chromatin and involves temporary displacement and/or modification of nucleosomes. RNAPII has to negotiate its way past nucleosomes by utilizing a number of distinct mechanisms which require histone chaperones, chromatin remodeling factors and histone modifying enzymes. RNAPII often has to overcome other obstacles such as DNA damage (see below) reviewed by (Selth et al., 2010). The final outcome is the formation of an mRNA molecule which is the exact copy of the coding strand. Multiple RNAPII molecules can function on a single DNA template, leading to multiple rounds of transcription and equal number of mRNA molecules produced rapidly from a single gene copy.

iv) Termination, in which RNAPII is released from the transcription machinery complex.

1.6.2. -- Transcription Fidelity

Transcription fidelity during elongation is ensured basically by two mechanisms. The first involves an important structure of RNAPII called the trigger

loop, a mobile element of Rpb1 subunit, which appears to play a key role in RNAPII fidelity (Brueckner and Cramer, 2008; Kaplan et al., 2008). The trigger loop, located beneath the active site is involved in multiple interactions with the incoming nucleotide (Wang et al., 2006) which ensures the correct alignment required for nucleophilic attack and phosphodiester bond formation.

Rpb9 subunit of RNAPII is also involved in ensuring transcription fidelity (Nesser et al., 2006) by delaying closure of the trigger loop on the incoming nucleotide (Walmacq et al., 2009).

Removal of a mispaired nucleotide is greatly enhanced by factors that stimulate transcript cleavage, such as TFIIS *in vitro* (Jeon and Agarwal, 1996; Thomas et al., 1998) although it is not clear if the same is true *in vivo* as well.

1.6.3.-- Transcript Elongation Through Chromatin

Because of the nucleosomes are a strong barrier for the RNAPII passage, it is necessary to be modified in order for the transcription to occur efficiently (Izban and Luse, 1991; Orphanides et al., 1998).

There exist at least three described mechanisms by which elongating RNAPII functions in order to produce the transcript of the gene [reviewed by (Selth et al., 2010)] (Figure 1.15). One mechanism is nucleosome disassembly in front of elongating RNAPII, not only in the promoter but also within the coding region (Kristjuhan and Svejstrup, 2004; Schwabish and Struhl, 2004) (Figure 1.15.A). Genome-wide analyses of nucleosome occupancy in yeast revealed an inverse relationship between the rate of transcription and the histone density in the coding regions on genes, further suggesting that nucleosomes are disassembled during transcription (Bernstein et al., 2004; Lee et al., 2004).

Nucleosome structure is tripartite natured (H2A/H2B, H3/H4, DNA). H2A/H2B histone dimers are localised on the exterior of the nucleosome with less protein-DNA contacts, thus they are rapidly exchanged during transcription elongation (Jamai et al., 2007; Kimura and Cook, 2001; Thiriet and Hayes, 2005). By contrast, H3/H4 histones are less mobile and their turnover is much more dependent on transcription (Jamai et al., 2007).

Nevertheless, it is possible that nucleosome removal does not always occur as RNAPII traverses the gene (Figure 1.15.B). *In vivo* data suggest that transcript elongation can be performed by two mechanisms: one based on the loss of nucleosomes (as described above) and another histone acetylation-dependent mechanism in which there is little or no net loss of nucleosomes (Kristjuhan and Svejstrup, 2004). Thus, there exists a mechanism by which RNAPII can pass through chromatin with the help of histone modifications rather than nucleosome disassembly *per se*.

1.6.4.-- Remodeling of Chromatin During Transcription Elongation

Distinct groups of factors have been evolved by cells in order to achieve the proper chromatin remodeling required for efficient transcription elongation.

Firstly, there are the ATP-dependent chromatin remodelers, complexes that use energy obtained by ATP to modify the structure of chromatin. The main four families are SWI-SNF, ISWI, CHD and INO80/SWR reviewed by (Clapier and Cairns, 2009). These remodelers can modify promoter chromatin architecture but also play an important role during transcription elongation.

Secondly, there are the histone chaperones which bind histones and are involved in their dynamics, as well as their storage and their replication-associated assembly reviewed by (Park and Luger, 2006). They are implicated in both disassembly and reassembly of chromatin, activities which are both required for transcription associated histone exchange (Figures 1.15.A; 1.15.C). They also co-operate with ATP-depemdent chromatin remodelers. Of the most studied histone chaperones are FACT members (Facilitates Chromatin Transcription) which destabilize nucleosome structure so that one core histone dimer (H2A/H2B) is removed during RNAPII passage (Figure 1.15.B) (Belotserkovskaya et al., 2003) and Spt6, a H3/H4 chaperone that is important for the maintenance of chromatin structure, as in its absence, histones are depleted from the coding regions of several yeast genes (Bortvin and Winston, 1996; Kaplan et al., 2003). It is worth mentioning that Rad9 was found by our group to interact with Hir1 corepressor of histone gene transcription (Voutsina et al., unpublished).

Thirdly, there are covalent histone modifications, namely acetylation, methylation and ubiquitylation.

Hyperacetylation during active transcription is mostly observed in the promoter region of the transcribing gene and to a lesser extend in coding region (Pokholok et al., 2005; Workman and Kingston, 1998). However histone acetyltransferases (HATs) and histone deacetylases (HDACs) are enriched in the coding regions of genes (Close et al., 2006; Gilbert et al., 2004a; Govind et al., 2007; Keogh et al., 2005; Wang et al., 2002). Histone acetylation in coding regions is dynamic and specifically coupled to transcribing polymerase (Svejstrup, 2003). Furthermore, RNAPII-coupled histone acetylation is being removed immediately in the wake of the elongation complex (Figure 1.15.C). Elongator HAT and Gcn5 (SAGA member) are of the most studied candidates which couple RNAPII movement to histone acetylation.

Methylation of histones is being done on lysine residues on one, two or three methyl groups. Histone methylation does not have a significant structural role but it rather acts as a tag for effector proteins containing methyl-binding domains, such as chromodomains, PHD finger domains and Tudor domains (Daniel et al., 2005). It is worth to mention again that Rad9 also contais a Tudor domain. The elongating form of RNAPII is phosphorylated at serine 2 of the CTD, which is specifically recognized by the histone methyltransferase Set2 which methylates histone H3 in lysine 36 (H3K36me is rich in coding regions) (Krogan et al., 2003; Li et al., 2002; Schaft et al., 2003; Xiao et al., 2003). The major role of H3K36me is probably to regulate the acetylation-deacetylation cycle connected to the transcript elongation (Figure 1.15.C).

Monoubiquitylation of H2B (uH2B) at K123 appears to be a general consequence of transcriptional activation and is found at both promoter and coding regions of genes (Henry et al., 2003; Kao et al., 2004; Xiao et al., 2005). The positive effect of uH2B on elongation is related to histone methylation and to structural changes of the nucleosome that might facilitate the disassembly in front of elongating RNAPII, and the reassembly in its wake.
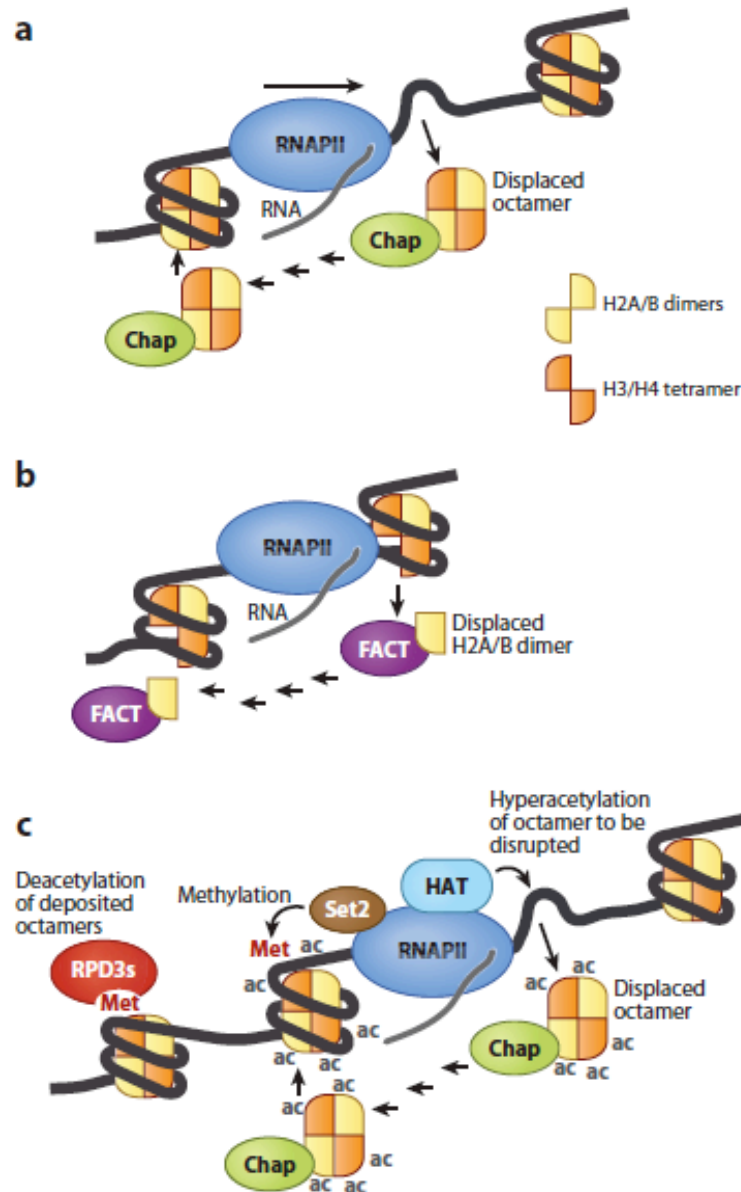
FIGURE 15: Transcript elongation through nucleosomes (Selth et al., 2010)
A) Transcription through a nucleosome can result in the release of histone proteins from DNA and their association with histone chaperones (Chaps).
B) Progression of RNAPII through a nucleosome may also occur without complete displacement of the histone proteins from DNA (see text for details).
C) Co-transcriptional histone modification (see text for details).

1.6.5.-- Transcription and DNA Damage

Taking into account the implication of Rad9 in transcription as described in Chapter 1.3.7, the role of Rad9 in TCNER (Chapters 1.4.1.1 & 1.4.1.2) and the fact

that we found Rad9 to be bound to the most actively transcribed genes (See Results Chapter 3.3.5.4) it is worth while examining a little further the interplay between transcription and DNA repair.

Apart from TCNER which we already described, another transcription-associated response to DNA damage is the polyubiquitylation of RNAPII (Svejstrup, 2007), which ultimately results in proteasome-dependent polymerase degradation (Bregman et al., 1996; Ratner et al., 1998). Like TCNER this process is triggered by RNAPII transcriptional arrest rather than DNA damage *per se* (Anindya et al., 2007; Somesh et al., 2005). Polyubiquitylation of RNAPII and its subsequent degradation is used as a last resort by the cell when RNAPII is persistently paused. The available data support the idea that TCNER and RNAPII ubiquitylation and degradation represent interconnected, but distinct, alternative cellular pathways for contending with DNA damage in active genes (Figure 16) (Anindya et al., 2007; Kvint et al., 2008; Somesh et al., 2005; Somesh et al., 2007; Svejstrup, 2007; Woudstra et al., 2002).
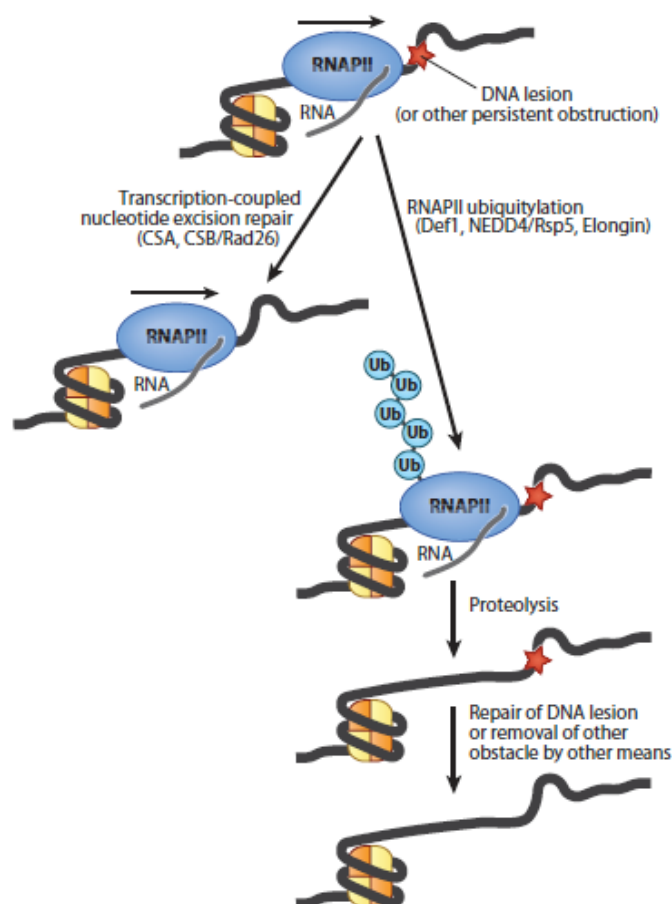
FIGURE 16: Alternative pathways for contending with transcript-obstructing DNA lesions (Selth et al., 2010)

Bulky DNA lesions, such as those generated by UV light, are an absolute block to the progression of RNA polymerase II (RNAPII). Factors such as CSA and CSB enable such lesions to be preferentially repaired by transcription-coupled nucleotide excision repair, TCNER (pathway on the left). This allows the polymerase to resume transcription. However, if such repair is not possible (or if the persistent block to transcription is caused by something else), the gene is unblocked by RNAPII ubiquitylation and proteolysis (pathway on the right). This presumably allows lesions and obstacles to be dealt with by other repair pathways [such as general (global) genome repair-GGNER] or by the next polymerase reaching the lesion being able to trigger TCNER.

Furthermore, it has been shown that there exists a proportional relation between the transcriptional activity of a gene and the mutation rate of a gene (Kim et al., 2007) and recent results show an increased accumulation of apurinic and apyrimidinic sites in highly transcribed DNA (Kim and Jinks-Robertson, 2009). This fact suggests a link between transcription and the fidelity of DNA replication. Highly transcribed genes are generally an impediment for replication forks (Azvolinsky et al., 2009). Situations like these have as a consequence the collision between the DNA replication and transcription machineries (Prado and Aguilera, 2005) which lead to transcription-associated recombination (dependent on replication) (Gottipati et al., 2008; Prado and Aguilera, 2005; Wellinger et al., 2006).

CHAPTER 3

RESULTS

3.3.1.-- Rad9 interaction with Aft1 is necessary for Rad9 localisation to specific genes

3.3.1.1.-- Rad9 interacts with Aft1 transcription factor

As I commented in the Introduction (Chapters 1.3.7 & 1.5), we have previously found in our group by performing Yeast Two Hybrid Screening and co-Immunoprecipitation Assays that Rad9 interacts *in vivo* and *in vitro* with Mac1 transcription factor (Voutsina and Gkouskou, unpublished). A new way for Rad9 recruitment on chromatin under unchallenged conditions in an RNA polymerase II transcription context, including Hir1 chaperone was described.

Another new interaction for Rad9 was found in the name of another metal-regulated transcription factor, namely Aft1, which, is the TF that regulates iron homeostasis (Introduction, Chapter 1.5). This is a novel Rad9-interacting protein and it establishes another possible connection between Rad9 and transcription regulation, as we previously showed in our lab for the Rad9-Mac1 case study (Gkouskou et al., unpublished). Rad9 could have potential role in transcription, since our group showed Rad9 localisation to promoter and coding regions of *CTR1* Mac1-regulated gene (on promoter and coding regions following RNAPII binding pattern) (Gkouskou et al., unpublished). Aft1 could also be a potential means driving Rad9 recruitment to genes and possibly other genomic regions.

Rad9 interaction with Aft1 was confirmed by performing co-Immunoprecipitation experiments using three alternative types of experiments (Figure 3.1):
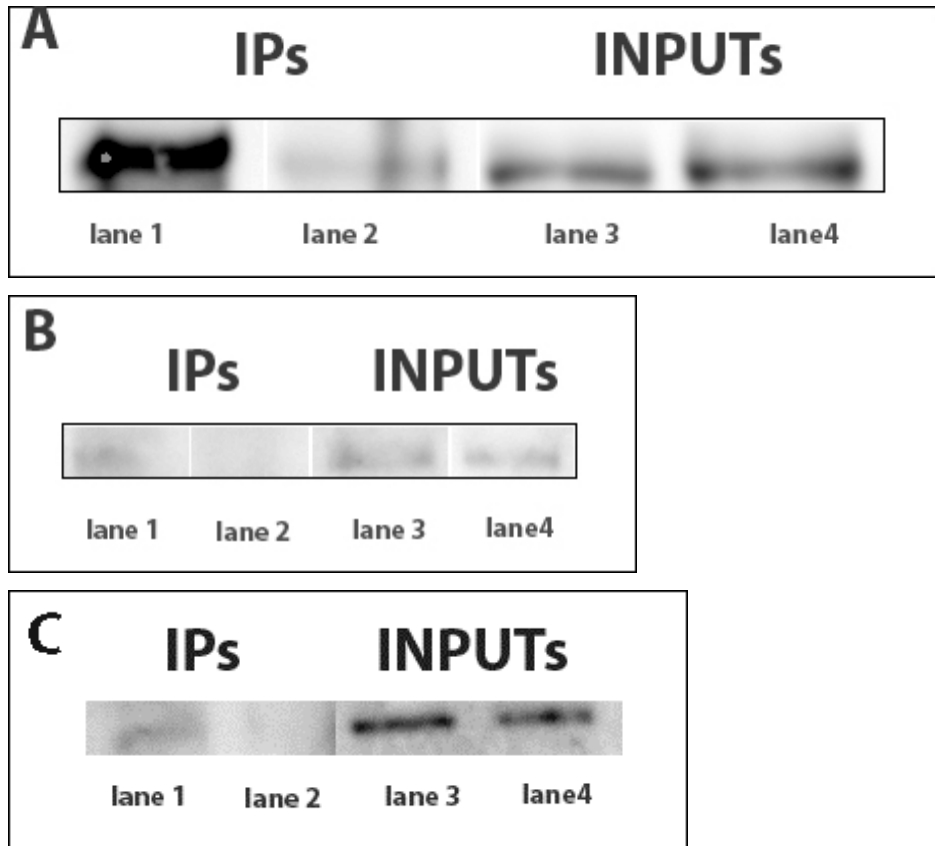
FIGURE 3.1: Rad9 interacts with Aft1 (Western blot)

A) In *rad9Δ* background, Aft1 was tagged with 9Myc epitopes. Rad9 tagged with flag epitope was inserted in the high copy plasmid pDB20 and this construct was inserted to *rad9Δ* strain in order to get *rad9Δ* Aft1-9Myc pDB20 Rad9-flag strain. As control we used the *rad9Δ* Aft1-9Myc pDB20 flag. We used Rad9 as a bait (flag) and we probed with Aft1 (Myc). The experiment was repeated twice. **Lanes 1,3**: *rad9Δ* Aft1-9Myc pDB20 Rad9-flag. **Lanes 2,4**: *rad9Δ* Aft1-9Myc pDB20 flag. The co-IP experiment was repeated twice.

B) In *rad9Δ* background, Aft1 was tagged with 3HA epitopes. Rad9 tagged with 9Myc epitopes was inserted in the high copy plasmid pYX142 and this construct was inserted to the first strain in order to get *rad9Δ* Aft1-3HA pYX142 Rad9-9Myc strain. As control we used the *rad9Δ* Aft1-3HA pYX142 9Myc. We used Rad9 as bait (Myc) and we probed with Aft1 (HA). **Lanes 1,3**: *rad9Δ* Aft1-3HA pYX142 Rad9-9Myc. **Lanes 2,4**: *rad9Δ* Aft1-3HA pYX142 9Myc.

C) Aft1 and Rad9 proteins were tagged in order to get Aft1-3HA Rad9-9Myc strain (both proteins tagged endogenously) in which we used Rad9 as bait (Myc) and then probed with Aft1 (HA). As control we used the strain Aft1-3HA. **Lanes 1,3**: Aft1-3HA Rad9-9Myc. **Lanes 2,4**: Aft1-3HA

For all three experiments, after the co-IP, we also confirmed by western blot analysis and using different antibodies that the bait protein was bound to the beads (not shown). The IP:INPUT ratio was approximately 15:1.

3.3.1.2.—Rad9 is recruited to genes regulated by Aft1 transcription factor

As previously mentioned, Rad9 was found by our group to be present to promoter and coding regions of *CTR1* Mac1-regulated gene (Gkouskou et al., unpublished). After confirming Rad9-Aft1 interaction, we wondered whether Rad9

was present, maybe as a complex with Aft1, on genes regulated by Aft1. That would be important because Rad9 would be further connected to the transcription complexes, since it interacts with both Aft1 and Mac1. That would establish a direct or indirect connection of Rad9 to transcribed genes. We have analyzed Rad9 binding pattern on *FTR1* (Aft1-regulated), *FRE1* (Aft1- and Mac1-regulated) and *FRE7* (Mac1-regulated) genes in SC medium under inducing conditions (genes were activated by adding the metal chelators BCS and BPS, see Materials and Methods). All experiments from now on are performed under these growth conditions unless otherwise specified. It is important to mention that BCS and BPS chelators do not cause DNA damage conditions to the cells as examined by Western blot analyses (Gkouskou K.). In Figure 3.2 the revealed binding pattern is visualized.
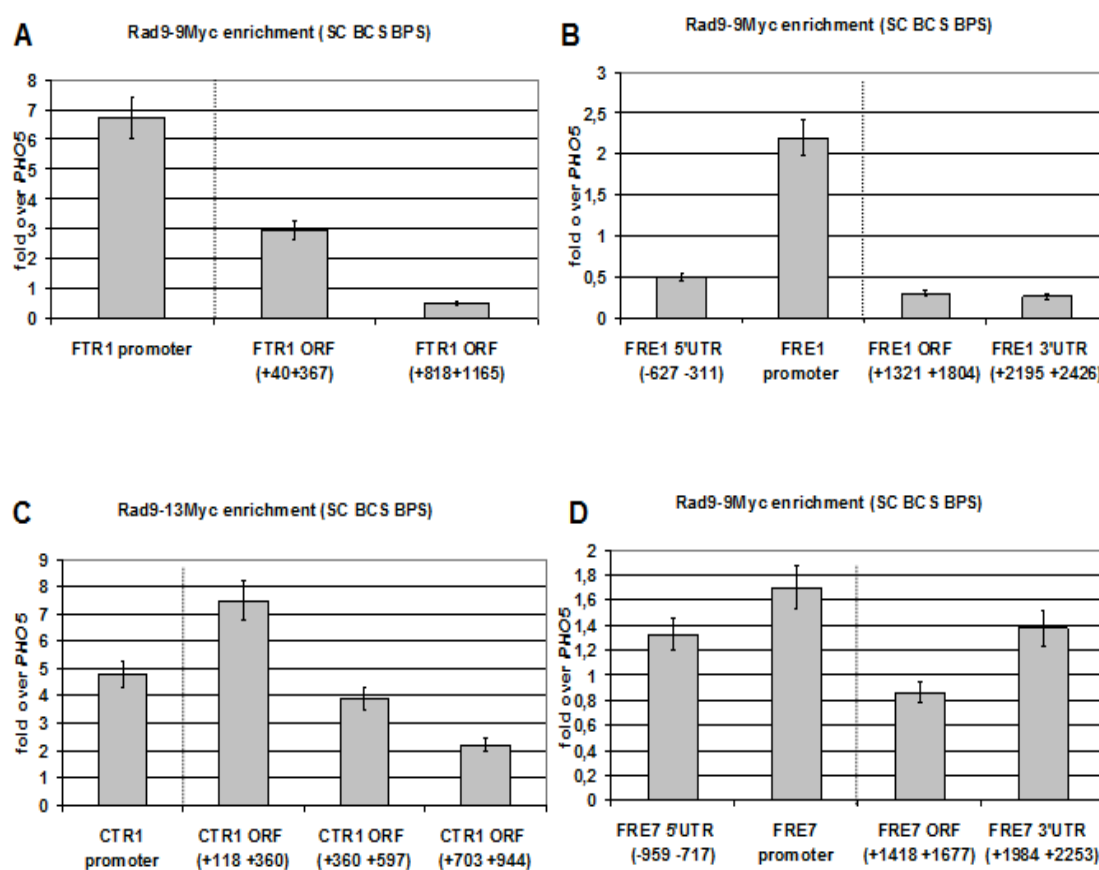
FIGURE 3.2: Binding pattern of Rad9 to Aft1 and/or Mac1 regulated genes
By ChIP analysis we studied the enrichment of Rad9 in each amplicon (x axis) on the genes A) *FTR1* (Aft1-regulated), B) *FRE1* (Aft1- and Mac1-regulated), C) *CTR1* (Mac1-regulated) D) *FRE7* (Mac1-regulated) is visualized after performing ChIP assay. Normalization was performed firstly over INPUT and secondly by measuring the binding of Rad9 on *PHO5* coding region, where Rad9 binding is minimal in any growth conditions (as tested by our group) and dividing to Rad9 enrichment in each case.

From the above manual chromatin immunoprecipitation analysis we showed that Rad9, apart from *CTR1,* was also present on both promoter and coding regions of *FTR1* gene and to a lesser extend on the promoters of *FRE1* and *FRE7*. The binding pattern was not similar between the genes tested since Rad9 was mainly present on the promoter of *FTR1* and *FRE1*, while it was mainly at the beginning of the *CTR1* ORF and Rad9 was localised rather evenly and not strongly to *FRE7* promoter and coding region. Nevertheless, Rad9 seems to be a part of Aft1 complex, since it is localised to promoter and coding region of the Aft1-regulated *FTR1* gene (and the promoter of *FRE1* Aft1/Mac1-regulated gene), along with Aft1 transcription factor (Results Chapter 3.3.3.1 and Figure 3.5).

3.3.1.3.—Rad9 recruitment to *CTR1* and *FTR1* is Aft1-dependent

After establishing that Rad9 interacts with Aft1 (as well as Mac1) and that it is localised to both promoter and coding regions of genes regulated by each transcription factor, we wondered whether this recruitment was dependent on Aft1. To address this question, we constructed a strain where Rad9 was tagged with 9Myc and *AFT1* or both *AFT1* and *AFT2* were deleted (*aft1*Δ Rad9-9Myc and *aft1*Δ*aft2*Δ Rad9-9Myc). We used these strains to perform manual Chromatin Immunoprecipitation experiments, to examine Rad9 localisation on promoter and coding regions of *CTR1* and *FTR1* genes. We examine the particular genes because the former has a consensus for Aft1 binding and Rad9 was found to be present on promoter of Aft1-regulated *FTR1* (Fragiadakis G). Furthermore, Aft1 is recruited to the promoter and coding region of the Mac1 regulated *CTR1* gene (see Chapter 3.3.2.1 and Figure 3.5). What we observed was that the binding of Rad9 in wild type strains was decreased by at least 2-4 fold when *AFT1* was deleted and slightly less when both *AFT1* and *AFT2* were deleted (Figure 3.3).
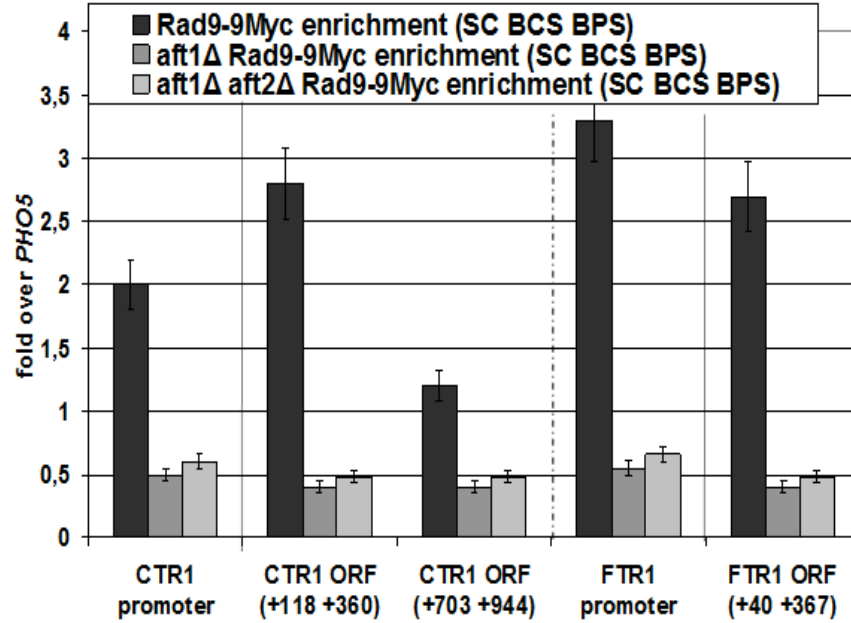
FIGURE 3.3: Binding pattern of Rad9 when *AFT1* or both *AFT1/AFT2* are absent
The enrichment of Rad9 on *CTR1* and *FTR1* promoter and coding regions as obtained by ChIP analyses in Rad9-9Myc, *aft1Δ* Rad9-9Myc and *aft1Δaft2Δ* Rad9-9Myc is visualized. The strains were grown under induced conditions (the genes tested were active) in synthetic complete medium. The normalization was done over the INPUT chromatin (x100). The conclusion was the same when the normalization was done over the background binding of a wild type strain. Similar results were obtained when the strains were grown in rich medium (YPD) in the absence of metal chelators (not shown).

We have also observed a considerable reduction on *CTR1* RNA accumulation when *AFT1* or both *AFT1* and *AFT2* were deleted in a *rad9Δ* background (*rad9Δaft1Δ* or *rad9Δaft1Δaft2Δ*) (Figure 3.4). Furthermore, Rad9 seemed to have a negative effect on *FTR1* expression, since in *rad9Δ* strains, *FTR1* transcript was increased two-fold (Figure 3.4) [(additional results show that this upregulation may be much lower; ~20% as compared to WT strain (Fragiadakis G.)]. These data show that Aft1 directly or indirectly affects the expression of *CTR1*, while Rad9 also has a mild effect (see also Results Chapter 3.3.3.1) and moreover that Rad9 could directly affect *FTR1* expression (Figure 3.4).
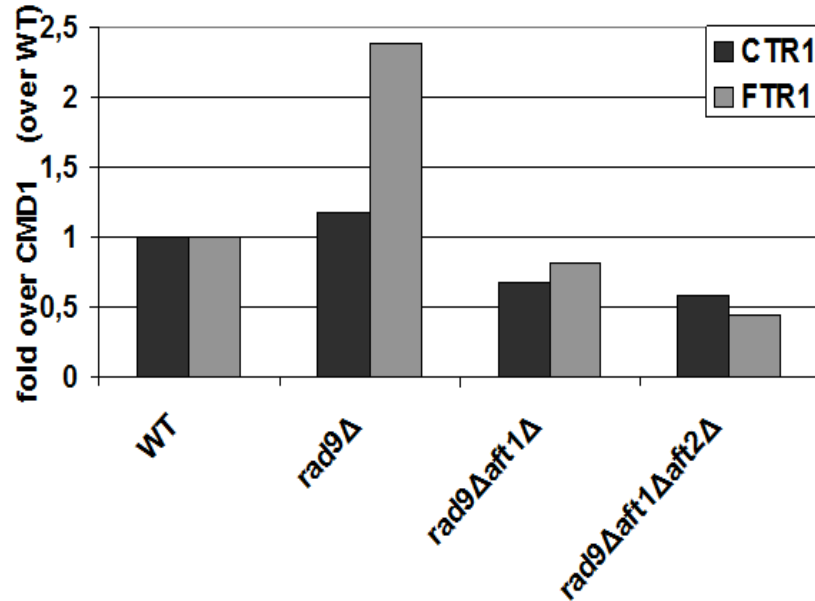
FIGURE 3.4: Rad9 negatively affects *CTR1* and *FTR1* expression, whilst Aft1 has a positive effect

RNA was isolated from strains (x axis) grown under induction conditions (*CTR1* was active) and Reverse Transcription assay (RT) was performed aiming to check changes in the levels of *CTR1* and *FTR1* transcripts. Normalization was done over change of CMD1 expression (which is not altered in the particular growth conditions), after a first normalization over the wild type (wt) strain (FT5). The experiment was performed twice and the average values are presented on the plot.

Having established that Rad9 localisation to promoter and coding regions of *CTR1* and *FTR1* genes is dependent on Aft1, we sought to investigate if the opposite situation of the Rad9-dependence of Aft1 localisation (Results Chapter 3.3.3.2) was also true.

3.3.2.1.-- Aft1 is recruited to the promoter and coding region of the Mac1 regulated *CTR1* gene

After confirming the Rad9-Aft1 interaction and Aft1-dependent recruitment of Rad9 to specific genes we investigated whether Aft1 recruitment was also dependent on Rad9.

We performed ChIP analysis to investigate if Aft1 transcription factor was recruited on promoter and coding regions of Mac1-regulated *CTR1* gene under induction conditions (when *CTR1* was active). In the regulatory regions of *CTR1,* there is one consensus sequence recognized by Aft1 (MacIsaac et al., 2006) although not of the canonical type. Surprisingly, we found that Aft1 transcription factor was

indeed recruited on both promoter and coding region of *CTR1* gene (Figure 3.5). This information is important because *CTR1* is a target known to be strongly regulated by Mac1 (it is member of the Mac1 regulon). Furthermore, it establishes a possible direct role for Aft1 in *CTR1* expression since in *aft1Δ* or *aft1Δaft2Δ* strains *CTR1* transcription drops considerably (Figure 3.4). Moreover, this information is important because it makes up an example of a locus where both Rad9 and Aft1 are recruited probably as part of a larger protein complex.
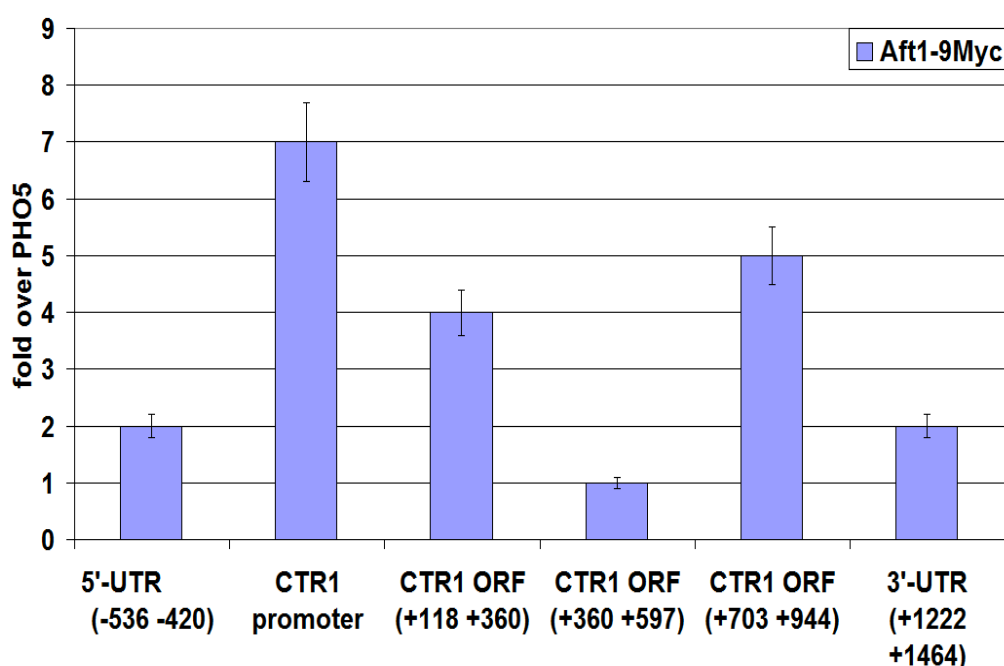
FIGURE 3.5: Binding pattern of Aft1 on *CTR1* gene
Chromatin Immunoprecipitation assay was perfomed in cells grown under induction conditions (SC BCS BPS, *CTR1* gene was active) and the enrichment of Aft1 on *CTR1* gene was examined by real time PCR. Normalisation was performed firstly over INPUT and secondly by measuring the binding of Rad9 on *PHO5* coding region, where Rad9 binding is minimal in any growth conditions (as tested by our group) and dividing to Rad9 enrichment in each case. Similar binding pattern was obtained after normalizing over *ACT1* or *TRP3* coding regions (not shown).

3.3.2.2.-- Aft1 recruitment on tested genes is independent of Rad9 presence

To examine whether Aft1 recruitment on *CTR1* and *FTR1* genes was dependent on Rad9 in the way that Rad9 recruitment on the same genes was dependent on Aft1 (Figure 3.3), we performed manual ChIP assay. We observed that the Aft1 recruitment on these genes was not dependent on Rad9 (Figure 3.6).
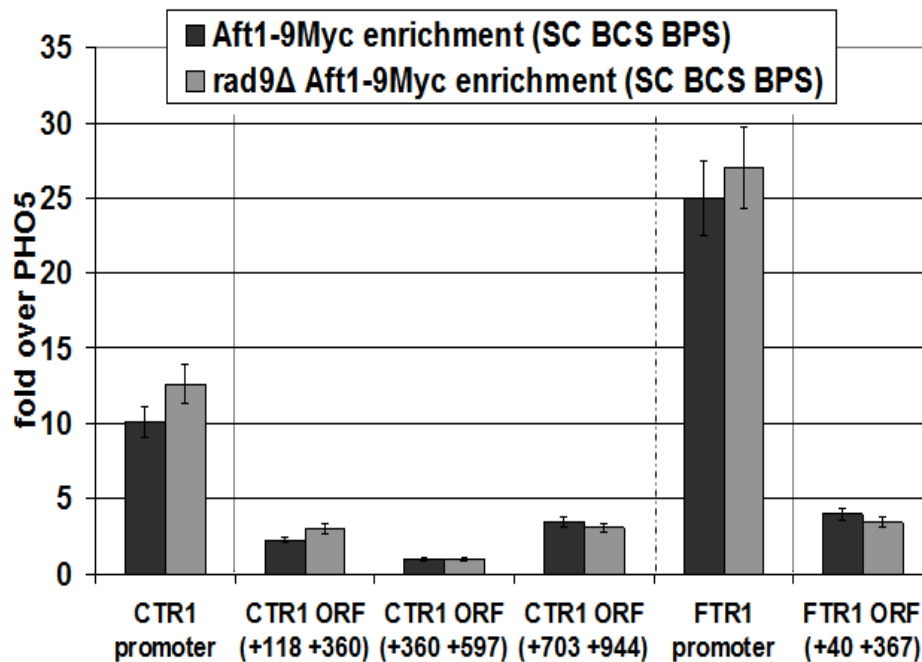
FIGURE 3.6: Aft1 is recruited on *CTR1* and *FTR1* genes independently of Rad9
Chromatin Immunoprecipitation assay was perfomed in cells grown under induction conditions (SC BCS BPS, *CTR1* and *FTR1* genes were active) and we examined the enrichment of Aft1 on *CTR1* and *FTR1* genes by real time PCR. Normalization was performed firstly over INPUT and secondly by measuring the binding of Rad9 on *PHO5* coding region, where Rad9 binding is minimal in any growth conditions (as tested by our group) and dividing to Rad9 enrichment in each case. The same binding pattern was also obtained after normalizing over *FRE2* coding region.

3.3.3.-- Rad9 affects the transcription of a small percentage of yeast genes

3.3.3.1.-- Establishing a connection of Rad9 (and Aft1) to transcription elongation

The finding that Rad9 is localised to both promoter and coding regions of specific genes (*CTR1* and *FTR1*), can be indicative of an implication in the transcription machinery of these genes, also since it was previously shown in our lab that Rad9 follows the RNAPII binding pattern to *CTR1* gene (Gkouskou et al., unpublished). Rad9 interaction with both Mac1 and Aft1 transcription factors was another reason why we speculated that it may be a part of a larger complex participating in the transcription of these genes.

Rad9 localisation to coding regions of genes lead us to test whether the protein has an effect on the transcription elongation in *Saccharomyces cerevisiae*. We performed 6-azauracil (6-AU) growth assay in *rad9Δ* strains as well as in *aft1Δ*, *aft2Δ*

and double or triple mutants. Azauracil is an inhibitor of enzymes that are involved in purine and pyrimidine biosynthesis, which leads to alterations in nucleotide pool levels *in vivo*. Subsequently, the depletion of nucleotide levels (GTP and UTP) by 6-azauracil can diminish transcription elongation rate and processivity (Mason and Struhl, 2005). In that way, 6-AU assay is considered a crude assay to test whether a protein has an effect in transcription elongation. The phenotype is smaller sized and fewer colonies, compared to the wild type strain, when tested in a serial dilutions growth assay. We have performed this assay in three different temperatures (30^0C, 25^0C, 16^0C) and analyzed the results (Figures 3.7A, 3.7B and 3.7C respectively). The different mutants had similar cell sizes (see Figure 3.31).
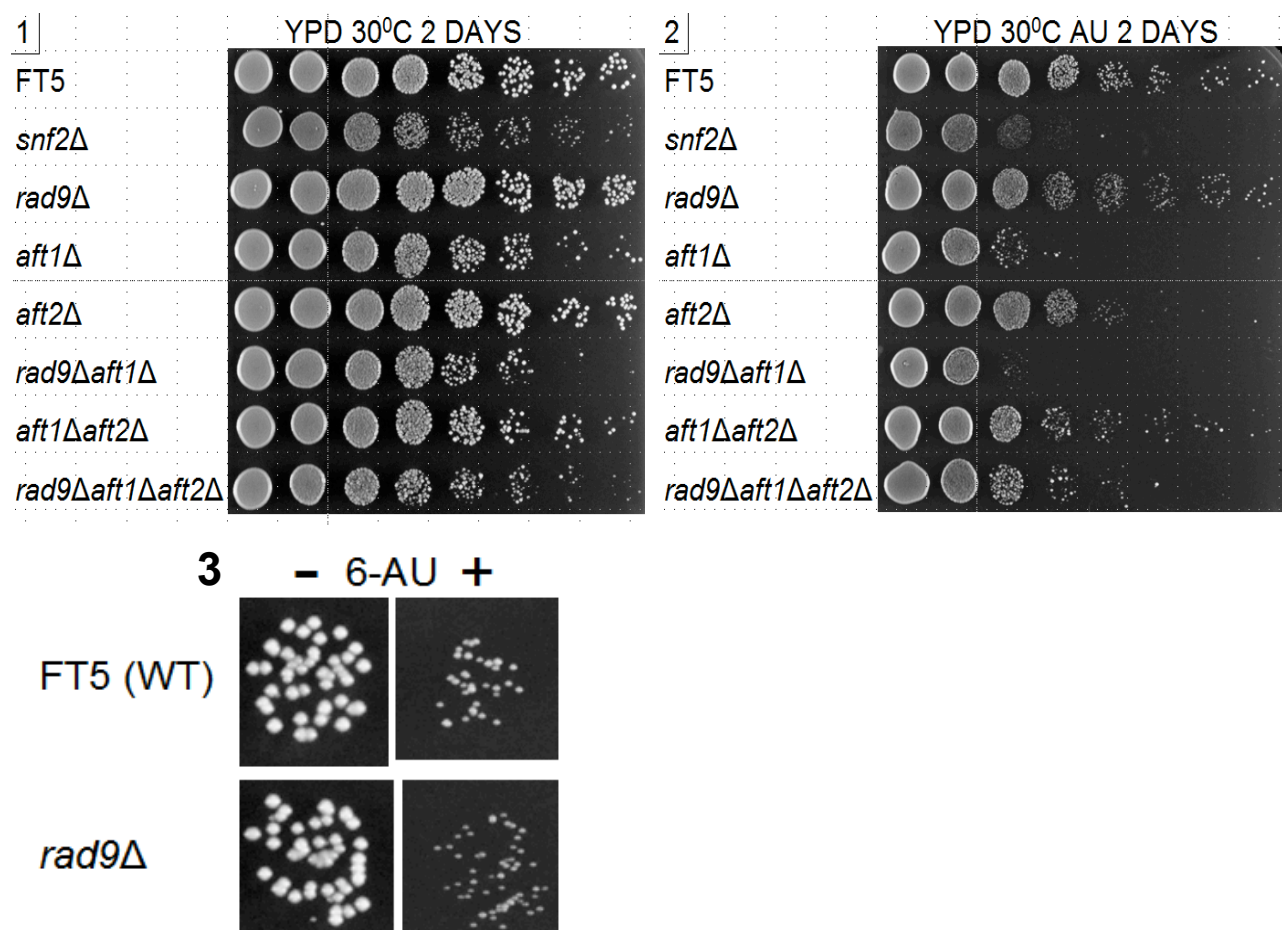
FIGURE 3.7A: 6-Azauracil growth assay in 30^0C
Cultures of the mutants noted above were grown in rich medium (YPD) until exponential phase (OD$_{550}$~0.5). All cultures were adjusted to the same optical density and 6-AU was added to a final concentration of 300μg/ml and incubation continued for 30 minutes. Untreated cells were also kept as control cultures (3.7A.1). After that, eight serial dilutions were spotted on YPD plates which also had (3.7A.2) or not (3.7A.1) 300μg/ml 6-AU. Plates were incubated for 2 days. s*nf2*Δ is used as a positive control for the slow growth phenotype in 6-AU. In panel 3, a the *rad9*Δ phenotype is shown magnified.

Based on Figure 3.7A, we can conclude the following:

i) *rad9Δ* strain has smaller sized colonies compared to the wt in 6-AU which means that in the particular growth conditions (the same as the ones where all of our experiments were performed) Rad9 does seem to affect transcription elongation. The phenotype is better visualized in Fig. 3.7A.3. The possibility for Rad9 to directly affect transcription is not very high since, as we observed from large scale expression microarray experiments, it affects the transcription of only a small percentage of the yeast's genes (1-2%) (See Results Chapter 3.3.3). Nevertheless, it is possible that Rad9 affects indirectly the transcription of genes related to growth and by that way, the present phenotype can be explained.

ii) *aft1Δ* strain has a severe slow growth phenotype (much stronger than Rad9's phenotype) in 6-AU which indicates that it can affect the transcription profile in yeast (although we cannot decipher if it does that directly or indirectly). It is probable that Aft1 achieves that through some of its other roles (see also Introduction Chapter 1.5.1.3), for example by influencing chromosome stability or chromatin structure (Berthelet et al., 2010). Another observation is that *aft1Δ* strain has mixed population of small and large colonies in both plain YPD and 6-AU.

iii) *aft2Δ* strain has a slow growth phenotype in 6-AU, though not as severe as aft1Δ.

iv) *rad9Δaft1Δ* strain has a synthetic slow growth phenotype compared to the single mutants both in plain YPD and in 6-AU where the colonies are also smaller sized compared to *aft1Δ* strain. That is a further indication of the two proteins acting together in some common pathway(s).

v) In plain YPD, *aft1Δaft2Δ* strain resembles more or less the growth of the single mutants. Double mutant in 6-AU seems to restore the slow growth phenotype of the single *aft1Δ* mutant. This may mean that a transcriptional defect is improved when both factors are absent.

vi) Triple mutant *rad9Δaft1Δaft2Δ* has a mild slow growth phenotype in plain YPD versus the wild type which is clear in 6-AU. In both cases the colonies are of mixed sizes. Also, triple mutant is slightly more slow growing in plain YPD compared to double *aft1Δaft2Δ* but it is clearly more slow growing in 6-AU. Rad9 seems to cause a defect in transcription, also apparent when it is combined with Aft1 action (*rad9Δaft1Δ*), whereas Aft2 seems to oppose this defect to a certain degree (*rad9Δaft1Δ* versus *rad9Δaft1Δaft2Δ* phenotype).
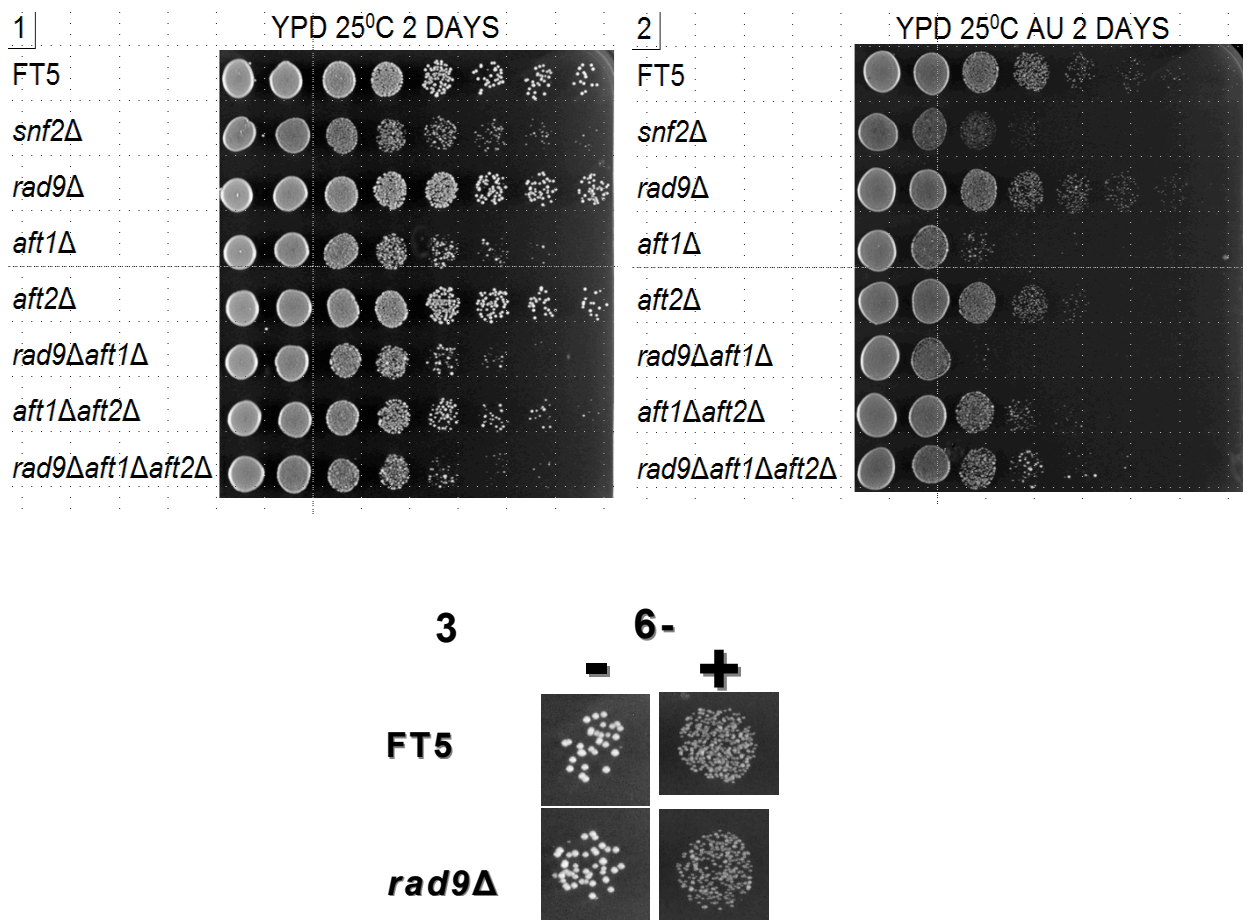
FIGURE 3.7B: 6-Azauracil growth assay in 25^0C

Cultures of the mutants noted above were grown in rich medium (YPD) until exponential phase ($OD_{550} \sim 0.5$). All cultures were adjusted to the same optical density and 6-AU was added to a final concentration of 300μg/ml and incubation continued for 30 minutes. Untreated cells were also kept as control cultures (3.7B.1). After that, eight serial dilutions were spotted on YPD plates which also had (3.7B.2) or not (3.7B.1) 300μg/ml 6-AU. Plates were incubated for 2 days. s*nf2Δ* is used as a positive control for the slow growth phenotype in 6-AU. Also presented is a magnification of the *rad9Δ* no phenotype (3).

Based on Figure 3.7B, we can conclude the following:

i) *rad9Δ* strain doesn't have a growth phenotype compared to the wt in 6-AU, opposite to what we observed in 30^0C. Thus, Rad9's effect in transcription elongation seems to be specific to 30^0C.

ii) *aft1Δ* has a severe slow growth phenotype in 6-AU (see also 3.7A, ii).

iii) *aft2Δ* has a slow growth phenotype in 6-AU, though not as severe as aft1Δ.

iv) *rad9Δaft1Δ* resembles *aft1Δ* in YPD and has a mild synthetic phenotype in 6-AU.

v) *aft1Δaft2Δ* has mildly better growth than single *aft1Δ* in YPD which is more apparent in 6-AU. Thus, Aft2 seems to be implicated in transcription elongation.

Double mutant in 6-AU does not seem to restore the slow growth phenotype of the single *aft1Δ* mutant, at least not to the same extend as in 30^0C.

vi) Triple mutant *rad9Δaft1Δaft2Δ* has a mild slow growth phenotype in plain YPD versus the wild type and also in 6-AU. The colonies are mixed sized in both cases. Also, triple mutant is more slow growing in plain YPD compared to double *aft1Δaft2Δ* but the growth is unchanged in 6-AU.

Thus, it seems that Rad9 does not have the same effect in transcription elongation which was apparent in 30^0C.
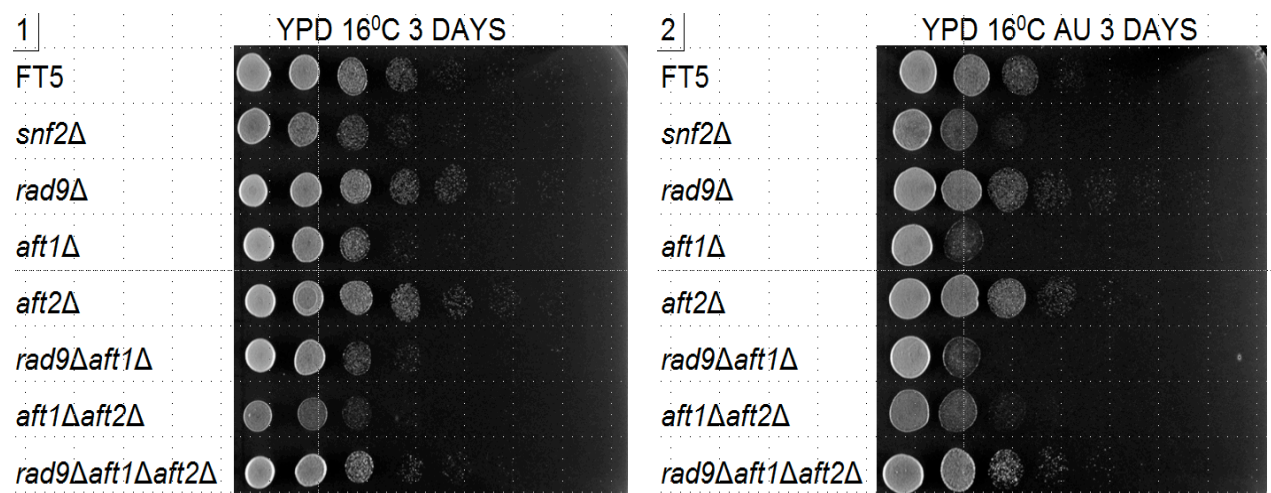
FIGURE 3.7C: 6-Azauracil growth assay in 16^0C
Cultures of the mutants noted above were grown in rich medium (YPD) until exponential phase (OD$_{550}$~0.5). All cultures were adjusted to the same optical density and 6-AU was added to a final concentration of 300μg/ml and incubation continued for 30 minutes. Untreated cells were also kept as control cultures (3.7C.1). After that, eight serial dilutions were spotted on YPD plates which also had (3.7C.2) or not (3.7C.1) 300μg/ml 6-AU. Plates were incubated for 3 days. s*nf2Δ* is used as a positive control for the slow growth phenotype in 6-AU.

Based on Figure 3.7C, we can conclude the following:

i) *rad9Δ* strain has actually a better growth phenotype than the wt in 6-AU growth conditions. It seems that Rad9 has not the same effect in transcription elongation compared to growth in 30^0C. Thus, Rad9 seems to be implicated in transcription elongation in 16^0C in a way opposite to the one in 30^0C.

ii) *aft1Δ* strain has a slow growth phenotype in 6-AU (see also 3.7A, ii).

iii) *aft2Δ* does not have a slow growth phenotype in 6-AU in 16^0C.

iv) *rad9Δaft1Δ* double mutant resembles *aft1Δ* in 6-AU and in plain YPD growth conditions. There isn't an indication of a synthetic growth phenotype in this temperature.

v) *aft1Δaft2Δ* has a mildly slower growth phenotype than single *aft1Δ* in YPD but mildly better in 6-AU growth conditions. Aft2 seems to affect transcription elongation in these conditions. Double mutant in 6-AU does not seem to restore the slow growth phenotype of the single *aft1Δ* mutant, in contrast to 30^0C and to a lesser extend to 25^0C.

vi) Triple mutant *rad9Δaft1Δaft2Δ* has almost no slow growth phenotype versus the wild type strain in both 6-AU and in plain YPD (it almost behaves like the wild type strain). The colonies are mixed sized in both cases. Furthermore, *RAD9* deletion improves the slow growth phenotype of the double mutants in both plain YPD and 6-AU growth conditions.

What is shown in the above-described 6-AU assays is that *rad9Δ* has a mild slow growth phenotype with smaller colonies in 30^0C (temperature at which the rest of the experiments were performed) which implies that it has an effect in transcription elongation. Furthermore, *rad9Δaft1Δ* strain has a synthetic slow growth phenotype and smaller sized colonies compared to the single mutants. This is a further indication of the two proteins acting together on some common pathway(s). The same conclusion can be deduced by the phenotype of the triple mutant *rad9Δaft1Δaft2Δ* when it is compared to *aft1Δaft2Δ*.

Notably *aft1Δ* show a stronger transcriptional elongation phenotype than *rad9Δ* . This is novel for this transcription factor and should be further investigated.

3.3.3.2.-- Genome-wide Expression Profiling of *rad9Δ* cells

After confirming the implication of Rad9 with transcription of particular metal-regulated genes and establishing a rough involvement of the protein to transcription elongation, we wondered whether Rad9 affects the transcription pattern of yeast on a genome-wide scale. To address this question we performed expression microarray analyses in *rad9Δ* cells grown in inducing (for copper and iron genes) conditions using the Affymetrix Platform Arrays. In the present work, we provide for the first time a comprehensive analysis of the transcriptional profile of yeast in the absence of Rad9.

We have found only a small percentage (~2%) of yeast genes to be transcriptionally altered with statistical significance (P<0.05). More specifically, 131 genes were differentially expressed as shown in Table 3.1. Although the fold change was mostly mild, the results were statistically important, as there was a ~98% overlap in the biological replicates. Out of the 131 genes, 61 were downregulated and 70 upregulated. In Figure 3.8 a synopsis of the experiment's results is illustrated.
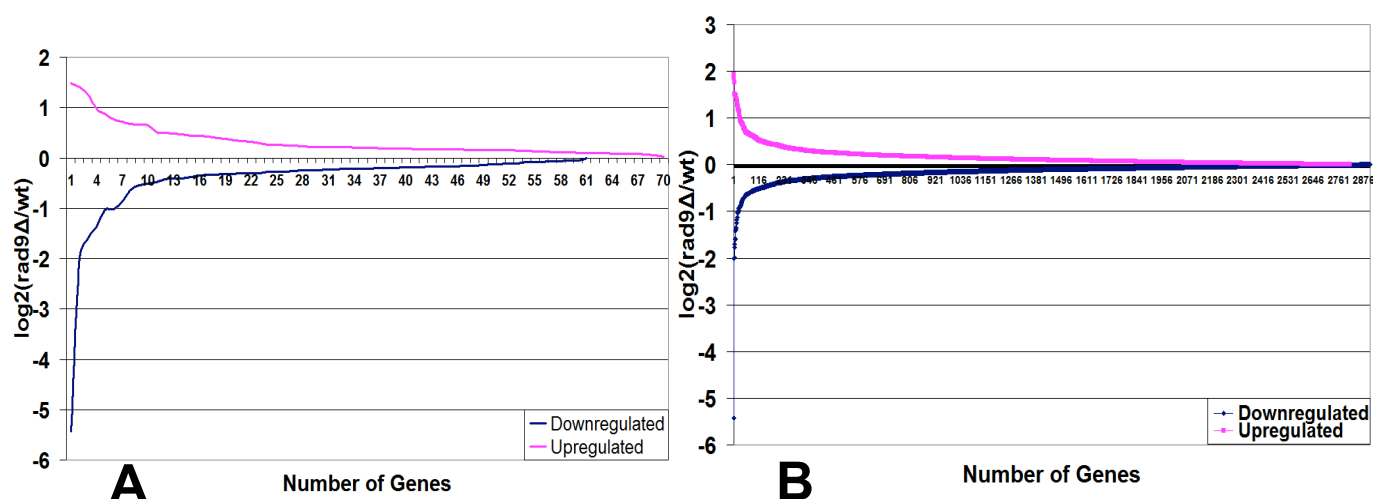
FIGURE 3.8: Transcriptionally altered genes in *rad9Δ* expression microarray experiment

After performing the experiment, as described in the text, we analyzed our results (see Materials and Methods), and selected the most statistically important genes that were transcriptionally altered **(A)** and plotted the $\log_2$ value of the *rad9Δ*/wt intensity ratio (the values of the downregulated genes were multiplied by -1 to visualize as negative). Of the 131 genes, 61 were downregulated and 70 were upregulated. In **(B)**, the same $\log_2$ *rad9Δ*/wt intensity ratio is plotted, but for the whole experiment (not only the statistically important genes). In both (A) and (B) plots, we observe similar numbers of up- and downregulated genes.

RANK	*rad9Δ*/WT	GENE	Description
1	-43,1833	RAD9	DNA damage-dependent checkpoint protein, required for cell-cycle arrest in G1/S, intra-S, and G2/M; transmits checkpoint signal by activating Rad53p and Chk1p; hyperphosphorylated by Mec1p and Tel1p; potential Cdc28p substrate
2	-3,96649	YJL052C-A	Putative protein of unknown function
3	-3,01535	YIR042C	Putative protein of unknown function; YIR042C is a non-essential gene
4	-2,58093	YRF1-1 /// YRF1-2 /// YRF1-3 /// YRF1-4 /// YRF1-5 /// YRF1-6 /// YRF1-7 /// YRF1-8	Helicase encoded by the Y' element of subtelomeric regions, highly expressed in the mutants lacking the telomerase component TLC1; potentially phosphorylated by Cdc28p; induced by treatment with 8-methoxypsoralen and UVA irradiation
5	-2,04289	YDR169C-A	Putative protein of unknown function; identified by fungal homology and RT-PCR

6	-2,02745	YLR157W-C	Putative protein of unknown function identified by gene-trapping, microarray-based expression analysis, and genome-wide homology searching; partially overlaps a Ty1 element
7	-1,82456	YGR126W	Putative protein of unknown function; green fluorescent protein (GFP)-fusion protein localises to both the cytoplasm and the nucleus and is induced in response to the DNA-damaging agent MMS
8	-1,55326	QCR8	Subunit 8 of ubiquinol cytochrome-c reductase complex, which is a component of the mitochondrial inner membrane electron transport chain; oriented facing the intermembrane space; expression is regulated by Abf1p and Cpf1p
9	-1,46029	YGR016W	Putative protein of unknown function
10	-1,43322	IDP2	Cytosolic NADP-specific isocitrate dehydrogenase, catalyzes oxidation of isocitrate to alpha-ketoglutarate; levels are elevated during growth on non-fermentable carbon sources and reduced during growth on glucose
11	-1,39843	YOL114C	Putative protein of unknown function with similarity to human ICT1 and prokaryotic factors that may function in translation termination; YOL114C is not an essential gene
12	-1,33521	KTR7	Putative mannosyltransferase involved in protein glycosylation; member of the KRE2/MNT1 mannosyltransferase family
13	-1,32802	AAD3	Putative aryl-alcohol dehydrogenase with similarity to P. chrysosporium aryl-alcohol dehydrogenase; mutational analysis has not yet revealed a physiological role
14	-1,32355	YGR153W	Putative protein of unknown function
15	-1,29953	APC9	Subunit of the Anaphase-Promoting Complex/Cyclosome (APC/C), which is a ubiquitin-protein ligase required for degradation of anaphase inhibitors, including mitotic cyclins, during the metaphase/anaphase transition
16	-1,27643	DET1	Acid phosphatase involved in the non-vesicular transport of sterols in both directions between the endoplasmic reticulum and plasma membrane; deletion confers sensitivity to nickel
17	-1,26459	SCM4	Potential regulatory effector of CDC4 function, suppresses a temperature-sensitive allele of CDC4, tripartite protein structure in which a charged region separates two uncharged domains, not essential for mitosis or meiosis
18	-1,25952	NTH2	Putative neutral trehalase, required for thermotolerance and may mediate resistance to other cellular stresses
19	-1,2495	GTS1	Arf3p GTPase Activating Protein (GAP) that localises to endocytic patches; gts1 mutations affect budding, cell size, heat tolerance, sporulation, life span, ultradian rhythms; localises to nucleus and induces flocculation when overexpressed
20	-1,24466	NOP53	Nucleolar protein; involved in biogenesis of the 60S subunit of the ribosome; interacts with rRNA processing factors Cbf5p and Nop2p; null mutant is viable but growth is severely impaired
21	-1,23476	SNX3	Sorting nexin required to maintain late-Golgi resident enzymes in their proper location by recycling molecules from the prevacuolar compartment; contains a PX domain and sequence similarity to human Snx3p
22	-1,2328	SIR3	Silencing protein that interacts with Sir2p and Sir4p, and histone H3 and H4 tails, to establish a transcriptionally silent chromatin state; required for spreading of silenced chromatin; recruited to chromatin through interaction with Rap1p
23	-1,23266	COX9	Subunit VIIa of cytochrome c oxidase, which is the terminal member of the mitochondrial inner membrane electron transport chain
24	-1,21483	HPA3	D-Amino acid N-acetyltransferase, catalyzes N-acetylation of D-amino acids through ordered bi-bi mechanism in which acetyl-CoA is first substrate bound and CoA is last product liberated; similar to Hpa2p, acetylates histones weakly in vitro
25	-1,20716	PPR1	Zinc finger transcription factor containing a Zn(2)-Cys(6) binuclear cluster domain, positively regulates transcription of genes involved in uracil biosynthesis; activity may be modulated by interaction with Tup1p
26	-1,20492	SDH1	Flavoprotein subunit of succinate dehydrogenase (Sdh1p, Sdh2p, Sdh3p, Sdh4p), which couples the oxidation of succinate to the transfer of electrons

			to ubiquinone as part of the TCA cycle and the mitochondrial respiratory chain
27	-1,19502	HOR7	Protein of unknown function; overexpression suppresses Ca2+ sensitivity of mutants lacking inositol phosphorylceramide mannosyltransferases Csg1p and Csh1p; transcription is induced under hyperosmotic stress and repressed by alpha factor
28	-1,19151	MRPL33	Mitochondrial ribosomal protein of the large subunit
29	-1,18738	CKB2	Beta' regulatory subunit of casein kinase 2, a Ser/Thr protein kinase with roles in cell growth and proliferation; the holoenzyme also contains CKA1, CKA2 and CKB1, the many substrates include transcription factors and all RNA polymerases
30	-1,18185	GLO2	Cytoplasmic glyoxalase II, catalyzes the hydrolysis of S-D-lactoylglutathione into glutathione and D-lactate
31	-1,17509	SPH1	Protein involved in shmoo formation and bipolar bud site selection; homologous to Spa2p, localises to sites of polarized growth in a cell cycle dependent- and Spa2p-dependent manner, interacts with MAPKKs Mkk1p, Mkk2p, and Ste7p
32	-1,16732	SWD3	Essential subunit of the COMPASS (Set1C) complex, which methylates histone H3 on lysine 4 and is required in transcriptional silencing near telomeres; WD40 beta propeller superfamily member and ortholog of mammalian WDR5
33	-1,16626	ICL2	2-methylisocitrate lyase of the mitochondrial matrix, functions in the methylcitrate cycle to catalyze the conversion of 2-methylisocitrate to succinate and pyruvate; ICL2 transcription is repressed by glucose and induced by ethanol
34	-1,16452	PUS6	tRNA:pseudouridine synthase, catalyzes the conversion of uridine to pseudouridine at position 31 in cytoplasmic and mitochondrial tRNAs; mutation of Asp168 to Ala abolishes enzyme activity; not essential for viability
35	-1,16446	GOS1	v-SNARE protein involved in Golgi transport, homolog of the mammalian protein GOS-28/GS28
36	-1,15826	UGP1	UDP-glucose pyrophosphorylase (UGPase), catalyses the reversible formation of UDP-Glc from glucose 1-phosphate and UTP, involved in a wide variety of metabolic pathways, expression modulated by Pho85p through Pho4p
37	-1,15198	SHG1	Subunit of the COMPASS (Set1C) complex, which methylates histone H3 on lysine 4 and is required in transcriptional silencing near telomeres
38	-1,14995	PEX32	Peroxisomal integral membrane protein, involved in negative regulation of peroxisome size; partially functionally redundant with Pex31p; genetic interactions suggest action at a step downstream of steps mediated by Pex28p and Pex29p
39	-1,14925	VPS70	Protein of unknown function involved in vacuolar protein sorting
40	-1,13846	TRK1	Component of the Trk1p-Trk2p potassium transport system; 180 kDa high affinity potassium transporter; phosphorylated in vivo and interacts physically with the phosphatase Ppz1p, suggesting Trk1p acitivy is regulated by phosphorylation
41	-1,13784	NCE101	Protein of unknown function, involved in secretion of proteins that lack classical secretory signal sequences
42	-1,13304	LSM4	Lsm (Like Sm) protein; part of heteroheptameric complexes (Lsm2p-7p and either Lsm1p or 8p): cytoplasmic Lsm1p complex involved in mRNA decay; nuclear Lsm8p complex part of U6 snRNP and possibly involved in processing tRNA, snoRNA, and rRNA
43	-1,13164	UTR4	Protein with sequence similarity to 2,3-diketo-5-methylthiopentyl-1-phosphate enolase-phosphatases, involved in methionine salvage; found in both the cytoplasm and nucleus
44	-1,13067	YIL161W	Putative protein of unknown function; green fluorescent protein (GFP)-fusion protein localises to the cytoplasm; mRNA is enriched in Scp160p-associated mRNPs; YIL161W is a non-essential gene
45	-1,12722	YDR514C	Protein of unknown function that localises to mitochondria; overexpression of

RANK		GENE	
			YDR514C affects endocytic protein trafficking
46	-1,12091	HSP10	Mitochondrial matrix co-chaperonin that inhibits the ATPase activity of Hsp60p, a mitochondrial chaperonin; involved in protein folding and sorting in the mitochondria; 10 kD heat shock protein with similarity to E. coli groES
47	-1,11316	YDL121C	Putative protein of unknown function; green fluorescent protein (GFP)-fusion protein localises to the endoplasmic reticulum; YDL121C is not an essential protein
48	-1,11052	MRPL31	Mitochondrial ribosomal protein of the large subunit
49	-1,09972	RPL8A	Ribosomal protein L4 of the large (60S) ribosomal subunit, nearly identical to Rpl8Bp and has similarity to rat L7a ribosomal protein; mutation results in decreased amounts of free 60S subunits
50	-1,09591	DHR2	Predominantly nucleolar DEAH-box ATP-dependent RNA helicase, required for 18S rRNA synthesis
51	-1,09371	ERV29	Protein localised to COPII-coated vesicles, involved in vesicle formation and incorporation of specific secretory cargo
52	-1,08295	MET1	S-adenosyl-L-methionine uroporphyrinogen III transmethylase, involved in the biosynthesis of siroheme, a prosthetic group used by sulfite reductase; required for sulfate assimilation and methionine biosynthesis
53	-1,07741	APT1	Acyl-protein thioesterase responsible for depalmitoylation of Gpa1p; green fluorescent protein (GFP)-fusion protein localises to both the cytoplasm and nucleus and is induced in response to the DNA-damaging agent MMS
54	-1,05682	PFA5	Palmitoyltransferase with autoacylation activity; likely functions in pathway(s) outside Ras; member of a family of putative palmitoyltransferases containing an Asp-His-His-Cys-cysteine rich (DHHC-CRD) domain
55	-1,05321	PEP4	Vacuolar aspartyl protease (proteinase A), required for the posttranslational precursor maturation of vacuolar proteinases; important for protein turnover after oxidative damage; synthesized as a zymogen, self-activates
56	-1,0529	APT1	Adenine phosphoribosyltransferase, catalyzes the formation of AMP from adenine and 5-phosphoribosylpyrophosphate; involved in the salvage pathway of purine nucleotide biosynthesis
57	-1,05032	RPL21A /// RPL21B	Protein component of the large (60S) ribosomal subunit, nearly identical to Rpl21Bp and has similarity to rat L21 ribosomal protein /// Protein component of the large (60S) ribosomal subunit, nearly identical to Rpl21Ap and has similarity to rat L21 ribosomal protein
58	-1,04322	CUP5	Proteolipid subunit of the vacuolar H(+)-ATPase V0 sector (subunit c; dicyclohexylcarbodiimide binding subunit); required for vacuolar acidification and important for copper and iron metal ion homeostasis
59	-1,04166	ATG26	UDP-glucose:sterol glucosyltransferase, conserved enzyme involved in synthesis of sterol glucoside membrane lipids; in contrast to ATG26 from P. pastoris, S. cerevisiae ATG26 is not involved in autophagy
60	-1,0329	YMR114C	Protein of unknown function; may interact with ribosomes, based on co-purification experiments; green fluorescent protein (GFP)-fusion protein localises to the nucleus and cytoplasm; YMR114C is not an essential gene
61	-1,00982	NDC1	Nuclear envelope protein with multiple putative transmembrane domains, required for nuclear pore complex assembly and spindle pole body duplication; required for meiosis II

RANK	rad9Δ/WT	GENE	Description
70	1,016753	TKL1	Transketolase, similar to Tkl2p; catalyzes conversion of xylulose-5-phosphate and ribose-5-phosphate to sedoheptulose-7-phosphate and glyceraldehyde-3-phosphate in the pentose phosphate pathway; needed for synthesis of aromatic amino acids
69	1,040667	LIP1	Ceramide synthase subunit; single-span ER membrane protein associated with Lag1p and Lac1p and required for ceramide synthase activity, null mutant grows extremely slowly and is defective in ceramide synthesis
68	1,048025	RPS12	Protein component of the small (40S) ribosomal subunit; has similarity to rat ribosomal protein S12
67	1,055077	SRV2	CAP (cyclase-associated protein) subunit of adenylyl cyclase complex; N-

			terminus binds adenylyl cyclase and facilitates activation by RAS; C-terminus binds ADP-actin monomers, facilitating regulation of actin dynamics and cell morphogenesis
66	1,056487	DRS2	Aminophospholipid translocase (flippase) that maintains membrane lipid asymmetry in post-Golgi secretory vesicles; contributes to clathrin-coated vesicle formation and endocytosis; mutations in human homolog ATP8B1 result in liver disease
65	1,058843	THR1	Homoserine kinase, conserved protein required for threonine biosynthesis; expression is regulated by the GCN4-mediated general amino acid control pathway
64	1,062765	TIF34	eIF3i subunit of the core complex of translation initiation factor 3 (eIF3), which is essential for translation
63	1,064679	RPL37B	Protein component of the large (60S) ribosomal subunit, has similarity to Rpl37Ap and to rat L37 ribosomal protein
62	1,071242	DIS3	Exosome core complex catalytic subunit; possesses both endonuclease and 3'-5' exonuclease activity; involved in 3'-5' RNA processing and degradation in both the nucleus and the cytoplasm; has similarity to E. coli RNase R and to human DIS3
61	1,072131	RPL18A	Protein component of the large (60S) ribosomal subunit, identical to Rpl18Bp and has similarity to rat L18 ribosomal protein; intron of RPL18A pre-mRNA forms stem-loop structures that are a target for Rnt1p cleavage leading to degradation
60	1,07405	CDC10	Component of the septin ring of the mother-bud neck that is required for cytokinesis; septins recruit proteins to the neck and can act as a barrier to diffusion at the membrane, and they comprise the 10nm filaments seen with EM
59	1,081554	KAP114	Karyopherin, responsible for nuclear import of Spt15p, histones H2A and H2B, and Nap1p; amino terminus shows similarity to those of other importins, particularly Cse1p; localisation is primarily nuclear
58	1,081998	GUS1	Glutamyl-tRNA synthetase (GluRS), forms a complex with methionyl-tRNA synthetase (Mes1p) and Arc1p; complex formation increases the catalytic efficiency of both tRNA synthetases and ensures their correct localisation to the cytoplasm
57	1,085589	KEX2	Subtilisin-like protease (proprotein convertase), a calcium-dependent serine protease involved in the activation of proproteins of the secretory pathway
56	1,092733	NAT1	Subunit of the N-terminal acetyltransferase NatA (Nat1p, Ard1p, Nat5p); N-terminally acetylates many proteins, which influences multiple processes such as the cell cycle, heat-shock resistance, mating, sporulation, and telomeric silencing
55	1,096039	COQ1	Hexaprenyl pyrophosphate synthetase, catalyzes the first step in ubiquinone (coenzyme Q) biosynthesis
54	1,09832	NET1	Core subunit of the RENT complex, which is a complex involved in nucleolar silencing and telophase exit; stimulates transcription by RNA polymerase I and regulates nucleolar structure
53	1,100275	MGM1	Mitochondrial GTPase related to dynamin, present in a complex containing Ugo1p and Fzo1p; required for normal morphology of cristae and for stability of Tim11p; homolog of human OPA1 involved in autosomal dominant optic atrophy
52	1,109273	ATS1	Protein required, with Elongator complex, Kti11p, and Kti12p, for modification of wobble nucleosides in tRNA; has a potential role in regulatory interactions between microtubules and the cell cycle
51	1,110028	IMH1	Protein involved in vesicular transport, mediates transport between an endosomal compartment and the Golgi, contains a Golgi-localisation (GRIP) domain that interacts with activated Arl1p-GTP to localise Imh1p to the Golgi
50	1,111372	MIP1	Catalytic subunit of the mitochondrial DNA polymerase; conserved C-terminal segment is required for the maintenance of mitochondrial genome; related to human POLG, which has been associated with mitochondrial diseases
49	1,115233	SRB5	Subunit of the RNA polymerase II mediator complex; associates with core polymerase subunits to form the RNA polymerase II holoenzyme; essential for

				transcriptional regulation; involved in telomere maintenance
48	1,11582	UBP15		Ubiquitin-specific protease that may play a role in ubiquitin precursor processing
47	1,119929	MIA40		Essential protein of the mitochondrial intermembrane space (IMS); promotes retention of newly imported proteins; may do so by stabilizing client protein folding as part of a disulfide relay system or transferring metal to client proteins
46	1,125142	ERG9		Farnesyl-diphosphate farnesyl transferase (squalene synthase), joins two farnesyl pyrophosphate moieties to form squalene in the sterol biosynthesis pathway
45	1,126969	STE23		Metalloprotease involved, with homolog Axl1p, in N-terminal processing of pro-a-factor to the mature form; member of the insulin-degrading enzyme family
44	1,12741	INN1		Essential protein that associates with the contractile actomyosin ring, required for ingression of the plasma membrane into the bud neck during cytokinesis; C2 domain, a membrane targeting module, is required for function
43	1,127553	OCA6		Cytoplasmic protein required for replication of Brome mosaic virus in S. cerevisiae, which is a model system for studying positive-strand RNA virus replication; null mutation confers sensitivity to tunicamycin and DTT
42	1,127832	ORC5		Subunit of the origin recognition complex, which directs DNA replication by binding to replication origins and is also involved in transcriptional silencing
41	1,129098	TYE7		Serine-rich protein that contains a basic-helix-loop-helix (bHLH) DNA binding motif; binds E-boxes of glycolytic genes and contributes to their activation; may function as a transcriptional activator in Ty1-mediated gene expression
40	1,131898	CDC24		Guanine nucleotide exchange factor (GEF or GDP-release factor) for Cdc42p; required for polarity establishment and maintenance, and mutants have morphological defects in bud formation and shmooing
39	1,135503	RIM11		Protein kinase required for signal transduction during entry into meiosis; promotes the formation of the Ime1p-Ume6p complex by phosphorylating Ime1p and Ume6p; shares similarity with mammalian glycogen synthase kinase 3-beta
38	1,140876	GID8		Protein of unknown function, involved in proteasome-dependent catabolite inactivation of fructose-1,6-bisphosphatase; contains LisH and CTLH domains, like Vid30p; dosage-dependent regulator of START
37	1,141554	DAM1		Essential subunit of the Dam1 complex (aka DASH complex), couples kinetochores to the force produced by MT depolymerization thereby aiding in chromosome segregation; Ipl1p target for regulating kinetochore-MT attachments
36	1,14383	ADE1		N-succinyl-5-aminoimidazole-4-carboxamide ribotide (SAICAR) synthetase, required for 'de novo' purine nucleotide biosynthesis; red pigment accumulates in mutant cells deprived of adenine
35	1,144662	CUP9		Homeodomain-containing transcriptional repressor of PTR2, which encodes a major peptide transporter; imported peptides activate ubiquitin-dependent proteolysis, resulting in degradation of Cup9p and de-repression of PTR2 transcription
34	1,146197	NAM2		Mitochondrial leucyl-tRNA synthetase, also has a direct role in splicing of several mitochondrial group I introns; indirectly required for mitochondrial genome maintenance
33	1,157914	HRD1		Ubiquitin-protein ligase required for endoplasmic reticulum-associated degradation (ERAD) of misfolded proteins; genetically linked to the unfolded protein response (UPR); regulated through association with Hrd3p; contains an H2 ring finger
32	1,158255	PMD1		Protein with an N-terminal kelch-like domain, putative negative regulator of early meiotic gene expression; required, with Mds3p, for growth under alkaline conditions
31	1,158859	VPS75		NAP family histone chaperone; binds to histones and Rtt109p, stimulating histone acetyltransferase activity; possesses nucleosome assembly activity in vitro; proposed role in vacuolar protein sorting and in double-strand break repair
30	1,162145	ENV11		Protein proposed to be involved in vacuolar functions; mutant shows defect in CPY processing and fragmented vacuoles; deletion mutant has increased

			glycogen accumulation and displays elongated buds; green fluorescent protein (GFP)-fusion protein localises to the nucleus
29	1,166127	SQS1	Stimulates the ATPase and helicase activities of Prp43p; acts with Prp43p to stimulate 18s rRNA maturation by Nob1p; overexpression antagonizes the suppression of splicing defects by spp382 mutants; component of pre-ribosomal particles
28	1,174081	BNI1	Formin, nucleates the formation of linear actin filaments, involved in cell processes such as budding and mitotic spindle orientation which require the formation of polarized actin cables, functionally redundant with BNR1
27	1,184722	PUF4	Member of the PUF protein family, which is defined by the presence of Pumilio homology domains that confer RNA binding activity; preferentially binds mRNAs encoding nucleolar ribosomal RNA-processing factors
26	1,185915	SEC63	Essential subunit of Sec63 complex (Sec63p, Sec62p, Sec66p and Sec72p); with Sec61 complex, Kar2p/BiP and Lhs1p forms a channel competent for SRP-dependent and post-translational SRP-independent protein targeting and import into the ER
25	1,19948	ATR1	Multidrug efflux pump of the major facilitator superfamily, required for resistance to aminotriazole and 4-nitroquinoline-N-oxide
24	1,203506	SKS1	Putative serine/threonine protein kinase; involved in the adaptation to low concentrations of glucose independent of the SNF3 regulated pathway
23	1,220709	ETP1	Putative protein of unknown function that is required for growth on ethanol; contains a zinc finger region and has homology to human BRAP2, which is a cytoplasmic protein that binds nuclear localisation sequences
22	1,251639	SLN1	Histidine kinase osmosensor that regulates a MAP kinase cascade; transmembrane protein with an intracellular kinase domain that signals to Ypd1p and Ssk1p, thereby forming a phosphorelay system similar to bacterial two-component regulators
21	1,256175	YHR086W-A	Putative protein of unknown function; identified by fungal homology and RT-PCR
20	1,271676	YNL277W-A	Putative protein of unknown function
19	1,296635	FYV6	Protein of unknown function, required for survival upon exposure to K1 killer toxin; proposed to regulate double-strand break repair via non-homologous end-joining
18	1,313831	MRS4	Iron transporter that mediates Fe2+ transport across the inner mitochondrial membrane; mitochondrial carrier family member, similar to and functionally redundant with Mrs3p; active under low-iron conditions; may transport other cations
17	1,336882	DBP1	Putative ATP-dependent RNA helicase of the DEAD-box protein family; mutants show reduced stability of the 40S ribosomal subunit scanning through 5' untranslated regions of mRNAs
16	1,354305	REV3	Catalytic subunit of DNA polymerase zeta, involved in translesion synthesis during post-replication repair; required for mutagenesis induced by DNA damage; involved in double-strand break repair
15	1,355659	YLH47	Mitochondrial inner membrane protein exposed to the mitochondrial matrix, associates with mitochondrial ribosomes, NOT required for respiratory growth; homolog of human Letm1, a protein implicated in Wolf-Hirschhorn syndrome
14	1,385679	DIN7	Mitochondrial nuclease functioning in DNA repair and replication, modulates the stability of the mitochondrial genome, induced by exposure to mutagens, also induced during meiosis at a time nearly coincident with commitment to recombination
13	1,39658	TOM70	Component of the TOM (translocase of outer membrane) complex responsible for recognition and initial import steps for all mitochondrially directed proteins; acts as a receptor for incoming precursor proteins
12	1,407796	VAM7	Component of the vacuole SNARE complex involved in vacuolar morphogenesis; SNAP-25 homolog; functions with a syntaxin homolog Vam3p in vacuolar protein trafficking
11	1,419912	UBP16	Deubiquitinating enzyme anchored to the outer mitochondrial membrane, probably not important for general mitochondrial functioning, but may perform a

			more specialized function at mitochondria
10	1,568563	YIR021W-A	Putative protein of unknown function; identified by expression profiling and mass spectrometry
9	1,584332	FRE5	Putative ferric reductase with similarity to Fre2p; expression induced by low iron levels; the authentic, non-tagged protein is detected in highly purified mitochondria in high-throughput studies
8	1,598547	KAR4	Transcription factor required for gene regulation in repsonse to pheromones; also required during meiosis; exists in two forms, a slower-migrating form more abundant during vegetative growth and a faster-migrating form induced by pheromone
7	1,647906	PEX18	Peroxin required for targeting of peroxisomal matrix proteins containing PTS2; interacts with Pex7p; partially redundant with Pex21p
6	1,706983	YGR226C	Dubious open reading frame, unlikely to encode a protein; not conserved in closely related Saccharomyces species; overlaps significantly with a verified ORF, AMA1/YGR225W
5	1,83138	FIG2	Cell wall adhesin, expressed specifically during mating; may be involved in maintenance of cell wall integrity during mating
4	1,970925	YNL034W	Putative protein of unknown function; YNL034W is not an essential gene
3	2,378028	FUS1	Membrane protein localised to the shmoo tip, required for cell fusion; expression regulated by mating pheromone; proposed to coordinate signaling, fusion, and polarization events required for fusion; potential Cdc28p substrate
2	2,641638	ASG7	Protein that regulates signaling from a G protein beta subunit Ste4p and its relocalisation within the cell; specific to a-cells and induced by alpha-factor
1	2,800618	YMR206W	Putative protein of unknown function; YMR206W is not an essential gene

TABLE 3.1: Transcriptionally altered genes in *rad9Δ* mutant

rad9Δ cells were grown under induction conditions (SC BCS BPS) and the protocol for Affymetrix expression Arrays was followed for two biological replicates (See Materials and Methods). Taking into account both experiments and after the proper normalization (see Materials and Methods) and using a P<0.05 cutoff, we have found 131 genes to be transcriptionally altered. Of these, 61 were downregulated (green colour) and 70 were upregulated (red colour). The second column (*rad9Δ*/WT) represents the increase or decrease of the transcript compared to the wild type (WT) strain (see also Materials and Methods).

After this first sorting of our expression microarray results, we sought to explore possible functional enrichments on the datasets. We used BiNGO plugin on Cytoscape platform (see Materials and Methods) in order to find overrepresented gene clusters for the genes that we found to be transcriptionally altered. We used Cytoscape analysis to find Gene Ontology (GO) groups depending on the Biological Process (BP), Molecular Function (MF), as well as the Cellular Component (CC) of which they are enriched. By this approach, we can see if Rad9 affects specific groups of genes and whether there exists interplay between them and other known pathways in yeast. Using a false discovery rate of 0.1-0.05 we found specific gene groups to be overrepresented which were similar in the up- and down-regulated genes (Table 3.1.1).

GO	Cellular Component	# of genes
133	Polarisome	2

GO		# of genes
5677	Chromatin silencing complex	2
35097	Histone methyltransferase complex	2
5739	Mitochondrion	30
31966	Mitochondrial membrane	12
5746	Mitochondrial respiratory chain	3
22625	large ribosomal subunit	6
16020	Membrane	45
5937	Mating projection	7
42575	DNA polymerase complex	2
781	Chromosome, telomeric region	3
5856	Cytoskeleton	8
GO	**Molecular Function**	**# of genes**
16790	Thiolester hydrolase activity	4
42393	Histone binding	3
15077	Monovalent inorganic cation transmembrane transporter activity	4
4843	Ubiquitin-specific protease activity	2
8135	Translation factor activity, nucleic acid binding	3
3724	RNA helicase activity	2
3824	Catalytic activity	51
GO	**Biological Process**	**# of genes**
31935	Regulation of chromatin silencing	3
746	Conjugation	7
6303	Double-strand break repair via nonhomologous end joining	3
6566	Threonine metabolic process	2
6081	Cellular aldehyde metabolic process	3
5991	Trehalose metabolic process	2
6081	Various metabolic genes	3

Table 3.1.1. Selected GO categories showing significant overrepresentation in *rad9Δ* cells grown in SC BCS BPS

As shown in the Table above, the overrepresented gene clusters included ones related to metabolic processes, mitochondria, ribosomes and translation factor activity, chromatin silencing, DSB repair, protein degradation, mating projection and conjugation.

Because the number of up- and down-regulated genes was small (70 and 61 respectively), the cytoscape functional analysis could not retrieve any significant

overrepresented clusters. Nevertheless, when we carefully studied the lists of up- and down-regulated genes with no use of software we observed that in the <u>downregulated</u> list, there exist metabolic genes (ranked 10, 13, 24, 26, 56), mitochondria-related (ranked 8, 23, 46, 48), ribosomal biogenesis- and structure-related (ranked 20, 28, 48, 49, 57), chromatin modification-transcriptional silencing-related (ranked 22, 32, 37), related to vacuole (ranked 21, 39, 55, 58), to subcellular transport (ranked 16, 35, 51) and helicase function (ranked 4, 50). Accordingly, in the <u>upregulated</u> genes list we were able to find metabolic genes (ranked 34, 36, 46, 48, 55, 56, 57, 58, 69), genes related to mitochondria in multiple ways like import (ranked 13, 47), membranes (ranked 11, 15), metabolism (ranked 14, 34), and other (ranked 50, 53). Furthermore, in the upregulated genes list we found genes related to ribosomal RNA processing and ribosomal structure (ranked 27, 29, 61, 63, 68), vacuolar-related (ranked 12, 30, 31), related to protein degradation (ranked 33, 38, 48), associated to DNA replication and repair (ranked 14, 16, 42), to transcription regulation (ranked 8, 35, 49), mating (ranked 3, 5) and iron homeostasis (ranked 9, 18).

Rad9 does not affect the global transcriptional pattern of yeast to a significant extend, which means that it is not likely for Rad9 to have a potential action of a transcriptional activator/repressor. The fact that the genes which are statistically transcriptionally altered include metabolic ones could explain the growth defect in 6-azauracil assay (Figure 3.7A).

It is worth mentioning that we have also observed in RNA accumulation experiments, a four-fold decrease of RNAPII (RPO21, the largest subunit) in *rad9Δ* strains (Figure 3.8A). We have also shown that Rad9 was present in both the coding and promoter region of RPO21 gene (Figure 3.8B). Nevertheless, this had no important effect on yeast transcriptome, since only ~2% of the genes were altered, which means that eventhough RNAPII is somewhat reduced, the amount is still enough for quite normal transcription.
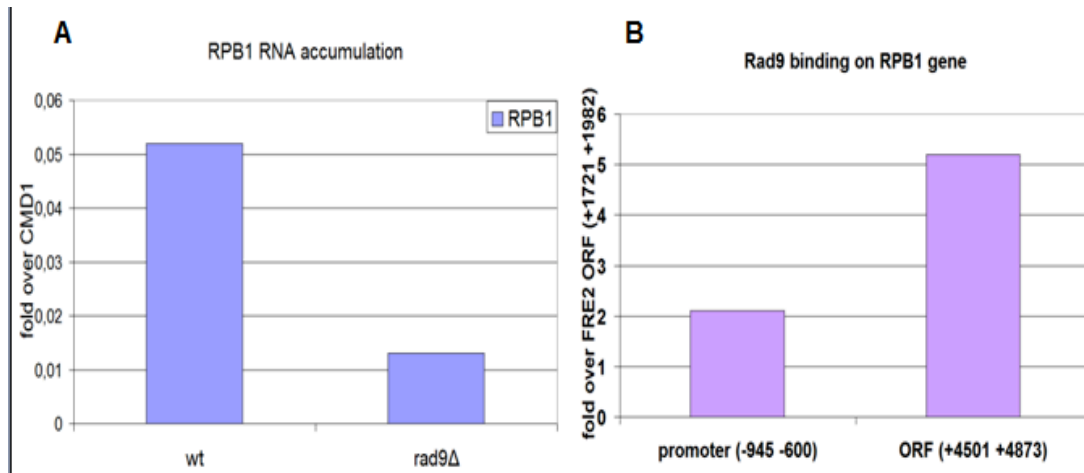
FIGURE 3.8: Expression of *RPB1* gene decreases in *rad9Δ*, while Rad9 localises to *RPB1* gene

A) wt and *rad9Δ* cells were grown in SC BCS BPS and RNA was extracted and used in RT analysis to check the change in the expression of *RPB1* transcript. B) The enrichment of Rad9 in promoter and ORF regions of *RPO21* (*RPB1*) gene (encoding for the largest subunit of RNAPII) is visualized after ChIP experiment. Normalization was performed firstly over INPUT and secondly by measuring the binding of Rad9 on *FRE2* coding region, where Rad9 binding is minimal in any growth conditions (as tested by our group) and dividing to Rad9 enrichment.

We have found that Rad9 affects a small number of genes transcriptionally but it also localizes to genes whose transcription is not affected significantly. For that reason we sought to explore Rad9 genome-wide localisation.

3.3.4.—Rad9 localisation to chromatin under non-DNA damaging conditions

3.3.4.1.—Rad9 localises to 1/5 of all yeast genes but to only a fraction of the genes whose transcription affects

As we mentioned in the Introduction (Chapter 1.3.4), Rad9 was previously found to chromatin fraction in unperturbed conditions throughout the cell cycle (Gilbert et al., 2001; Hammet et al., 2007). Nevertheless, very little is known about the role that Rad9 has there. This is one of the big questions we have aimed to explore in this study by performing a high resolution analysis of Rad9 binding pattern on the whole genome.

We have used the Affymetrix *Saccharomyces cerevisiae* Tiling 1.0R Array (See Materials and Methods) to analyse in depth the binding pattern of Rad9. By this approach, we examined whether Rad9 effect in yeast's transcriptional profile is direct or indirect, as well as whether there are specific loci for which Rad9 has a binding bias. In the first experiment we applied the same growth conditions which were used

for the expression microarray (SC medium with BCS/BPC in which the iron/copper-regulated genes were induced).

The first question we wanted to address was whether Rad9 affects the transcription of the genes listed in Results Chapter 3.3.3.2 (*rad9Δ* expression array) directly or indirectly.

As described in Materials and Methods, after the scanning of our hybridized sample, we obtained the intensity values of each area spotted on the Array and normalized to the identically trained INPUT sample grown in the same conditions using the proper software. We then used the Integrated Genome Browser (IGB) to visualize our results and set a threshold in order to obtain the intensity values corresponding to two different P-values (10^{-3} and 5×10^{-3}). By this sorting, we found that Rad9 was localised to about one fifth (~16-23% depending on the threshold) of the 5757 annotated yeast genes. More specifically it was present to 1308 (P=5×10^{-3}) or 935 genes (P=10^{-3}). Thus, only a small percentage (~2.5%) of the genes where Rad9 is localised is also affected transcriptionally by its absence (*rad9Δ*) (Figure 3.9). From another point of view, in 31 out of 131 (~24%) genes that are transcriptionally altered in *rad9Δ*, Rad9 is present (P=5×10^{-3}).
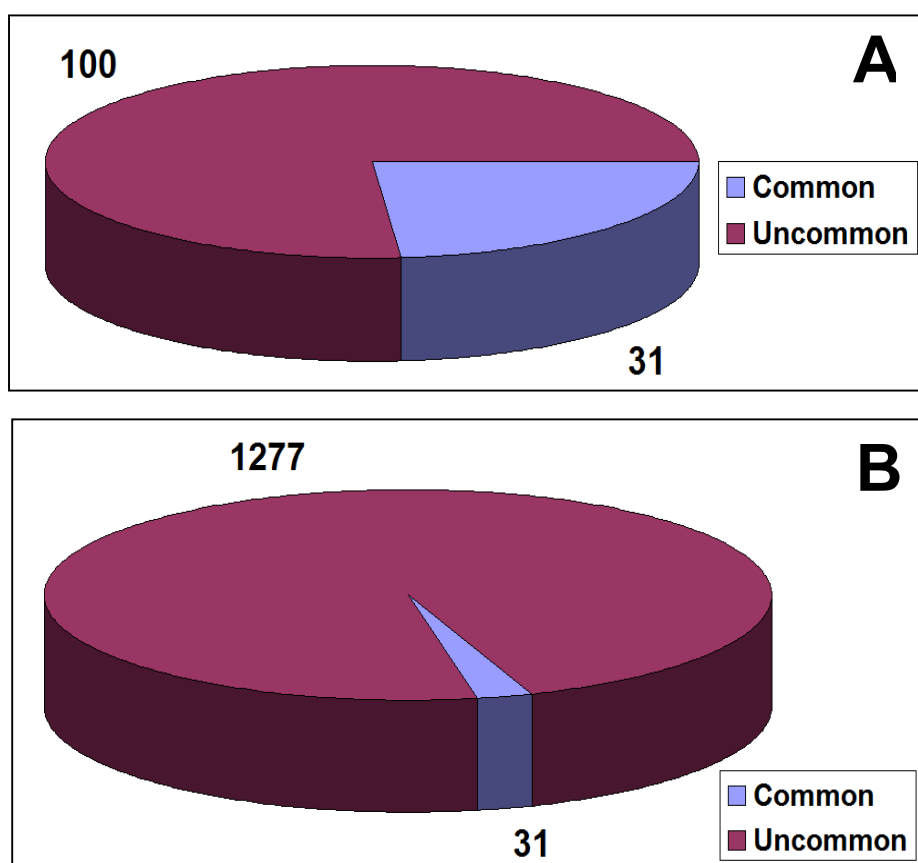
FIGURE 3.9: Rad9 presence in chromatin is not likely to be associated with transcription regulation

Rad9 affected the transcription of 131 genes as we saw on our expression study described in Results Chapter 3.3.3.2 in SC BCS BPS growth conditions. We have also found Rad9 to be present in 1308 genes (when we used $P=5x10^{-3}$ threshold) in the same growth conditions. Similar results were obtained when a $P=10^{-3}$ threshold was used.

(A) Illustrated in the chart is the proportion of the 131 genes whose transcription is affected by Rad9. Of these, the 31 have Rad9 localised on them (~24%).

(B) Illustrated in the chart is the proportion of the 1308 genes on which Rad9 is localised. Of these, only 31 are also transcriptionally altered (~2.5%)

From the above it is further established that Rad9 does not affect transcription in general.

In spite of the small number of genes whose transcription Rad9 affected and was localized to, we wanted to examine whether these genes could be clustered to specific GO groups depending on the Molecular Function (MF) of the encoded proteins, the Biological Process (BP) they were participating in or their subcellular localisation (Cellular Component, CC). To do that, we used BiNGO plugin in Cytoscape platform (see Materials and Methods). In addition to that, we grouped the genes to which Rad9 was localised, into categories depending on whether Rad9 was present on their coding regions, non coding regions, or both and we applied Cytoscape Analysis. Subsequently, we would be able to decipher whether there were functional groups to which Rad9 localised and affected transcription (direct role), affected transcription without binding (indirectly) or localised without affecting transcription.

Rad9 was localised to and also affected the transcription (direct role) of 31 genes (as shown above). In 30 out of the 31 genes, Rad9 was on coding regions; in 6 out of the 31 was in non coding regions and in 3 out of the 31 it was present in coding and non coding region of the same gene. The sole statistically important (FDR=0.05) overrepresented GO category was the one related to metabolic processes. In the case where Rad9 had an indirect role in transcription, no clusters were formed.

Moreover, the case where Rad9 was localised without affecting transcription consisted the largest group (1277 out of 1308 genes when $P=5x10^{-3}$). In Table 3.2, there are listed the clusters overrepresented for all of the categories (coding, non coding, coding-non coding of the same gene), according to the P-value significance (see Materials and Methods).

TOTAL	CODING	NON CODING	CODING & NON CODING OF SAME GENE
BP	**BP**	**BP**	**BP**
-**metabolic** process (oxoacid, carboxylic acid, organic acid, cellular ketone) (10^{-15})	-**metabolic** process (oxoacid, carboxylic acid, organic acid, cellular ketone) (10^{-17})	-**regulation of translation** (10^{-1})	-**regulation of translation** (10^{-3})
-**regulation of translation** (10^{-17})	-**regulation of translation** (10^{-18})	-**regulation** of cellular protein **metabolic process** (10^{-1})	-cellular metabolic process (10^{-3})
-**post trascriptional regulation of gene expression** (10^{-17})	-**post trascriptional regulation of gene expression** (10^{-18})	-**post transcriptional regulation** of gene expression (10^{-1})	-post transcriptional regulation of gene expression (10^{-3})
-**amine and aminoacid and derivative metabolic process** (10^{-7})	-cellular **amine metabolic process** (10^{-10})	**MF**	-small molecule metabolic/catabolic process (10^{-1})
-**glucose catabolic** process (10^{-6})	-**glucose catabolic** process (10^{-6})	-structural constituent of **ribosome** (10^{-3})	-regulation of cellular protein metabolic process (10^{-2})
-cellular aromatic compound metabolic process (10^{-7})	-gluconeogenesis, glycolysis (10^{-5})	-**rRNA** binding (10^{-1})	**MF**
And with higher P-value:	And with higher P-value:	-structural molecule activity (10^{-1})	-**structural constituent of ribosome** (10^{-4})
-transition metal ion transport (10^{-3})	-transition metal ion transport (10^{-4})	**CC**	-**rRNA binding** (10^{-2})
-**iron** assimilation (10^{-2})	-**iron** assimilation/transport (10^{-3})	-cytosolic **ribosome** (10^{-7})	-**structural** molecule activity (10^{-1})
-iron ion transport (10^{-3})	-vacuolar protein catabolic process (10^{-4})	-small ribosomal subunit (10^{-2})	-**oxidoreductase** activity, acting on paired donors, with incorporation or reduction of molecular oxygen (10^{-1})
-oxidation reduction (10^{-4})	-oxidation reduction (10^{-4})	-cell wall (10^{-2})	-SSU rRNA binding (10^{-1})
-siderophore iron transport (10^{-1})	-siderophore iron transport (10^{-1})		**CC**
MF	**MF**		-**ribosome** (10^{-7})
	-**catalytic** activity (10^{-22})		-cytosolic large/small **ribosomal subunit** (10^{-2})
	-purine (ribo)nucleotide binding (10^{-10})		-ribonucleoprotein complex (10^{-2})
	-ATP binding (10^{-8})		
	-vitamin binding (10^{-4})		

-catalytic activity (10^{-20}) **-** nucleotide binding (10^{-11}) -purine nucleoside binding (10^{-9}) -ATP binding (10^{-8}) **-oxidoreductase** activity (10^{-3}) -ion binding (10^{-1}) -hydrolase and glucosidase activity (10^{-2}) -transmembrane transporter activity (10^{-2}) **CC** **-cell wall** (10^{-8}) -anchored to membrane (10^{-6}) -cytosolic ribosome (10^{-5}) -membrane fraction (10^{-3})	**-oxidoreductase** activity (10^{-4}) -translation elongation factor activity (10^{-2}) -lyase activity (10^{-1}) -metal ion binding (10^{-2}) -transmembrane transporter activity (10^{-2}) **CC** **-cell wall** (10^{-7}) -external encapsulating structure (10^{-7}) -plasma membrane (10^{-7}) -cytosolic ribosome (10^{-5})		

TABLE 3.2: Clusters of genes where Rad9 is localised without affecting transcription

The "P-value" in the parentheses represents the significance level as obtained from the hypergeometric test performed in BiNGO application on Cytoscape platform (see Materials and Methods). The lower the P-value the higher the statistical significance of the clustered groups. The "Total" column includes the clusters derived from all the genes that Rad9 binds without affecting their transcription (as obtained from the Rad9 SC BCS BPS ChIP on chip experiment with P-value=5×10^{-3}). The rest three columns include the clusters which correspond to the three categories of loci where Rad9 localises (Coding, Non Coding and Coding/Non-Coding of the same gene). The clusters are presented in ascending P-value (descending statistical significance). BP: Biological Process, MF: Molecular Function, CC: Cellular Component.

Taking into account the clustering presented in Table 3.2 we conclude that there is a strong bias of Rad9 localisation to genes that are related to metabolic processes of glucose, aminoacids and other carbohydrates, as well as genes related to

regulation of translation and gene expression. Catalytic and oxidoreductase activities are strongly overrepresented among the genes where Rad9 is localised. As far as subcellular localisation is concerned, cell wall and ribosomes are the most profound categories. These gene groups are related to high transcriptional activity, which is discussed in detail in Results Chapter 3.3.5.4. Confirmatory RT experiments for differentially expressed genes have been performed by using RT PCR for selected genes (*YIR042C, YGL212W, YCL027W, YCR089W, YLR102C, YJL166W*) (Figure 3.9B)
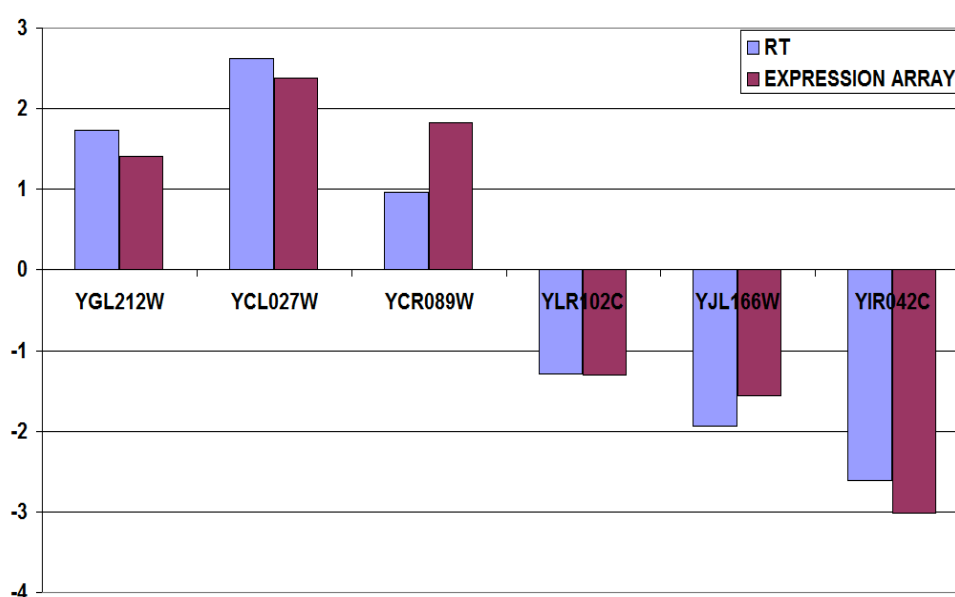
FIGURE 3.9B: Confirmatory RT PCR for *rad9Δ* expression microarray
RNA was extracted from WT and *rad9Δ* cells grown in SC BCS BPS and RT Analysis was performed. Three up- and three downregulated genes were selected and their RNA accumulation was examined. The genes are depicted on the *x*-axis. The results represent the ratio *rad9Δ*:WT as fold over *UBC6* gene RNA accumulation (whose transcription is not changed under these conditions).

We have also performed an overrepresentation functional analysis for the genes whose transcription Rad9 affects but to which is not localised (100 out of 131). These genes were not possible to group into statistical significant categories. Nevertheless, the most apparent groups included the ones for "thiolester hydrolase activity" (GO 16790), "histone binding" (GO 42393), "monovalent inorganic cation transmembrane transporter activity" (GO 15077), "membrane" (GO 16020), "chromatin silencing complex" (GO 5677), "mitochondrial outer membrane translocase complex" (GO 5742).

3.3.4.2.-- Rad9 is localised mostly on protein coding regions of genes, rather than non-coding (intergenic)

The ChIP on chip experiments for Rad9-13Myc SC BCS BPS were performed twice and results were analysed separately. Both gave similar results and conclusions in all of the differential analyses performed. The numbers presented in this analysis correspond to one experiment, unless otherwise mentioned. The methodology, software and algorithms for normalization used in the analysis are presented in detail in Materilas and Methods (Chapter 11: Chromatin Immunoprecipitation on chip). Briefly, after the chromatin immunoprecipitation experiment the sample is hybridized on the Array slide which is scanned and the intensities are visualized using the Integrated Genome Browser (IGB) where a threshold is set in order to obtain the statistically important values (we used a P-value of 10^{-3} or 5×10^{-3}). One of the controls used in our experiments was the localization pattern of His3-9Myc protein which is not nuclear, as well as the input chromatin (not treated with antibody) localization which shows any endogenous bias for localisation of proteins to specific loci. Figure 3.9C shows an example of the visualization of our results.
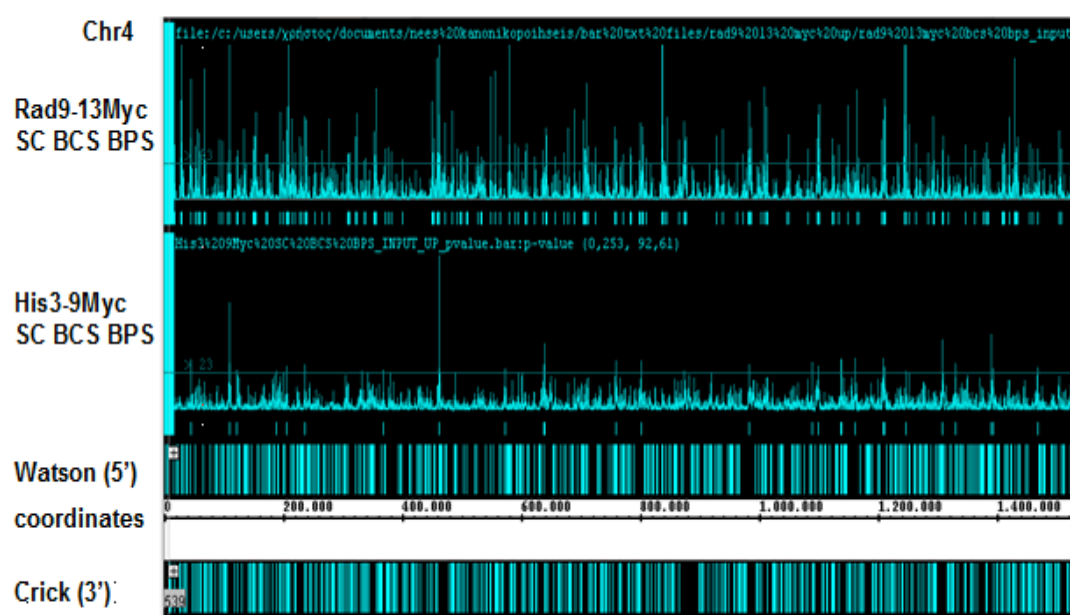
FIGURE 3.9C: Example of visualisation of chromatin immunoprecipitation results

The intensities of the localisation of Rad9-13Myc and control protein His3-9Myc along chromosome 4 are visualized in the IGB browser (in P-value form as -10log10). An enrichment of the protein is depicted as a peak. The horizontal line over the peaks is the selected 10^{-3} threshold in the same scale for both proteins. The genes along Watson and Crick strands are shown as full boxes.

One of the first observations from analyzing our results was that Rad9 had a strong preference to localise to coding regions of genes rather than intergenic. This may be another indication of Rad9 binding on transcriptionally active genes, in addition to what we have mentioned in Results Chapter 3.3.4.1 where we found it on transcriptionally active gene clusters.

The ChIP on chip experiments of Rad9-13Myc in SC under induction conditions (BCS BPS), have showed that approximately 3/4 of the genes where Rad9 localises are related to coding regions (Figure 3.10). The remaining 1/4 is in either non-coding/intergenic regions or in both coding and non-coding areas of the same gene.

We have also performed a ChIP on chip analysis of Rad9 localisation when Aft1 transcription factor is absent, under the same growth conditions, in order to further investigate the effect of Aft1 in Rad9 distribution on the genome, as well as the interdependency between the two proteins, as we shall see in following chapters. When Aft1 is absent, we found Rad9 to be localised to ~20% less targets. When we analysed the binding pattern of Rad9 in this strain, we observed a similar localization with the wt strain (preferably to coding regions), however the non-coding areas where Rad9 was present doubled (Figure 3.10, grey versus black columns). This may be because of Rad9 is present in the same complex as Aft1; in this way, Aft1 could tether Rad9 in coding regions and when absent, part of Rad9 molecules could move to non coding regions.

The presence of Rad9 mostly to coding regions is in accordance with the 6-AU phenotype and the implication to transcription elongation.
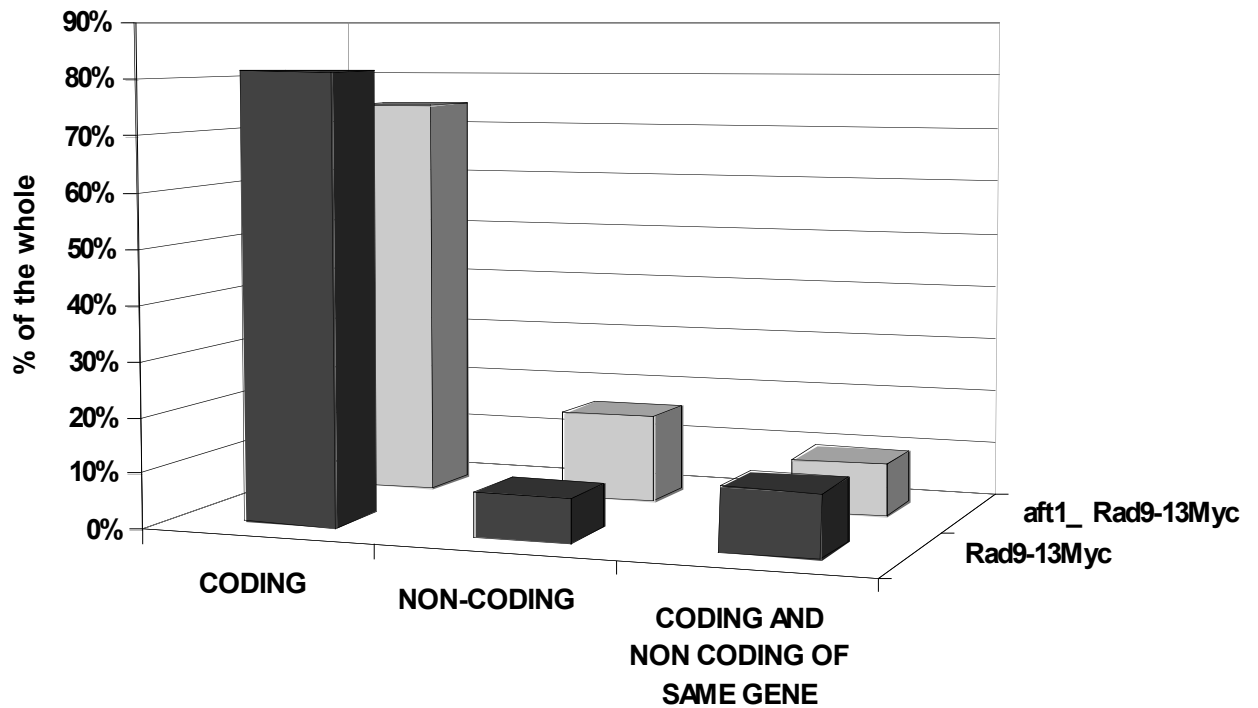
FIGURE 3.10: Distribution of Rad9 localisation sites
After performing the ChIP on chip experiments of Rad9 in wt and in *aft1*Δ strains (z axis), we analyzed the distribution of Rad9 pattern in coding and non-coding areas (x axis). The genes to which Rad9 is localised in each occasion are expressed as percentage of the whole number of genes (*y* axis).

3.3.4.3.-- Rad9 localisation to non-ORF features

We have then investigated whether Rad9 was present on non-ORF features of yeast. We obtained the list of non-ORF elements from Saccharomyces Genome Database (SGD) for each of the chromosomes and examined the binding pattern of Rad9. A snapshot of *Saccharomyces cerevisie* non-ORF features is presented in Figure 3.11. This was used for the comparison to our results.
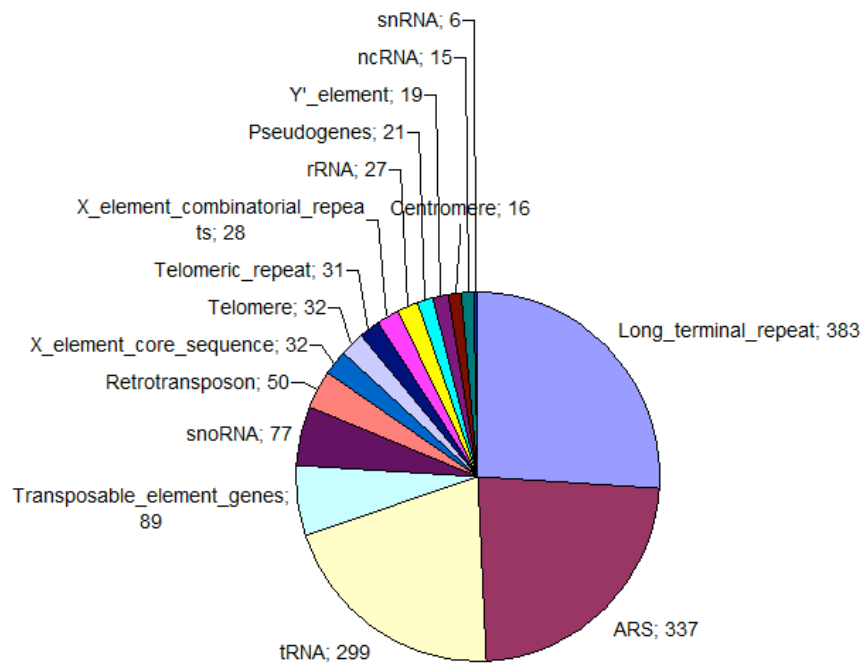
FIGURE 3.11: Snapshot of *S. cerevisiae* non-ORF features
The yeast's non-coding features are presented along with the numbers of their population. ARS: Autonomous Replicating Sequence.

When we compared Rad9 localisation sites on non-ORF areas to the list of the features presented in Figure 3.11, we found that Rad9 was present in all the Left and two Right Telomeres, in 51 out of 89 Transposable element genes, in 29 out of 383 Long Terminal Repeats (LTRs), in 7 out of 27 rRNA genes, in 19 out of 337 ARSs and few tRNA genes. The centromeric sequences are not represented in the Tiling Arrays, so we performed manual ChIP analysis for all 16 yeast centromeres and found that Rad9 was present in more than half of them (9 out of 16, see also Results Chapter 3.3.4.4).

We have also examined the localization of Rad9 to non-ORF elements in the absence of Aft1 transcription factor, in order to reveal any possible effect. A summary of the results is presented in Figure 3.12 and its accompanying table.

Experiment (P=5x10^{-3})	Rad9-13Myc SC BCS BPS		*aft1*Δ Rad9-13Myc SC BCS BPS	
	#	%	#	%
ARS	20/337	5.9	31/337	9.19
Telomeres	15/32	45.3	14/32	43.75
Retrotransposons	27/89	29.77	1/89	1.12

LTRs	24/383	6.1	34/383	8.87	
rRNAs	5/27	16.66	4/27	14.81	

The non-ORF features that were most represented in Rad9 Tiling Arrays are shown in the table, in the presence or absence of Aft1 transcription factor. The results for the Rad9-13Myc experiment are an average of two replicates. The number of the features included in each experiment is presented, along with the corresponding percentage value of the total number of features in each category in the yeast genome. ARS: Autonomous Replicating Sequence; LTR: Long Terminal Repeat.
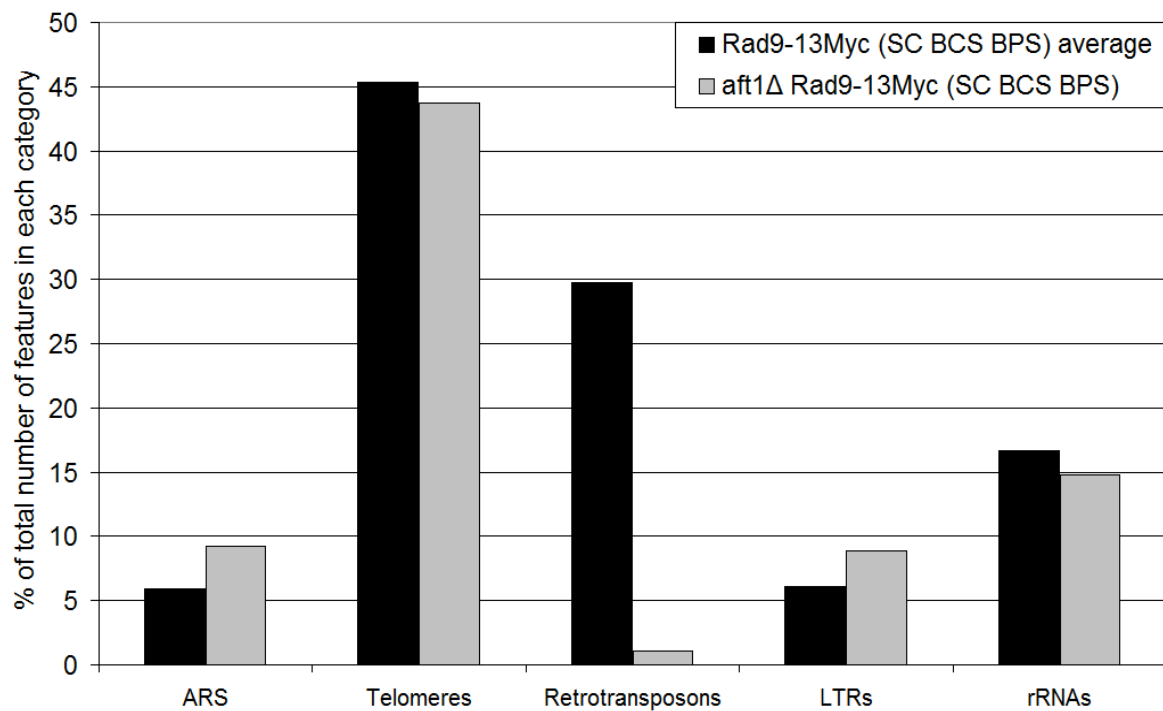
FIGURE 3.12: Rad9 in non-ORF features
The five non-ORF feature categories that were most represented in Rad9 Tiling Arrays are presented in the chart, as percentage of the total number of features in each category in the yeast genome. Rad9 is localised to ~7% of ARSs, ~60% of telomeres, ~30% of retrotransposon genes, ~7% of LTRs and 15-20% of rRNA genes. Data from a single experiment of each strain and growth condition are presented.

We will now focus on the above-presented results in order to evaluate any possible significance.

ARSs

Rad9 was present in a small number of autonomously replicating sequences (ARSs) (~7% of all ARSs in genome). ARSs function as chromosomal replication origins in *Saccharomyces cerevisiae*, and play an essential role in chromosome maintenance (Deshpande and Newlon, 1992; Yang et al., 1999). Each chromosome initiates replication at multiple sites at intervals of 40-100 kb, with each origin regulated to fire only once per cell cycle, mostly around mid-S phase, although

different origins are activated continuously throughout S phase (Raghuraman et al., 2001). Origins also fire in a characteristic order, which appears to be independent of the origin itself, but often correlates with the transcriptional activity of surrounding genes, with early-firing origins associated with active genes, and late-firing origins associated with silent genes (Vujcic et al., 1999).

We wondered whether there was a special connection to a specific category of ARSs (early or late firing) to which Rad9 was localised. We compared the data of (Wyrick et al., 2001), as well as (Yabuki et al., 2002), who mapped the posititions of ARSs, to our own Rad9 localisation data and have found that there is no correlation between localisation of Rad9 and early or late firing type of ARS (almost half were late firing and the other half early). This may mean that Rad9 binding on ARSs is stochastic.

Telomeres

The chromosome ends of *Saccharomyces cerevisiae* are complex mosaics of several different types of telomeric and subtelomeric elements known as X element core sequences, X element combinatorial repeats, telomeric repeats, and Y' elements (Louis et al., 1994). The X element core sequence, a small conserved element of ~475 bp containing an ARS sequence and in most cases an Abf1 binding site, is the only region shared by all chromosome ends. The X element combinatorial repeats, formerly known as subtelomeric repeats or STRs, are located between the X element core sequence and the telomeric end and are usually present as a combination of one or more of several types of smaller elements designated D, C, B, or A. The telomeric repeat is a G-rich terminal sequence of the form $(TG_{1-3})_n$ that is maintained by telomerase (Louis, 1995). The Y' element is a helicase-encoding repetitive sequence found in many but not all subtelomeric regions next to the telomeric repeats, or adjacent X element combinatorial repeats, either as a single copy or tandem repeat of two to four copies. Possible functions of telomeric regions include roles in chromosomal segregation, maintenance of chromosome stability, recombinational sequestering, or as a barrier to transcriptional silencing (Louis, 1995; Louis et al., 1994).

We have found Rad9 present to at least half of the chromosome telomeres in yeast. A role of Rad9 in telomeres has also been proposed in the past (Lazzaro et al., 2008). Lazzaro et al (2008) propose potential mechanisms for the role of Rad9 in

resection inhibition in response to DSBs and uncapped telomeres: Rad9, while bound to the methylated by Dot1 (histone methyl-transferase) H3K79, it interferes with the action of the nuclease(s) or generates a non permissive chromatin configuration, thus inhibiting exonucleolytic processing of DNA. (see also Introduction Chapter 1.3.5). Rad9 may also act as part of an "anticheckpoint" mechanism in telomeres, which most likely exists to prevent healthy telomeres from constitutively activating checkpoint signaling (Michelson et al., 2005).

Table 3.3 summarizes the results of our findings on the localisation of Rad9 to telomeres, in wild type or in *aft1*Δ cells, as well as the localisation of His3 control protein (cytoplasmic). Rad9 showed a preference to localise to Left Telomere ends rather than Right ones, predominantly after grown in minimal medium (SC). His3-9Myc control protein does not seem to have this kind of preference, although the pattern is similar to the one for Rad9-9Myc grown in YPD. Since growth medium does not seem to affect the localization, the pattern observed may have to do with something associated with the 9Myc tagging. In support of this, when Rad9 is tagged with 13Myc (in the presence or absence of Aft1) it seems to have a similar localization pattern mostly to Left telomeres, different from the respective of the Rad9-9Myc in YPD or His3-9Myc in SC BCS BPS). A ChIP on chip experiment with a strain containing 9 or 13Myc tag inserted in a neutral locus should confirm if this is the case. His3-9Myc in SC BCS BPS has lower intensity values than Rad9-13Myc in the same growth conditions (Figure 3.3C), hence the intensity parameter cannot explain the His3-9Myc presence in additional Right telomeres compared to the Rad9 grown in SC BCS BPS. To the best of our knowledge, there is no difference – structural, topological or other- between the Right and Left yeast chromosome ends.

Experiment ($P=5 \times 10^{-3}$) → chromosome	**Rad9-13Myc SC BCS BPS**	*aft1*Δ **Rad9-13Myc SC BCS BPS**	**Rad9-9Myc YPD**	**His3-9Myc SC BCS BPS**
I	L	L	L	L
II	L	L	L	L
III	L	L	L	L
IV	L	L	L, R	L, R
V			R	R

VI	L	L	L	L
VII	L	L	L, R	L, R
VIII	L, R		L, R	L, R
IX	L	L	L	L, R
X	L	L	L	L
XI	L	L	L	L, R
XII	L, R	L	L, R	L, R
XIII	L	L	L	L
XIV	L	L	L	L, R
XV	L	L	L, R	L, R
XVI	L	L	L, R	L, R

Table 3.3: Rad9 localisation on telomeres
Rad9 localisation on Left (L) or Right (R) Telomere end is presented, as well as for His3.

Retrotransposons and LTRs

Rad9 was localised to ~30% of yeast retrotransposons in wild type strains (Figure 3.12). This fact can be of importance, as we will discuss later, since Ty elements are present in loci prone to participate in chromosome rearrangements.

Ty elements (*t*ransposon-*y*east) are DNA sequences that move from one chromosomal site to another via an RNA intermediate. The DNA segment is transcribed into RNA (by host's RNAPII), then reverse-transcribed into cDNA (by the self-encoded reverse transcriptase) which is reinserted into the nuclear genome, usually at a different site. The original retrotransposon stays in place, and the new retrotransposon takes with it copies of any adjacent genes or regions that may have been duplicated during the process, making transposition a major source of gene expansion during genome evolution. The insertion event can also influence genomic evolution by disrupting coding or transcriptional control elements, or by promoting chromosomal rearrangements via homologous recombination (Kim et al., 1998).

There are approximately 50 retrotransposons in the yeast genome, comprising 5 types (Ty1 through Ty5), which represent two distinct groups of eukaryotic LTR-retrotransposons known as Ty1-*copia* (Pseudoviridae) and Ty3-*gypsy* (Metaviridae) elements. Ty1, Ty2, Ty4, and Ty5 are all Ty1-*copia* retrotransposons, whereas the Ty3 retrotransposons are the only representatives of the Ty3-*gypsy* group (Kim et al., 1998). Transposition is a non-random process, and insertion hotspots vary with Ty

element type (Natsoulis et al., 1989). Ty1, Ty2, Ty3 and Ty4 elements tend to integrate near tRNAs or other genes transcribed by RNA polymerase III (Kim et al., 1998), and Ty5 elements preferentially integrate into heterochromatin at telomeres and silent mating loci (Xie et al., 2001).

There are 4 types of LTRs (Long Terminal Repeats) associated with Ty elements: delta (Ty1 and Ty2), sigma (Ty3), tau (Ty4), and omega (Ty5). These LTRs are present in the retrotransposons as flanking direct terminal repeats, and are also scattered about the genome as single LTRs, which have been abandoned through recombination between the two LTRs of a full-length Ty element (Lesage and Todeschini, 2005). Delta sequences are by far the most abundant, at nearly 300, followed by sigma and tau at a few dozen each, and omega at less than 10. These distributions reflect the relative abundances of each of the types of Ty elements with which they are associated.

Since Rad9 was found to be localised to a significant number of retrotransposons and LTRs, we further investigated this result, to see if there was a bias of Rad9 binding to a particular type of retrotransposon/LTR. The results from this analysis are summarized in Table 3.4. We didn't find Rad9 to have a significant tendency to localise to a particular type of these elements as compared to the His3 control protein respective pattern.

Rad9 grown in YPD or in SC BCS BPS was localised to ~50% of retrotransposons. Nevertheless, the replicate experiment of Rad9 in SC BCS BPS showed that Rad9 was localised to much less retrotransposons, comparable of the situation of *aft1*Δ Rad9-13Myc SC BCS BPS. Rad9 grown in SC BCS BPS was localised to ~25% of yeast retrotransposons (as averaged from two biological replicates). This could mean that Rad9 localisation to these elements is not quite specific and is dependent on factors that are not yet established. However, it seems that in the absence of Aft1 transcription factor, Rad9 preference to localise to retrotransposons is diminished. This means that Aft1 is important for Rad9 localisation to these loci which are prone to chromosome rearrangements (Figure 3.12) We speculate that Rad9 plays a safeguarding role in these areas, protecting the cell from possible future DNA damage events by being in the adjacent area ready to act (in a rapid DNA damage response). Aft1-dependency could further highlight the implication of this transcription factor to DNA damage which is in agreement to previous reports (Berthelet et al., 2010).

Experiment (P=5x10^{-3})	Rad9-13Myc SC BCS BPS		Rad9-13Myc SC BCS BPS (replicate)		*aft1*Δ Rad9-13Myc SC BCS BPS		Rad9-9Myc YPD		His3-9Myc SC BCS BPS	
LTRs	#	%	#	%	#	%	#	%	#	%
Ty1	18/297	6.06	13/297	4.37	30/297	10.1	18/297	6.06	23/297	7.74
Ty2	8/45	17.77	1/45	2.22	0/45	0	8/45	17.77	4/45	8.88
Ty3	0/44	0	0/44	0	0/44	0	3/44	6.81	0/44	0
Ty4	0/38	0	2/38	5.26	2/38	5.26	0/38	0	0/38	0
Ty5	3/9	33.33	2/9	22.22	2/9	22.22	1/9	11.11	1/9	11.11

TABLE 3.4: Rad9 localisation to LTRs
The analyzed results are categorized into the 5 different types of Ty elements and depicted as both numbers and percentage of the total number of elements in each category. For this analysis, we took into account only the "pure" Ty categories (that had elements of only one type). Data from a single experiment of each strain and growth condition are presented.

3.3.4.4.-- Rad9 is localised to the centromeres

It is known that DNA damage checkpoint proteins are localised to centromeres in mammalian systems reviewed by (Shimada and Komatsu, 2009). Aft1 has also been found in these loci interacting with centromeric proteins, thus it may be implicated to genome stability (Hamza and Baetz, 2011; Measday et al., 2005) (see also Introduction Chapter 5.1.3). A reasonable question is whether Rad9 is also present in centromeres as an Aft1-interacting protein, or as part of the DNA damage checkpoint group of proteins.

Due to the fact that Affymetrix *S.cerevisiae* 1.0R Tiling Arrays do not include the centromeric regions (because of the high A+T content), we designed primers for each of the 16 yeast chromosomes and performed manual ChIP experiments to investigate Rad9 localisation under induction conditions.

Lee et al. (2002) have determined how most of the transcriptional regulators encoded in the eukaryote *Saccharomyces cerevisiae* associate with genes across the genome in living cells. Aft1 and Mac1 were among the transcription factors included in the study and they also investigated their binding pattern on the centromeres. In the present study, in addition to Rad9, we have also investigated Mac1 and Aft1 localisation to centromeres.

Our results are summarized in Figure 3.13 and in its accompanying table, where we show the distribution of Rad9 on the centromeres, along with Aft1 and Mac1 transcription factors.
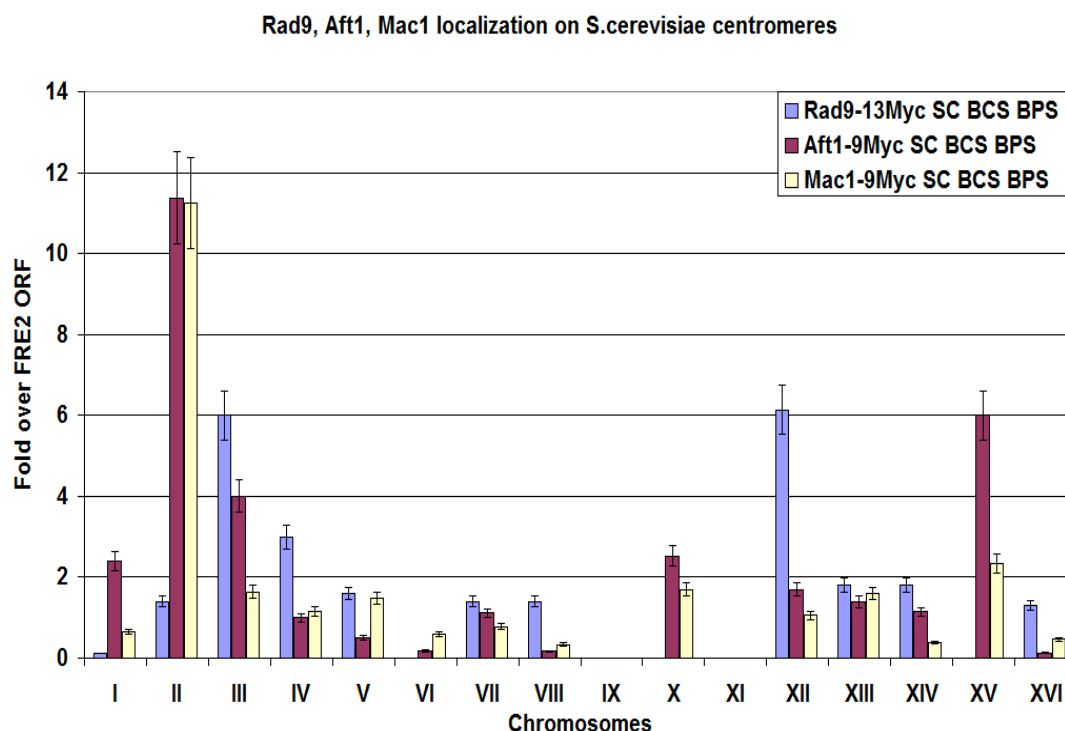
FIGURE 3.13: Rad9, Aft1 and Mac1 localisation on centromeres
Manual ChIP experiments were performed at least as duplicates for each of the 16 yeast chromosomes (*x* axis). Normalization was performed firstly over INPUT and secondly by measuring the binding of each protein on *FRE2* coding region, where binding of these proteins is minimal and dividing to their enrichment in each case. The same binding pattern was also obtained after normalizing over *PHO5* coding region and the results were similar. Due to high content in AT nucleotides in centromeric areas, some of the primers were not functional in Real Time PCR (chr IX and XI).

CEN	I	II	III	IV	V	VI	VII	VIII	IX	X	XI	XII	XIII	XIV	XV	XVI
Rad9		+	++	+	+		+	+				++	+	+		+
Aft1	+	++	++	Lee		Lee	+			+	Lee	+ Lee	+	+	++	
Mac1		++	+	Lee	+ Lee					+			+		+	

Lee et al. (2002) in their study found Aft1 localised to chromosomes IV, VI, XI (where we found minimal or no enrichment) and XII. We confirmed Aft1 localisation to additional centromeres, while it is probable that it is localised to all of the centromeres and may not be able to be detected because of the nature of the loci (AT rich, hard to design functional primers). We can see that Rad9 and Aft1 coincide in centromeres of chromosomes II, III, VII, XII, XIII and XIV. Furthermore, Rad9 localised to ten out of sixteen centromeres. Rad9 presence in centromeres is in

agreement with results from mammalian systems where DNA damage checkpoint proteins were found in centromeres (including Rad9's partial homolog Brca1) reviewed by (Shimada and Komatsu, 2009). Thus, Rad9 may have a role in preservation of genome integrity, in co-operation with Aft1, in centromeric regions.

Furthermore, Aft1 recruitment was also checked on centromeres CEN3, CEN12 and CEN15 by manual ChIP in the presence or absence of Rad9 and we found that the Aft1 binding was not changed (data not shown). Thus, it seems that Rad9 does not affect Aft1 recruitment to all tested targets.

3.3.5.-- Study of Rad9 localisation regions on the genome

We have checked whether Rad9 has a consensus binding sequence but we could not find any (N. Papanikolaou). After establishing the binding of Rad9 on genomic regions, we sought to investigate what characterizes the Rad9 localisation sites. Is it the transcriptional activity? Does Rad9 prefer to localize to DNA damage-prone loci? Is it the nucleotide content of the sequences? Does it follow special epigenetic marks?

3.3.5.1.-- Rad9 is recruited to GC-rich regions of the genome

Considering that specific areas of the genome, which are rich in GC nucleotides tend to be more active, having a more extended chromatin conformation than AT-rich isochores (Dekker, 2007; Gilbert et al., 2004b; Yokota et al., 1997), we wanted to examine if that was the case with Rad9 as well. To address this question we obtained the sequences where Rad9 was bound in the genome, extracted their GC-content information and compared to a randomized group of sequences of the same number and length (see Materials and Methods). What we found was that the median GC content of the regions where Rad9 was bound was ~43%, while the respective value from the randomized sequences was 38% (t-test P-value of 10^{-127}) (Figure 3.14 and Table 3.5). This shows that Rad9 has a tendency to localise to areas rich in GC nucleotides and subsequently areas that are more active. When the replicate experiment is incorporated, the averaged median GC content for Rad9 is 41%.
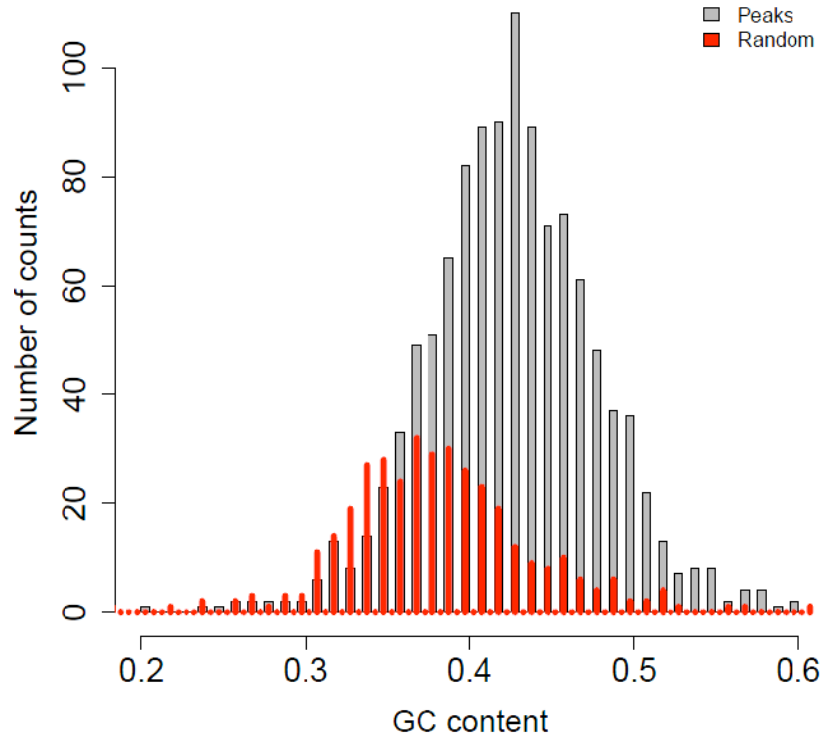
FIGURE 3.14: Rad9 localises to GC-rich regions
After obtaining the sequence content of the genomic areas where Rad9 was localised (in SC BCS BPS or YPD), we calculated the GC percentage. We compared this value to the one obtained by a randomized group of sequences of the same number and length (see Materials and Methods). The median of GC content is presented in *x* axis and the median of sequences with the corresponding content on *y* axis. Rad9 data information is plotted with grey colour and randomized information with redx. Results were obtained from one experiment.

	GC median: experiment	GC median: random
Rad9-13Myc SC BCS BPS P=10^{-3}	0.43	0.38
*aft1*Δ Rad9-13Myc SC BCS BPS P=10^{-3}	0.37	0.38
Aft1-9Myc SC BCS BPS P=10^{-3}	0.41	0.38

TABLE 3.5: GC Median values

When we performed the same kind of analysis for Aft1 ChIP on chip experiment, a similar pattern to the one in Figure 3.14 was observed, with Aft1 binding to GC-rich sequences with a median of 41%. On the other hand, we have found that this preference of Rad9 to localize to GC-rich regions is Aft1-dependent, since when Aft1 is absent, Rad9 does not exhibit the particular binding bias (Figure 3.15). In fact, the median of GC content was 37%, almost the same as the randomized sequences.
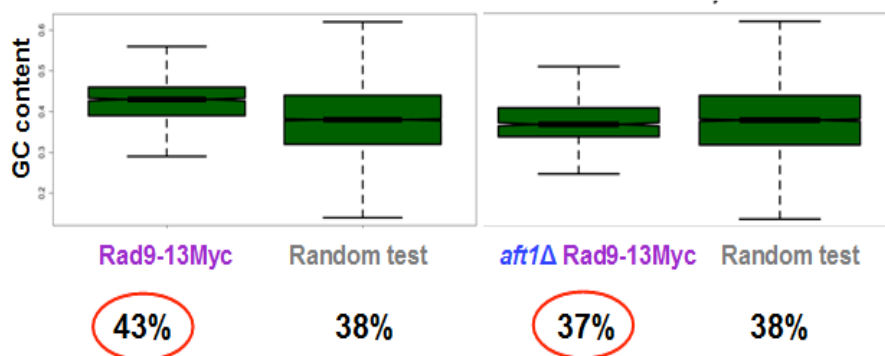
FIGURE 3.15: Rad9 localisation to GC-rich regions is Aft1-dependent
After obtaining the sequence content of the genomic areas where Rad9 was localised (in SC BCS BPS) in the presence or absence of Aft1, we calculated the GC percentage. We compared this value to the one obtained by a randomized group of sequences of the same number and length (see Materials and Methods). The median of GC content is presented for the two experiments and the corresponding random tests. Results were obtained from one experiment.

3.3.5.2.—Rad9 has a binding bias to genes longer than the average

We next wondered whether Rad9 had a localisation preference to genes of specific size. To address this question, we grouped yeast genes into 20 bins depending on their size and compared to Rad9 binding pattern from the ChIP on chip experiments to examine how many statistically significant peaks were included in each bin (Figure 3.16). Furthermore, we performed this analysis for Rad9 in *aft1Δ* cells, for Aft1 transcription factor, as well as for the His3 control protein. We compared our results to the distribution of all yeast genes depending on their size.

We observed that Rad9 showed a binding bias to genes longer than 1800bp. Furthermore, when Aft1 transcription factor was absent, there was a shift to even longer genes (Figure 3.16). Aft1 also showed a binding bias to longer genes (as well as His3). It has been shown that genes with long ORFs are connected to higher H4 acetylation in *set2Δ* cells (deficient of H3 methylation) (Li et al., 2007b) and this could have been a mark which Rad9 follows in its recruitment to the chromatin. As we will see in a following chapter this was not the case for Rad9.

Furthermore, we have observed that there was a particularly high percentage of Rad9 localisation to very long genes (>6000bp) (Figure 3.16). We have analysed these genes and tried to find if there was an overrepresentation of particular GO groups (regarding molecular function-MF, biological process-BP or subcellular localisation-CC), by performing Cytoscape Analysis (see Materials and Methods). We

have found that, of the 52 genes included in this category, ~40% encoded for proteins localised in mitochondrion, with an overrepresentation of groups for fatty acid biosynthesis, lipid kinase activity and acetyl-coA carboxylase activity. In addition, six out of the 52 genes were unique for their molecular function (mainly biosynthetic enzymes: *CYR1, FAS1, URA2, FAB1, GLT1, ACC1*). This localisation of Rad9 on genes related to energy production is important, since it shows a connection to vital cellular processes. This particular connection may also be related to Rad9-Aft1 interaction, since iron metabolism through Aft1 is strongly connected to mitochondria (see also Introduction Chapter 5.1.2). In addition, we have found that Aft1 is localised to 43 out of the 52 long genes. We have also found that from the list of the 304 genes whose transcription seems to be affected in *aft1Δ* cells (as obtained by Shakoury-Elizeh et al., 2004) only *LSC1* (*YOR142W*; alpha subunit of succinyl-CoA ligase, which is a mitochondrial enzyme) was included in the list of the 52 long genes. The above results show that the presence of Aft1 on these long genes is not related to the Aft1-regulon.
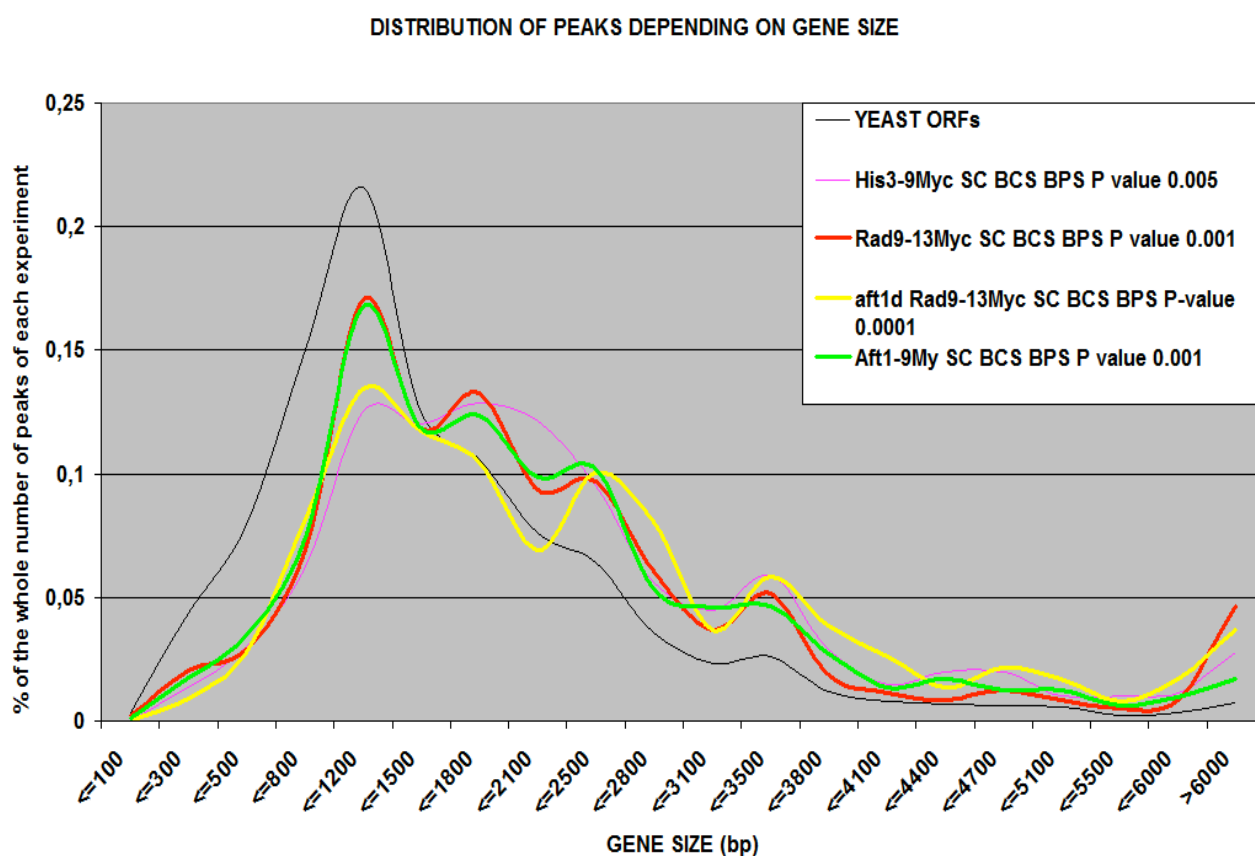
FIGURE 3.16: Rad9 has a binding bias to larger than the average size of genes
S. cerevisiae genes were grouped in 20 bins depending on their size (*x* axis). We have then examined how many of the peaks from each experiment fit each of the bins. The result is expressed as percentage of the total number of peaks from each experiment. The distribution of all yeast genes is also plotted with black line.

3.3.5.3.-- Frequency of Rad9 binding sites. Distribution of Rad9 on chromosomes.

Having analysed the Rad9 binding pattern in relation to the size of genes, we wondered whether there was a special bias regarding the frequency with which Rad9 localises to its targets, as well as how Rad9 localisation pattern is distributed on chromosomes.

First we obtained the annotated Rad9 localisation peaks and we examined every how many base pairs per chromosome they appear. We have found that there is one peak (localisation site) of Rad9 every 10-12000 base pairs. In the case where Aft1 is absent, Rad9 is bound less frequently (every 15-18000 base pairs). In *aft1Δ* strain we observed that in chrI and chrIV, Rad9 is present even less frequently (every 30-37000 base pairs) (Figure 3.17). The same analysis was performed for Aft1 transcription factor which showed a similar pattern to Rad9, except for chromosomes IV and XIII in which the peaks were less frequent.
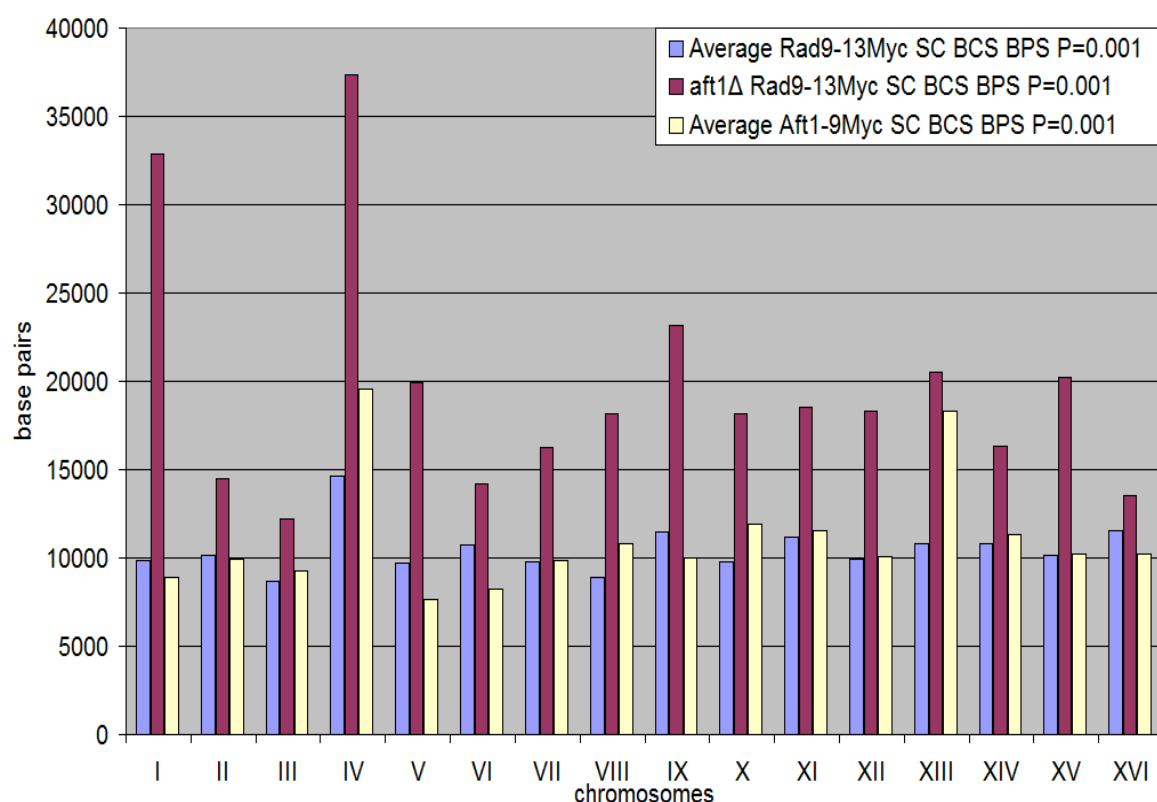
FIGURE 3.17: Frequency of Rad9 and Aft1 localisation sites (peaks)
The frequency of Rad9 localisation sites is presented as an average of every how many base pairs there is a peak present (*y* axis) in each of the sixteen yeast chromosomes (*x* axis) and in strains where Aft1 is present (blue columns) or absent (red columns). The average obtained by two replicates is plotted for Rad9 and Aft1 proteins. Aft1 is shown in yellow.

We then examined if there was a connection between Rad9 localisation sites and the size of the chromosomes. For that reason, we plotted the number of peaks (as percentage of all peaks) for each chromosome. We also did the same analysis for Aft1 transcription factor. The results are presented in Figure 3.18. What we can see is that Rad9 and Aft1 have a similar distribution on the chromosomes. Furthermore, the number of peaks is generally relative to the chromosome size (see chromosome sizes in smaller graph-green columns). When Aft1 is absent, Rad9 localisation sites were found to be proportionally more in chrII and chrXVI and less in chrI and chIV (red columns compared to blue ones). As in Figure 3.17, it was again obvious that in chromosome IV, the peaks were less than expected, regarding the chromosome size.
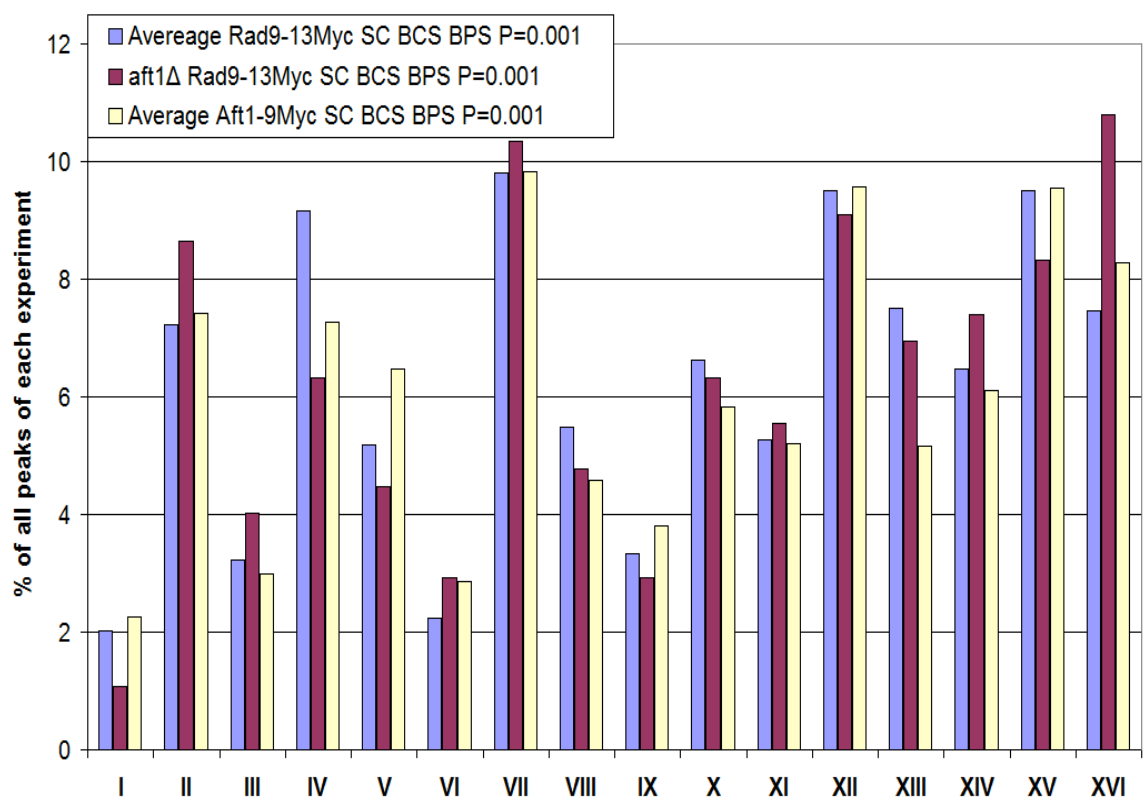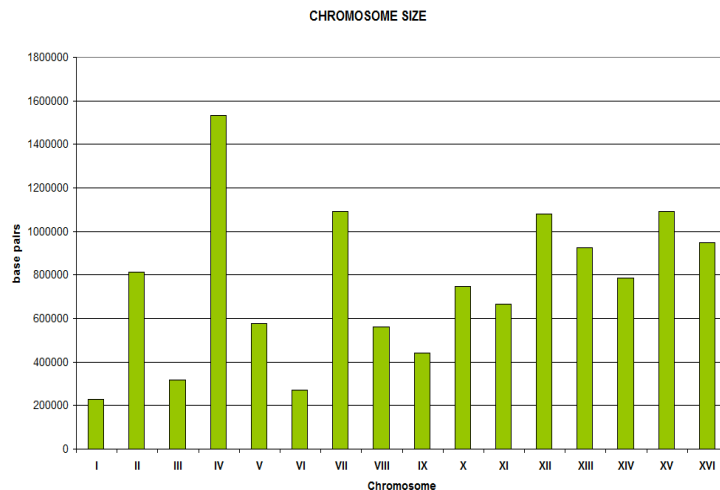
FIGURE 3.18: Distribution of Rad9 and Aft1 on chromosomes
The distribution of Rad9 and Aft1 localisation sites are presented as percentage of all the peaks of each experiment, distributed in each chromosome. The average obtained by two replicates is plotted for Rad9 and Aft1 proteins. In the smaller graph, the yeast chromosomes are plotted according to their size (in base pairs).

Based on the results deduced by Figures 3.17 and 3.18, we wondered if there was a specific characteristic in any of the chromosomes, such as different percentage of GC content compared to average, which would be a notion towards the activity of the genes that they contain, since higher GC content is connected to higher transcriptional activity. We examined the GC-content of each of the chromosomes, but it was of average value to all 16 chromosomes (38-39%).

3.3.5.4.-- Rad9 is localised to the most highly active yeast genes in an Aft1-dependent manner

After the indications of a Rad9 binding bias to regions which are highly transcriptionally active (GC-rich loci, binding to coding rather than intergenic regions, binding to gene groups that are highly active such as the ones for aminoacid biosynthesis or metabolism), we sought to examine this relation in depth.

For that reason, we grouped yeast genes into 6 groups depending on their activity based on our expression microarray experiments performed in the same growth conditions as the ChIP on chip experiments. We then compared these groups to the statistically significant localisation sites obtained from the ChIP on chip experiments, in order to see how they fit into each of the groups (Figure 3.19).
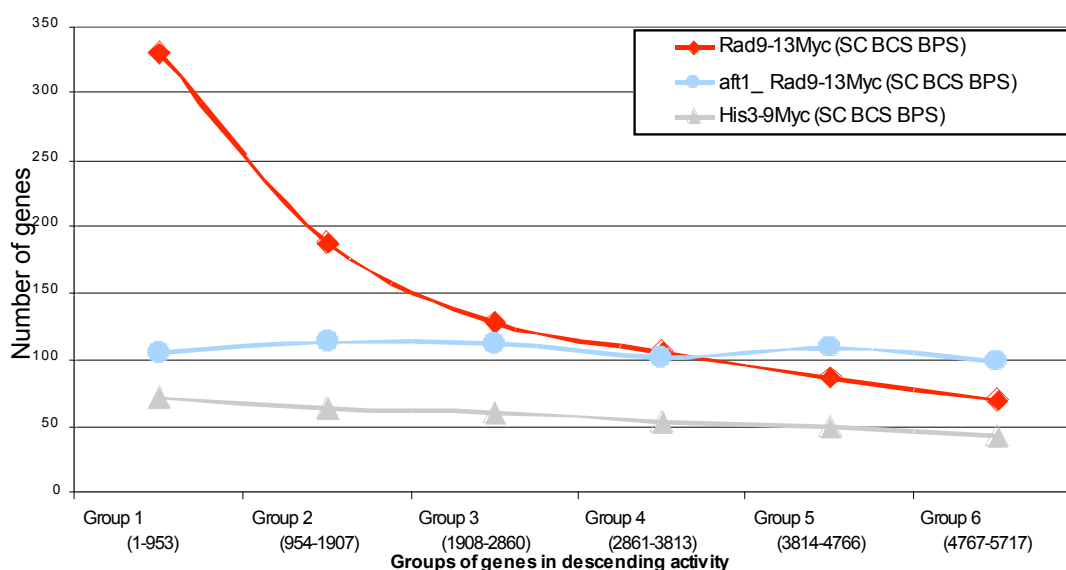
FIGURE 3.19: Rad9 is localised to the most highly active yeast genes in an Aft1-dependent manner

Yeast genes were grouped in 6 groups (*x* axis), containing ~1000 genes each, in descending transcriptional activity in SC BCS BPS growth conditions (obtained by our expression microarrays experiments). We then compared the localisation sites of Rad9 (coding and/or non-coding), in the presence or absence of Aft1 (red and blue line respectively), and plotted the number of genes that fit each group (*y* axis). His3 control protein is shown in grey.

This analysis showed us that Rad9 has a strong binding bias to highly active genes. This was further reinforced by the fact that this Rad9 binding bias is even stronger to the most highly active genes (Figure 3.19B). Similar Rad9 binding pattern was also observed in our ChIP on chip experiment with cells grown in rich medium (YPD). What was striking was the fact that this bias was completely abolished in the absence of Aft1. Thus, Aft1 plays a vital role to the binding of Rad9 to highly active genes.
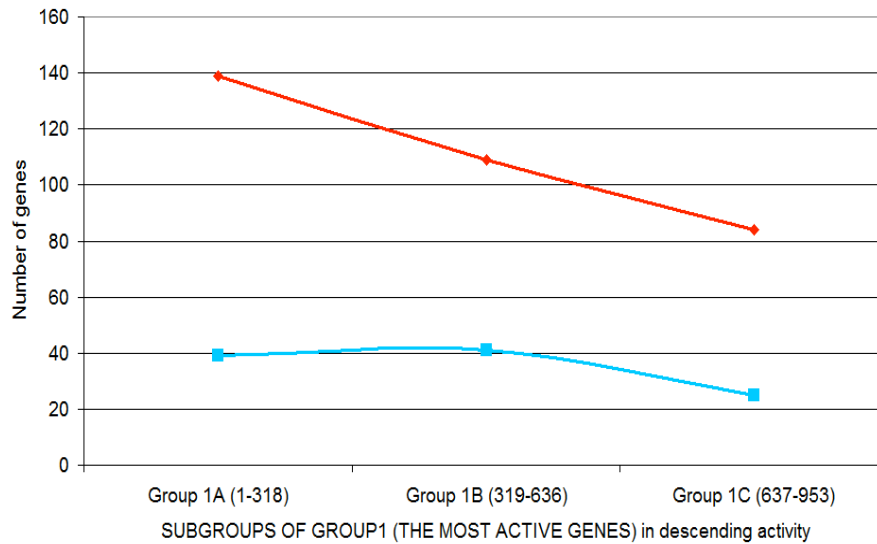
FIGURE 3.19B: Rad9 has a strong binding bias within the most highly active genes
We divided Group1 (see Figure 3.19 legend) into 3 subgroups and performed the same analysis for Rad9 in WT (red line) and *aft1Δ* (blue line).

The same analysis described in Figures 3.19 and 3.19B was performed for the overlapping targets between Rad9 and Aft1. The results showed that the common targets between Rad9 and Aft1 exhibit an even stronger binding correlation to the most highly active genes (Figures 3.19C-3.19D).
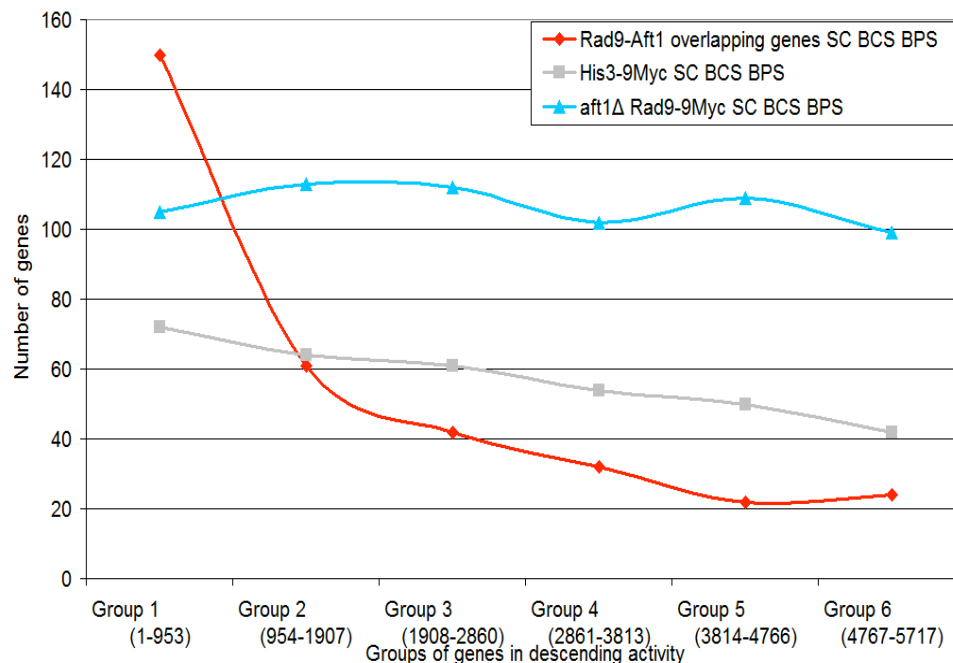
FIGURE 3.19C: Rad9 and Aft1 overlapping targets show a strong binding bias to the most highly active genes in an Aft1-dependent manner
The analysis described in the legend of Figure 3.19 was performed on the common targets of Aft1 and Rad9.

Rad9-Aft1 overlapping genes in GROUP1
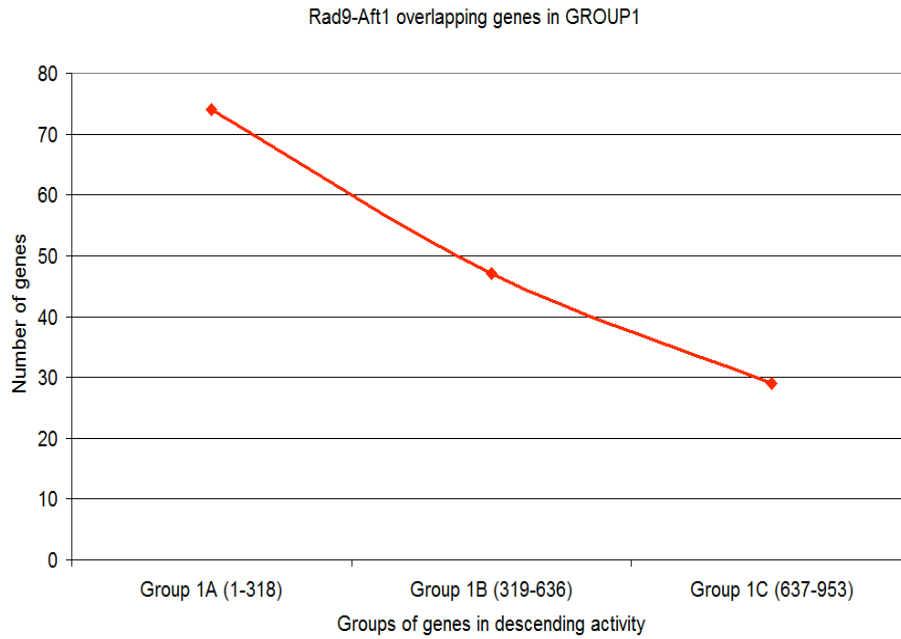
FIGURE 3.19D: Rad9-Aft1 common targets have a strong binding bias within the most highly active genes
We divided Group1 (see Figure 3.19 legend) into 3 subgroups and performed the same analysis for the overlapping targets of Rad9 and Aft1.

Subsequently, we wanted to see what was the connection between Aft1 binding pattern and the activity of these loci, so we performed the same kind of analysis for the Aft1 ChIP on chip experiment. Furthermore, we also performed a genome-wide analysis of Aft1 binding pattern when Rad9 was absent and compared the outcome. The result of the analysis is presented in Figure 3.20.
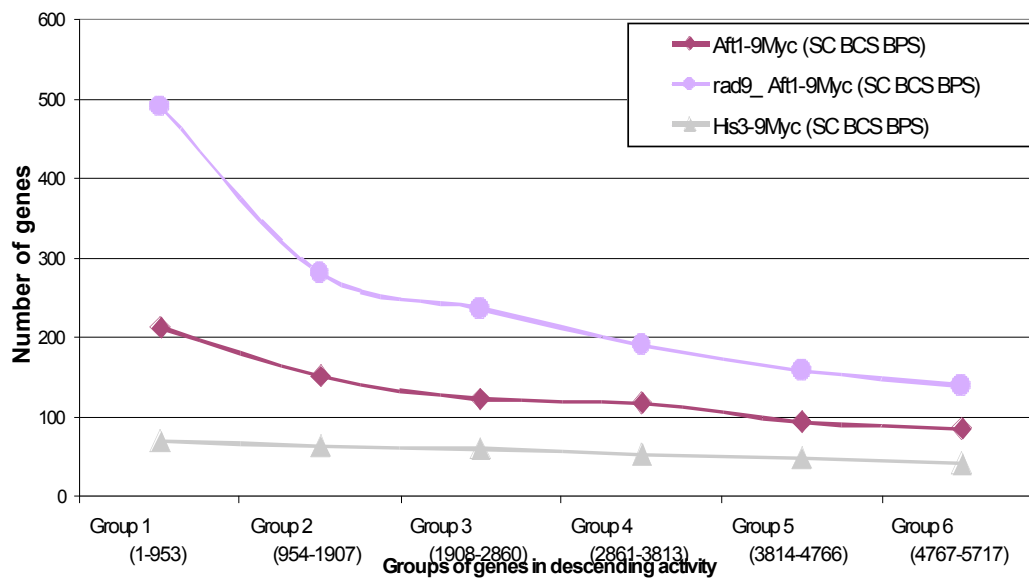
FIGURE 3.20: Aft1 is localised to highly active yeast genes

111

Yeast genes were grouped in 6 groups (*x* axis), containing ~1000 genes each, in descending transcriptional activity in SC BCS BPS growth conditions (obtained by our expression microarrays experiments). We then compared the localisation sites of Aft1, in the presence or absence of Rad9 (brown and purple line respectively), and plotted the number of genes that fit each group (*y* axis). His3 control protein is shown in grey.

In Figure 3.20 we show that Aft1 also has a tendency to bind to highly active genes, though not in the level that Rad9 does. Furthermore, it seems that Rad9 may have a mild inhibitory effect in Aft1 binding on active regions, since when it is absent, there is a 5% increase of Aft1 binding to the first group of genes (most active).

We will further investigate the connection between Rad9 and transcriptionally active genes in Results Chapter 3.3.6.6.

3.3.5.5.-- Rad9 and meiotic recombination hotspots

The studies by three individual groups (Buhler et al., 2007; Gerton et al., 2000; Robine et al., 2007) provided a comprehensive mapping of the meiotic recombination hotspots and hotORFs i.e. genomic regions that the probability of DSB formation is 100–1000 times higher than the average. As mentioned in the Introduction, hotspot activity is primarily determined by local features of chromatin structure, notably absence of nucleosomes (Introduction Chapter 1.4.2).

Hotspots and hotORFs have a significant overrepresentation of metabolic and aminoacid biosynthetic genes as well as ionic homeostasis genes. These groups of genes are also overrepresented in our experiments for Rad9. This fact led us to do a comparison between the above-mentioned studies (Buhler et al., 2007; Gerton et al., 2000; Robine et al., 2007) and our own, to see if there is a coincidence of Rad9 binding sites and of meiotic recombination hotspot regions. We first made a rough comparison between Rad9 localisation pattern and the mapped meiotic recombination hotspots and noticed that eventhough our experiments were performed in vegetative cells, such a coincidence roughly existed (Figure 3.21).
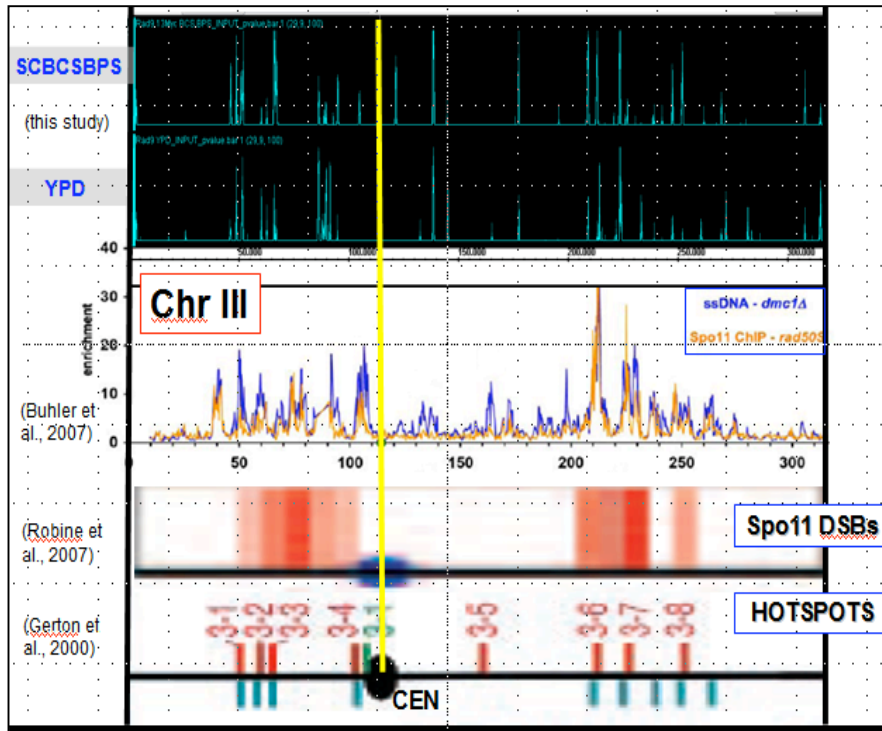
FIGURE 3.21: Rad9 binding pattern in vegetative cells follows the loci which are hotspots for meiotic recombination

On top of the figure, the binding pattern of Rad9 in chromosome III from our ChIP on chip experiments (grown in SC BCS BPS or in YPD) is visualized through Integrated Genome Browser (see Materials and Methods). The peaks are the areas where Rad9 is enriched. Below, there are the areas of meiotic recombination hotspots as mapped by three different studies (Buhler et al., 2007; Gerton et al., 2000; Robine et al., 2007). Similar overlapping pattern we have also observed for the rest chromosomes.

We have then examined in detail the relation of Rad9 with the hotspots of meiotic recombination in WT and *aft1Δ* cells. Furthermore, we performed the same analysis for the Rad9-Aft1 overlapping targets and for the Aft1 localisation sites (Figure 3.22).
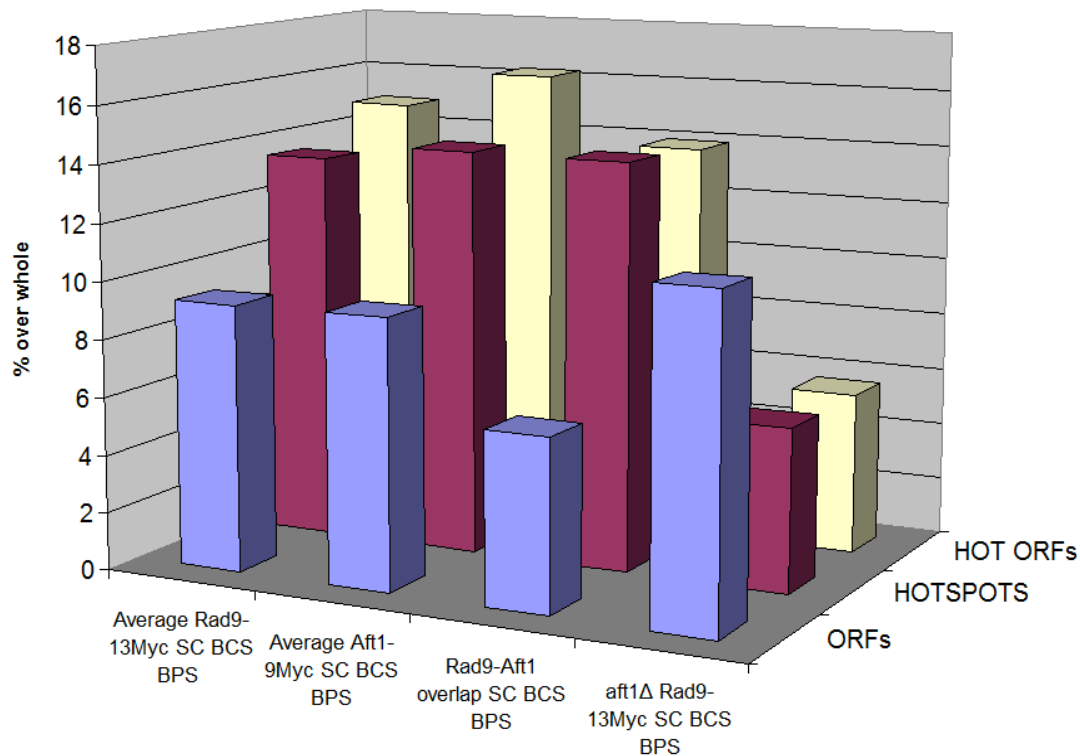
FIGURE 3.22: Rad9 is localised to hotspots and hotORFs of meiotic recombination in an Aft1-dependent manner

The list of mapped hotspots and hotORFs of meiotic recombination (obtained by Gerton et al., 2000), was compared to our results from Rad9 ChIP on chip experiments in the presence or absence of Aft1 transcription factor as well as the Rad9-Aft1 overlapping targets and the Aft1 targets alone. Rad9 and Aft1 common targets as obtained by two replicates were used in this analysis. We then plotted the percentage of the whole number in each case. To evaluate the significance of Rad9 binding to these loci, we also plotted the number of yeast ORFs from each experiment (as percentage of the whole number of yeast ORFs-blue columns).

In Figure 3.22 it is shown that Rad9 is localised to hotspots and hotORFs of meiotic recombination with high probability (vs ORF, blue column)- it is localised with higher percentage to these areas compared to the percentage of the overall targets in each experiment. Furthermore, that this binding bias is grossly diminished when Aft1 is absent. Thus, Rad9 localisation to meiotic recombination hotspots is Aft1-dependent. Meiotic recombination hotspots are prone to DNA damage and characterised by high content in GC which is in agreement to our previous results for Rad9 localisation pattern. Our results are indicative of Rad9 presence to DNA damage-prone chromatin. This is in accordance to the fact that Rad9 is localised to highly transcribed areas where the probability of a DSB occurrence is higher than the average (Kim et al., 2007).

3.3.5.6.-- Rad9, chromatin modifications and transcription under the scope of average gene analysis; dependence on Aft1. Aft1 average gene analysis; dependence on Rad9.

We sought to investigate whether there were further characteristics or epigenetic marks on chromatin which may drive Rad9 localisation to the genome. Genome-wide analyses for the distribution of RNAPII have been performed by other groups (Bermejo et al., 2009; Sun et al., 2009), as well as for methylation and acetylation of histone residues and for H3, H4 histone occupancy (Pokholok et al., 2005).

When we compared the RNAPII genome-wide distribution as mapped by Bermejo et al. (2009), we found that Rad9 has a partial overlapping pattern with RNAPII (Figure 3.23I). Most of this overlap is lost when Aft1 is absent (Figure 3.23II). This is in accordance to Rad9 localisation bias to active genes, but since the overlapping is not complete, it seems that the activity state of the chromatin is not the sole factor that affects Rad9 binding. When we performed the same comparison for the *aft1Δ* cells, the pattern became less overlapping (also in accordance to what we have observed in Figure 3.19).

FIGURE 3.23: Rad9 localisation on chromosome III in comparison to RNAPII binding pattern in WT and *aft1Δ* cells grown in SC BCS BPS

We obtained the signal log ratio values for RNAPII localisation pattern on chromosome III by Bermejo et al. (2009) as shown in the Rpb3 IP panels. I) We compared this pattern to Rad9 signal log ratio values, visualized as blue peaks or valleys by the Integrated Genome Browser. The first 3×10^5 base pairs of chromosome III are visualised. II) The same analysis was performed for *aft1Δ* Rad9 signal log ratio values.

As I commented in the Introduction, Rad9 recognizes H3K79 methylated histones after DNA damage through its Tudor domain. We sought to investigate whether this histone mark plays a role in Rad9 localisation pattern on the genome under non DNA damage induced conditions as well. Pokholok et al. (2005) have studied the genome-wide acetylation and methylation distribution in yeast and found that nucleosome methylation correlates with transcriptional activity. They found that, on average, the H3K79 trimethylation (H3K79me3) peaks within the transcribed regions of genes (ORFs), forming a bell-shaped curve. In general, this methylation mark occurs in ~90% of all histones and furthermore it is associated with telomeric silencing control in yeast (Ng et al., 2003; van Leeuwen et al., 2002), but global ChIP profiles of dimethylated H3K79 in *Drosophila* have linked this modification to active transcription (Schubeler et al., 2004).

We have observed that Rad9 is localised mostly to ORFs (see Results Chapter 3.3.4.2 and Figure 3.10), and we sought to compare this pattern to different types of methylation, acetylation and H3-H4 histones occupancy. To address this question, we have performed average gene analysis (see Materials and Methods) with which we obtained the relative occupancy of Rad9 protein from our ChIP on chip experiments and fitted the results across a model "average" gene. Subsequently, we compared our data to other relevant studies (Pokholok et al., 2005) (Figure 3.23A). By this analysis, we reconfirmed Rad9 localisation pattern to coding rather than non-coding regions and observed a bias to the 3' end. Under the examined conditions, Rad9 localisation pattern was more similar to H3K36me3 and H3K4me patterns rather than the H3K79 trimethylation mark (the one recognized by its Tudor domain). When Aft1 was absent (Figure 3.23Aii), Rad9 localisation pattern showed a shift towards the 3' end of the average gene (and 3'-UTR region) and lost the bell shaped pattern that was characteristic in the presence of Aft1 (Figure 3.23Ai).

When we compared the localization pattern of Aft1 on the average gene in the presence or absence of Rad9 (Figure 3.23Ax versus 3.23Axi respectively), we found

that Rad9 did not have an effect in Aft1 localisation pattern. This is in agreement to the Rad9-Aft1 relation that we have established so far.

i) Rad9-13Myc

ii) *aft1Δ* Rad9-13Myc

iii H3K9ac

iv H3K14ac

v H4ac

vi H3K4me1/me2/me3

vii H3K36me3

viii H3K79me3

ix H3 and H4 histones

x) Aft1-9Myc

xi) rad9Δ Aft1-9Myc
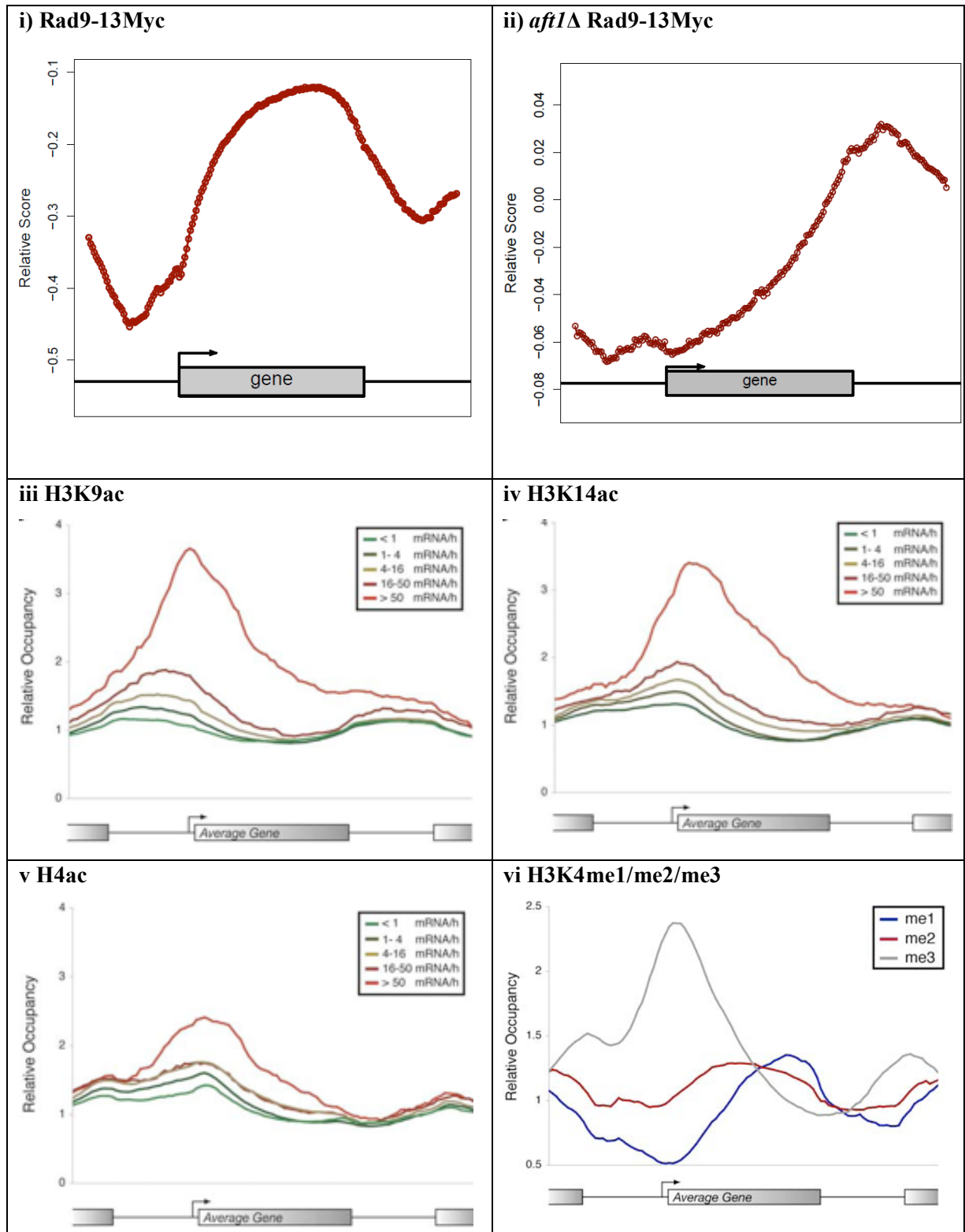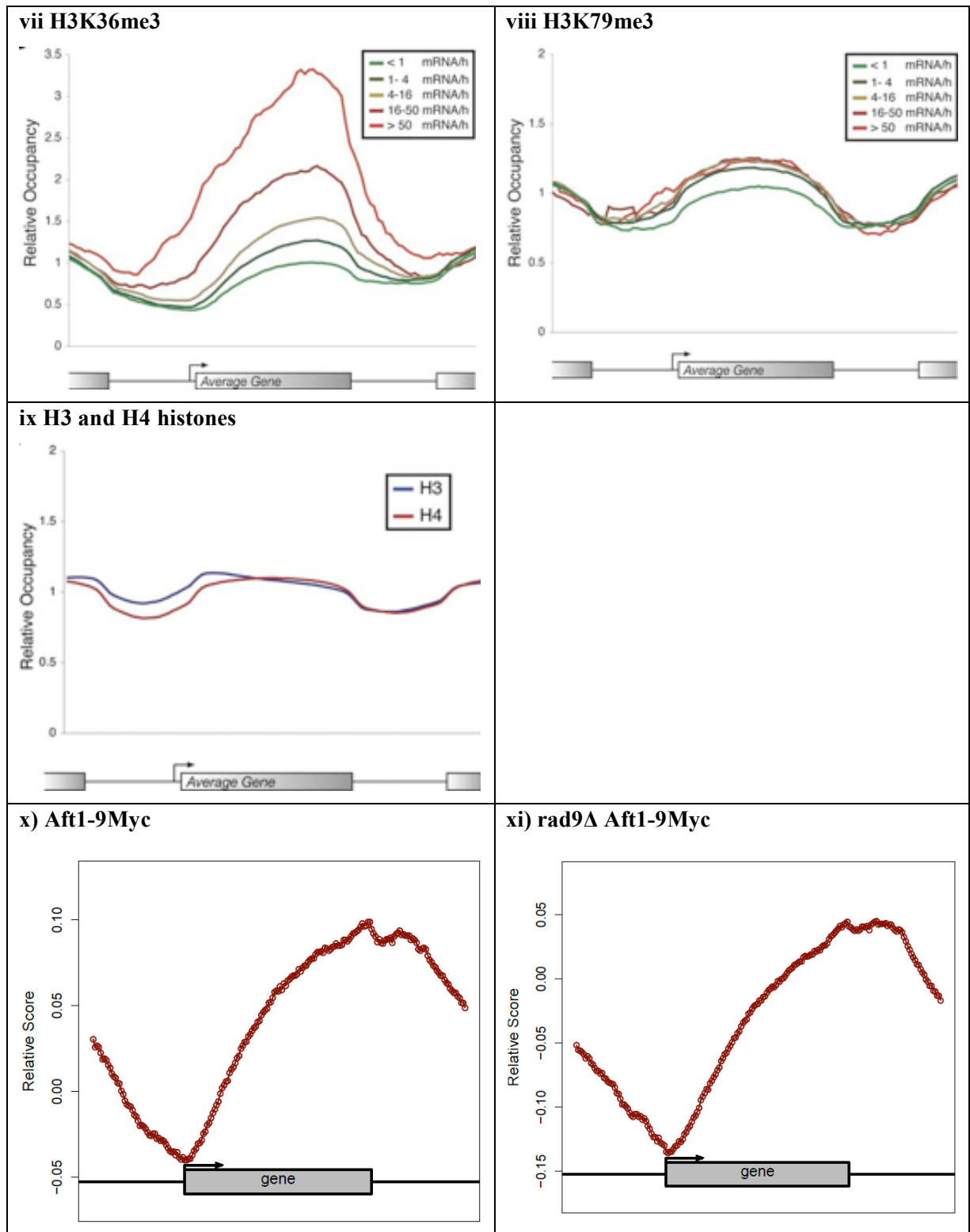
FIGURE 3.23A: Relative occupancy of Rad9 across an average gene in comparison to other epigenetic marks

Average gene analysis was performed for Rad9 genome-wide experiment as described in Materials and Methods. Relative occupancies of (i): Rad9 in SC BCS BPS, (ii): *aft1Δ* Rad9-13Myc SC BCS BPS, (iii): H3K9 acetylation, (iv): H3K14 acetylation, (v): H4 acetylation, (vi): H3K4 mono/di/trimethylation, (vii): H3K36 trimethylation, (viii): H3K79 trimethylation, (ix) H3 and H4 histones, (x) Aft1-9Myc SC BCS BPS, (xi) *rad9Δ* Aft1-9Myc SC BCS BPS. iii-ix: multiple curves for different activity gene groups are shown [obtained from (Pokholok et al., 2005)].

3.3.6.-- Qualitative analysis of Rad9 and of Rad9-Aft1 relation

After establishing the relation between Rad9 protein and Aft1 transcription factor and performed the genome-wide ChIP on chip analyses for both of them under non-induced DNA damage conditions (see previous chapters), we wanted to analyse our results qualitatively, namely to which functional categories they may group into. To address that, we obtained the coordinates of the localisation sites of the proteins for two different P-values (10^{-3} and 5×10^{-3}, see Materials and Methods). We then clustered these sites into three groups, depending on their binding value. The highest binding value corresponded to the lowest P-value, in order to finally have three groups formed in a descending binding value (Group1>Group2>Group3). We emphasized on the groups containing the genes where Rad9 and Aft1 were localised with the highest binding value. These were further analysed for possible overrepresented GO categories. This analysis was performed by using BiNGO, a Java-based tool used as a plugin in Cytoscape platform.

3.3.6.1.-- Qualitative analysis of Rad9 localisation pattern in the genome in the presence or absence of Aft1

Using a P-value cutoff of 0.001 we found that of the 935 genes to which Rad9 is localised in SC BCS BPS, the 221 (~24%) were common to the respective ones when Aft1 was absent, or else of the 648 genes to which Rad9 is localised when Aft1 is absent, the 221 (34.1%) were common to the respective ones in the case in which Rad9 is present (Figure 3.23B).
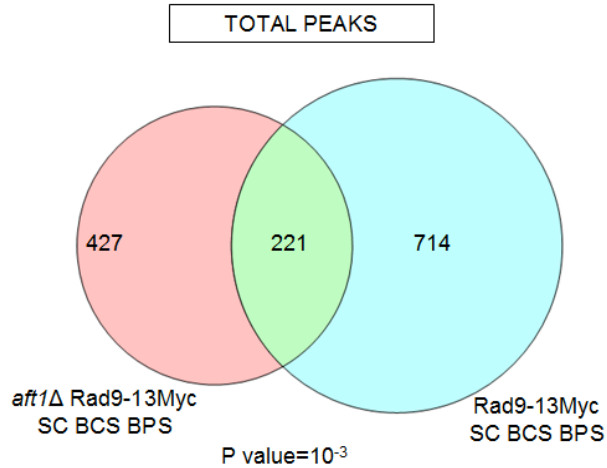
FIGURE 3.23B: Overlap of Rad9 targets in the presence or absence of Aft1 TF
Venn diagram showing the overlap (green) between the targets of Rad9 in WT background grown in SC BCS BPS (blue) and the targets of Rad9 in *aft1*Δ background grown in the same conditions (red).

 This comparison shows that a number of different additional genes is included in each case and this fact indicates the role of Aft1 in directing the Rad9 localisation. We separately examined the three different GO categories (BP-biological process, MF-molecular function, CC-cellular component) in the presence or absence of Aft1, in order to gather qualitative information on the effect of Aft1 in Rad9 binding. The most statistically important gene clusters that appeared are presented in the following tables.

GO: MOLECULAR FUNCTION	
Rad9-13Myc SC BCS BPS	*aft1*Δ **Rad9-13Myc SC BCS BPS**
Translation elongation factor activity (10^{-3}) [7/14]	Adenyl nucleotide binding (10^{-1}) [71/616]
Catalytic activity (10^{-2}) [127/2123]	**ATP binding** (10^{-1}) [67/575]
Ligase activity (10^{-2}) [4/4]	**ATPase** activity (10^{-1}) [32/229]
Vitamin binding (10^{-2}) [11/61]	
Biotin binding (10^{-2}) [4/5]	
Oxidoreductase activity, acting on paired donors, with incorporation or reduction of molecular oxygen (10^{-2}) [5/18]	
Oxidoreductase activity (10^{-2}) [29/307]	
Hydrolase activity, acting on carbon-nitrogen (but not peptide) bonds, in cyclic amidines (10^{-1}) [6/17]	

Glyceraldehyde-3-phosphate dehydrogenase (phosphorylating) activity (10^{-1}) [3/3]	
Lyase activity [11/96], NAD binding [5/19], Metal ion binding [44/812] (10^{1})	
Other clusters with higher P-values	

TABLE 3.6: GO Molecular Function overrepresentation of gene clusters in Rad9 ChIP on chip, in the presence or absence of Aft1

Numbers in parentheses correspond to hypergeometric test P-value as obtained from BiNGO analysis in Cytoscape (see Materials and Methods). Numbers in brackets correspond to the number of genes contained in our input fitting in each cluster, over the total number of yeast genes included in each cluster.

In Table 3.6, firstly we observed that the clusters formed in the presence of Aft1, are more that in its absence. Secondly, we see a qualitative difference: in the presence of Aft1, Rad9 is localised to clusters related to catalylic activity, translation elongation factor activity, ligase-, vitamin-, biotin-binding activity, oxidoreductase activity, among others. Groups like the one for oxidoreductase activity are connected to high transcriptional activity. In the absence of Aft1, the most apparent gene clusters are related to ATP-binding and ATPase activity. These latter gene clusters are also formed in the presence of Aft1, but are ranked in Group 3 (lower binding values). It should also be highlighted, that a lot of clusters overrepresented in the Rad9-13Myc strain, do not appear in the *aft1*Δ Rad9-13Myc strain. These clusters include among others, the clusters related to translation elongation factor activity, ligase activity, vitamin/biotin binding activity, oxidoreductase activity, hydrolase activity, glyceraldehyde-3-phosphate dehydrogenase activity, metal ion binding, cyclohydrolase activity, lyase activity. This is consistent to our previous observations that in the absence of Aft1, Rad9 loses its preference to bind the mostly active genes.

GO: BIOLOGICAL PROCESS	
Rad9-13Myc SC BCS BPS	***aft1*Δ Rad9-13Myc SC BCS BPS**
Pyruvate **metabolic** process (10^{-8}) [14/29]	Protein **import into nucleus** (10^{-5}) [13/49]
Carboxylic acid metabolic process (10^{-8}) [46/363]	**Regulation of metabolic** process (10^{-3}) [223/1154] (Group2)

Hexose **biosynthetic** process (10^{-7}) [12/22]	Regulation of cellular metabolic process (10^{-3}) [214/1101] (Group2)
Monosaccharide biosynthetic process (10^{-7}) [13/27]	Regulation of biological process (10^{-2}) [277/1500] (Group2)
Organic acid metabolic process (10^{-7}) [46/369]	**Nuclear transport** (10^{-2}) [40/133] (Group2)
Gluconeogenesis (10^{-7}) [11/19]	Nucleocytoplasmic transport (10^{-2}) [40/133] (Group2)
Alcohol biosynthetic process (10^{-6}) [15/47]	**Regulation** of cellular **biosynthetic** process (10^{-2}) [97/436] (Group2)
Glucose catabolic process (10^{-5}) [14/44]	**Regulation** of **translation** (10^{-1}) [92/417] (Group2)
Glycolysis (10^{-5}) [12/32]	**Regulation** of cellular protein **metabolic** process (10^{-1}) [95/438] (Group2)
Hexose catabolic process (10^{-5}) [14/49]	RNA localisation (10^{-1}) [32/107] (Group2)
Glucose metabolic process (10^{-4}) [16/67]	**Posttranscriptional regulation** of gene expression (10^{-1}) [92/426] (Group2)
Regulation of cellular protein metabolic process (10^{-4}) [45/438]	Regulation of protein metabolic process (10^{-1}) [102/490] (Group2)
Posttranscriptional regulation of gene expression (10^{-4}) [44/426], more in Group 3	Regulation of macromolecule metabolic process (10^{-1}) [198/1071] (Group2)
Regulation of **translation** (10^{-4}) [43/417]	**Iron** assimilation (10^{1}) [6/8] (Group2)
Regulation of cellular biosynthetic process (10^{-4}) [43/436]	
Oxidation reduction (10^{-2}) [29/279]	
Amino acid biosynthetic process (10^{-2}) [17/128] (Group 2)	
Metal ion transport (10^{-1}) [19/84] (Group 3)	
Iron ion transport (10^{-1}) [10/32] (Group 3)	

TABLE 3.7: GO Biological Process overrepresentation of gene clusters in Rad9 ChIP on chip, in the presence or absence of Aft1

Numbers in parentheses correspond to hypergeometric test P-value as obtained from BiNGO analysis in Cytoscape (see Materials and Methods). Numbers in brackets correspond to the number of genes contained in our input fitting in each cluster, over the total number of yeast genes included in each cluster.

In Table 3.7, we observe Rad9 localisation to genes which are clustered in groups related to glucose, hexose and organic acid metabolism. Groups for regulation

of metabolic processes, translation and posttranscriptional regulation of gene expression are also present, although exhibiting higher P-value. Thus, Rad9 is localized to genes required for cell growth. The presence of metal ion/iron transport groups is indicative of the induction growth conditions used (BCS/BPS), since these groups are absent from the clustering when Rad9-9Myc strain was grown on plain rich medium (YPD). When Aft1 is absent, Rad9 is localised with higher signal value (lower P-value) to genes encoding for proteins which participate to the import into nucleus. Furthermore, the categories for the regulation of metabolic processes, of transaltion, and of posttranscriptional regulation of gene expression are maintained in the absence of Aft1. Clusters related to metabolic and catabolic processes *per se* (including the highly active aminoacid biosynthetic genes), are not overrepresented in *aft1Δ* strains, which means that Aft1 assists Rad9 on its binding to genes related to cell growth.

GO: CELLULAR COMPONENT	
Rad9-13Myc SC BCS BPS	*aft1Δ* **Rad9-13Myc SC BCS BPS**
Fungal-type **cell wall** (10^{-7}) [21/90]	**Nuclear** lumen (10^{-1}) [114/560]
External encapsulating structure (10^{-5}) [21/107]	Nuclear pore complex (10^{1}) [19/57]
Cytosolic **ribosome** (10^{-2}) [20/156]	
Anchored to membrane (10^{1}) [9/47]	
COPII vesicle coat (ER→Golgi transport) (10^{1}) [4/9]	

TABLE 3.8: GO Cellular Component overrepresentation of gene clusters in Rad9 ChIP on chip, in the presence or absence of Aft1
Numbers in parentheses correspond to hypergeometric test P-value as obtained from BiNGO analysis in Cytoscape (see Materials and Methods). Numbers in brackets correspond to the number of genes contained in our input fitting in each cluster, over the total number of yeast genes included in each cluster.

In Table 3.8, we observe that the gene clusters to which Rad9 is localised, encode for proteins which are localised primarily to cell wall and secondarily to cytosolic ribosome. Cell wall protein-encoding genes are connected to high transcriptional activity (as we found in our genome-wide expression experiments), also consistent to our previous results for Rad9. These categories are absent from the *aft1Δ* strain, also consistent to our observations that Aft1 assists Rad9 on binding to highly active regions.

3.3.6.2.-- Aft1 genome-wide localisation pattern: a qualitative comparison to Rad9's localisation pattern

After examining the binding pattern of Rad9 in the genome in the presence or absence of Aft1, we sought to further investigate the interaction of the two proteins as it is reflected on their localisation to the genome.

Furthermore, Aft1 is a well studied transcription factor known for its role in the regulation of iron-related genes and for its more recent implications to genome integrity, chromosome and cell wall stability, DNA damage. What was unexpected is the fact that we have found Aft1 to be localised to coding regions of genes as shown in Figure 3.23C.
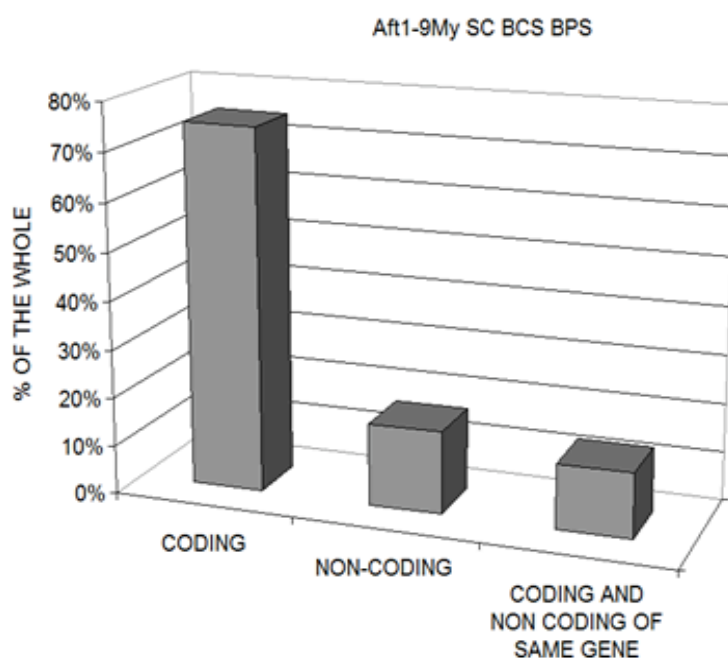
FIGURE 3.23C: Distribution of Aft1 localisation sites
After performing the ChIP on chip experiments of Aft1 in SC BCS BPS, we analyzed the distribution of Aft1 pattern in coding and non-coding areas (x axis). The genes to which Aft1 is localised in each occasion are expressed as percentage of the whole number of genes (*y* axis).

We performed ChIP on chip analysis for the Aft1 transcription factor on the same growth conditions used in the previous Rad9 experiments (SC BCS BPS). The overlap between the binding sites of the two proteins in the two experiments was

~40%. We performed Cytoscape analysis as described above (Chapter 3.3.6.1) and the results of the analysis are presented in the following tables.

GO: MOLECULAR FUNCTION	
Rad9-13Myc SC BCS BPS	**Aft1-9Myc SC BCS BPS**
Translation elongation factor activity (10^{-3}) [7/14]	**Iron** ion binding (10^{-6}) [20/116]
Catalytic activity (10^{-2}) [127/2123]	**Oxidoreductase** activity, oxidizing metal ions (10^{-3}) [6/10]
Ligase activity (10^{-2}) [4/4]	**Iron** ion transmembrane **transporter** activity (10^{-3}) [6/11]
Vitamin binding (10^{-2}) [11/61]	Transition metal ion transmembrane transporter activity (10^{-3}) [9/34]
Biotin binding (10^{-2}) [4/5]	**Ferric chelate reductase** activity (10^{-2}) [5/8]
Oxidoreductase activity, acting on paired donors, with incorporation or reduction of molecular oxygen (10^{-2}) [5/18]	Di-, tri-valent inorganic cation transmembrane transporter activity (10^{-2}) [9/41]
Oxidoreductase activity (10^{-2}) [29/307]	**Translation elongation** factor activity (10^{-1}) [5/14]
Hydrolase activity, acting on carbon-nitrogen (but not peptide) bonds, in cyclic amidines (10^{-1}) [6/17]	**DNA helicase** activity (10^{1}) [6/30]
Glyceraldehyde-3-phosphate dehydrogenase (phosphorylating) activity (10^{-1}) [3/3]	FAD binding (10^{1}) [6/34]
Lyase activity [11/96], NAD binding [5/19], Metal ion binding [44/812] (10^{1})	**Electron carrier** activity (10^{1}) [9/77]
Other clusters with higher P-values	Acetolactate synthase activity (10^{1}) [2/2]
	Fatty-acyl-CoA synthase activity (10^{1}) [2/2]

TABLE 3.9: GO Molecular Function overrepresentation of gene clusters in Rad9 ChIP on chip, in comparison to Aft1

Numbers in parentheses correspond to hypergeometric test P-value as obtained from BiNGO analysis in Cytoscape (see Materials and Methods). Numbers in brackets correspond to the number of genes contained in our input fitting in each cluster, over the total number of yeast genes included in each cluster.

In Table 3.9, we observe that some of the overrepresented groups between Rad9 and Aft1 ChIP on chip experiments are overlapping. These include oxidoreductase activity and translation elongation factor clusters. In the case of Aft1,

the iron binding/transporter cluster was, as expected, at the highest ranking. Some of the clustered groups that Aft1 was localised to, such as the ones for DNA helicase activity or electron carrier activity were not present in Rad9 ChIP on chip.

GO: BIOLOGICAL PROCESS	
Rad9-13Myc SC BCS BPS	**Aft1-9Myc SC BCS BPS**
Pyruvate **metabolic** process (10^{-8}) [14/29]	**Iron** ion **transport** (10^{-8}) [13/32]
Carboxylic acid metabolic process (10^{-8}) [46/363]	Transition metal ion transport (10^{-6}) [15/57]
Hexose **biosynthetic** process (10^{-7}) [12/22]	**Iron assimilation** (10^{-6}) [7/8]
Monosaccharide biosynthetic process (10^{-7}) [13/27]	Di-, tri-valent inorganic cation transport (10^{-5}) [13/47]
Organic acid metabolic process (10^{-7}) [46/369]	**Siderophore** transport (10^{-4}) [6/9]
Gluconeogenesis (10^{-7}) [11/19]	Iron ion homeostasis (10^{-3}) [10/37]
Alcohol biosynthetic process (10^{-6}) [15/47]	Cellular ion homeostasis (10^{-1}) [14/116]
Glucose catabolic process (10^{-5}) [14/44]	**Regulation** of biological quality (10^{-1}) [28/377]
Glycolysis (10^{-5}) [12/32]	**Oxidation reduction** (10^{-1}) [23/279]
Hexose catabolic process (10^{-5}) [14/49]	**Copper** ion import (10^{-1}) [4/8]
Glucose metabolic process (10^{-4}) [16/67]	**Regulation** of **translation** (10^{1}) [28/417]
Regulation of cellular protein metabolic process (10^{-4}) [45/438]	**Post transcriptional regulation** of gene expression (10^{1}) [28/426]
Posttranscriptional regulation of gene expression (10^{-4}) [44/426], more in Group 3	**Organic acid metabolic** process (10^{1}) [25/369]
Regulation of **translation** (10^{-4}) [43/417]	**Regulation** of cellular biosynthetic process (10^{1}) [28/436]
Regulation of cellular biosynthetic process (10^{-4}) [43/436]	**Amino acid metabolic** process (10^{1}) [17/235]
Oxidation reduction (10^{-2}) [29/279]	Fatty acid biosynthetis process (10^{1}) [4/17]
Amino acid biosynthetic process (10^{-2}) [17/128] (Group 2)	**Telomere maintenance** via recombination (10^{1}) [4/19]
Metal ion transport (10^{-1}) [19/84] (Group 3)	**Amino acid** and derivative **metabolic**

	process (10^{-1}) [38/255] (Group 2)
Iron ion transport (10^{-1}) [10/32] (Group 3)	**Carboxylic acid metabolic** process (10^{-2}) [50/363]
	Glucose catabolic process (10^{1}) [11/44] (Group 2)

TABLE 3.10: GO Biological Process overrepresentation of gene clusters in Rad9 ChIP on chip, in comparison to Aft1
Numbers in parentheses correspond to hypergeometric test P-value as obtained from BiNGO analysis in Cytoscape (see Materials and Methods). Numbers in brackets correspond to the number of genes contained in our input fitting in each cluster, over the total number of yeast genes included in each cluster.

In Table 3.10, we observe that the gene clusters related to iron transport/assimilation are, as expected, higher in the overall rank in Aft1 experiment. Groups for oxidation reduction, regulation of translation and post transcriptional regulation of gene expression are also overrepresented, similar to Rad9 clustering pattern. Glucose catabolic process cluster is also present in Aft1 BP clustering but in lower rank compared to Rad9. In general, we observe an overall similarity of the overrepresented clusters between Rad9 and Aft1, which reflects a participation of both in similar pathways (maybe co-operatively). Nevertheless, we will also see some differences in our in depth analysis of the two experiments in Results Chapter 3.5.3.

GO: CELLULAR COMPONENT	
Rad9-13Myc SC BCS BPS	**Aft1-9Myc SC BCS BPS**
Fungal-type **cell wall** (10^{-7}) [21/90]	**Eukaryotic translation elongation factor 1 complex** (10^{-2}) [4/5]
External encapsulating structure (10^{-5}) [21/107]	Fungal-type **cell wall** (10^{1}) [11/90]
Cytosolic **ribosome** (10^{-2}) [20/156]	Plasma membrane (10^{1}) [25/351]
Anchored to membrane (10^{1}) [9/47]	External encapsulating structure (10^{1}) [11/107]
COPII vesicle coat (ER→Golgi transport) (10^{1}) [4/9]	Anchored to membrane (10^{1}) [7/47]
	High affinity **iron permease** complex (10^{1}) [2/2]
	Acetolactate synthase complex (10^{1}) [2/2]
	Fatty acid synthase complex (10^{1}) [2/2]

TABLE 3.11: GO Cellular Component overrepresentation of gene clusters in Rad9 ChIP on chip, in comparison to Aft1
Numbers in parentheses correspond to hypergeometric test P-value as obtained from BiNGO analysis in Cytoscape (see Materials and Methods). Numbers in brackets correspond to the number of genes contained in our input fitting in each cluster, over the total number of yeast genes included in each cluster.

In Table 3.11, we see that, Aft1 is –similarly to Rad9- localised to gene clusters related to cell wall. Eukaryotic translation elongation factor 1 complex is also among the overrepresented categories for Aft1 binding.

3.3.6.3.1-- In depth analysis of the Rad9-Aft1 relation as it is reflected in their genome-wide localisation pattern

After the analysis of the genome-wide ChIP on chip experiments of Rad9 in the presence or absence of Aft1, we obtained the statistically significant loci to which each protein is localised, corresponding to two different P-values (10^{-3} and $5x10^{-3}$), as described in Materials and Methods. We then grouped the genomic loci to which each protein was localised into four categories: a) Total peaks (which included all the statistically significant loci), b) Peaks corresponding to coding regions, c) Peaks corresponding to non-coding regions and d) Peaks corresponding to coding and non-coding regions of the same gene. We compared the respective gene lists for each of these four categories between the two experiments in order to find:

i)   Genes to which Rad9 is localised only when Aft1 transcription factor is absent (Table 3.12).

ii)   Genes to which Rad9 is localised only when Aft1 transcription factor is present but is not when it is absent (Table 3.13).

iii)   Genes to which Rad9 is localised regardless the Aft1 presence (Table 3.14).

For each of these three categories we performed qualitative analysis using the BiNGO plugin in Cytoscape platform as described in Materials and Methods, in order to find any overrepresented gene clusters in each of the three GO categories (Molecular Function-MF, Biological Process-BP, Cellular Component-CC). The results obtained by this analysis are presented below.

TOTAL PEAKS
(MF) No clustering
(BP)
- Establishment of localization in cell (10^{-7}) [78/659]
- Intracellular **transport** (10^{-6}) [72/610]
- **Nuclear transport** (10^{-4}) [23/148]
- **rRNA metabolic** process (10^{-4}) [34/262]
- Golgi vesicle transport (10^{-4}) [26/185]

(CC)
- **Nuclear** lumen (10^{-2}) [96/546]

CODING
(MF)
- **ATPase** activity (10^{-5}) [29/242]
- Nucleoside-triphosphate activity (10^{-4}) [36/356]
- **Fatty acid synthase** activity (10^{-3}) [4/9]
- **Protein Ser/Thr kinase** activity (10^{-3}) [16/119]
- Pyrophosphatase activity/ hydrolase activity, acting on acid anhydrides (10^{-3}) [36/374]

(BP)
- Establishment of localization in cell (10^{-7}) [69/659]
- Intracellular **transport** (10^{-6}) [63/610]
- Cellular localization (10^{-6}) [73/757]
- Protein import into nucleus (10^{-6}) [13/54]
- **rRNA metabolic** process (10^{-5}) [31/262]
- **Ribosome biogenesis** (10^{-3}) [39/372]

(CC)
- **Nuclear lumen** (10^{-4}) [49/546]
- Microtubule organizing center (10^{-4}) [12/70]
- **Spindle pole** body (10^{-4}) [12/70]
- **Golgi transport** complex (10^{-4}) [4/8]
- **Mating** projection (10^{-3}) [16/121]

ONLY NON CODING
(BP) No clustering
(MF) No clustering
(CC) No clustering

TABLE 3.12: Gene Clusters to which Rad9 is localised only when Aft1 is absent

See text for experimental procedure. Numbers in parentheses correspond to hypergeometric test P-value as obtained from BiNGO analysis in Cytoscape (see Materials and Methods). Numbers in brackets correspond to the number of genes contained in our input fitting in each cluster, over the total number of yeast genes included in each cluster. When no clustering was possible, it is mentioned respectively. MF: Molecular Function, BP: Biological Process, CC: Cellular Component.

TOTAL PEAKS

(MF)
- **Catalytic** activity (10^{-15}) [343/2192]
- **Hydrolase** activity, hydrolyzing O-glycosyl compounds (10^{-7}) [17/41]
- **Oxidoreductase** activity (10^{-7}) [66/323]
- transferase activity, transferring acyl groups, acyl groups converted into alkyl on transfer (10^{-6}) [8/11]
- Ion binding (10^{-6}) [129/791]
- **Glucosidase** activity (10^{-5}) [10/20]
- **Translation elongation factor** activity (10^{-5}) [9/17]
- **Vitamin** binding (10^{-5}) [18/58]
- **Lyase** activity (10^{-5}) [25/97]
- **Siderophore** transporter activity (10^{-4}) [4/4]

(BP)
- **Biosynthetic/metabolic/catabolic** process (glucose, organic acid) (10^{-16}-10^{-11})
- Translation regulation (10^{-11}) [54/192]
- **Amino acid metabolic** process (10^{-10}) [63/247]
- Glucose metabolic process (10^{-10}) [34/98]
- **Posttranscriptional regulation** of gene expression (10^{-10}) [55/206]
- **Oxidation reduction** (10^{-8}) [75/363]
- **Siderophore** transport (10^{-7}) [8/9]
- **Iron-ion** transport (10^{-5}) [13/31]

(CC)
- External encapsulating structure (10^{-10}) [36/108]
- Anchored to membrane (10^{-10}) [26/59]
- Fungal-type **cell wall** (10^{-11}) [36/100]
- Cytosolic **ribosome** (10^{-6}) [40/169]
- Alpha,alpha-trehalose-phosphate synthase complex (UDP-forming) (10^{-4}) [4/4]
- **Tubulin** complex (10^{-3}) [3/3]

ONLY CODING

(MF)
- **Catalytic** activity (10^{-16}) [334/2192]
- **Oxidoreductase** activity (10^{-7}) [64/323]
- Hydrolase activity, hydrolyzing O-glycosyl compounds (10^{-6}) [16/41]
- **Cation/metal ion** binding (10^{-6}) [123/791]
- **Translation elongation factor activity** (10^{-5}) [9/17]
- **Vitamin** binding (10^{-5}) [18/58]
- Lyase activity (10^{-5}) [24/97]
- Substrate specific transmembrane transporter activity (10^{-4}) [50/274]
- **Siderophore** transporter activity (10^{-4}) [4/4]
- **Transcription repression** activity (10^{-4}) [14/51]
- rRNA binding (10^{-3}) [12/44]

(BP)
- **Carboxylic acid metabolic** process (10^{-18}) [98/377]
- Cellular ketone metabolic process (10^{-16}) [98/391]
- **Glucose catabolic** process (10^{-12}) [25/51]
- **Amine metabolic** process (10^{-11}) [73/303]
- Cellular **aminoacid and derivative metabolic** process (10^{-11}) [74/315]
- Regulation of translation (10^{-11}) [53/192]
- **Post transcriptional regulation** of gene expression (10^{-10}) [54/206]
- **Siderophore** transport (10^{-6}) [7/9]
- **Iron** assimilation (10^{-5}) [6/8]
- Iron-ion transport (10^{-4}) [11/31]
- A lot of other clusters with higher P-value

(CC)
- Extracellular region (10^{-14}) [39/95]
- Fungal-type **cell wall** (10^{-12}) [37/100]
- Anchored to membrane (10^{-10}) [25/59]
- External encapsulating structure (10^{-11}) [37/108]
- Cytosolic **ribosome** (10^{-7}) [41/169]

NON CODING

(MF)
- Structural constituent of **ribosome** (10^{-7}) [25/233] (P=0.005)
- Structural molecule activity [28/375] (P=0.005)
- SSU rRNA binding (10^{-5}) [3/4]

(BP) No clustering

(CC)
- Cytosolic part (10^{-7}) [20/219]
- Cytosolic **ribosome** (10^{-6}) [16/169]
- Fungal-type **cell wall** (10^{-4}) [10/100]

TABLE 3.13: Gene clusters to which Rad9 is localised only when Aft1 transcription factor is present but is not when it is absent

See text for experimental procedure. Numbers in parentheses correspond to hypergeometric test P-value as obtained from BiNGO analysis in Cytoscape (see Materials and Methods). Numbers in brackets correspond to the number of genes contained in our input fitting in each cluster, over the total number of yeast genes included in each cluster. When no clustering was possible, it is mentioned respectively. MF: Molecular Function, BP: Biological Process, CC: Cellular Component.

TOTAL

(MF)
- **Nucleoside** (purine) binding (10^{-9}) [55/703]
- Adenyl nucleotide binding (10^{-7}) [50/694]
- **ATP binding** (10^{-6}) [47/652]
- Purine ribonucleotide binding (10^{-6}) [50/752]
- **Catalytic** activity (10^{-4}) [104/2192]
- Ligase activity, forming carbon-carbon bonds (10^{-4}) [3/4]
- Biotin binding (10^{-4}) [3/5]
- CoA carboxylase activity (10^{-3}) [2/2]

(BP)
- **Translation regulation** (10^{-7}) [23/192]
- Regulation of cellular **protein metabolic process** (10^{-7}) [24/215]
- **Post transcriptional regulation** of gene expression (10^{-7}) [23/206]
- **Regulation of protein metabolic** process (10^{-6}) [26/279]
- Carboxylic acid **metabolic** process (10^{-4}) [27/377]
- Protein import into nucleus (10^{-4}) [8/54]
- Fatty acid biosynthetic process (10^{-4}) [5/22]
- Iron assimilation (10^{-8}) [7/8] [$P=5 \times 10^{-3}$]

(CC)
- Plasma **membrane** (10^{-7}) [54/366]
- 90S **preribosome** (10^{-5}) [17/83]
- Fungal-type **cell wall** (10^{-4}) [19/100]
- **Mating projection** (10^{-4}) [20/121]

ONLY CODING

(MF)
- **Nucleoside** binding (10^{-3}) [45/703]
- Adenyl nucleotide binding (10^{-2}) [42/694]
- **Catalytic** activity (10^{-7}) [201/2192] (P=0.005)
- ATP binding (10^{-6}) [83/652] (P=0.005)
- Ligase activity, forming carbon-carbon bonds (10^{1}) [3/4]
- Biotin binding (10^{1}) [3/5]

(BP)
- **Regulation of translation** (10^{-4}) [22/192]
- Regulation of cellular protein **metabolic process** (10^{-4}) [23/215]
- **Post transcriptional regulation** of gene expression (10^{-3}) [22/206]
- **Regulation of protein metabolic** process (10^{-3}) [25/279]
- Iron assimilation (10^{-4}) [7/8] (P=0.005)
- Carboxylic acid metabolic process (10^{1}) [25/377]
- **Siderophore** iron transport (10^{-2}) [5/6] (P=0.005)
- **Ribosome** biogenesis (10^{-2}) [46/372] (P=0.005)

(CC)
- **Plasma membrane** (10^{-2}) [47/366] (P=0.005)
- 90S **preribosome** (10^{-1}) [16/83] (P=0.005)
- **Mating projection** tip (10^{-1}) [19/110] (P=0.005)

ONLY NON CODING

(MF)
- **Helicase** activity (10^{-6}) [6/107]
- **ATPase** activity, coupled (10^{-4}) [5/172]
- Purine NTP dependent helicase activity (10^{-5}) [5/76]
- **Hydrolase** activity, acting on acid anhydrides (10^{-3}) [6/374]

(BP) Premeiotic DNA synthesis (10^{-3}) [3/6]

(CC) No clustering

TABLE 3.14: Gene clusters to which Rad9 is localised regardless the Aft1 presence

See text for experimental procedure. Numbers in parentheses correspond to hypergeometric test P-value as obtained from BiNGO analysis in Cytoscape (see Materials and Methods). Numbers in brackets correspond to the number of genes contained in our input fitting in each cluster, over the total number of yeast genes included in each cluster. When no clustering was possible, it is mentioned respectively. MF: Molecular Function, BP: Biological Process, CC: Cellular Component.

In Tables 3.12, 3.13 and 3.14, we observed once more that Aft1 is required for Rad9 localisation to highly transcriptionally active gene clusters, since in its absence Rad9 is not localised to well known active groups such as the ones related to oxidoreductase activity, amino acid metabolic process and cell wall (Table 3.13). Gene clusters, such as the ones related to catalytic activity, post-transcriptional regulation of gene expression, presence to cell wall, are much more represented quantitatively when Aft1 is present rather than regardless its presence (Table 3.13 versus Table 3.14). This means that Aft1 association to Rad9 assists the binding of the latter to the particular gene clusters.

Furthermore, we conclude that Aft1 is very important in establishing the Rad9 localisation to genes related to cell growth (such as metabolic, or biosynthetic of glucose and amino acids, encoding ribosomal proteins). Rad9 presence on genes related to cell growth, in an Aft1-dependent manner, can be of great importance since it connects a DNA damage checkpoint protein to vital cellular processes in non DNA damage induced conditions.

Furthermore, for the group of genes to which Rad9 is localised only when Aft1 is absent, as we can see a difference in the list of the overrepresented gene clusters, since there are clusters related to nuclear transport, rRNA metabolic process, ribosome biogenesis, ATPase activity (Table 3.12), compared to the biosynthetic/metabolic gene clusters or the ones related to catalytic activity, regulation of translation, cell wall and ribosomes, which are apparent when Aft1 is present (Table 3.13). This qualitative difference highlights the importance of Aft1 in directing Rad9 localisation to specific sites of the genome.

The quality of the genome-wide analysis is confirmed by the iron related gene clusters, which are significantly more apparent in Rad9's localisation pattern when Aft1 is present.

3.3.6.3.2.-- Rad9 localisation to the coding and non-coding region of the same gene in the presence or absence of Aft1

We further examined the case in which Rad9 was localised to the coding and non-coding region of the same gene, as was the case of *CTR1* gene. To address that, we performed the analysis described in the previous chapter (Results Chapter

3.3.6.3.1) for the group of genes that were characterized by this specificity and the results are presented in Table 3.15. The analysis was performed for the cases where Aft1 was present or absent.

Rad9-9Myc SC BCS BPS
(MF)
- **SSU rRNA (**10^{-5}) [3/4]
- Structural **constituent of ribosome (**10^{-5}) [14/233]
- **rRNA** binding (**10^{-5}) [6/44]
- **Translation elongation** factor activity (**10^{-4}) [4/17]
- **Structural** molecule activity (**10^{-4}) [16/375]
- **Oxidoreductase** activity (**10^{-3}) [14/323]

(BP)
- Cellular **metabolic** process (**10^{-6}) [86/3827]
- **Regulation of translation** (**10^{-5}) [13/192]
- Post transcriptional regulation of gene expression (**10^{-5}) [13/206]
- Regulation of **translational elongation** (**10^{-5}) [5/24]
- **Carboxylic acid metabolic process** (**10^{-5}) [18/377]
- Glucose **catabolic** process (**10^{-4}) [6/51]
- **Glucose metabolic** process (**10^{-3}) [7/98]
- Regulation of cellular protein metabolic process (**10^{-5}) [13/215]
- NADPH regeneration (**10^{-4}) [4/21]
- Ribosome biogenesis (**10^{-3}) [15/372]
- **Oxidation** reduction (**10^{-3}) [14/363]

(CC)
- **Ribosome** (**10^{-7}) [18/275]
- Cytosolic small **ribosomal** subunit (**10^{-5}) [8/64]
- Extracellular region (**10^{-5}) [9/95]
- **Fungal-type cell wall** (**10^{-5}) [9/100]
- External encapsulating structure (**10^{-5}) [9/108]
- Chaperonin containing T-complex (**10^{-4}) [3/8]
- 90S **preribosome** (**10^{-3}) [6/83]
- Eucaryotic translation elongation factor 1 complex (**10^{-3}) [2/5]

aft1Δ Rad9-13Myc SC BCS BPS
(MF)
- **Siderophore-iron transmembrane** transporter activity (**10^{-5}) [3/4] (P=0.005)

(BP)
- Transport (**10^{-6}) [56/1221] (P=0.005)
- Establishment of localization (**10^{-5}) [56/1226] (P=0.005)
- Di-, trivalent inorganic **cation transport** (**10^{-5}) [8/45] (P=0.005)
- **Iron assimilation** (**10^{-5}) [4/8] (P=0.005)
- **Siderophore** transport (**10^{-5}) [4/9] (P=0.005)
- Transmembrane transport (**10^{-4}) [23/381] (P=0.005)
- **Iron ion transport** (**10^{-4}) [6/31] (P=0.005)
- Iron assimilation by chelation and transport (**10^{-4}) [3/6] (P=0.005)
- Iron chelate transport (**10^{-4}) [3/6] (P=0.005)

(CC)   No clustering

TABLE 3.15: Gene clusters to which Rad9 is localised to both their coding and non coding regions
See text for experimental procedure. Numbers in parentheses correspond to hypergeometric test P-value as obtained from BiNGO analysis in Cytoscape (see Materials and Methods). Numbers in brackets correspond to the number of genes contained in our input fitting in each cluster, over the total number of yeast genes included in each cluster. When no clustering was possible, it is mentioned respectively. MF: Molecular Function, BP: Biological Process, CC: Cellular Component.

In the case where Rad9 is localised to the coding and non-coding region of the same gene, the overrepresented clusters include genes related to ribosomal subunits, rRNA binding, translation elongation factor activity and regulation of translation. The presence of Rad9 on such genes is an indication of a more solid role of Rad9 in cellular mechanisms related to protein synthesis. This is a further indication of Rad9 possible implication in regulation of cell growth genes.

3.3.6.4.-- Aft1 localisation pattern in the presence or absence of Rad9

After examining the effect of Aft1 on Rad9 localisation to the genome (Results Chapter 3.3.6.3.1 and 3.3.6.3.2), we sought to investigate what was the effect of Rad9 on Aft1 localisation to the genome in order to obtain a comprehensive view of the Aft1-Rad9 relation. To address this matter, we performed ChIP on chip analysis of Aft1 in the absence of Rad9 protein and compared qualitatively the results to the ones from ChIP on chip analysis of Aft1 in the presence of Rad9 after taking into account the binding value of Aft1 (clustered the genes into Groups 1, 2, 3 in descending binding values as described in Results Chapter 3.3.6). The two experiments between the two strains had an overlap of ~55%.

A general overview of the Aft1 binding pattern in the presence or absence of Rad9 in each of the three GO categories is presented in Tables 3.16, 3.17 and 3.18.

GO: MOLECULAR FUNCTION	
rad9Δ Aft1-9Myc SC BCS BPS	Aft1-9Myc SC BCS BPS
Structural **constituent of ribosome** (10^{-4}) [43/233]	**Iron** ion binding (10^{-6}) [20/116]
Catalytic activity (10^{-3}) [212/2192]	**Oxidoreductase** activity, oxidizing metal ions (10^{-3}) [6/10]
Structural molecule activity (10^{-3}) [55/375]	**Iron** ion transmembrane **transporter** activity (10^{-3}) [6/11]
Vitamin binding (10^{-1}) [15/58]	Transition metal ion transmembrane transporter activity (10^{-3}) [9/34]
Co-factor binding (10^{-1}) [28/162]	**Ferric chelate reductase** activity (10^{-2}) [5/8]

Purine nucleotide binding (10^{-1}) [89/793]	Di-, tri-valent inorganic cation transmembrane transporter activity (10^{-2}) [9/41]
Lyase activity (10^{-1}) [20/97]	**Translation elongation** factor activity (10^{-1}) [5/14]
rRNA binding (10^{-1}) [12/44]	**DNA helicase** activity (10^{1}) [6/30]
Oxidoreductase activity (10^{-1}) [43/323]	FAD binding (10^{1}) [6/34]
Translation elongation factor activity (10^{1}) [7/17]	**Electron carrier** activity (10^{1}) [9/77]
Transition metal ion transmembrane transporter activity (10^{1}) [9/28]	Acetolactate synthase activity (10^{1}) [2/2]
Di-, tri-valent inorganic cation transmembrane transporter activity (10^{1}) [10/36]	Fatty-acyl-CoA synthase activity (10^{1}) [2/2]
Ferric-chelate reductase activity (10^{1}) [5/9]	
Metal ion transmembrane transporter activity (10^{1}) [11/45]	
Copper ion transmembrane transporter activity (10^{1}) [4/6]	
ATP binding (10^{1}) [70/652]	
Iron ion transmembrane transporter activity (10^{1}) [5/11]	
siderophore-iron transmembrane transporter activity (10^{1}) [3/4]	

TABLE 3.16: Gene clusters of GO Molecular Function to which Aft1 is localised in the presence or absence of Rad9
See text for experimental procedure. Numbers in parentheses correspond to hypergeometric test P-value as obtained from BiNGO analysis in Cytoscape (see Materials and Methods). Numbers in brackets correspond to the number of genes contained in our input fitting in each cluster, over the total number of yeast genes included in each cluster. MF: Molecular Function, BP: Biological Process, CC: Cellular Component.

In Table 3.16, we observe that the types of gene clusters to which Aft1 is localised are of similar content in the presence or absence of Rad9. Nevertheless, a shift in their ranking is apparent since iron-related gene clusters are lower in the rank when Rad9 is absent.

GO: BIOLOGICAL PROCESS	
rad9Δ Aft1-9Myc SC BCS BPS	Aft1-9Myc SC BCS BPS
Regulation of translation (10^{-15}) [54/192]	**Iron** ion **transport** (10^{-8}) [13/32]
Posttranscriptional **regulation of gene expression** (10^{-15}) [56/206]	Transition metal ion transport (10^{-6}) [15/57]
Carboxylic acid **metabolic** process (10^{-14}) [78/377]	**Iron assimilation** (10^{-6}) [7/8]
Cellular ketone metabolic process (10^{-14}) [79/391]	Di-, tri-valent inorganic cation transport (10^{-5}) [13/47]
Cellular **amino acid metabolic** process (10^{-13}) [60/247]	**Siderophore** transport (10^{-4}) [6/9]
Regulation of cellular protein metabolic process (10^{-13}) [55/215]	Iron ion homeostasis (10^{-3}) [10/37]
Cellular **amine metabolic** process (10^{-12}) [61/270]	Cellular ion homeostasis (10^{-1}) [14/116]
Cellular amino acid and derivative metabolic process (10^{-11}) [65/315]	**Regulation** of biological quality (10^{-1}) [28/377]
Regulation of protein metabolic process (10^{-8}) [56/279]	**Oxidation reduction** (10^{-1}) [23/279]
Cellular nitrogen compound biosynthetic process (10^{-6}) [55/310]	**Copper** ion import (10^{-1}) [4/8]
Cellular aromatic compound metabolic process (10^{-4}) [32/146]	**Regulation** of **translation** (10^{1}) [28/417]
Transition metal ion transport (10^{-3}) [17/55]	**Post transcriptional regulation** of gene expression (10^{1}) [28/426]
Glucose catabolic process (10^{-3}) [16/51]	**Organic acid metabolic** process (10^{1}) [25/369]
Glutamine family amino acid metabolic process (10^{-3}) [18/64]	**Regulation** of cellular biosynthetic process (10^{1}) [28/436]
Iron-ion transport (10^{-3}) [12/31]	**Amino acid metabolic** process (10^{1}) [17/235]
Monosaccharide catabolic process (10^{-2}) [17/61]	Fatty acid biosynthetis process (10^{1}) [4/17]
Di-, tri-valent inorganic cation transport (10^{-2}) [14/45]	**Telomere maintenance** via recombination (10^{1}) [4/19]
Alcohol catabolic process (10^{-2}) [17/66]	**Amino acid** and derivative **metabolic**

	process (10^{-1}) [38/255] (Group 2)
Iron assimilation (10^{-2}) [6/8]	**Carboxylic acid metabolic** process (10^{-2}) [50/363]
Iron ion homeostasis (10^{-2}) [12/38]	**Glucose catabolic** process (10^{1}) [11/44] (Group 2)

TABLE 3.17: Gene clusters of GO Biological Process to which Aft1 is localised in the presence or absence of Rad9

See text for experimental procedure. Numbers in parentheses correspond to hypergeometric test P-value as obtained from BiNGO analysis in Cytoscape (see Materials and Methods). Numbers in brackets correspond to the number of genes contained in our input fitting in each cluster, over the total number of yeast genes included in each cluster. MF: Molecular Function, BP: Biological Process, CC: Cellular Component.

In Table 3.17, we can see that the absence of Rad9 does not affect the localisation of Aft1 to clusters containing highly active genes such as the ones related to oxidoreductase activity or amino acid metabolic process. Nevertheless, there is again a shift in the ranking of the clusters, such as the iron related ones, which are higher in rank when Rad9 is present. "Regulation of translation" and "metabolic processes"-related gene clusters are lower in rank when Rad9 is present. It seems though that the absence of Rad9 does not have a serious qualitative effect on Aft1 localisation. Rad9 effect on Aft1 localisation pattern is not as serious as Aft1 effect on Rad9 as previously shown (Results Chapters 3.3.6.1 and 3.3.6.3.1).

GO: CELLULAR COMPONENT	
rad9Δ Aft1-9Myc SC BCS BPS	**Aft1-9Myc SC BCS BPS**
Cytosolic **ribosome** (10^{-10}) [44/169]	**Eukaryotic translation elongation factor 1** complex (10^{-2}) [4/5]
Cytosolic large ribosomal subunit (10^{-5}) [25/93]	Fungal-type **cell wall** (10^{1}) [11/90]
Plasma membrane enriched fraction (10^{-4}) [23/89]	Plasma membrane (10^{1}) [25/351]
Fungal-type **cell wall** (10^{-3}) [23/100]	External encapsulating structure (10^{1}) [11/107]
Cytosolic small ribosomal subunit (10^{-2}) [17/64]	Anchored to membrane (10^{1}) [7/47]
External encapsulating structure (10^{-2}) [23/108]	High affinity **iron permease** complex (10^{1}) [2/2]
Eukaryotic translation elongation factor 1 complex (10^{1}) [3/5]	**Acetolactate synthase** complex (10^{1}) [2/2]

	Fatty acid synthase complex (10^1) [2/2]

TABLE 3.18: Gene clusters of GO Cellular Component to which Aft1 is localised in the presence or absence of Rad9
See text for experimental procedure. Numbers in parentheses correspond to hypergeometric test P-value as obtained from BiNGO analysis in Cytoscape (see Materials and Methods). Numbers in brackets correspond to the number of genes contained in our input fitting in each cluster, over the total number of yeast genes included in each cluster. MF: Molecular Function, BP: Biological Process, CC: Cellular Component.

In Table 3.18, we can see that gene clusters related to cell wall and eukaryotic translation elongation factor 1 complex are included in the list where Aft1 is localised regardless the Rad9 presence, although in a different ranking. In all three GO categories, there is a higher overrepresentation of clusters related to ribosome structure and function when Rad9 is absent. Nevertheless, we can again see that the impact of *RAD9* deletion on the gene categories where of Aft1 localises is not severe compared to the impact of *AFT1* deletion on Rad9 localisation pattern.

We further analyzed the above-presented results in order to get an insight on:

i)　　　Where Aft1 is localised only when Rad9 is absent

ii)　　　Where Aft1 is localised only when Rad9 is present

iii)　　　Where Aft1 is localised regardless the Rad9 presence

The results are presented in Tables 3.19, 3.20 and 3.21 respectively.

TOTAL (MF)

- **structural constituent of ribosome** (10^{-14}) [96/233]
- structural molecule activity (10^{-11}) [125/375]
- substrate-specific **transmembrane transporter** activity (10^{-2}) [79/374]
- substrate-specific transporter activity (10^{-2}) [91/330]
- transmembrane transporter activity (10^{-2}) [87/318]
- transporter activity (10^{-2}) [101/392]
- electron carrier activity (10^{-1}) [22/56]

TOTAL (CC)

- Cytosolic **ribosome** (10^{-26}) [94/169]
- Cytosolic large ribosomal subunit (10^{-15}) [54/93]
- Cytosolic small ribosomal subunit (10^{-8}) [35/64]
- Ribonucleoprotein complex (10^{-7}) [156/556]
- Intrinsic to membrane (10^{-1}) [272/1295]
- Mitochondrial nucleoid (10^1) [12/23]

TOTAL (BP)

- **Regulation of translation** (10^{-10}) [77/192]
- **Posttranscriptional regulation of gene expression** (10^{-10}) [80/206]
- Regulation of cellular protein metabolic process (10^{-8}) [79/215]
- **Intron homing** (10^{-4}) [10/10]
- **Regulation** of protein **metabolic** process (10^{-4}) [84/279]
- **Ribonucleoprotein** complex **biogenesis** (10^{-2}) [110/423]
- **Ribosome biogenesis** (10^{-2}) [99/372]
- Pyruvate metabolic process (10^{-2}) [16/28]
- Transmembrane transport (10^{-2}) [100/381]
- Small molecule biosynthetic process (10^{-2}) [100/390]
- Nucleotide metabolic process (10^{-1}) [61/214]
- rRNA export from nucleus (10^{-1}) [19/43]
- nucleobase, nucleoside and nucleotide metabolic process (10^{-1}) [67/245]
- Gluconeogenesis (10^1) [10/17]
- Amine metabolic process (10^1) [74/303]
- Hexose biosynthetic process (10^1) [10/20]
- Glycine catabolic process (10^1) [4/4]

TABLE 3.19: Gene clusters to which Aft1 transcription factor is localised only when Rad9 is absent

See text for experimental procedure. Numbers in parentheses correspond to hypergeometric test P-value as obtained from BiNGO analysis in Cytoscape (see Materials and Methods). Numbers in brackets correspond to the number of genes contained in our input fitting in each cluster, over the total number of yeast genes included in each cluster. When no clustering was possible, it is mentioned respectively. MF: Molecular Function, BP: Biological Process, CC: Cellular Component.

As in Table 3.18, we can again see in Table 3.19 that when Rad9 is absent, Aft1 is localised to gene clusters related to protein synthesis regulation and structure and biogenesis of ribosome (to a greater extend compared to the *rad9Δ* cells). This could show a possible implication of Aft1 transcription factor in regulation of protein synthesis.

TOTAL (MF)

- **Helicase activity** (10^{-6}) [25/107]
- ATP-dependent helicase activity (10^{-4}) [18/76]
- DNA helicase activity (10^{-3}) [12/35]
- ATPase activity, coupled (10^{-3}) [27/172]
- Pyrophosphatase activity (10^{-3}) [43/374]
- Hydrolase activity, acting on acid anhydrides, in phosphorus containing anhydrides (10^{-3}) [43/374]
- Nucleoside triphosphatase activity (10^{-2}) [40/356]
- Transcription regulator activity (10^{-2}) [40/361]
- Purine ribonucleotide binding (10^{-1}) [67/752]
- ATPase activity (10^{-1}) [30/242]
- ATP binding (10^{-1}) [59/652]
- Transcription activator activity (10^{-3}) [43/374]

TOTAL (BP)

- **Regulation of transcription** (10^{-2}) [63/669]
- **Regulation of nucleobase**, nucleoside, nucleotide and nucleic acid **metabolic process** (10^{-2}) [68/759]
- Regulation of RNA metabolic process (10^{1}) [46/489]
- Regulation of biosynthetic process (10^{1}) [72/910]
- Other with higher P-values

TOTAL (CC)
No clustering

TABLE 3.20: Gene clusters to which Aft1 transcription factor is localised only when Rad9 is present

See text for experimental procedure. Numbers in parentheses correspond to hypergeometric test P-value as obtained from BiNGO analysis in Cytoscape (see Materials and Methods). Numbers in brackets correspond to the number of genes contained in our input fitting in each cluster, over the total number of yeast genes included in each cluster. When no clustering was possible, it is mentioned respectively. MF: Molecular Function, BP: Biological Process, CC: Cellular Component.

Table 3.20 contains the gene clusters to which Aft1 is localised only when Rad9 is present. It is shown that Rad9 is necessary for Aft1 localisation to genes related to DNA helicase activity.

TOTAL (MF)
- **Purine nucleotide binding** (10^{-4}) [101/793]
- Adenyl **nucleotide binding** (10^{-3}) [91/694]
- Transition **metal ion transmembrane transporter** activity (10^{-3}) [12/28]
- Purine ribonucleotide binding (10^{-3}) [94/752]
- **ATP binding** (10^{-3}) [84/652]
- **Catalytic** activity (10^{-2}) [214/2192]
- **Translation elongation factor** activity (10^{-1}) [8/17]
- **Siderophore-iron** transmembrane transporter activity (10^{-1}) [4/4]
- **Iron-ion** transmembrane transporter activity (10^{-1}) [6/11]
- Pyrophosphatase activity (10^{1}) [49/374]
- Hydrolase activity, acting on acid anhydrides, in phosphorus containing anhydrides (10^{1}) [49/374]
- Translation factor activity, nucleic acid binding (10^{1}) [14/60]
- Copper-ion transmembrane transporter activity (10^{1}) [4/6]
- Vitamin binding (10^{1}) [12/58]

TOTAL (CC)
- **Fungal-type cell wall** (10^{-3}) [24/100]
- External encapsulating structure (10^{-2}) [24/108]
- Extracellular region (10^{-2}) [21/95]
- Anchored to membrane (10^{-1}) [15/59]
- **Eukaryotic translation elongation** factor-1 complex (10^{1}) [4/5]
- Cytoskeleton (10^{1}) [35/245]
- Cellular bud (10^{1}) [29/201]
- Cortical actin cytoskeleton (10^{1}) [13/64]
- Ribosome (10^{1}) [35/275]
- Nup82 complex (10^{1}) [3/5]

TOTAL (BP)
- **Regulation of translation** (10^{-12}) [51/192]
- **Post transcriptional regulation of gene expression** (10^{-11}) [52/206]
- **Regulation** of cellular protein **metabolic process** (10^{-10}) [52/215]
- Regulation of protein metabolic process (10^{-8}) [57/279]
- Transition **metal ion transport** (10^{-6}) [21/55]
- Regulation of gene expression (10^{-3}) [114/874]
- Regulation of macromolecule biosynthetic process (10^{-5}) [114/878]
- Carboxylic acid **biosynthetic process** (10^{-4}) [36/172]
- Oxoacid metabolic process (10^{-4}) [60/377]
- Cellular ketone metabolic process (10^{-4}) [61/391]
- Amine metabolic process (10^{-3}) [50/303]
- **Metal ion** transport (10^{-3}) [22/86]
- Cellular aminoacid and derivative metabolic process (10^{-3}) [50/315]
- di-, trivalent inorganic cation transport (10^{-3}) [15/45]
- Cellular aminoacid biosynthetic process (10^{-3}) [28/133]
- **Iron ion** transport (10^{-2}) [12/31]
- Siderophore transport (10^{-1}) [6/9]
- More with higher P-values

TABLE 3.21: Gene clusters to which Aft1 transcription factor is localised regardless Rad9 presence

See text for experimental procedure. Numbers in parentheses correspond to hypergeometric test P-value as obtained from BiNGO analysis in Cytoscape (see Materials and Methods). Numbers in brackets correspond to the number of genes contained in our input fitting in each cluster, over the total number of yeast genes included in each cluster. When no clustering was possible, it is mentioned respectively. MF: Molecular Function, BP: Biological Process, CC: Cellular Component.

In Table 3.21, we can see that Aft1 does not need Rad9 in order to accomplish its classic role as a transcriptional activator of the iron regulon. A localisation pattern of Aft1 to gene clusters related to metabolic processes is apparent. It is important that Aft1 is present on groups of genes further the ones belonging to the iron regulon. This result will be discussed in Chapter 3.3.8 in which we compare our results to data about novel Aft1 roles (Berthelet et al., 2010; Shakoury-Elizeh et al., 2004).

3.3.6.5—Overexpression of Rad9 does not increase its localization targets

As mentioned in previous chapters, we have found Rad9 localised to 16-20% of yeast genes (~900-1200 out of 5757 depending on the growth conditions). It was found by GFP analyses that Rad9 protein is present in about 400 molecules per yeast cell grown in rich medium (YPD) (Ghaemmaghami et al., 2003). Since the number of Rad9 molecules is small compared to the sites that we found it localised to the genome, we sought to examine what would be the outcome in the case Rad9 was present in more molecules per cell. Would it still have some specificity in its binding pattern or would it bind unselectively to more genomic loci?

To address this question we have made a construct where Rad9 protein tagged with 13Myc epitopes was introduced to the high copy plasmid pYX142. The produced amount of Rad9 protein was at least 10 times higher, as we checked by Western blot analysis (Figure 3.24).

FIGURE 3.24: Rad9 protein overexpressed in pYX142 versus the endogenously tagged
We have grown cultures of Rad9-9Myc (tagged and inserted in the genome) (*lane B*) and Rad9-9Myc inserted in pYX142 plasmid (see Materials and Methods) which was transformed into *rad9Δ* yeast strain (*lane A*). The conditions used for the growth were the same as in our ChIP on chip experiment (SC BCS BPS). We then isolated protein extract from 2×10^7 cells of both cultures and run them on a 6% SDS gel and analysed by Western blot.

We used this Rad9-9Myc-pYX142 strain for a large scale ChIP on chip experiment in order to decipher whether Rad9 protein would be localised to more loci. In addition, we performed Cytoscape analysis, using BiNGO plugin, to see if the overrepresented GO categories of the gene clusters remained similar. In our interpretation, it must be taken into account that this is a case of a not normal condition for the cell and the results from this genome-wide experiment must be evaluated under this perspective.

We have found that the number of genes to which Rad9 was localised was of similar order compared to the respective number from the ChIP on chip experiment with the endogenously tagged protein (624 versus 935 genes respectively, using a similar P-value cut-off). The fewer genes could be explained by the fact that during the particular experiment we faced a technical problem: the scanner used for the scanning of the hybridized samples was malfunctioning and the hybridized slides waited a two-week period before scanned.

The similar number of Rad9 targets regardless its overexpression indicates that Rad9 does not localise unselectively to the genome. Nevertheless, we also observed that the binding bias to the most highly active genes was not so apparent (Figure 3.24B).
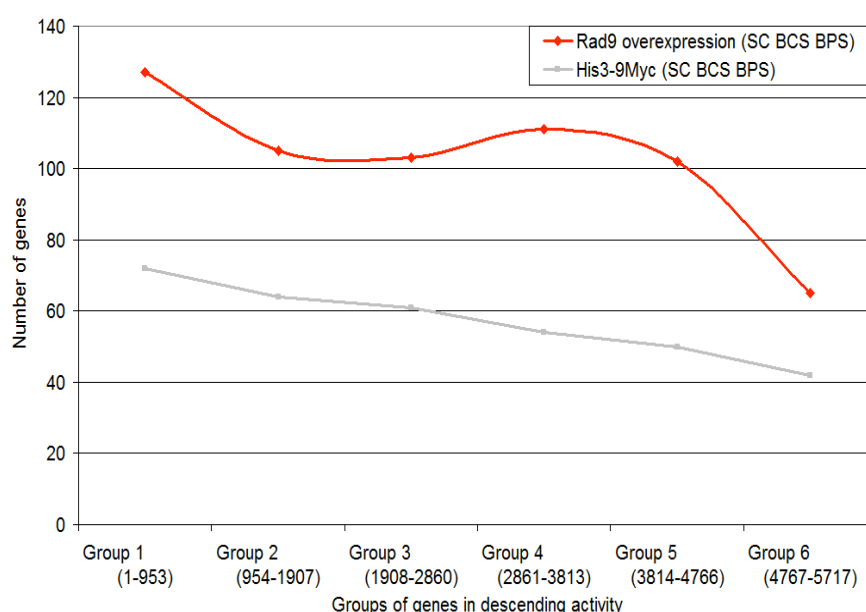
FIGURE 3.24B: Distribution of Rad9 localisation, when overexpressed, according to gene activity
Yeast genes were grouped in 6 groups (*x* axis), containing ~1000 genes each, in descending transcriptional activity in SC BCS BPS growth conditions (obtained by our expression microarrays experiments). Illustrated in red is the binding pattern of Rad9 when it is overexpressed in pYX142 plasmid (see Materials and Methods) plotted as the number of common genes in each group (*y* axis). His3 control protein is shown in grey.

Furthermore, although Rad9 had again a preference to localise to coding regions, we observed a higher localization percentage to non coding regions compared to the experiment with the endogenously tagged Rad9. This differential outcome can be attributed to the overexpression of Rad9 which may affect other pathways in the cell creating abnormal conditions. Such possible abnormality is also reflected on the fact that the overlap in number of genes between the two experiments was low (~38%). The results from the qualitative analysis, performed as described in Chapter 3.3.6, are presented in Table 3.22.

Rad9-9Myc-pYX142 SC BCS BPS (overexpression)	
GO: Molecular Function	GO: Biological Process
Iron ion binding (10^{-1}) [9/116]	**Iron** ion **transport** (10^{-3}) [7/32]
Iron ion **transmembrane transporter** activity (10^1) [3/11]	**Iron** ion **homeostasis** (10^{-3}) [7/37]
Translation elongation factor activity (10^1) [3/14]	Transition metal ion transport (10^{-2}) [8/57]
Siderophore-iron transmembrane transporter activity (10^1) [2/4]	Cellular di-, tri-valent inorganic cation homeostasis (10^{-2}) [8/65]
ATPase activity (10^{-2}) [44/229] (Group 2)	**Siderophore** transport (10^1) [3/9]
Pyrophosphatase activity / **Hydrolase** activity, acting on acid anhydrides, in phosphorus-containing anhydrides (10^{-2}) [56/330] (Group 2)	**Regulation** of biological process (10^{-7}) [208/1500] (Group 2)
Purine ribonucleotide binding (10^{-1}) [96/673] (Group 2)	Organelle **organization and biogenesis** (10^{-6}) [213/1579] (Group 2)
Transcription regulator activity (10^1) [55/353] (Group 2)	**Regulation of gene expression** (10^{-4}) [144/1011] (Group 2)
GO: Cellular Component	**Regulation of biosynthetic** process (10^{-4}) [143/1014] (Group 2)
High affinity **iron permease complex** (10^1) [2/2]	**Chromatin modification** (10^{-4}) [48/231] (Group 2)
Cellular **bud** (10^{-3}) [37/169] (Group 2)	**Establishment and/or maintenance of chromatin architecture** (10^{-3}) [50/260] (Group 2)

Chromatin remodeling complex (10^{-2}) [23/82] (Group 2)	Chromosome organization and biogenesis (10^{-2}) [67/398] (Group 2)
Cellular bud neck (10^{-2}) [30/134] (Group 2)	Regulation of transcription (10^{-2}) [95/631] (Group 2)
Site of polarized growth (10^{-1}) [34/169] (Group 2)	Regulation of metabolic process (10^{-2}) [153/1154] (Group 2)
Nuclear lumen (10^{-1}) [82/560] (Group 2)	Microtubule cytoskeleton organization and biogenesis (10^{-2}) [23/85] (Group 2)
Nucleoplasm (10^{-1}) [56/343] (Group 2)	t-RNA export from nucleus (10^{-2}) [12/28] (Group 2)
Cytoskeleton (10^{-1}) [40/220] (Group 2)	A lot of other groups with higher P-values (Group 2)

TABLE 3.22: GO overrepresentation of gene clusters in Rad9 overexpression ChIP on chip

Numbers in parentheses correspond to hypergeometric test P-value as obtained from BiNGO analysis in Cytoscape (see Materials and Methods). Numbers in brackets correspond to the number of genes contained in our input fitting in each cluster, over the total number of yeast genes included in each cluster.

In Table 3.22, we can see that Rad9 has a different pattern of overrepresented gene clusters to which it is localised, if we compare to Tables 3.6, 3.7 and 3.8. When it is overexpressed, the iron binding/transport/homeostasis groups which are induced are higher in rank. Moreover, clusters related to chromatin modification and architecture appear. The cell wall subcellular localisation groups are not apparent as in the ChIP on chip for the endogenous Rad9.

It seems that in the case when Rad9 is overexpressed, the cell's physiological processes are somewhat impaired. To further examine this matter, we performed a genome-wide expression microarray experiment in non induced conditions (SC), with a strain which had *RAD9* inserted in a high copy plasmid (pDB20), as described in Materials and Methods. We discovered that ribosomal gene clusters were downregulated while others related to sugar transporter activity were upregulated (Figure 3.25 and Table 3.23). Also genes related to chromatin cohesion (Smc1, Mcd1, Ibd2) were downregulated. From ChIP on chip Tiling Arrays we noted that Rad9 was localised to *SMC1* gene. Smc1 protein is a subunit of the
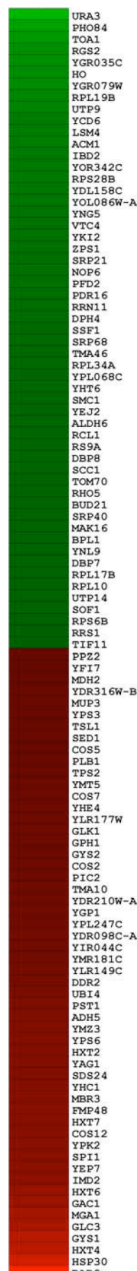
multiprotein cohesin complex, is essential and involved in chromosome segregation.

FIGURE 3.25: Expression Array of Rad9 overexpression
Analysis was performed as described in Materials and Methods. The genes that had a two-fold change and fit a statistical cut-off of 5% FDR-adjusted P-value were visualized with the use of MeV software. Red colour: upregulation; Green colour: downregulation.

The effect of Rad9 overexpression in the expression of such genes can partly explain the altered Rad9 localisation pattern because vital cell functions such as protein synthesis could be impaired.

UPREGULATED GO: MF	P-value	Freq	DOWNREGULATED GO: BP	P-value	Freq
mannose transporter activity	10^{-5}	4/15	ribosome biogenesis and assembly	10^{-5}	8/233
fructose transporter activity	10^{-5}	4/15	cytoplasm organization and biogenesis	10^{-5}	8/233
glucose transporter activity	10^{-5}	4/16	ribosome biogenesis	10^{-4}	7/196
hexose transorter activity	10^{-5}	4/17	rRNA processing	10^{-4}	6/162
monosaccharide trasporter activity	10^{-5}	4/17	rRNA metabolism	10^{-4}	6/171
sugar transporter activity	10^{-4}	4/21			
glycogen (starch) synthase activity	10^{-4}	2/2			
carbohydrate transporter activity	10^{-4}	4/26			
RNA-directed DNA polymerase activity	10^{-4}	5/51			
DNA-directed DNA polymerase activity	10^{-3}	5/63			
transporter activity	10^{-3}	12/365			

TABLE 3.23: Up- and downregulated gene clusters in Rad9 overexpression expression Array
BiNGO Analysis in Cytoscape Platform has been performed as described in Materials and Methods. P-value numbers correspond to hypergeometric test as obtained from BiNGO analysis in Cytoscape (see Materials and Methods). Numbers in Freq column correspond to the number of genes contained in our input fitting in each cluster, over the total number of yeast genes included in each cluster. MF: Molecular Function, BP: Biological Process

3.3.6.6.-- Rad9 and localisation pattern to active and induced genes

We have shown that Rad9 has a strong Aft1-dependent binding bias to transcriptionally active genes (see also Results Chapters 3.3.5.4 and 3.3.6.3.1 and Table 3.13). But how selective is Rad9 localisation to highly active genes? To address this question we performed a genome-wide experiment for Rad9 localisation when the strain was grown in medium with galactose instead of glucose, where it is known that particular gene groups are transcriptionally activated (being repressed in glucose) (Lashkari et al., 1997). If Rad9 had a tendency to bind to transcriptionally active regions with no selectivity we would expect to find it onto all genes transcriptionally

active in galactose. We have compared our results to the ones by Lashkari et al. (1997) and the results are presented in Table 3.24.

Row	A	GLUCOSE YPD	GALACTOSE RAF GAL	SC BSC BPS	RAF GAL NON-CODING	CODING
1	Glucose vs. galactose expression data (Lashkari et al., 1997, PNAS 94:13056)	GLUCOSE	GALACTOSE			
2	Ratio of					
3	gene expression	ChIP on chip experiments groups (Group1=the highest binding)			RAF GAL	
4	Glucose Galactose ORF Gene Description	YPD	RAF GAL	SC BSC BPS	NON-CODING	CODING
5	2.1 YHR018 ARG4 Arginosuccinate lyase	2	NO	3	~~~	~~~
6	3.5 YPR035 GLN1 Glutamate--ammonia ligase	1 high	NO	1	~~~	~~~
7	2.8 YML116 ATR1 Aminotriazole and 4-nitroquinoline resistance protein	NO	NO	3	~~~	~~~
8	2.0 YMR303 ADH2 Alcohol dehydrogenase II	NO	NO	3	~~~	~~~
9	3.7 YBR145 ADH5 Alcohol dehydrogenase V	NO	NO	NO	~~~	~~~
10	3.2 YBL030 AAC2 ADP, ATP carrier protein 2	NO	NO	NO	~~~	~~~
11	2.9 YBR085 AAC3 ADP, ATP carrier protein	NO	NO	NO	~~~	~~~
12	2.7 YDR298 ATP5 H1-transporting ATP synthase d chain precursor	NO	2	NO	+	~~~
13	2.5 YBR039 ATP3 H1-transporting ATP synthase g chain precursor	NO	NO	NO	~~~	~~~
14	5.5 YML054 CYB2 Lactate dehydrogenase cytochrome b2	NO	NO	3	~~~	~~~
15	3.4 YML054 CYB2 Lactate dehydrogenase cytochrome b2	NO	NO	3	~~~	~~~
16	2.3 YKL150 MCR1 Cytochrome-b5 reductase	NO	NO	NO	~~~	~~~
17	4.2 YBL045 COR1 Ubiquinol--cytochrome c reductase 44K core protein	NO	2	3	+	~~~
18	3.5 YDL067 COX9 Cytochrome c oxidase chain VIIA	NO	NO	NO	~~~	~~~
19	2.7 YLR038 COX12 Cytochrome c oxidase, subunit VIB	NO	NO	NO	~~~	~~~
20	2.6 YHR051 COX6 Cytochrome c oxidase subunit VI	NO	NO	NO	~~~	~~~
21	2.4 YLR395 COX8 Cytochrome c oxidase chain VIII	NO	NO	NO	~~~	~~~
22	2.3 YFR033 QCR6 Ubiquinol--cytochrome c reductase 17K protein	NO	NO	3	~~~	~~~
23	23.7 YLR081W GAL2 Galactose (and glucose) permease	NO	YES	NO	+++	+++
24	21.9 YBR018C GAL7 UDP-glucose-hexose-1-phosphate uridylyltransferase	NO	1 high	NO	+++	+++
25	21.8 YBR020W GAL1 Galactokinase	3	YES high	3	+++	+++
26	19.5 YBR019C GAL10 UDP-glucose 4-epimerase	2	YES high	3	+++	+++
27	14.7 YLR081 GAL2 Galactose (and glucose) permease	NO	YES	NO	+++	+++
28	8.6 YDR009W GAL3 Galactokinase	3	2	NO	~~~	+++
29	3.0 YML051 GAL80(1) Negative regulator for expression of galactose-induced genes	NO	2	NO	++	++
30	2.8 YML051 GAL80(2) Negative regulator for expression of galactose-induced genes	NO	2	NO	++	++
31	2.7 YER055 HIS1 ATP phosphoribosyltransferase	3	1	3	+++	~~~
32	3.4 YBR248 HIS7 Glutamine amidotransferase/cyclase	2	NO	3	~~~	~~~
33	7.4 YCL030 HIS4 Phosphoribosyl-AMP cyclohydrolaseyphosphoribosyl-ATP pyrophosphataseyhistidinol dehydrogenase	2	NO	1	~~~	~~~
34	5.8 YKR080 MTD1 Methylenetetrahydrofolate dehydrogenase (NAD1)	NO	NO	3	~~~	~~~
35	6.0 YDR019 GCV1 Glycine decarboxylase T subunit	NO	NO	2	~~~	~~~
36	6.1 YLR058 SHM2 Serine hydroxymethyltransferase	NO	NO	NO	~~~	~~~
37	8.1 YML123 PHO84 High-affinity inorganic phosphate/H1 symporter	1	NO	NO	~~~	~~~
38	3.5 YDR408 ADE8 Phosphoribosylglycinamide formyltransferase (GART)	NO	NO	NO	~~~	~~~
39	3.6 YDR408 ADE8 Phosphoribosylglycinamide formyltransferase (GART)	NO	NO	NO	~~~	~~~
40	4.4 YAR015 ADE1 Phosphoribosylamidoimidazole-succinocarboxamide synthase	3	NO	3	~~~	~~~
41	5.6 YMR300 ADE4 Amidophosphoribosyltransferase	NO	NO	3	~~~	~~~
42	5.6 YOR128 ADE2 Phosphoribosylaminoimidazole carboxylase	1	NO	1	~~~	~~~
43	6.0 YGL234 ADE5,7 Phosphoribosylamine-glycine ligase and phosphoribosylformylglycinamidine cyclo-ligase	1	NO	1	~~~	~~~
44	6.3 YBL015 ACH1 Acetyl-CoA hydrolase	1	NO	3	~~~	~~~

TABLE 3.24: Rad9 is localised to highly active genes under galactose induction
We used (Lashkari et al., 1997) expression data in glucose versus galactose (Column A) to obtain a list with the most highly transcribed genes in galactose (pink) and some of the highly transcribed in glucose (yellow). We then compared the strength of Rad9 binding on these genes, as obtained by the ChIP on chip analysis of three experimets: strains grown in YPD (column B), in galactose (column C) and in SC BCS BPS (column D). We grouped the genes where Rad9 was localised into three groups (Group1 had the highest binding). NO: no binding, YES high: very high binding, 1>2>3: binding with different strength.In columns I and J, is depicted the localization of Rad9 under galactose induction to non-coding and/or coding regions.

In Table 3.25, there is a summary of the qualitative analysis of Rad9 localisation in galactose growth conditions. The analysis was performed as previously described by using BiNGO plugin in Cytoscape platform. For the clustering, we used mainly the genes where Rad9 had the highest statistical significanct binding values.

Total (MF)

- **Structural** constituent of **ribosome** (10^{-21}) [36/222]

- Structural molecule activity (10^{-16}) [38/354]

Total (CC)

- **Cytosolic ribosome** (10^{-28}) [37/156]

- Cytosolic large ribosomal subunit (10^{-19}) [24/83]

- **Ribonucleoprotein** complex (10^{-15}) [43/500]

- Cytosolic small ribosomal subunit (10^{-7}) [13/62]

- eukaryotic translation elongation factor 1 complex (10^{1}) [2/5]

Total (BP)

- **Translation** (10^{-16}) [44/499]

- Cellular **biosynthetic** process (10^{-10}) [56/1141]

- Macromolecule biosynthetic process (10^{-5}) [56/1457]

- **Gene expression** (10^{-4}) [53/1448]

- Cellular protein **metabolic process** (10^{-2}) [54/1702]

- Cellular macromolecule metabolic process (10^{-1}) [54/1753]

- **Response to** cycloheximide (10^{-1}) [3/4]

- Response to cycloalkane (10^{-1}) [3/4]

- Response to organic cyclic substance (10^{-1}) [3/5]

- Response to antibiotic (10^{1}) [3/10]

- Response to organic substance (10^{1}) [4/24]

- Regulation of translational fidelity (10^{1}) [3/11]

- Negative regulation of translation (10^{1}) [3/11]

- Trehalose catabolic process (10^{1}) [2/3]

TABLE 3.25: GO gene clusters to which Rad9 is localised in galactose

Rad9-13Myc cells were grown in medium containing galactose as carbon source. Numbers in parentheses correspond to hypergeometric test P-value as obtained from BiNGO analysis in Cytoscape (see Materials and Methods). Numbers in brackets correspond to the number of genes contained in our input fitting in each cluster, over the total number of yeast genes included in each cluster. When no clustering was possible, it is mentioned respectively. MF: Molecular Function, BP: Biological Process, CC: Cellular Component.

In Table 3.25, we observe a high overrepresentation of gene clusters related to structural constituents of ribosome, translation and response to external stimuli, consistent with the different carbon source we used during growth. When we compared our results to the ones by (Lashkari et al., 1997), we found that Rad9 was present to most of the genes induced in galactose (Table 3.24). However, it was also present to other groups of genes as well (Table 3.25), which showed that Rad9 does not bind exclusively to induced active regions. Nevertheless, this experiment shows a very strong Rad9 binding bias to the highly active genes, since its localisation to these genes in galactose growth conditions is accompanied by a high binding value and a statistically important P-value (Figure 3.26).

DISTRIBUTION OF EACH PROTEIN BINDING PATTERN ON GENES REGARDING THEIR ACTIVITY
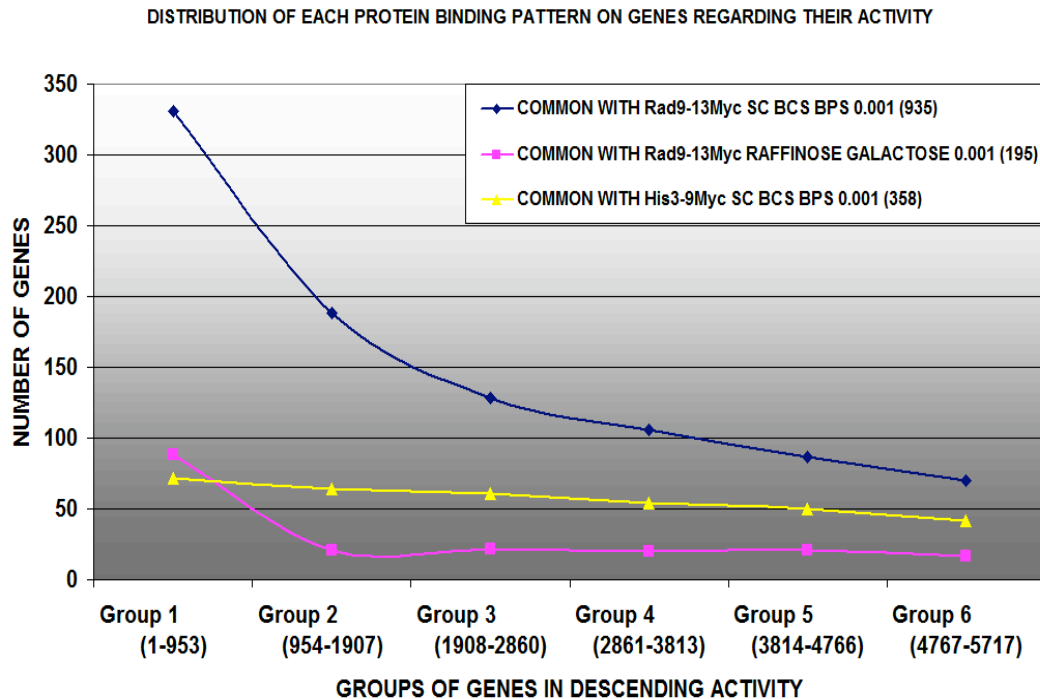
FIGURE 3.26: Rad9 is localised to the most highly active yeast genes in galactose
Yeast genes were grouped in 6 groups (*x* axis), containing ~1000 genes each, in descending transcriptional activity in SC BCS BPS growth conditions (obtained by our expression microarrays experiments). Illustrated is the binding pattern of Rad9 in raffinose-galactose growth conditions (pink line) as well as in SC BCS BPS (blue line) plotted as the number of genes that fit each group (*y* axis). His3 control protein is shown in yellow.

Worth mentioning is the fact that in galactose growth conditions, Rad9 was localised to 50% less genes compared to the glucose SC BCS BPS growth conditions and also that there was a shift to binding to more non-coding regions with a non coding: ORF ratio of about 1:1 (versus the 1:4 respective ratio in SC BCS BPS growth conditions). It seems that the kinetics in galactose favor the localization of more components to the promoter loci.

3.3.7.1.-- Rad9 in DNA damage conditions

We have so far studied Rad9 in non-DNA damage induced conditions. What happens when exogenous DNA damage is applied to the growing culture? How is the localisation pattern of Rad9 affected? Does Rad9 DNA damage checkpoint protein show any specificity in its distribution to the genome? If so, is it recruited to specific areas of the genome?

To address these questions we performed a genome-wide ChIP on chip analysis of Rad9 in SC BCS BPS growth conditions and used the drug zeocin to apply dsDNA damage randomly (see Materilas and Methods).

The analysis of the results (as described above and in Materials and Methods) showed that when DNA damage was applied, Rad9 distribution in ORF or non-coding regions remained similar as in the SC BCS BPS experiment (Figure 3.27). The overlap between the two experiments was ~40%.
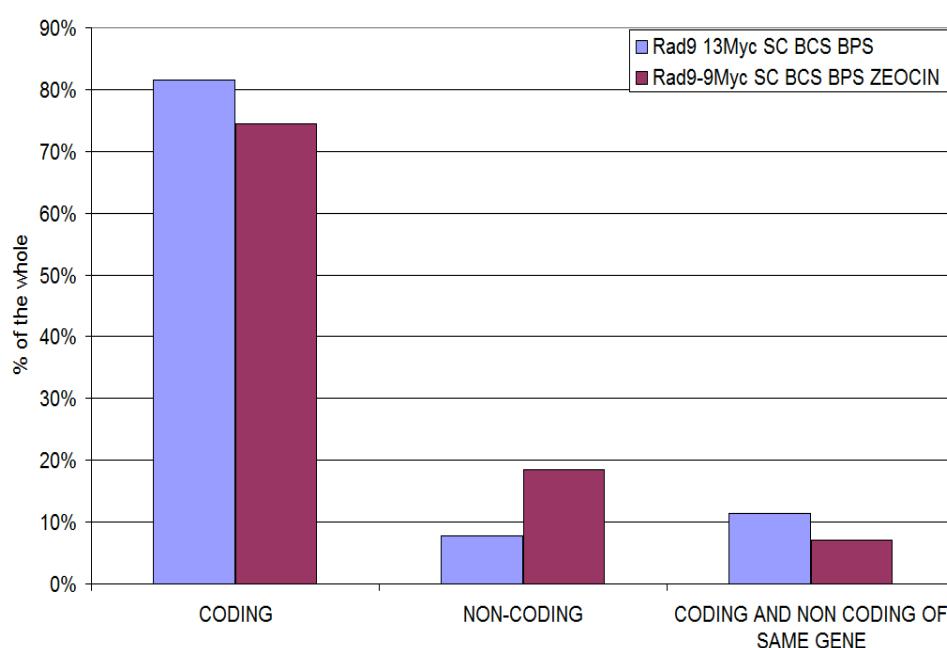
FIGURE 3.27: Distribution of Rad9 localisation sites
After performing the ChIP on chip experiments of Rad9 in SC BCS BPS zeocin (blue) or SC BCS BPS (red), we analyzed the distribution of Rad9 pattern in coding and non-coding areas (*x* axis). In the top legent, we can see the strains used, the growth conditions and the P-value that we set in order to obtain the list of genes where Rad9 binds (see Materials and Methods). The genes were Rad9 is localised in each occasion are expressed as percentage of the whole number of genes in each experiment and category (*y* axis).

We have then analyzed the activity state of the genes to which Rad9 was localised upon DNA damage and found that Rad9 again had a binding bias to the most transcriptionally active genes (Figure 3.28).

DISTRIBUTION OF EACH PROTEIN BINDING PATTERN ON GENES REGARDING THEIR ACTIVITY
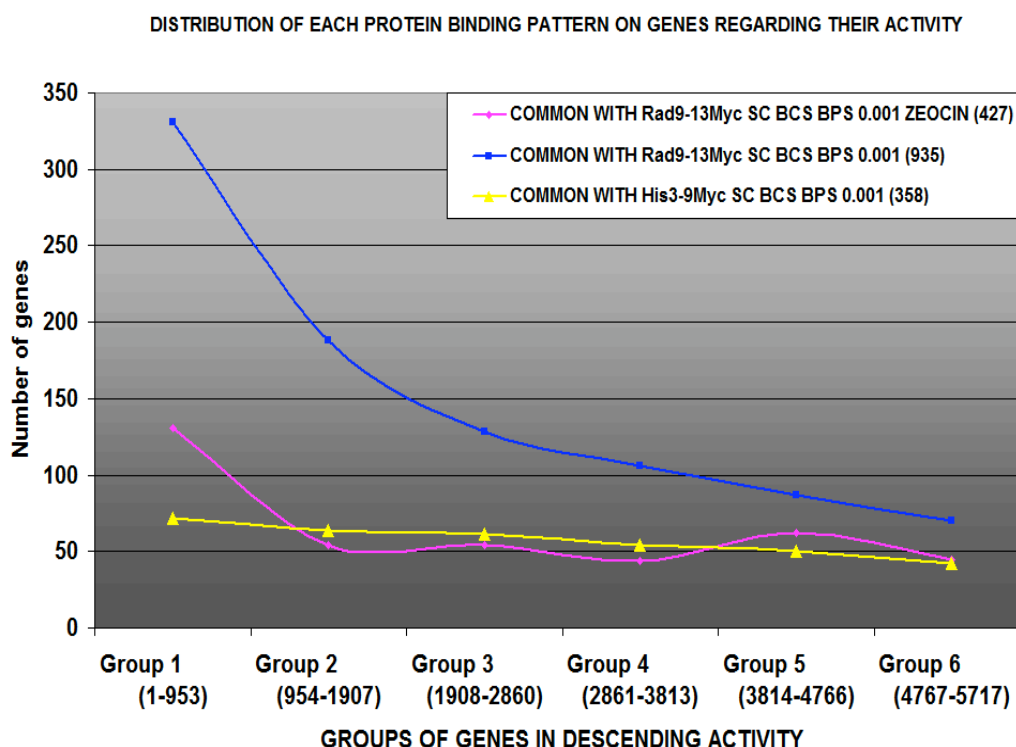
FIGURE 3.28: Rad9 is still localised to the most highly active yeast genes upon zeocin treatment

Yeast genes were grouped in 6 groups (*x* axis), containing ~1000 genes each, in descending transcriptional activity in SC BCS BPS growth conditions (obtained by our expression microarrays experiments). Illustrated is the binding pattern of Rad9 upon DNA damage (zeocin) growth conditions (pink line) as well as in SC BCS BPS (blue line) plotted as the number of common genes in each group (*y* axis). His3 control protein is shown in yellow.

The fact that Rad9 is localised strongly in genomic areas which are highly active under DNA damage conditions is consistent with the fact that highly active regions are more vulnerable and prone to DNA damage. Furthermore Rad9 is localised to genomic areas with an average of 43% GC content. We have shown that Rad9 also has the same strong binding bias to highly active regions even in the absence of DNA damage induced conditions. This could be indicative of a strong presence of Rad9 in loci which are prone to DNA damage, before the actual damage occurs. This means that Rad9 plays an important role in protecting genome integrity by performing a constant surveillance of chromatin which is prone to DNA damage. When we compared the highly active genes to which Rad9 is localised in both DNA damage and normal conditions we found that vital groups of genes were included, such as ones encoding for translation elongation factors, metabolic enzymes, Y'-Help1 DNA helicase (Y'-HELicase Protein 1) with role in telomere maintenance.

151

We have also performed a qualitative analysis of the results from the Rad9 ChIP on chip upon DNA damage as previously described by using BiNGO plugin in Cytoscape platform in order to obtain the overrepresented GO groups. For the clustering, we primarily used the genes where Rad9 had the highest statistical significanct binding values. The results are presented in the following tables (3.26-3.28).

GO: MOLECULAR FUNCTION	
Rad9-13Myc SC BCS BPS ZEOCIN	**Rad9-13Myc SC BCS BPS**
Iron ion binding (10^{-4}) [19/116]	**Translation elongation factor** activity (10^{-3}) [7/14]
ATP-dependent **helicase** activity (10^{-3}) [15/73]	**Catalytic** activity (10^{-2}) [127/2123]
Iron ion transmembrane **transporter** activity (10^{-2}) [6/11]	**Ligase** activity (10^{-2}) [4/4]
Siderophore iron transmembrane transporter activity (10^{-2}) [4/4]	**Vitamin** binding (10^{-2}) [11/61]
ATPase activity (10^{-2}) [24/229]	**Biotin** binding (10^{-2}) [4/5]
Pyrophosphatase activity (10^{-1}) [30/330]	**Oxidoreductase** activity, acting on paired donors, with incorporation or reduction of molecular oxygen (10^{-2}) [5/18]
Hydrolase activity, acting on acid anhydrides (10^{-1}) [30/332]	Oxidoreductase activity (10^{-2}) [29/307]
Purine nucleotide binding (10^{-1}) [49/711]	**Hydrolase** activity, acting on carbon-nitrogen (but not peptide) bonds, in cyclic amidines (10^{-1}) [6/17]
Translation elongation factor activity (10^{1}) [5/14]	Glyceraldehyde-3-phosphate dehydrogenase (phosphorylating) activity (10^{-1}) [3/3]
Oxidoreductase activity, oxidizing metal ions (10^{1}) [4/10]	Lyase activity [11/96], NAD binding [5/19], Metal ion binding [44/812] (10^{1})
More clusters with higher P-value	Other clusters with higher P-values

TABLE 3.26: GO Molecular Function gene clusters to which Rad9 is localised in zeocin (DNA damage)
See text for experimental procedure. Numbers in parentheses correspond to hypergeometric test P-value as obtained from BiNGO analysis in Cytoscape (see Materials and Methods). Numbers in brackets correspond to the number of genes contained in our input fitting in each cluster, over the total number of yeast genes included in each cluster.

In Table 3.26, we see common function gene clusters such as the ones related to oxidoreductase activity, translation elongation factor activity and hydrolase activity placed in different ranking. In addition, new clusters such as the one related to helicase activity is apparent. The higher ranking of iron-related genes is explained by a side-effect of the use of zeocin: the drug needs copper ions in order to function properly, so, when applied to the growing culture it leads to *CTR1* downregulation (unpublished results) which in turn leads to non-functional Fet3 oxidase which is necessary for iron-metabolism (see also Introduction Chapter 5.1.1 and Introduction Figure 1.10). Hence, an iron depletion is secondarily created, Aft1 is activated and the transcription of genes which promote the iron uptake is induced. Rad9 in the presence of zeocin is localised to the iron related genes because they are highly active due to the above-mentioned *CTR1* copper transporter side-effect. Nevertheless, the binding of Rad9 to highly active genes is again apparent.

GO: BIOLOGICAL PROCESS	
Rad9-13Myc SC BCS BPS ZEOCIN	**Rad9-13Myc SC BCS BPS**
Iron assimilation (10^{-5}) [7/8]	Pyruvate **metabolic** process (10^{-8}) [14/29]
Iron ion **transport** (10^{-4}) [11/32]	Carboxylic acid metabolic process (10^{-8}) [46/363]
Siderophore transport (10^{-3}) [6/9]	Hexose **biosynthetic** process (10^{-7}) [12/22]
Biological regulation (10^{-3}) [103/1722]	Monosaccharide biosynthetic process (10^{-7}) [13/27]
Iron-ion homeostasis (10^{-3}) [10/37]	Organic acid metabolic process (10^{-7}) [46/369]
Telomere maintenance via recombination (10^{-2}) [7/19]	**Gluconeogenesis** (10^{-7}) [11/19]
Cell **adhesion** (10^{-2}) [5/9]	Alcohol biosynthetic process (10^{-6}) [15/47]
Regulation of **translation** (10^{-1}) [35/417]	**Glucose catabolic** process (10^{-5}) [14/44]
Regulation of cellular biosynthetic process (10^{-1}) [36/436]	Glycolysis (10^{-5}) [12/32]
Posttranscriptional regulation of gene expression (10^{-8}) [14/29]	Hexose catabolic process (10^{-5}) [14/49]
Regulation of biological quality (10^{-1}) [32/377]	**Glucose metabolic** process (10^{-4}) [16/67]
Regulation of cellular protein metabolic	**Regulation** of cellular protein metabolic

process (10^{-1}) [35/438]	process (10^{-4}) [45/438]
Vacuolar protein catabolic process (10^{-1}) [15/119]	**Posttranscriptional regulation** of gene expression (10^{-4}) [44/426], more in Group 3
Positive regulation of transcription (DNA dependent) (10^{1}) [13/115]	Regulation of **translation** (10^{-4}) [43/417]
Mitotic recombination (10^{1}) [7/38]	Regulation of cellular biosynthetic process (10^{-4}) [43/436]
Glycolysis (10^{1}) [6/32]	**Oxidation reduction** (10^{-2}) [29/279]
Amine transport (10^{1}) [8/56]	**Amino acid biosynthetic** process (10^{-2}) [17/128] (Group 2)
Glucose catabolic process (10^{1}) [7/44]	**Metal** ion transport (10^{-1}) [19/84] (Group 3)
Branched chain family amino acid biosynthetic process (10^{1}) [4/14]	**Iron** ion transport (10^{-1}) [10/32] (Group 3)
Telomere maintenance (10^{1}) [8/59]	
Leucine metabolic process (10^{1}) [3/8]	
Loss of chromatin silencing during replicative cell aging (10^{1}) [3/8]	
Progressive alteration of chromatin during replicative cell aging (10^{1}) [3/9]	

TABLE 3.27: GO Biological Process gene clusters to which Rad9 is localised in zeocin (DNA damage)

See text for experimental procedure. Numbers in parentheses correspond to hypergeometric test P-value as obtained from BiNGO analysis in Cytoscape (see Materials and Methods). Numbers in brackets correspond to the number of genes contained in our input fitting in each cluster, over the total number of yeast genes included in each cluster.

In Table 3.27, we observe that highly active gene clusters, such as the ones related to amino acid metabolism or other metabolic processes, are included both in the clustering upon zeocin or without zeocin. Furthermore, genes related to telomere maintenance are also part of the list. The iron-related gene clusters are higher in the rank due to the side-effect of zeocin, as mentioned above.

GO: CELLULAR COMPONENT	
Rad9-13Myc SC BCS BPS ZEOCIN	**Rad9-13Myc SC BCS BPS**
Plasma membrane (10^{-5}) [38/351]	Fungal-type **cell wall** (10^{-7}) [21/90]
Fungal-type **cell wall** (10^{-3}) [16/90]	**External encapsulating** structure (10^{-5}) [21/107]

External encapsulating structure (10^{-2}) [16/107]	Cytosolic **ribosome** (10^{-2}) [20/156]
Anchored to membrane (10^{-1}) [10/47]	Anchored to membrane (10^{1}) [9/47]
Polysome (10^{1}) [5/15]	COPII vesicle coat (ER→Golgi transport) (10^{1}) [4/9]
Cortical actin cytoskeleton (10^{1}) [8/51]	
High affinity iron permease complex (10^{1}) [2/2]	

TABLE 3.28: GO Cellular Component gene clusters to which Rad9 is localised in zeocin (DNA damage)

See text for experimental procedure. Numbers in parentheses correspond to hypergeometric test P-value as obtained from BiNGO analysis in Cytoscape (see Materials and Methods). Numbers in brackets correspond to the number of genes contained in our input fitting in each cluster, over the total number of yeast genes included in each cluster.

Gene clusters related to cell wall and ribosome are among the most overrepresented ones in both physiological and under zeocin conditions (Table 3.28). This is yet another element pointing to Rad9 implication in highly active loci.

We took our analysis one step further by comparing our results from Rad9 ChIP on chip upon DNA damage to the one performed after growth in physiological conditions in order to get an insight of:

i) Gene clusters to which Rad9 localises only in DNA damage

ii) Gene clusters to which Rad9 localises only in physiological conditions

iii) Gene clusters to which Rad9 localises regardless DNA damage

The results of this analysis are presented in the following tables, starting from Table 3.29, which includes the gene clusters overrepresented only in DNA damage induced conditions.

Rad9 localises only in DNA damage (zeocin) GO: MOLECULAR FUNCTION			
P-value	n	X	Gene cluster
10^{-3}	17	56	**electron carrier** activity
10^{-2}	41	274	substrate-specific **transmembrane transporter** activity
10^{-1}	35	242	**ATPase** activity
10^{-1}	20	107	**helicase** activity
10^{1}	23	150	ion transmembrane transporter activity
10^{1}	8	30	**histone binding**
10^{1}	43	374	**pyrophosphatase** activity
10^{1}	43	374	**hydrolase** activity, acting on acid anhydrides
10^{1}	8	31	**heme** binding

P-value	n	X	Gene cluster
			Rad9 localises only in DNA damage (zeocin) **GO: BIOLOGICAL PROCESS**
10^{-8}	10	10	**intron homing**
10^{-3}	146	1458	**nucleic acid metabolic** process
10^{-2}	51	381	**transmembrane** transport
10^{-1}	167	1793	biological regulation
10^{-1}	100	965	**response to stimulus**
10^{-1}	15	67	mRNA export from nucleus
10^{-1}	61	532	RNA processing
10^{0}	72	669	**regulation** of **transcription**
10^{0}	5	9	polyphosphate metabolic process
10^{0}	20	118	**conjugation**
10^{0}	53	460	**DNA metabolic** process
10^{0}	78	759	**regulation of nucleobase**, nucleoside, nucleotide and nucleic acid **metabolic process**
10^{0}	90	905	regulation of cellular biosynthetic process
10^{0}	5	10	**vitamin** transport
10^{0}	22	144	RNA splicing
10^{0}	28	205	**positive regulation of nucleobase**, nucleoside, nucleotide and nucleic acid **metabolic process**
10^{0}	28	205	positive regulation of nitrogen compound metabolic process
10^{0}	139	1545	regulation of biological process
10^{0}	100	1045	regulation of cellular metabolic process
10^{0}	83	837	**RNA metabolic** process
10^{0}	32	248	positive regulation of cellular metabolic process
10^{0}	72	704	**response to stress**
10^{0}	12	58	amine transport
10^{0}	87	888	**regulation** of macromolecule **biosynthetic** process
10^{0}	21	139	nucleobase, nucleoside, nucleotide and nucleic acid transport
10^{0}	31	240	positive **regulation** of macromolecule **metabolic** process
10^{1}	13	70	nucleus organization
10^{1}	165	1922	cellular nitrogen compound metabolic process
10^{1}	16	98	interphase
10^{1}	9	39	regulation of multi-organism process
10^{1}	9	39	regulation of conjugation
10^{1}	20	136	cation transport
10^{1}	20	136	multi-organism process
10^{1}	8	32	respiratory electron transport chain
10^{1}	34	285	regulation of transcription from RNA polymerase II promoter
10^{1}	25	192	positive regulation of gene expression
10^{1}	25	192	chromatin modification
10^{1}	39	345	cell division

P-value	n	X	Gene cluster
			Rad9 localises only in DNA damage (zeocin) **GO: CELLULAR COMPONENT**
10^{-1}	112	1141	nuclear part
10^{0}	45	366	plasma membrane

TABLE 3.29: GO Gene clusters to which Rad9 is localised only upon DNA damage

See text for experimental procedure. Numbers in "P-value" column correspond to hypergeometric test
P-value as obtained from BiNGO analysis in Cytoscape (see Materials and Methods). Numbers in "n"

column correspond to the number of genes contained in our input fitting in each cluster, over the total number of yeast genes included in each cluster ("X" column).

In Table 3.29, we see that upon DNA damage (zeocin) Rad9 is localised to gene clusters related to electron carrier, transporter and helicase activities, DNA metabolism and regulation of nucleic acids metabolism, chromatin modification and that there is an overrepresentation of genes encoding for proteins localised to the nucleus. These results give Rad9 protein another potential in the downstream components of DNA repair mechanisms to which effector proteins could normally act.

Table 3.30, illustrates the gene clusters overrepresented in the case of Rad9 binding only in physiological conditions.

P-value	n	X	Gene cluster
	Rad9 localises only in physiological conditions GO: Molecular Function		
10^{-15}	446	2192	**catalytic** activity
10^{-3}	25	58	**vitamin binding**
10^{-2}	46	162	cofactor binding
10^{-1}	76	323	**oxidoreductase** activity
10^{-1}	25	71	isomerase activity
10^{-1}	176	908	nucleotide binding
10^{-1}	12	24	**oxidoreductase** activity, acting on the aldehyde or oxo group of donors
10^{-1}	154	793	purine nucleotide binding
10^{0}	6	8	thiamin pyrophosphate binding
10^{0}	25	83	oxidoreductase activity, acting on CH-OH group of donors
10^{0}	11	24	transferase activity, transferring nitrogenous groups
10^{0}	171	923	**hydrolase** activity
10^{0}	11	25	exopeptidase activity
10^{0}	9	18	oxidoreductase activity, acting on the aldehyde or oxo group of donors, NAD or NADP as acceptor
10^{0}	4	4	AMP binding
10^{0}	126	654	adenyl ribonucleotide binding
10^{0}	27	97	lyase activity
10^{0}	15	42	vitamin B6 binding
10^{0}	15	42	pyridoxal phosphate binding
10^{0}	148	791	cation binding
10^{0}	15	43	metallopeptidase activity
10^{0}	13	35	peptide binding
10^{0}	124	652	ATP binding
10^{1}	22	76	oxidoreductase activity, acting on the CH-OH group of donors, NAD or NADP as acceptor
10^{1}	67	318	transmembrane transporter activity
10^{1}	143	775	metal ion binding
10^{1}	14	41	hydrolase activity, hydrolyzing O-glycosyl compounds
10^{1}	8	17	aminopeptidase activity
10^{1}	8	17	carboxylic acid binding
10^{1}	9	21	transaminase activity
10^{1}	10	25	intramolecular transferase activity

Rad9 localises only in physiological conditions GO: Biological Process			
P-value	n	X	Gene cluster
10^{-12}	221	912	small molecule **metabolic** process
10^{-11}	118	396	organic acid **metabolic** process
10^{-10}	97	315	cellular **amino acid** and derivative metabolic process
10^{-10}	110	377	**carboxylic** acid **metabolic** process
10^{-9}	112	391	cellular **ketone metabolic** process
10^{-8}	84	270	cellular **amine metabolic** process
10^{-7}	54	146	cellular aromatic compound metabolic process
10^{-7}	77	247	**cellular amino acid metabolic** process
10^{-7}	88	303	amine metabolic process
10^{-5}	56	172	organic acid biosynthetic process
10^{-5}	56	172	**carboxylic acid** biosynthetic process
10^{-5}	60	192	regulation of translation
10^{-5}	63	206	**posttranscriptional regulation of gene expression**
10^{-5}	46	133	cellular amino acid biosynthetic process
10^{-5}	64	215	regulation of cellular protein metabolic process
10^{-4}	69	240	alcohol metabolic process
10^{-4}	41	118	hexose metabolic process
10^{-3}	78	310	cellular nitrogen compound biosynthetic process
10^{-3}	29	78	cellular carbohydrate catabolic process
10^{-2}	33	98	**glucose metabolic** process
10^{-2}	70	279	regulation of protein metabolic process
10^{-2}	85	363	**oxidation reduction**
10^{-1}	34	118	vacuolar protein catabolic process
10^{0}	41	159	coenzyme metabolic process
10^{0}	10	20	hexose biosynthetic process
10^{0}	13	31	glycolysis
10^{0}	15	39	serine family amino acid metabolic process
10^{0}	9	17	gluconeogenesis
10^{0}	11	24	NADP metabolic process
10^{0}	10	21	NADPH regeneration
10^{0}	5	6	acetyl-CoA biosynthetic process

Rad9 localises only in physiological conditions GO: Cellular Component			
P-value	n	X	Gene cluster
10^{-2}	662	4074	**cytoplasm**
10^{0}	6	8	chaperonin-containing T-complex
10^{0}	13	31	vesicle coat
10^{0}	42	169	cytosolic **ribosome**
10^{0}	5	6	MCM complex
10^{0}	4	4	alpha,alpha-trehalose-phosphate synthase complex (UDP-forming)
10^{0}	50	219	cytosolic part

TABLE 3.30: GO Gene clusters to which Rad9 is localised only in physiological conditions

See text for experimental procedure. Numbers in "P-value" column correspond to hypergeometric test P-value as obtained from BiNGO analysis in Cytoscape (see Materials and Methods). Numbers in "n" column correspond to the number of genes contained in our input fitting in each cluster, over the total number of yeast genes included in each cluster ("X" column).

As expected, in physiological conditions Rad9 was localised in gene clusters related to transcriptionally active groups of genes as we have already established, including clusters related to catalytic and oxidoreductase activities, amino acid and glucose metabolism and ribosomes (Table 3.30).

Table 3.31 contains the overrespresented Rad9 GO gene clusters to which Rad9 localises regardless DNA damage induction.

P-value	n	X	Gene cluster
	Rad9 localises regardless DNA damage GO: Molecular Function		
10^{-9}	92	703	**nucleoside binding**
10^{-9}	90	698	purine nucleoside binding
10^{-8}	106	908	nucleotide binding
10^{-8}	88	694	adenyl nucleotide binding
10^{-8}	84	652	**ATP binding**
10^{-8}	84	654	adenyl ribonucleotide binding
10^{-7}	94	793	purine nucleotide binding
10^{-7}	90	752	purine ribonucleotide binding
10^{-7}	90	752	ribonucleotide binding
10^{-4}	38	242	**ATPase activity**
10^{-4}	50	374	pyrophosphatase activity
10^{-4}	50	374	**hydrolase** activity, acting on acid anhydrides
10^{-2}	8	17	translation elongation factor activity
10^{-1}	4	4	**siderophore-iron transmembrane** transporter activity
10^{-1}	4	4	mannose binding
10^{-1}	5	7	cyclohydrolase activity
10^{-1}	9	28	transition metal ion transmembrane transporter activity
10^{0}	168	2192	**catalytic** activity
10^{0}	7	20	glucosidase activity
10^{0}	10	44	rRNA binding
10^{0}	5	11	**iron ion transmembrane transporter** activity
10^{0}	10	45	metal ion transmembrane transporter activity
10^{0}	4	7	monosaccharide binding
10^{0}	5	12	**oxidoreductase activity**, oxidizing metal ions
10^{0}	11	57	iron ion binding
10^{0}	9	41	hydrolase activity, hydrolyzing O-glycosyl compounds
10^{0}	16	107	helicase activity
10^{1}	18	147	RNA polymerase II transcription factor activity
10^{1}	5	18	hexose transmembrane transporter activity
10^{1}	2	2	copper-transporting ATPase activity
10^{1}	17	137	transcription factor activity
10^{1}	3	6	hydroxymethyl-, formyl- and related transferase activity
10^{1}	25	233	structural constituent of ribosome
10^{1}	20	174	ligase activity
10^{1}	6	27	oxidoreductase activity, acting on paired donors, with incorporation or reduction of molecular oxygen
10^{1}	15	119	protein serine/threonine kinase activity

P-value	n	X	Gene cluster
10^1	4	13	sugar binding
10^1	4	13	cofactor transporter activity
10^1	9	56	electron carrier activity
10^1	9	56	specific RNA polymerase II transcription factor activity
10^1	3	7	beta-glucosidase activity
10^1	31	323	oxidoreductase activity
			More with higher P-values

Rad9 localises regardless DNA damage GO: Biological process			
P-value	n	X	Gene cluster
10^{-13}	183	1794	biological regulation
10^{-10}	157	1546	regulation of biological process
10^{-8}	39	192	**regulation** of **translation**
10^{-7}	40	206	**posttranscriptional regulation of gene expression**
10^{-6}	39	215	**regulation** of cellular protein **metabolic process**
10^{-6}	96	874	**regulation of gene expression**
10^{-5}	97	905	regulation of cellular biosynthetic process
10^{-5}	104	1003	**regulation** of macromolecule metabolic process
10^{-5}	112	1116	regulation of metabolic process
10^{-5}	43	279	regulation of protein metabolic process
10^{-5}	13	31	**iron ion transport**
10^{-4}	17	55	transition metal ion transport
10^{-4}	40	254	**cellular cell wall organization**
10^{-4}	40	254	**external encapsulating structure organization**
10^{-4}	7	8	**iron assimilation**
10^{-4}	30	162	regulation of localisation
10^{-4}	15	45	di-, tri-valent inorganic cation transport
10^{-4}	29	155	regulation of transport
10^{-4}	104	1045	**regulation of primary metabolic** process
10^{-4}	7	9	**siderophore** transport
10^{-2}	12	38	**iron ion homeostasis**
10^{-2}	5	6	iron assimilation by chelation and transport
10^{-2}	5	6	siderophore-iron transport
10^{-2}	5	6	iron chelate transport
10^{-2}	22	126	**fungal-type cell wall organization**
10^{-2}	7	14	positive regulation of transport
10^{-1}	19	104	**regulation of cell size**
10^{-1}	22	135	**monocarboxylic acid metabolic** process
10^{-1}	20	117	regulation of cellular component size
10^{-1}	20	117	regulation of anatomical structure size
10^{-1}	15	74	purine nucleotide biosynthetic process
10^{-1}	173	2245	biosynthetic process
10^{-1}	36	295	positive regulation of biological process
10^{-1}	12	51	**glucose catabolic** process
10^{-1}	5	8	**flocculation**
10^{-1}	170	2212	cellular biosynthetic process

Rad9 localises regardless DNA damage GO: Cellular Component			
P-value	n	X	Gene cluster
10^{-11}	31	95	extracellular region

P-value	n	X	
10^{-10}	30	100	**fungal-type cell wall**
10^{-10}	31	108	cell wall
10^{-10}	31	108	**external encapsulating** structure
10^{-3}	35	237	**site of polarized growth**
10^{-3}	28	169	cytosolic **ribosome**
10^{-2}	32	212	**membrane** fraction
10^{-2}	32	212	insoluble fraction
10^{-2}	17	74	**plasma membrane** part
10^{-1}	35	275	ribosome
10^{-1}	4	5	**eukaryotic translation elongation factor 1** complex
10^{-1}	27	201	cellular bud
10^{0}	54	556	ribonucleoprotein complex
10^{0}	17	110	**mating projection tip**
10^{0}	15	93	cytosolic large ribosomal subunit
10^{1}	11	64	cytosolic small ribosomal subunit
10^{1}	11	64	cortical actin cytoskeleton
10^{1}	2	2	high affinity iron permease complex
10^{1}	2	2	transcriptional repressor complex
10^{1}	12	83	90S preribosome

TABLE 3.31: GO Gene clusters to which Rad9 is localised regardless DNA damage

See text for experimental procedure. Numbers in "P-value" column correspond to hypergeometric test P-value as obtained from BiNGO analysis in Cytoscape (see Materials and Methods). Numbers in "n" column correspond to the number of genes contained in our input fitting in each cluster, over the total number of yeast genes included in each cluster ("X" column).

Gene clusters which were overrepresented for Rad9 binding regardless DNA damage induced conditions included the ones related to nucleotide, ATP-binding, ATPase, hydrolase, siderophore transmembrane, catalytic and oxidoreductase activities, regulation of translation, gene expression and metabolic processes, and clusters encoding for cell wall and ribosomal proteins.

3.3.7.2.—Rad9 and Aft1 in DNA damage induced conditions

We wanted to further investigate whether Aft1 and Rad9 show a special phenotype when growing in DNA damage induced conditions. This would offer further information to the Aft1-Rad9 relation in these specific conditions. To address this matter, we performed growth assay experiments of a series of mutants upon DNA damage conditions, using the drug zeocin (Figure 3.29). As expected, *rad9Δ* strain exhibited serious growth defect (no growth). The *aft1Δ* strain showed the same serious phenotype, which highlights the importance of these two proteins in DNA damage response. *aft2Δ* strain showed a very mild -almost no defective- phenotype, it

nevertheless added to the growth defect of *rad9Δaft1Δ*, since the triple mutant (*rad9Δaft1Δaft2Δ*) has a more serious slow growth phenotype. *aft1Δ* phenotype dominated over *aft2Δ* phenotype, as shown in the double mutant *aft1Δaft2Δ* in which there was no growth observed. Rad9 deletion compensated for the defective phenotype of the double mutant *aft1Δaft2Δ* as shown in the triple *rad9Δaft1Δaft2Δ* strain. It is also shown that the combination of deletion of both *RAD9* and *AFT1* released the growth defect of the single mutants. These observations show that Aft1 and Rad9 indeed have a special interdependency in DNA damage induced conditions.
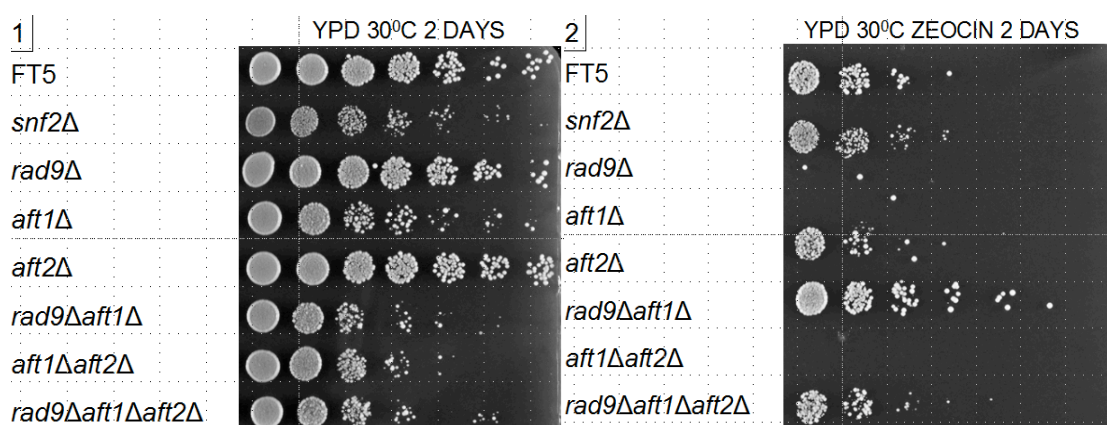
FIGURE 3.29: Growth assay in DNA damage conditions (zeocin)
Cultures of the depicted mutants were grown in rich medium (YPD) until exponential phase (OD$_{550}$~0.5). All cultures were adjusted to the same optical density and the drug zeocin was added to a final concentration of 150μg/ml and incubation continued for 2 hours. Untreated cells were also kept as control cultures. After that, seven serial dilutions from each culture were spotted on YPD plates. Plates were incubated for 2 days.

Both Rad9 and Aft1 were produced in lower amounts in DNA damage conditions as shown by Western blot (Figure 3.30A).

A)
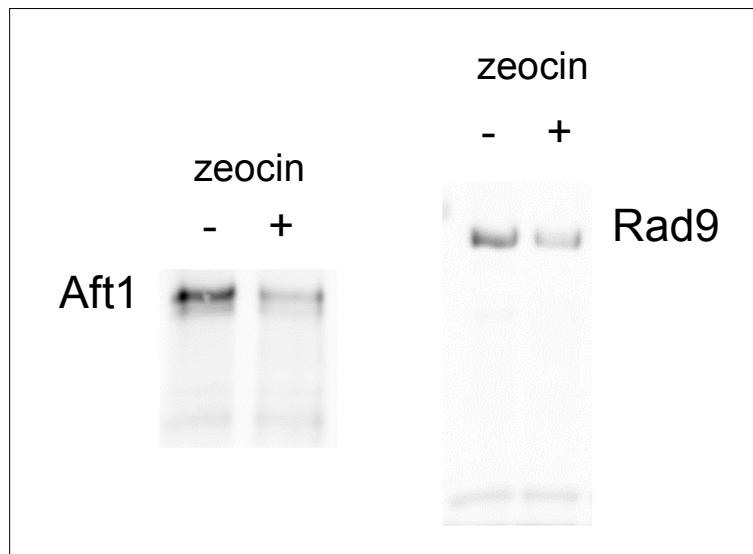
B)
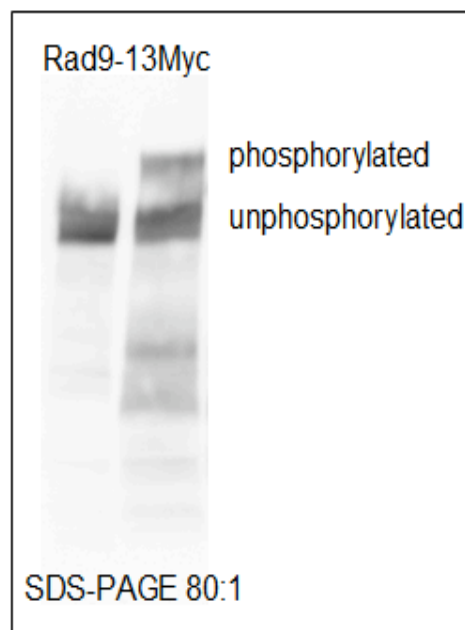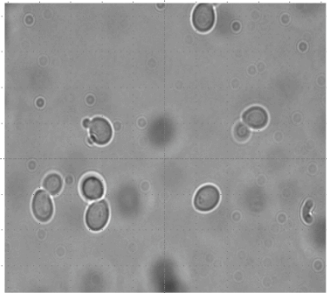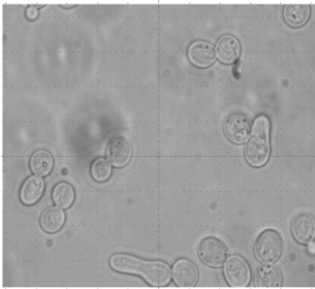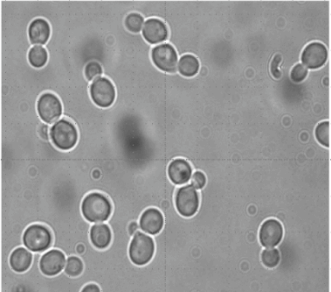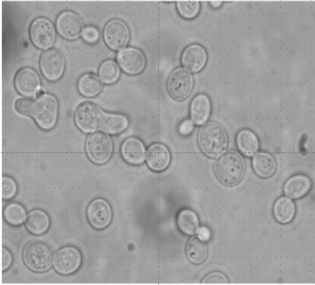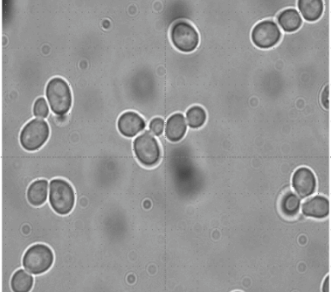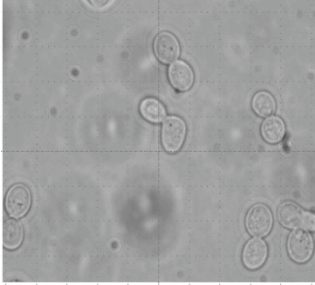
FIGURE 3.30: Rad9 and Aft1 are produced in lower amounts upon DNA damage

A) Strains with tagged Rad9-13Myc and Aft1-9Myc proteins were cultured in SC BCS BPS until OD$_{550}$=0.5. Zeocin was then added at a final concentration 150μg/ml and cultures were incubated for 2 hours. Untreated cultures were also kept. Protein extract from ~2x10^7 cells was isolated and used for SDS-PAGE analysis. B) SDS PAGE analysis in gel 80:1(acrylamide:bisacrylamide) where the phosphorylated form of Rad9 after zeocin treatment is visible (right column), compared to the non-phosphorylated in normal growth conditions (left column, used in the majority of the experiments of this thesis).

Having performed the growth assays for Rad9, Aft1 and Aft2 single, double and triple mutants, we subsequently performed a microscopic analysis of the mutants

in the presence or absence of induced DNA damage. To address this question, we prepared cultures of the mutants in the same growth conditions, and collected exponentially growing cells, treated or untreated with the drug zeocin and examined them microscopically (Figure 3.31). We observed that in the strains where Rad9 is absent in combination to Aft1 or both Aft1/Aft2 (*rad9Δaft1Δ*, *rad9Δaft1Δaft2Δ*), the phenotype of the wt cells (prolonged cells, stopped in G2/M phase) is much more mild, which is consistent with our growth assay results presented in Figure 3.29. Thus, this combination of mutants seems to give the cells resistance to the drug zeocin and subsequently DNA damage.

SC	SC + 150μg/ml zeocin	Notes on zeocin
WT (FT5)	WT (FT5) +ZEOCIN	large cells and buds (G2/M stopped, no cytokinesis), prolonged cell morphology present, low percentage of apoptotic cells
rad9Δ	rad9Δ +ZEOCIN	resemble WT
aft1Δ	aft1Δ +ZEOCIN	less in number, many cysts (maybe vacuoles)→indication of apoptosis (?), not many prolonged cells
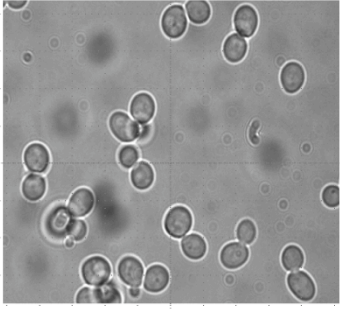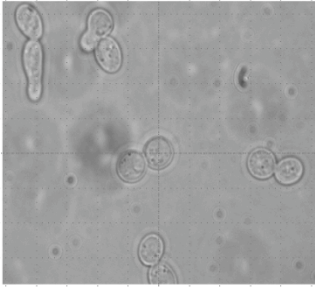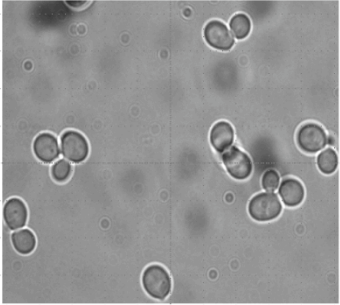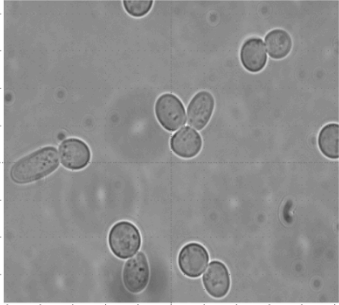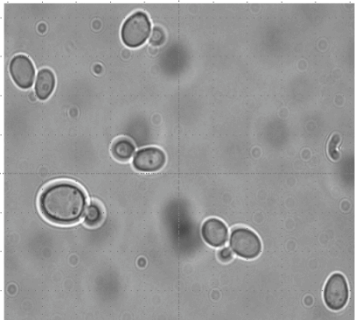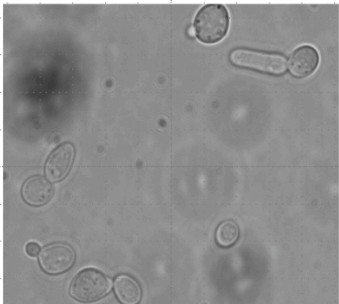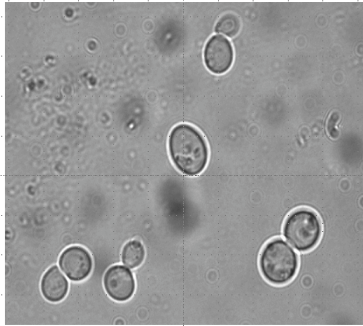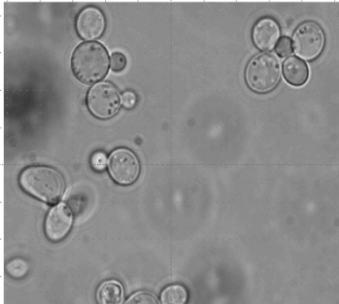
aft2Δ	*aft2Δ +ZEOCIN*	cysts are present, not so large prolonged cell population
rad9Δaft1Δ	*rad9Δaft1Δ +ZEOCIN*	resemble FT5, not a lot of cysts present
aft1Δaft2Δ	*aft1Δaft2Δ +ZEOCIN*	smaller sized cells, apoptotic cells are singe (vs the previous which were in division phase), do they die earlier?
rad9Δaft1Δaft2Δ	*rad9Δaft1Δaft2Δ +ZEOCIN*	less cells, round with black spots inside, no multi-cyst phenotype

FIGURE 3.31: Microscopic analysis of Rad9 and Aft1 mutants in the presence or absence of DNA damage

Yeast cells were grown in SC medium until $OD_{550}=0.5$. Zeocin was added to a final concentration of 150μg/ml and incubation continued for another 2 hours. Cells were then collected and examined microscopically (optical microscope, 100X lens).

3.3.8.-- Deconstructing Aft1: A focus on the multifunctional transcription factor

As we discussed in Introduction Chapter 5.1.3, Aft1 is a transcription factor with roles extending further than being the classic regulator of iron-responsive genes under iron depletion. Aft1 associates with the kinetochore complex by interacting with members of the complex such as Cbf1 and Iml3, while it is also co-localised with Ndc10 inner kinetochore protein (Hamza and Baetz, 2011; Measday et al., 2005). Furthermore, Aft1 is required for the increased association of cohesin with pericentric chromatin and *aft1Δ* cells display chromosome segregation defects in meiosis, hence a role in chromosome integrity becomes apparent (Measday et al., 2005).

As we have previously shown by ChIP analyses, Aft1 is present to most of the centromeres. Furthermore, we showed that *aft1Δ* strains have a serious growth defect in 6-AU assays, which associates Aft1 to transcription elongation. We have also established that Aft1 transcription factor interacts with Rad9 DNA damage checkpoint protein and examined the effect of Aft1 in Rad9 genome-wide binding pattern. We have also studied the genome-wide localisation pattern of Aft1 and found it to be localised mostly to ORFs rather than promoter regions of genes. The number of the genes on which Aft1 was present was bigger than the ones consisting the iron regulon (25 genes). In Results Chapter 3.3.6.2 we have examined qualitatively the loci to which Aft1 was localised and found that apart from the expected iron-related clusters, there were also overrepresented others related to translation elongation and metabolic processes of amino acids and glucose.

In this Chapter we will examine our results in the light of published data about Aft1 new targets and genetic interactants. We wanted to check whether Aft1 localisation to the centromeres was dependent on Cbf1 inner kinetochore protein with which Aft1 was found to genetically and physically interact (Measday et al., 2005). To address this question we constructed a *cbf1Δ* Aft1-9Myc strain and performed ChIP analysis to see whether Aft1 localisation to centromeres was altered. In our analysis we included *CTR1* promoter and ORF regions as well as *FTR1* promoter to see if this interaction was necessary for Aft1 binding to other targets as well. The results are presented in Figure 3.32. We can see that Aft1 localisation on centromeres and the other targets tested is Cbf1-independent, since the Aft1 binding pattern does not change significantly in the absence of Cbf1. Aft1 presence in the centromeres may be related to its interaction to other kinetochore proteins such as Iml3 with which it

was recently found to interact (Hamza and Baetz, 2011) or it can be due to an own property.

Aft1 dependence on Cbf1
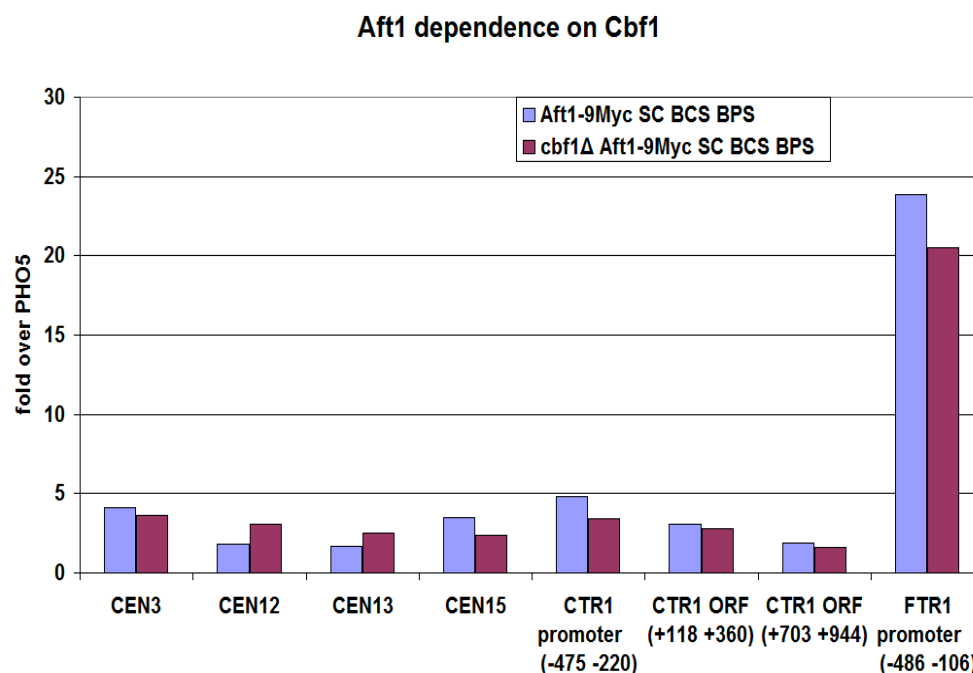
FIGURE 3.32: Aft1 localisation on centromeres, *CTR1* and *FTR1* is Cbf1-independent
Chromatin Immunoprecipitation assay was perfomed in cells grown under induction conditions (SC BCS BPS, *CTR1, FTR1* genes were active) and we examined the enrichment of Aft1 on CEN3, CEN12, CEN13, CEN15, *CTR1* promoter and ORF, *FTR1* promoter by real time PCR. Normalization was performed firstly over INPUT and secondly by measuring the binding of Rad9 on *PHO5* coding region, where Rad9 binding is minimal in any growth conditions (as tested by our group) and dividing to Rad9 enrichment in each case.

A recent functional genomic analysis of Aft1 revealed new iron-independent functions (Berthelet et al., 2010). The genetic network that Berthelet group constructed revealed that Aft1 affects a diverse range of cellular processes, including the *RIM101* pH pathway, cell wall stability, DNA damage, protein transport, chromosome stability and mitochondrial function. We have compared the results from our Aft1 genome-wide analysis to their functional analysis to see if Aft1 was localised to the genes with which it genetically interacted. We indeed found 13 genes (out of 48) that fit into this category (Table 3.32) which enhances the multifunctional character of Aft1 transcription factor.

GENE	DESCRIPTION
CCS1	Copper chaperone, involved in oxidative stress protection
FET4	Low-affinity Fe(II) transporter of the plasma membrane
CBF1	Transcription factor and component of the kinetochore

CLN2	G1 cyclin involved in regulation of the cell cycle
SSH1	Subunit of the Ssh1 translocon complex
DRS2	Cdc50-Drs2 endosome complex that regulates cell polarity
RPS21B	Protein component of the small (40S) ribosomal subunit
MIT1	Transcriptional regulator of pseudohyphal growth
HUR1	Protein of unknown function
GDS1	Protein of unknown function
CHO2	Phosphatidylethanolamine methyltransferase (PEMT)
IRA2	GTPase-activating protein that negatively regulates RAS
TIM18	Component of the mitochondrial TIM22 complex

TABLE 3.32: Genes with which Aft1 genetically interacts (Berthelet et al., 2010) and is localised to (this study)
See text for details.

As we can see from Table 3.32, Aft1 seems to have the potential to affect directly cellular processes related not only to iron regulation but also others, such as chromosome stability (*CBF1*), cell cycle process (*CLN2*), protein transport (*SSH1, DRS2*), structure of ribosome (*RPS21B*).

Aft1 was also found to affect the transcription of genes other than the ones included in the iron regulon (Shakoury-Elizeh et al., 2004). Shakoury-Elizeh et al. showed that when yeast is subjected to iron deprivation, it undergoes a transcriptional remodeling, resulting in a shift from iron-dependent to parallel, but iron-independent, metabolic pathways such as biotin uptake and biosynthesis, nitrogen assimilation, and purine biosynthesis. Two enzymes active in these pathways, biotin synthase and glutamate synthase, require an iron-sulfur cluster for activity. Iron deprivation activates transcription of the biotin importer and simultaneously represses transcription of the entire biotin biosynthetic pathway. Multiple genes involved in nitrogen assimilation and amino acid metabolism are induced by iron deprivation, whereas glutamate synthase, a key enzyme in nitrogen assimilation, is repressed. A CGG palindrome within the promoter of glutamate synthase confers iron-regulated expression, suggesting control by a transcription factor of the binuclear zinc cluster family.

We have compared our results from ChIP on chip experiments of Rad9 and Aft1 to the results from Shakoury-Elizeh et al. (2004) to see if there exists a direct role of these proteins to the newly revealed Aft1 target genes. The results are

presented in Table 3.33. We can see that Aft1 and Rad9 proteins are present to the majority of the newly identified Aft1 targets which points to a direct role of Aft1 in their altered expression and also highlights the Aft1-Rad9 interdependency in metabolic genes, consistent with the results of our study.

Gene	Aft1 SC BCS BPS	Rad9 SC BCS BPS
New genes in Iron Dependent response		
SMF3	++ PO	-
COT1	++ O	+ O
VHT1	_	+ O
HMX1	+++ PO	++ PO
TIS11	+++ PO	+ O
Regulation of nitrogen metabolism		
MEP2	-	++ O
GDH1	+ O	+ O
CAR1	-	-
GDH3	+++ O	-
CHA1	++ PO	-
AGP1	-	-
CAN1	+ O	-
GAT1	++ O	+ O
ARO9	+ O	-
DUR3	+ P	-
DAL3	-	-
BAT2	-	-
Purine biosynthetic pathway		
GVC1	-	++ O
GVC2	-	++ O
GVC3	-	+ O
SER1	++ O	+ O
SER2	-	-
SHM2	++ O	-
MTD1	-	+ O
ADE3	+ O	+++ O

ADE4	-	+ O
ADE5,7	++ O	+++ O
ADE8	-	-
ADE6	++ O	++ O
ADE2	+ O	+++ O
ADE1	-	+ O
ADE13	+ O	-
ADE17	+ O	++ O
ADE16	++ O	+ O
ADE12	-	-

TABLE 3.33: Aft1 and Rad9 protein localisation to new Aft1 targets
The first column contains the genes found in Shakoury-Elizeh et al (2005) study (see text for description), while the other two columns describe the binding or not of Aft1 or Rad9 proteins. Value of binding is also noted accordingly [- < + (Group3) < ++ (Group2) < +++ (Group1)]. P:Promoter, O: ORF.

CHAPTER 4

DISCUSSION

RAD9 was the first DNA damage-dependent checkpoint gene identified in yeast (Weinert and Hartwell, 1988); however the exact molecular details regarding the function of the corresponding protein are not yet fully understood. Rad9 has been up to now studied almost entirely under DNA-damage induced conditions with the vast majority of the existing studies being focused on its role in the DDR. The dynamics of Rad9 recruitment to chromatin have not been studied before under a general functional perspective. In the present thesis, the localization and functionality of Rad9 protein was studied by genome-wide expression and localisation (ChIP on chip) microarray analyses. This is the first time in which Rad9 role is examined in a genome-wide scale, under no DNA damage-induced conditions.

Furthermore, we have found a new Rad9-interacting protein, the Aft1 transcription factor which is primarily responsible for the iron homeostasis in the cell. The combined study of the localisation pattern of Rad9 in relation to Aft1 in yeast's genome under certain growth conditions revealed a strong interdependency between the two proteins. In addition, we provide for the first time a genome-wide localisation analysis of Aft1 which has already proved to be a multifunctional protein with roles extending further than the classic regulation of iron-responsive genes.

Rad9 DNA damage checkpoint protein interacts with Aft1 transcription factor

We have found that Rad9 interacts with Aft1 transcription factor (Figure 3.1) and is recruited to genes of the iron regulon in an Aft1-dependent manner (Figure 3.3) under physiological growth conditions. Performing such small scale ChIP analyses, we have also shown Aft1 recruitment to the Mac1-regulated *CTR1* gene independently of Rad9. This is an example of a locus where both Rad9 and Aft1 are recruited, maybe as part of a larger protein complex. The presence of Aft1 on *CTR1* is indicative of another possible level of transcription regulation of this gene. In addition, since we found that in *aft1Δ* or *aft1Δaft2Δ* strains, *CTR1* transcription decreases considerably, we believe that Aft1 has a possible direct role in *CTR1* expression.

Rad9 affects the transcription of a small percentage of yeast genes

We have established a connection between Rad9 as well as Aft1 and transcription elongation, as shown by 6-AU assays including a synthetic phenotype in *rad9Δaft1Δ* (Figure 3.7) which is a further indication of the two proteins acting together on some common pathway(s). Rad9 implication with transcription has not been previously shown under unperturbed or non-DNA damage inducing conditions. It was shown that the *RAD9*-dependent gene transactivation is required for excision repair of active genes but not for repair of non-transcribed DNA (Al-Moghrabi et al., 2009). The same group showed that the role of Rad9 in NER is through the up-regulation of genes involved in this repair process and that Rad9 is required for repair of the transcribed and non-transcribed strands of active genes but not for repair of transcriptionally inactive DNA sequences. However, Rad9 has not up to now been connected to transcription *per se* under non DNA damage-inducing conditions.

By our genome-wide expression profiling in *rad9Δ* strains we found ~2% of yeast genes to be transcriptionally altered with statistical significance ($P<0.05$). Since Rad9 does not affect the global transcriptional pattern of yeast to a significant extend, it is not likely for Rad9 to act as a general transcriptional activator/repressor. The functional analysis of the transcriptionally altered genes revealed that they include genes related to metabolism, to ribosomal biogenesis, processing and structure, related to mitochondria (import, membranes, metabolism), to vacuoles, to chromatin silencing and to transcription regulation. There is not a general transcription regulator which is affected by Rad9. The fact that metabolic and ribosomal genes are affected in *rad9Δ* could explain the growth defect in 6-AU assay (Figure 3.7A).

When we compared the genome-wide expression analysis results from *rad9Δ* strains to the Rad9 localisation pattern to the genome, we found that Rad9 is localized to only a small fraction of the genes whose transcription affects (Figure 3.9). These overlapping genes were related to metabolism.

Rad9 is present to chromatin under non DNA damage-inducing conditions

Our study is the first example of a high resolution genome-wide analysis of the Rad9 localisation pattern. Although it has been previously shown that a significant proportion of Rad9 is already chromatin-bound in unperturbed conditions throughout the cell cycle (Gilbert et al., 2001; Granata et al., 2010; Hammet et al., 2007), the studies were rather focused on the molecular basis of this interaction rather than its

function. Under untreated conditions, Rad9 is chromatin bound through the interaction of its Tudor domain with H3K79me and its BRCT-mediated dimerization. Upon DNA damage, the activated Rad9 may change its conformation, interacting also with γ-H2A. In M-phase, an alternative means of Rad9 recruitment near DNA lesions involves its interaction with Dpb11 replication initiation protein (Granata et al., 2010). Although Rad9 seems to have the capability of binding to ssDNA through its Tudor domain (Lancelot et al., 2007), we could not find a possible motif that it may recognize by performing *in silico* analysis. In our study, we provide a comprehensive analysis of the Rad9 localisation pattern under unperturbed conditions and we focus on the functional aspects of the Rad9 chromatin binding.

We believe that Rad9 localisation to the genome is to certain extend stochastic, since more than ¼ of the Rad9 localisation targets were different between the replicate experiments. Nevertheless, our analysis showed that the common targets of Rad9 are characterised by well defined traits, pointing to a non-random localisation of Rad9 in the genome.

Features of Rad9 genome-wide localisation map

Our Rad9 genome-wide localization analyses provide a fine structured map of Rad9 localisation pattern in multiple growth conditions. We found that Rad9 has a strong preference on localization to coding regions of genes (~75% of the peaks) rather than on intergenic ones (Figure 3.10).

We found Rad9 localised in at least half of the yeast's telomeres, especially at the Left ends, mainly in X rather than Y elements. X elements are repressed and Y' elements are active (Zhu and Gustafsson, 2009). Although Rad9 has a tendency to localize to active regions (see below), it is also present to telomeric repressed and devoid of nucleosomes regions, possibly because of their vital fuction for the cell survival. Our results confirm previous studies which have examined the role of Rad9 in these loci. In budding yeast, shortened telomeres activate a DNA damage response similar to the one triggered by DSBs (AS and Greider, 2003; Enomoto et al., 2004). (Michelson et al., 2005) has included Rad9 in an anticheckpoint mechanism which most likely exists to prevent healthy telomeres from constitutively activating checkpoint signaling. This mechanism is based on the fact that the subtelomeric repeat sequences, because of their high copy number and proximity, allow efficient repair of DNA breaks near the telomere. The nuclease Exo1, is involved in the

generation of ssDNA and contributes to the activation of the DNA damage checkpoint in *cdc13-1* mutants (Maringele and Lydall, 2002; Zubko et al., 2004); this involves the Exo1 phosphorylation in a checkpoint-dependent manner (which includes Mec1, Rad17, Rad24, Rad9 and Rad53) when telomeres are uncapped (hence unprotected) (Morin et al., 2008). Lazzaro et al. (2008) proposed that Rad9, when bound to chromatin, may represent a direct structural impediment to nuclease activity or it may promote the formation of a chromatin structure that inhibits exonucleolytic processing of DNA; this could be due to the interaction of the Tudor domain of Rad9 with methylated H3 or due to the interaction of BRCT domain of Rad9 with phosphorylated checkpoint proteins, or histones at sites of DNA damage and thus inhibiting nuclease activity (Du et al., 2006; Hammet et al., 2007). Furthermore, it has been shown that repeated elements (such as Ty and Y' elements) play a central role in the dynamic organisation of genome architecture by interacting with specific non-repetitive loci leading to inter- and intrachromosomal interactions as a part of an epigenomic regulatory system (O'Sullivan et al., 2009). It is worth studying if and how Rad9 may be involved in such a system.

Rad9 is present to ~50% of yeast retrotransposons, although the result was not reproducible in our replicate experiment, pointing towards a not quite specific Rad9 localisation to these featutres. Ty elements are present in loci prone to participate in chromosome rearrangements; they are associated with genomic "fragile" sites, where replication pauses and chromosomes are more likely to break (Cha and Kleckner, 2002). RNA can serve as a template for DNA synthesis (through reverse transcriptase encoded by Ty elements) during repair of a chromosomal DSB in yeast (Storici et al., 2007). Thus, the localisation of Rad9 in such loci is rather expected. Furthermore, there is an example of a Rad9-dependent signaling pathway activation of a Ty1 element in *est2* mutants (defective for reverse transcription) (Scholes et al., 2003). Transposition is a major source of gene expansion during genome evolution. The insertion event can also influence genomic evolution by disrupting coding or transcriptional control elements, or by promoting chromosomal rearrangements via homologous recombination (Kim et al., 1998). We believe that Rad9 plays a safeguarding role in such vital genomic loci ensuring that chromosome rearrangements occur with no alterations due to possible future DSB events. It is important that Rad9 presence in such loci seems to be Aft1-dependent.

We found both Rad9 and Aft1 proteins localised to centromeres which is in agreement with results from mammalian systems where DNA damage checkpoint proteins were found in centromeres (including Rad9's partial homolog Brca1) reviewed by (Shimada and Komatsu, 2009). Thus, Rad9 may have a role in preservation of genome integrity, through a possible co-operation with Aft1 in centromeric regions. We found that Aft1 localisation on centromeres is Rad9-independent, whereas Rad9 localisation is Aft1-dependent. Rad9 does not have a crucial effect on Aft1 localisation to centromeres. Furthermore, it has recently been shown that there exists endogenous transcription at the centromeres regulated by Cbf1 and Ste12 transcription factors in an RNAPII-dependent manner (Ohkuni and Kitagawa, 2011). This group proposes that *CEN* transcription might be responsible for the proper topology of *CEN* DNA. Our findings are in agreement with Okhuni and Kitagawa data since Aft1 transcription factor is localised on centromeric chromatin, as shown by us and others (Lee et al., 2002b) and also in complex with Rad9. We describe new elements in the centromeric region which are worth examining to see if and how they contribute to endogenous transcription in these loci.

We have shown that Rad9 is recruited in an Aft1-dependent manner to highly active genomic regions and GC-rich loci. These loci have a more extended chromatin conformation than AT-rich isochores (Dekker, 2007; Gilbert et al., 2004b; Yokota et al., 1997). GC-rich genes display higher levels of H3 and H4 acetylation compared to more AT-rich genes (Dekker, 2007). GC-rich regions have been connected to high rates of meiotic recombination DSBs (see below). It is possible that the GC content-dependent differences in chromatin conformation, the histone modification status and the transcriptional activity are determinants of Rad9 binding pattern in the genome.

Our analysis revealed that Rad9 has a binding bias to genes longer than the average which was even stronger in *aft1*Δ strains. Bibliography lacks studies that correlate specific traits or localisation of proteins to sizes of genes. Nevertheless, it has been shown that genes with long ORFs are correlated to higher H4 acetylation in *set2*Δ cells (deficient of H3 methylation) (Li et al., 2007b; Xue-Franzen et al., 2010) and this may also be a mark which drives Rad9 recruitment to specific genes. Furthermore, we observed that the number of Rad9 localisation sites correlated to the chromosome size except for chrIV (which is significantly the largest yeast chromosome), where the sites were proportionally less than expected. This unique case of the largest yeast chromosome can be explained by the fact that large

chromosomes cross over less often per kilobase than shorter chromosomes (Kaback et al., 1992). Large chromosomes also have lower hotspot density and less meiotic recombination DSBs (Blitzblau et al., 2007; Gerton et al., 2000; Kaback et al., 1992; Martini et al., 2006); and, as we will discuss below, we found Rad9 localised to a significant percentage of meiotic recombination hotspots. We speculate that Rad9 is present on these loci because of they are prone to DSB events; hence Rad9 is in the vicinity to play a surveillance role, ensuring a rapid response.

Rad9 interaction with Aft1 is a critical factor on the genome-wide localisation pattern of the former to the most highly active genes

Our expression and genome-wide localisation studies for Rad9 showed that Rad9 is localised under non DNA damage inducing conditions to the most highly active genes in an Aft1-dependent manner (Figure 3.19). The strong binding bias of Rad9 to highly active genes was completely abolished in *aft1Δ* strains, since the distribution shifted to being even in all activity groups. Highly transcribed regions are more prone to DNA damage since they have largely open chromatin conformation. Rad9 presence (with high binding value) to the highly active genes under galactose growth conditions confirmed the result observed under SC growth conditions. The binding bias of Rad9 to highly active genes is also supported by the fact that in the genome-wide localisation experiment performed in SC BCS BPS growth conditions (where iron- and copper-regulated genes are up-regulated) we observed strong binding of Rad9 to these targets.

Rad9 is also localized to the most highly active genes upon DNA damage (Figure 3.28). The fact that Rad9 is localised strongly in genomic areas which are highly active under DNA damage conditions is in agreement with the fact that highly active regions are more vulnerable and prone to DNA damage. It has been shown that there exists a proportional relation between the transcriptional activity of a gene and the mutation rate of a gene (Kim et al., 2007) and recent results show an increased accumulation of apurinic and apyrimidinic sites in highly transcribed DNA (Kim and Jinks-Robertson, 2009). This fact suggests a link between transcription and the fidelity of DNA replication. Highly transcribed genes are generally an impediment for replication forks (Azvolinsky et al., 2009). Situations like these have as a consequence the collision between the DNA replication and transcription machineries (Prado and Aguilera, 2005) which lead to transcription-associated recombination

(Gottipati et al., 2008; Prado and Aguilera, 2005; Wellinger et al., 2006). The fact that Rad9 has a strong binding bias to highly active regions under unperturbed conditions as well as under DNA damage-induced conditions is indicative of a strong presence in loci which are prone to DNA damage, even before the actual damage occurs. Rad9 seems to play an important role in protecting genome integrity by performing a constant surveillance of chromatin which is prone to DNA damage.

It has been shown that Rad9 is required for the repair of the TS and Non TS (NTS) of active genes but not for the repair of transcriptionally inactive sequences (Al-Moghrabi et al., 2009). It was also shown that UV-dependent *de novo* protein synthesis is required for efficient repair of NTS of active genes but not for repair of non-transcribed DNA (Al-Moghrabi et al., 2003). This fact highlights a connection of Rad9 protein and transcriptionally active sequences which is in consistency to our work. Furtheremore, Al-Moghrabi et al. have shown that the inhibition of UV-mediated *de novo* protein synthesis, which is required for efficient NER, does not have any effect on the efficiency of excision repair in the *rad9Δ* cells. This suggests that *RAD9* and *de novo* protein synthesis may act through the same pathway/mechanism. Therefore it is logical to attribute the role of Rad9 in NER to its UV-dependent trans-activator role which leads to the up-regulation of genes involved in this repair process after UV-exposure such as *RAD2, RAD7, RAD16* and *RAD23* which are in fact part of the *RAD9* regulon (Friedberg et al., 1995). Based on Al-Moghrabi et al (2009) work, it can be pointed out that in the absence of the coupling between transcription and NER, UV-dependent *de novo* protein synthesis becomes dispensable for NER, despite the fact that the target gene is actively transcribed (Lee et al., 2001, 2002a). This suggests that UV-dependent gene trans-activation is required for NER only when the repair process is coupled to transcription, a process that cells have evolved to allow prompt removal of DNA damage by favoring repair of the TS to the detriment of the complementary NTS.

In addition, it has recently been found in embryonic stem cells that a DNA repair complex, namely the trimeric XPC nucleotide excision repair complex, is selectively required for the synergistic activation of the *Nanog* gene by Oct4 and Sox2 (Fong et al., 2011). This study identified a transcriptional coactivator with diversified functions in maintaining ES cell pluripotency and safeguarding genome integrity. Although, Rad9 protein cannot be considered a transcriptional coactivator *per se*, the two systems may be comparable, since Rad9 is a DNA damage repair protein and

interacts with two transcription factors (Mac1 and Aft1) (Gkouskou et al., unpublished and this study).

Hotspots of meiotic recombination and Rad9 in mitosis

Rad9 localises to hotspots and hotORFs of meiotic recombination with high probability in an Aft1-dependent manner (Figure 3.22). This was shown after comparing our genome-wide localization data with the data by three individual groups who provided a quite comprehensive mapping of these loci (Buhler et al., 2007; Gerton et al., 2000; Robine et al., 2007). We believe that the presence of Rad9 to these loci is related to their nature: prone to DNA damage, absence of nucleosomes, GC-rich. It supports the model in which Rad9 is distributed on chromatin under non DNA damage-induced conditions, with a localization bias to loci which are sensitive to DNA damage, playing a safeguarding role and ensuring a rapid and effective response after the damage, securing genome integrity. Aft1 seems again to play a vital role in Rad9 localisation to DNA damage prone regions, since in *aft1Δ* cells, Rad9 binding in hotspots and hotORFs is diminished. This interplay between the transcription factor and the DNA damage checkpoint protein seems to be very important for the preservation of genome fidelity.

Localisation pattern of Rad9 to average gene reveals common patterns with epigenetic marks

By performing average gene analysis, we have found that Rad9 follows a characteristic localisation pattern forming a bell-shaped curve in the coding region of the average gene, with a tendency to bind stronger to the 3' portion of the ORF (Figure 3.23A). This pattern is shifted in the absence of Aft1, forming a peak at the 3' end (and 3'UTR) of the average gene. The relative occupancy of Aft1 on the average gene is not changed by the absence of Rad9. Rad9 and Aft1 have similar localization patterns on the average gene, consistent with the model of the two proteins participating in the same complex.

In an attempt to decipher whether Rad9 follows an epigenetic mark as a means which determine its localization, we compared our average gene analysis results to the relative occupancy of different types of methylation and acetylation, and H3 and H4 histones occupancy as calculated by other groups (Li et al., 2007b; Pokholok et al., 2005). Even though Rad9 can recognize the H3K79 methylated histones through its

Tudor domain, we found that H3K36me3 and H3K4me relative occupancy patterns were more similar to the one of Rad9. Further experiments would be informative in order to examine whether Rad9 can indeed directly or indirectly recognize H3K36 methylated histones (see Future Experiments below). Furthermore, in *set2Δ* strains (absence of H3 methylation) the AcH4 shows a peak at the 3'portion of gene coding regions (Li et al., 2007a), resembling that of H3K36 trimethylation and the pattern of Rad9 localisation. We could not find similarities to H3K9, H3K14 and H4 acetylation, H3K4 trimethylation versus Rad9 relative occupancy.

Rad9 localises to highly active genes related to cell growth in an Aft1-dependent manner

The qualitative analysis of our results from the genome-wide binding pattern of Rad9 showed that it is localised to clusters related to catalylic activity, oxidoreductase activity, metabolic processes, translation elongation factor activity, ligase-, vitamin-, biotin-binding activity, cell wall localisation. Groups like the one for oxidoreductase activity, metabolic or cell wall-related are connected to high transcriptional activity, which is in consistence to the results from the multiple analyses that we performed. Rad9 is found on genes required for cell growth. The importance of Rad9 localisation to such genes is supported by the fact that we found Rad9 localised to both coding and non-coding regions of genes related to protein synthesis.

Aft1 is required for Rad9 localisation to highly transcriptionally active gene clusters, since in *aft1Δ* cells Rad9 localisation to well known active groups such as the ones related to oxidoreductase activity, amino acid metabolic process and cell wall is absent or underrepresented (Table 3.13). Aft1 association to Rad9 is important for the localisation of the latter to further gene clusters, such as the ones related to catalytic activity, post-transcriptional regulation of gene expression, presence to cell wall (Table 3.13 versus Table 3.14).

We show that Aft1 is very important in establishing the Rad9 localisation to genes related to cell growth (such as metabolic, or biosynthetic of glucose and amino acids, encoding ribosomal proteins). Rad9 presence on genes related to cell growth, in an Aft1-dependent manner, can be of great importance since it connects a DNA damage checkpoint protein to vital cellular processes under non DNA damage induced conditions.

Rad9 can act together with Aft1 under DNA damage conditions

We found that under DNA damage conditions[4] Rad9 is localised strongly in highly active genomic areas which is consistent with the fact that these regions are more vulnerable and prone to DNA damage. The same is also true in unperturbed conditions. This is indicative of a strong localisation of Rad9 in loci which are prone to DNA damage, before the actual damage occurs. We speculate that Rad9 plays an important role in protecting genome integrity by performing a constant surveillance of chromatin which is prone to DNA damage. When we compared the highly active genes to which Rad9 is localised in both DNA damage and normal conditions we found that vital groups of genes were included, such as ones encoding for translation elongation factors, metabolic enzymes and Y'-Help1 DNA helicase (Y'-HELicase Protein 1) which has a role in telomere maintenance.

Upon DNA damage, Rad9 is localised to gene clusters related to electron carrier, transporter and helicase activities, DNA metabolism and regulation of nucleic acids metabolism and chromatin modification. These results point to a potential implication of Rad9 protein in the actual DNA repair mechanisms, which is further to its classic role as a mediator protein of the damage signal.

Our functional assays revealed that Aft1 and Rad9 have a special interdependency in DNA damage conditions (zeocin) (Figure 3.29). The single mutants exhibited serious growth defect (no growth), whereas the combination of deletion of both *RAD9* and *AFT1* released the growth defect of the single mutants. Rad9 deletion compensated for the defective phenotype of the double mutant *aft1Δaft2Δ* as shown in the triple *rad9Δaft1Δaft2Δ* strain. These results are in consistency with our microscopic analysis of the mutants under DNA damage (Figure 3.31): in the strains where Rad9 is absent in combination to Aft1 or both Aft1/Aft2 (*rad9Δaft1Δ*, *rad9Δaft1Δaft2Δ*), the phenotype of the WT cells (prolonged cells, stopped in G2/M phase) is much more mild. We have found a series of cell growth-related genes (such as metabolic and ribosomal genes) to be downregulated in *rad9Δ* cells (Table 3.1). If Rad9's absence can cause reduction of glucose metabolism, this can explain the compensation of the defective phenotype of the double mutant

---

[4] Add of zeocin, a drug that randomly created dsDNA breaks.

aft1Δaft2Δ when we delete Rad9, since it is has been shown that cells grown in low glucose survive better upon DNA damage (MMS) (Kitanovic et al., 2009).

Aft1 is a multifunctional transcription factor

Aft1 has been connected with roles beyond iron metabolism: it contributes to the preservation of genome integrity by localising to centromeres and interacting with kinetochore proteins (Cbf1, Ndc10, Iml3) (Hamza and Baetz, 2011; Measday et al., 2005). We have performed manual ChIP analysis for all chromosome centromeres and confirmed Aft1 presence to most of them. In addition, we have shown that Aft1 localisation to centromeres is Cbf1-independent. Further experiments should be performed to decipher the nature of Aft1 presence in the centromeres. It may be related to its interaction to other kinetochore proteins (such as Iml3 or Ndc10) or it can be due to an own property.

Shakoury-Elizeh et al. (2004) studied the transcriptional response to iron deprivation and identified new Aft1 target genes. They showed that when yeast is subjected to iron deprivation, it undergoes a transcriptional remodeling, resulting in a shift from iron-dependent to parallel, but iron-independent, metabolic pathways. It was found that other metabolic pathways are also regulated by iron: biotin uptake and biosynthesis, nitrogen assimilation, and purine biosynthesis. Furthermore, they found that multiple genes involved in nitrogen assimilation and amino acid metabolism were induced by iron deprivation, whereas glutamate synthase, a key enzyme in nitrogen assimilation, was repressed. We have found Aft1 localised to gene clusters related to metabolic processes such as of glucose and aminoacids. Aft1 and Rad9 proteins are present to the majority of the newly identified by Shakoury-Elizeh et al. Aft1 targets which points to a direct role of Aft1 in their altered expression and also highlights its interdependency with the interacting Rad9 protein in metabolic genes, consistent with the results of our study (Table 3.33).

We found that Aft1 does not need Rad9 in order to accomplish its classic role as a transcriptional activator of the iron regulon. In *rad9Δ* cells Aft1 is localised to gene clusters related to protein synthesis regulation and structure and biogenesis of ribosome. This is indicative of a possible implication of Aft1 transcription factor in regulation of protein synthesis which is more apparent in *rad9Δ* cells.

A recent functional genomic analysis of Aft1 revealed new iron-independent functions (Berthelet et al., 2010). The genetic network that they constructed showed

that Aft1 affects a diverse range of cellular processes, including the *RIM101* pH pathway, cell wall stability, DNA damage, protein transport, chromosome stability and mitochondrial function. By comparing the results from our Aft1 genome-wide analysis to their functional analysis to examine whether Aft1 was localised to the genes with which it genetically interacted, we found that Aft1 seems to directly affect cellular processes related not only to iron regulation but also to others, such as chromosome stability (*CBF1*), cell cycle process (*CLN2*), protein transport (*SSH1, DRS2*), structure of ribosome (*RPS21B*).

Furthermore, our Aft1 genome-wide analysis showed that it was localized mostly to coding rather than promoter regions of genes. We have also shown a connection of Aft1 to transcription elongation, since *aft1Δ* strains have a serious growth defect in 6-AU assays (no growth). This may point to an implication of Aft1 to transcription elongation (see Future Experiments Chapter below).

Aft1 complex as a means to stimulate DNA repair

The preferential repair of the transcribed strand of genes (Mellon et al., 1987) as well as promoter surrounding sequences (Tu et al., 1996) has established a functional link between transcription and DNA repair. In mammalian systems transcriptional activators were shown to stimulate DNA repair. Using chromatin templates and purified NER factors, (Frit et al., 2002) showed that transcriptional activators Gal4-VP16 and RAR stimulate the removal of DNA damage in promoter regions (and the surroundings of their binding site) as a result of a specific function of activators in local chromatin remodeling (by attracting cofactors) to give access to the DNA repair factors. The way transcriptional activators stimulate the removal of DNA damage can be more direct: by interacting with DNA repair factors and recruiting them to the damage site. Gal4-VP16 and RAR are shown to interact with RPA and TFIIH essential NER factors respectively (He et al., 1993; Li and Botchan, 1993; Rochette-Egly et al., 1997), which are recruited once XPC/HR23B is bound to the damaged DNA to initiate the GGR subpathway of NER (Volker et al., 2001).

Frit et al (2002) showed that transcriptional activators stimulate the removal of DNA lesions on both DNA strands and in the vicinity of their DNA binding sites, which usually include the transcription initiation site. In that way, in the damaged loci, they are ready to act fast when they are needed. Following induction of DNA damage, activators would locally derepress chromatin to facilitate the repair process

and to further allow accurate transcription initiation. This hypothesis is also supported by studies demonstrating that DNA repair was much faster and without strand selectivity near the transcription start site of the human JUN gene that is surrounded to up to five activator DNA binding sites (Tu et al., 1996). This, along with the fact that the formation of the transcription complex requires both the coding and the non coding strands (Kim et al., 2000; Robert et al., 1998), emphasizes the importance of such a transcription initiation associated repair (TIAR) that operates without strand bias. There is a preferential repair of the transcribed strand, which may mean that once RNA synthesis is initiated, the elongating RNA pol II and its accompanying factors would fulfill the role previously assumed by the activator in surveying the integrity of the gene to be transcribed- this transcription elongation coupled repair (TECR) targeting specifically the transcribed strand. This scenario is also supported by the fact that RNA pol II is associated not only with transcription factors but also with DNA repair factors such as RPA, XPG and XPF (Maldonado et al., 1996; Tantin et al., 1997).

The above studies in mammalian systems show a potential for a similar model in *Saccharomyces cerevisiae* for the Rad9 DNA damage checkpoint protein which is involved in NER and interacts with Aft1 and Mac1 transcription factors. We found Aft1 and Mac1 TFs localised to more targets than the ones known from the bibliography (Aft1 and Mac1 regulons). The fact that Rad9 is localised to more genes than these TFs are localised to, can be indicative of a more complex regulation of Rad9 distribution to the genome. Even so, Rad9 is localised to some genes that neither of these factors is present. This may mean that either Rad9 interacts with more transcription regulators or that it acts as part of a larger DNA damage response complex which is always near highly transcribed genes ready to act fast when DNA damage occurs (surveillance role).

Model

We showed that Rad9 protein is distributed on chromatin under no DNA damage induced conditions. This distribution is not random but it is connected to loci which exhibit high levels of transcriptional activity. This constitutive dynamic recruitment on chromatin may facilitate the speed and efficiency of Rad9-dependent response to DNA damage. Rad9 protein interacts with Aft1 transcription factor and this interaction is critical for its localization to the genome. We showed that Rad9

localisation to active sites and sites prone to DNA-damage is to a great extend Aft1-dependent. It is possible that Aft1 transcription factor facilitates Rad9 localisation by making the chromatin accessible. Epigenetic marks on chromatin such as methylation may rule this genome-wide binding pattern of Rad9. Rad9 is localised mostly in coding regions of genes and we showed that it participates in transcription elongation in cooperation with Aft1. Aft1 transcription factor may act with Rad9 in order to stimulate DNA repair possibly by attracting other cofactors which give access to the repair machinery (Figure 3.33), a hypothesis resembling the one that has already been established for mammalian systems (Frit et al., 2002). The interplay between Aft1 transcription factor and Rad9 DNA damage checkpoint protein seems to be very important for the preservation of genome fidelity.
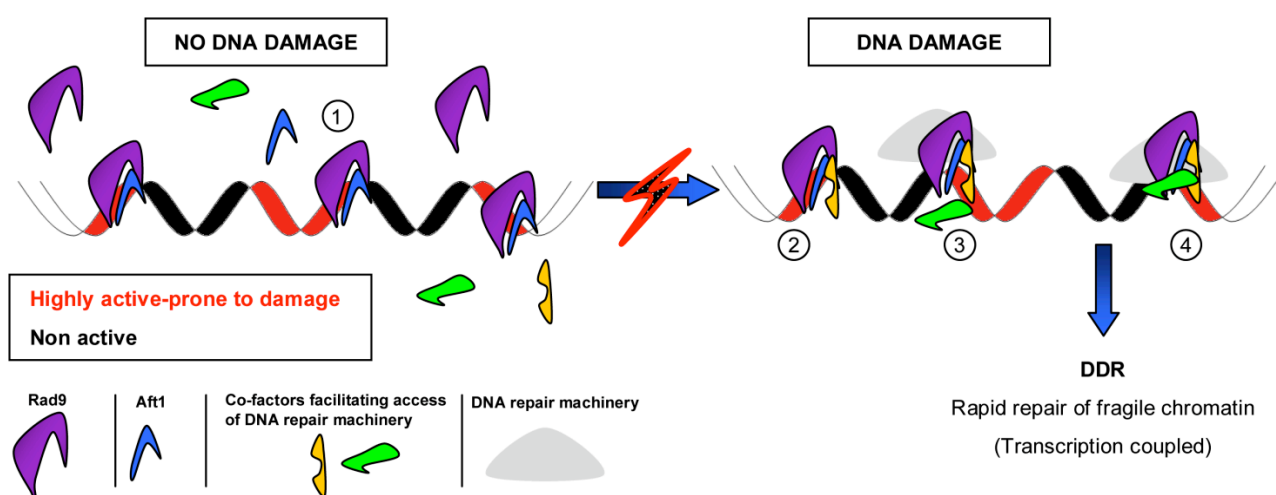
FIGURE 3.33: Surveillance of DNA damage-prone chromatin by Rad9 and Aft1
(1) Under no DNA damage-induced conditions, Rad9 (in purple) is recruited to DNA damage-prone chromatin along with Aft1 (in blue) in an Aft1-dependent manner. **(2)** When a DNA damage event occurs, Aft1 transcription factor could recruit other co-factors (in yellow and green). **(3)** The co-factors facilitate the access of the DNA repair machinery (in grey). **(4)** The whole DNA repair machinery is recruited at the DNA damage site, ensuring a rapid DDR leading to an effective repair of the damaged chromatin.

FUTURE EXPERIMENTS

In the present study we describe a novel way of protection of sensitive to DNA damage genomic regions. Rad9 protein is localized to these loci, under non DNA damage-induced conditions, in a non-random way. These regions are highly transcriptionally active, have high content in GC and are DNA damage-prone. The localization to such regions is driven by the Aft1 transcription factor, since Rad9 loses this preference in *aft1Δ* cells. Aft1 TF is also identified as a new Rad9-interacting protein. The present study provides information on the cell's protective mechanisms against the DNA damage before the actual damage occurs.

We propose that future experiments should further focus on Aft1 transcription factor and its role in the protection of DNA damage prone loci that we have established in this study. This is of great importance since Aft1 is –in the last decade-gradually being established as a multifunctional transcription factor which is implicated to vital cellular processes such as genome integrity, chromosome and cell wall stability, mitochondrial function and protein transport (Berthelet et al., 2010; Hamza and Baetz, 2011; Measday et al., 2005; Shakoury-Elizeh et al., 2004), apart from its classic role as the main regulator of iron homeostasis. We found Aft1 localised to gene clusters related to metabolic processes of aminoacids, organic acids, glucose (Figure 3.10) and also localized to clusters related to cell growth such as regulation of translation, translation elongation factor activity, ribosomes (Figures 3.9-3.11). This localisation is novel for Aft1 and *aft1Δ* expression microarray experiments in the same growth conditions as the ones used in the tiling Arrays (SC BCS BPS) would address the question of whether Aft1 can affect directly the transcription of these gene targets. In addition to that, because we provide the first high resolution genome-wide localization map of Aft1, one could further investigate individual genes of interest.

Furthermore, the characteristic localisation pattern of Aft1 to the coding regions of genes rather than to the promoter regions deserves further insight, since this is novel for a transcription factor. We showed by average gene analysis (Figure 3.23A) that Rad9 does not influence Aft1 localisation pattern. What drives Aft1 inside the coding regions of genes? Proteomic analyses of Aft1 would reveal possible novel Aft1-interacting proteins which may explain this localization pattern. One should also take into account the novel strong phenotype that we found for Aft1 in 6-AU assay

which relates it –directly or indirectly- to transcription elongation (Figure 3.7A). The relation of Aft1 to transcription elongation could be further analysed by examining by co-IP analyses whether Aft1 interacts with any of the components of the transcription elongation machinery. Subsequently, depending on the co-IP results, a genome wide localisation analysis of Aft1-interacting components of transcription elongation machinery should be performed under the same growth conditions in order to compare to the Aft1 localisation pattern that we already have. Mutant genetic analyses of transcription elongation factors in combination with *aft1Δ* cells should give additional insights as to how a transcription factor such as Aft1 could affect transcription elongation in the yeast cell.

Average gene analyses in the possible overlapping gene targets of Aft1 and other Aft1-interacting component(s) of transcription elongation machinery (as found by genome-wide analyses) can indicate whether Aft1 is related to transcription elongation through a transcription elongation machinery component. The large scale experiments could include RNA polII localisation (or other transcription elongation component) analysis in *aft1Δ* cells.

We have also showed that *aft1Δ* cells exhibit a strong phenotype under DNA damage induced conditions (zeocin) (Figure 3.29). This should be verified by performing the functional growth assay by using other DNA damage-inducing drugs as well[5]. If the phenotype is reproducible it could be informative to perform a genome-wide localization analysis of Aft1 under DNA damage-inducing conditions. This experiment should be examined in parallel with i) Aft1 genome-wide analysis in *rad9Δ* cells and ii) Rad9 genome-wide analysis under the same DNA damage-induced conditions. It would be valuable to study the Rad9-Aft1 relation under DNA damage-induced conditions, especially since we have observed a synthetic phenotype in the double mutant compared to the single ones in zeocin (Figure 3.29).

As far as Rad9 is concerned, a similar experimental approach as the one described for Aft1 can be followed in order to confirm its implication to transcription in general and to transcription elongation in particular. By expression microarray analyses, we have found that Rad9 affects the transcription levels of ~2% of yeast

---

[5] The use of different DNA damage-inducing agent is important, since we have found that zeocin is implicated in the iron-regulation in the cell: This copper-chelated form of zeocin is inactive. When the antibiotic enters the cell, the copper cation is reduced from $Cu2+$ to $Cu1+$ and removed by sulfhydryl compounds in the cell. Increase of copper in the cell causes downregulation of Fet3 copper-regulated ferroxidase, causing –secondarily- iron deprivation. Upon removal of the copper, zeocin is activated, binds DNA and cleaves it, causing cell death.

genes and we have also observed a "small colonies" phenotype in 6-AU assay which showed a -direct or indirect- implication of Rad9 with transcription elongation. Proteomic analyses can reveal novel Rad9-interacting proteins which could explain the relation of Rad9 with transcription. Another indicative experiment for showing such a relation could be the genome-wide localisation analysis of RNA polII in *rad9Δ* cells.

By performing average gene analyses we showed that Rad9 localisation pattern to the average gene under non DNA damage-induced conditions was similar to the respective pattern of specific chromatin epigenetic marks such as H3K36me3, H3K4me and H3K79me3 (Figure 3.23A). In order to examine whether or not Rad9 is driven to chromatin by these epigenetic marks, one could construct mutants of these methylation marks and perform genome-wide localisation analyses of Rad9 to see if and how Rad9 localisation pattern is changed.

Furthermore, *in silico* experiments of average gene analyses on specific clusters of genes to which Rad9 and/or Aft1 are localised (as found by BiNGO plugin in Cytoscape platform for WT and *rad9Δ* or *aft1Δ*) would give additional insights as to how the recruitment of these proteins could be differentially affected in distinct gene clusters. The above analyses could include a comparison with the respective pattern of epigenetic marks, in order to examine possible means of recruitment to chromatin.

We have established the Aft1-dependent recruitment of Rad9 to genomic regions which are DNA damage prone. It would be important to know whether other proteins of the DNA damage response cascade are also present to these regions and if Aft1 is important for their possible localisation. Candidate proteins for this analysis could be the upstream kinases Mec1 (and its interacting protein Ddc2) and Tel1, the members of the MRX complex (Mre3, Rad50, Xrs2), the members of the 9-1-1 complex (Rad17, Mec3, Ddc1) and the Rad53 downstream kinase. Presence of these proteins in the proximity of DNA damage-prone loci will be in support of our model for the surveillance role of Rad9 in fragile chromatin before the actual DNA damage occurs.

CHAPTER 2

MATERIALS AND METHODS

2.A. GENERAL MATERIALS

General materials used in this study include:

- Chemicals of Sigma, Merck, Amersham, AppliChem
- Media by Difco (yeast nitrogen base without aminoacids, bactopeptone)
- Restriction enzymes by Minotech and New England Biolabs (NEB)
- **Antibodies**

The antibodies used in this study include sc-789 c-myc rabbit polyclonal IgG (Santa Cruz) used in Westerns (in 1:1000 dilution) and ChIP experiments, sc-805 HA probe rabbit polyclonal IgG (Santa Cruz) (1:250 in Westerns), 5131 RNA pol II CTD (Abcam) (1:2000 in Westerns), KS736 hexokinase1 rabbit IgG (1:1000 in Westerns), HSP70 rabbit IgG, flag F3165 (Sigma) (1:1000 in Westerns), sc-40 c-Myc mouse monoclonal IgG (Santa Cruz) (1:1000 in Westerns), sc-7392 HA probe mouse monoclonal IgG (Santa Cruz) (1:1000 in Westerns), secondary goat anti-rabbit 111-035-003 (Jackson) (1:20000 in Westerns), HRP mouse 5S (1:10000 in Westerns).

- Radioisotopes $[\alpha\text{-}^{32}P]dATP$ and $[\alpha\text{-}^{32}P]dCTP$
- JetQuick Plasmid mini prep spin kit (400250) and Macherey-Nagel Nucleospin Extract II (740609.50) and SuperSignal West Pico Chemiluminescent Substrate kit (Thermo Scientific; 34077)
- Glass beads unwashed 425-600μm (Sigma G9268)
- Membranes by Scheischer & Schuell, Bioscience (for RNA transfer) (Nytran-N 10416196) and Whatman Protran Nitrocellulose Membrane BA83 for transfer of proteins
- Autoradiography film (Fuji, 90224)
- G sepharose beads (GE Healthcare 17-0618-01)
- BCS (bathocuproine disulfonic acid-Na_2 salt) (SERVA 14470), BPS (bathophenanthroline disulfonic acid-Na_2 salt) (SERVA 14483 and Fluka 11890)
- 6-Azauracil (Sigma A1757)
- Geneticin G418 Sulfate (11811-023)

- Oligonucleotides from Microchemistry laboratory of IMBB and Metabion
- The program ImageQuant (for the PhosporImager Use) and Scion Image for quantification of bands
- SYBR gree (Invitrogen S7563)
- All Affymetrix equipment for hybridization, scanning of expression and tiling arrays and the software mentioned in the respective protocol (IGB, TAS, Galaxy). Cytoscape software for functional clustering with BiNGO plugin as mentioned in the respective protocols of the genome-wide experiments
- SGD database

2.B. MEDIA AND GROWTH CONDITIONS

Growth of bacterial cells was done in LB, while yeast cells were grown in Synthetic Complete (SC) or Yeast Peptone Dextrose (YPD) media as described (Sambrook, 1989). SC medium contains 0.67% nitrogen base (including 1.23μM FeCl$_3$ and 0.25μM CuSO$_4$), the 20 aminoacids, uracil, adenine and 2% glucose. The copper dependent transcription was induced by the addition of BCS chelator of Cu^{+1} and Cu^{+2} (bathocuproine disulfonic acid-Na$_2$ salt) in a final concentration of 100μM. The metal dependent transcription was induced by the addition in a final concentration of 100μM of the chelator of Cu^{+1} and Cu^{+2} and Fe^{+1} and Fe^{+2} BPS (bathophenanthroline disulfonic acid-Na$_2$ salt). More specifically, the culture conditions used in this study were
- SC
- SC plus BCS added 3hrs before the harvesting of the cells
- SC plus BCS added 3hrs before the harvesting of the cells plus BPS added 6hrs before the harvesting of the cells
- SC plus BCS added 3hrs before the harvesting of the cells plus BPS added 6hrs before the harvesting of the cells plus zeocin (a drug that causes dsDNA breaks) added 2 hours before the harvesting in a final concentration of 150μg/ml
- YPD
- YPD plus 6-Azauracil (6-AU), a drug that binds GTP and UTP.
- YPD plus zeocin added 2 hours before the harvesting in a final concentration of 150μg/ml

- YP Raffinose plus galactose induction for 1hr 15mins. The protocol followed was from Haber lab (www.bio.brandeis.edu/haberlab/jehsite/protocol.html)

2.C. STRAINS

The background strain used in this study is the BJ5457 that lacks proteases (MATa ura3-52 trp1 lys2-801 his3[Delta]200 pep4::HIS3 prb1[Delta]1.6R can1 Gal+). Based on this strain, a series of other strains (see table below) have been constructed, having either specifically tagged or deleted genes.

FT5 Rad9-13Myc (TRP)	Christos Andreadis
FT5 Rad9-9Myc (TRP)	Kalliopi Gkouskou
FT5 Aft1-9Myc (TRP)	George Fragiadakis
FT5 His3-9Myc (TRP)	Kalliopi Gkouskou
FT5 Mac1-9Myc (TRP)	Alexandra Voutsina
FT5 *aft1Δ::KAN* Rad9-13Myc (TRP)	George Fragiadakis
FT5 *aft1Δ::URA3 aft2Δ::KAN* Rad9-13Myc (TRP)	George Fragiadakis
FT5 *rad9Δ* Aft1-9Myc (TRP)	George Fragiadakis
FT5 *cbf1Δ* Aft1-9Myc (TRP)	Christos Andreadis
FT5 Aft1-3HA (KAN)	George Fragiadakis
FT5 Aft1-3HA (KAN) Rad9-9Myc (TRP)	Christos Andreadis
FT5 *rad9Δ::KAN* Aft1-3HA (TRP)	Christos Andreadis
FT5 *rad9Δ::KAN*	Kalliopi Gkouskou
FT5 *snf2Δ::KAN*	Kalliopi Gkouskou
FT5 *aft1Δ::URA*	George Fragiadakis
FT5 *aft2Δ::KAN*	George Fragiadakis
FT5 *aft1Δ::URA aft2Δ::KAN*	George Fragiadakis
FT5 *rad9Δ::KAN aft1Δ::URA*	George Fragiadakis
FT5 *rad9Δ::TRP aft1Δ::KAN aft2Δ::URA*	George Fragiadakis

DNA

2.1. PLASMIDS AND CONSTRUCTS

The plasmids used in this study include the pYM1 *kanMX6* (3HA), the pYM6 *k1TRP1* (9Myc) (Knop et al., 1999) and the pFA6a-13Myc-TRP1 and pFA-3HA-KANMX6 (Longtine et al., 1998), which were used for taggings or deletion of genes as described above. Also, the pDB20-flag-URA plasmid which was used for the insertion of Rad9 in the co-IP experiments (constructed by K. Gkouskou). Finally, the

pYX142-LEU plasmid was used for the insertion of Rad9-9Myc (in NcoI-SlaI positions) and 9Myc (in SmaI-SlaI positions) to construct the strains that we used in our co-IP experiments. Rad9-9Myc sequence was extracted from genomic DNA of Rad9-9Myc strain. pDB20-flag-URA and pYX142-LEU are multi-copy plasmids used for the overexpression of our proteins in co-IP or ChIP experiments.

2.2. PCR-PRIMERS

i) PCR

Polymerase Chain Reaction (PCR) was used extensively in this study to amplify DNA regions of interest in multiple experiments. PCR includes the typical denaturation step (denaturation of the template DNA), the annealing step (where the primers recognise their complementary sequences on the template DNA) and the extension step (where the polymerisation of the DNA takes place).

The typical PCR reaction used in this study was set as follows ($V_f=20\mu l$):

> 7μl H_2O
>
> 5μl IP/INPUT sample
>
> 1μl forward primer 200ng/μl
>
> 1μl reverse primer 200ng/μl
>
> 0.5μl dNTPs 10mM
>
> 2μl $MgCl_2$ 25mM
>
> 2.5μl Taq buffer 5 u/μl
>
> 1μl Taq polymerase

The typical PCR programme used was set as follows: a) 5mins 94^0C (denaturation), b) 30sec 94^0C, c) 30sec 52^0C (annealing temperature depends on the primer content in AT), d) 1min extension in 72^0C for every 1000bp of amplicon, e) 10mins 72^0C final extension.

ii) PRIMERS

The primers used in this study have been designed in Vector NTI software setting the specifications needed each time and produced by Micro-chemistry laboratory of IMBB. They have been used in the ChIP on chip experiments, clonings, Northern probe production, RT PCRs, diagnostic PCRs for the new strains (with deleted genes or tagged proteins). They are mentioned in the table below:

NAME	SEQUENCE	Comments
FRE2 +1721 F	5'- TGATTGCAGTTAGAGGATTC-3'	FRE2 ORF
FRE2 +1982 R	5'- AGTTCCTTAACATTTGGTCG-3'	FRE2 ORF
FRE2 -921 F	5'-ATTTCTGGAACACGGATAAG-3	FRE2 5'-UTR
FRE2 -631 R	5'- GGCTGAGAGACATTATGATG-3'	FRE2 5'-UTR
FRE2 +2302 F	5'- TGTGAAAGTCGTAGTGTGTC-3'	FRE2 3'-UTR
FRE2 +2533 R	5'- TTATCTTCCTTGCATCTGTG-3'	FRE2 3'-UTR
FRE7 +1418 F	5'- GAGATGAAATGTGTACCCTC-5'	FRE7 ORF
FRE7 +1677 R	5'- AGGAATAATGGTGATGAGAC-5'	FRE7 ORF
FRE7 -355 F	5'- TCCTCGTCTGCGCAAATTG-3'	FRE7 PROM
FRE7 -111 R	5'- TCTTGAGAACAAACGAGTGC-3'	FRE7 PROM
FRE7 -959 F	5'-AATACAGAGACAACAAGGAC-3'	FRE7 5'-UTR
FRE7 -717 R	5'- AGAGAATATCAATCACTCCC-3'	FRE7 5'-UTR
FRE7 +1984 F	5'- TCTAGAAGACAATACAACGC-3'	FRE7 3'-UTR
FRE7 +2253 R	5'- AAGTAATGTTGCAGGAAGTG-3'	FRE7 3'-UTR
FRE1 +411 F	5'- TATCCATCTTAACCTAATGC-3'	FRE1 ORF
FRE1 +664 R	5'- AAATTAATACGACGAGACCC-3'	FRE1 ORF
FRE1 -627 F	5'- CCCTTGATGATACTCTAAAC-3'	FRE1 5'-UTR CRR1 ORF
FRE1 -311 R	5'- TAGATTCTCACCAAGATTGC-3'	FRE1 5'-UTR CRR1 ORF
FRE1 +2195 F	5'- ATGCGGGTTCTAAATCTAAG-3'	FRE1 3'-UTR CDC 123 ORF
FRE1 +2426 R	5'- TCCGAAGAATGATGTTGAAG-3'	FRE1 3'-UTR CDC 123 ORF
FRE1 -409	5'-GTTGAAGAATACCCGATA-3'	FRE1 PROMOTER
FTR1 -486 F	5'-CCACGGTCACTACTAACTCC-3'	FTR1 PROMOTER
FTR1 -106 R	5'-AGCTCAAGGTCGAACTACAG-3'	FTR1 PROMOTER
FTR1 +40F	5'-TGT GTT CAG AGA GTG CTT GG-3'	FTR1 ORF
FTR1 +367 R	5'-CGCAATCTTCACTCTCCACT-3'	FTR1 ORF
FTR1 +818 F	5'-TGGACAATGGGTGGGATATC-3'	FTR1 ORF
FTR1 +1165 R	5'-TTTGAGACGAGGAATGACTG-3'	FTR1 ORF

FRE2 -617F	5'-AAT ACT GAC TTT GCG AAT GC -3'	FRE2 PROM
FRE2 -245R	5'-ATG GCA CGA ATG ATA CAC CC -3'	FRE2 PROM
ACT1 +1415F	5'-TTT GTG CGC GTA TGT TTA TG - 3'	ACT1 3'UTR
ACT1 +1722R	5'-ACA CGG TCC AAT GGA TAA AC – 3'	ACT1 3'UTR
ACT1 -622F	5'-AAG TAA ATA AGA CAC ACG CG – 3'	ACT1 5'UTR
ACT1 -302R	5'-TAT TTA TGC AAG AGG ACG TG – 3'	ACT1 5'UTR
CTR1 +118F	5'-CGA TAT TAT CGA GCA TGT CAT C-3'	CTR1 ORF
CTR1 -220R	5'-CCT CTC GAG ATG ACA ATA C-3'	CTR1 PROM
FRE1 +101F	5'-CGCTATACCAATTTGGATGT-3'	FRE1 ORF
FRE1 +388R	5'-AATGATACGCTGTCTCGTTC-3'	FRE1 ORF
CRR1 +80F	5'-ACTCCATTTCTTGTTCTCCA-3'	CRR1 ORF
CRR1 +348R	5'-CTTGGTATTTGCCTTATTCG-3'	CRR1 ORF
RAD50 -300 F	5'-ATCTTGCAATACTTTCACGG-3'	RAD50 OUT 5'-UTR
RAD50 +4113R	5'-TACCGACTTGGAAACGATAG-3'	RAD50 OUT 3'-UTR
RAD9 F2	5'-GATATTAC GGACAATGAT ATATACAACA CTATTTCTGA GGTTAGA CGG ATC CCC GGG TTA ATT AA-3'	For Rad9-13Myc tagging in pFA6a cassette
RAD9 R1	5'-AATCG TCCCTTTCTA TCAATTATGA GTTTATATAT TTTTATAATT GAA TTC GAG CTC GTT TAA AC-3'	For Rad9-13Myc tagging in pFA6a cassette
RAD50Δ S3	5'-AGC AAC CAT TGA GAG GCA AAA ACA AGG GAA CGA CGG AAA GCA GGC CGT ACG CTG CAG GTC GAC -3'	Deletion in pYM plasmid
RAD50 S2	5'-TTA ATC AAT CAA AGT CTA TCC CTT CGT AGA TAT TAT GGG GTC TTT ATC GAT GAA TTC GAG CTC G-3'	Deletion in pYM plasmid
R1 SMALL	5'-*GAA TTC* GAG CTC *GTT TAA AC*-3'	CHECK pFA6a CASSETTE
F2 SMALL	5'- C*GG ATC* CCC GGG *TTA ATT AA*-3'	CHECK pFA6a CASSETTE
HIS4 -296F	5'-ATCACAATCCTGACAACCAG-3'	HIS4

		PROMOTER
HIS4 -35R	5'-ACTATTACACAGCGCAGTTG-3'	HIS4 PROMOTER
HIS4 +113F	5'-AAGAGATTCTCCAGTTCTCC-3'	HIS4 ORF
HIS4 +511R	5'-TTTGGTCAACATATCCTTGC-3'	HIS4 ORF
HIS4 +821F	5'-TGTTAGATGCCAAGATCAAG-3'	HIS4 ORF
HIS4 +1116R	5'-CTTCTGCACACCAACTTTGT-3'	HIS4 ORF
HIS4 +1853F	5'-AAGCTGAACACGGTATTGAC-3'	HIS4 ORF
HIS4 +2215R	5'-ACTGCCTAGCGTAACCATAG-3'	HIS4 ORF
FTR1 -348F	5'-TATTAAGTGCGCGAATACTG-3'	FTR1 promoter
FTR1 -48R	5'-GTACAATCCGTCGTGTTATG-3'	FTR1 promoter
CEN1 -103F	5'- TTACCAGCTTCAATAACTCG-3'	Whole centromere
CEN1 +221R	5'- CGCCTAGTGCTTAAGAGTTC-3'	Whole centromere
CEN2 -67F	5'- GCTATTCAACTGGCACCTAC-3'	Whole centromere
CEN2 +261R	5'- TAAATGCGAAGAAGGTATGG-3'	Whole centromere
CEN3 -206F	5'- TGCTACCACTTCTATTACAC-3'	Whole centromere
CEN3 +188R	5'- ATGAGCAAAACTTCCACCAG-3'	Whole centromere
CEN4 -63F	5'-CACGAGCCAGAAATAGTAAC-3'	Whole centromere
CEN4 +196R	5'- TAAGCTATGAAAGCCTCGGC-3'	Whole centromere
CEN5 -101F	5'- CCTACATGCTACATAAGTCC-3'	Whole centromere
CEN5 +250R	5'- CCTTCAACATTGTTTAGCAG-3'	Whole centromere
CEN6 -163F	5'- GGAAGAGGTAAAGTAGTCGG-3'	Whole centromere
CEN6 +218R	5'- CGTCCAATATCATCGTAAAC-3'	Whole centromere
CEN7 -178F	5'- CTTCCTGAACATTCTAATGG-3'	Whole centromere
CEN7 +268R	5'- CATTAACTTTCATTGAACCG-3'	Whole centromere
CEN8 -122F	5'- TGGTGCATTACATTCCTTAC-3'	Whole centromere
CEN8 +199R	5'- ACTCTCCCTTAGTGCTTGTG -3'	Whole centromere
CEN9 -110F	5'- CTGCGAACGGATGAATATTG-3'	Whole centromere
CEN9 +181R	5'- CACCTGTTTTCATTACCCTG -3'	Whole centromere
CEN10 -138F	5'- CAGTTTAGTTGTTGTGGATG -3'	Whole centromere
CEN10 +350R	5'- CGACAAAGTATCTCAGAAGG -3'	Whole centromere
CEN11 -60F	5'- CATTGTATTGATTGATTCTGC-3'	Whole centromere
CEN11 +246R	5'- CTGTAATCACTTGTCAACGC-3'	Whole centromere
CEN12 -63F	5'- CTTGTAGTACGAGGTTAAC-3'	Whole centromere
CEN12 +238R	5'- GCTAATATCAACGAGTAAACG-3'	Whole centromere

CEN13 -49F	5'- AGCGATTTACTACACTTGAG-3'	Whole centromere
CEN13 +349R	5'- AGCCAGAACTTCTCATCAAC-3'	Whole centromere
CEN14 -55F	5'- AAGCAAGTAGATGTGAAGCC-3'	Whole centromere
CEN14 +257R	5'- TCATTCTTATCAGTCCAGCG-3'	Whole centromere
CEN15 -141F	5'- TTTCAGAAGTCATAACGCAC-3'	Whole centromere
CEN15 +237R	5'- AACTTCCTTGACAGAACCAT-3'	Whole centromere
CEN16 -100F	5'- GTTGAAGCCGTTATGTTGTC -3'	Whole centromere
CEN16 +275R	5'- TCAGTGTGGAGTAAGTCATC-3'	Whole centromere
RPO21 -945F	5'-TAACGATAGCGAGGCAAGCG-3'	RPO21 promoter (UAS)
RPO21 -600R	5'-GTTTGTCCACTTGTTGCCAC-3'	RPO21 promoter (UAS)
RPO21 +4501F	5'-AATGACGCTATGGCTGGAGG-3'	RPO21 coding
RPO21 +4873R	5'-TTGGCGACGTGGGAGAGTAG-3'	RPO21 coding
YRF1-5 -478F	5'-GAGAGCGGAAGAAGTTGTAG-3'	YRF1-5 promoter
YRF1-5 -216R	5'-CACTAAGATAAGCGACTGTC-3'	YRF1-5 promoter
YRF1-5 +3486F	5'-AGGCTGTATAACCGAACAGG-3'	YRF1-5 coding
YRF1-5 +3742R	5'-TGTCGCTGTCCTCATCACTG-3'	YRF1-5 coding
YML039W -325F	5'-CATTTGTTTAGTAGTATTCG-3'	YML039W promoter
YML039W -103R	5'-TACGATTATTCCTCATTCCG-3'	YML039W promoter
YML039W +49F	5'-GCCTGTGCTTCGGTTACTTC-3'	YML039W coding
YML039W +410R	5'-ACTGATGATGGATACTGCGG-3'	YML039W coding
TEF1 -509F	5'-ATCACATAGGAAGCAACAGG-3'	TEF1 promoter
TEF1 -310R	5'-ATTTAGTATGCTGTGCTTGG-3'	TEF1 promoter
TEF1 +339F	5'-CTTGATTATTGCTGGTGGTG-3'	TEF1 coding
TEF1 +712R	5'-TAGATGGTTGTTCAATGGCG-3'	TEF1 coding
CDC48 -294F	5'-GGGTGTGTTTGCTTCCATTC-3'	CDC48 promoter
CDC48 -17R	5'-TGTAGTTGAGCCAGTTATCG-3'	CDC48 promoter
CDC48 +1355F	5'-TCGATTCTTTAGGAGTCACC-3'	CDC48 coding
CDC48 +1695R	5'-CGATTCACCATACCACATAC-3'	CDC48 coding
9Myc F (SmaI)	5'-TCCCCCGGGCGTACGCTGCAGGTCGACTCC-3'	pYX142 construct
9Myc R (SlaI)	5'-TCCGCTCGAGGCTAGTGGATCCGTTCAA-3'	pYX142 construct
RAD9 +3F	5'-TCAGGCCAGTTAGTTCAATGGAAAAGC-3'	

CMD1 +3F (BamHI)	5'-CGGGATCCGTCCTCCAATCTTACCGAAG-3'	pBluescript SK construct
CMD1 +403R (BamHI)	5'-CGGGATCCCGCCTGATCCATCACTAACC-3'	pBluescript SK construct
CTR1 +48F (HindIII)	5'-CCCAAGCTTTAGTGCATCCAAGACAGTAG-3'	pBluescript SK construct
CTR1 +1116R (HindIII)	5'-CCCAAGCTTATTCTTTCCTGAGTCTGTGG-3'	pBluescript SK construct
CTR1 +944R	5'-TGTCTACCACATTGGCAGTTAC-3'	
CMD1 +75F	5'-TGGCTCTATCTCATCAAGTG-3'	CMD1 ORF
CMD1 +343R	5'-CACCAATGGATGTTAGCACG-3'	CMD1 ORF
TFIIS -250F	5'-GAGATACTTCACTAGCCCAC-3'	TFIIS 3'-UTR for THIIS delta check with KAN reverse primer
TFIIS +239F	5'-CGTTCCAGGCAAGCACAGC-3'	TFIIS ORF
TFIIS +577R	5'-CTTCGTTGGTGTCACAGTTG-3'	TFIIS ORF
COX1 +12394F	5'-AGGTCTACCTATCGGGATAC-3'	COX1 LAST CDS
COX1 +12622R	5'-GCGAAAGCATCAGGATAATC-3'	COX1 LAST CDS
ATP6 +456F	5'-CTCATTATTCGTACCTGCTG-3'	ATP6 ORF
ATP6 +721R	5'-CCTGAATGATACCAATAGCG-3'	ATP6 ORF
COX3 +373F	5'-CCACCCGTAGGTATTGAAG-3'	COX3 ORF
COX3 +623R	5'-CCAGCATAGAATACTGAACC-3'	COX3 ORF
GAL1 -179F	5'-CAGCGAAGCGATGATTTTTG-3'	GAL1 probe
GAL1 +102R	5'-CTTAATTATGCTCGGGCACTT-3'	GAL1 probe
KAN&HIS	5'-TGGGCCTCCATGTCGCTGG-3'	Check in pYM cassette
RAD9 +3109F	5'-AACTTCACTCATCCGCTAGC-3'	RAD9 ORF
RAD9 +3878R	5'-TGAAAACCAGTGTCCTCG-3'	RAD9 ORF
RAD9 -83F	5'-GCAACGATGAGCAATGTG-3'	
TRP primer	5'-GCTATTCATCCAGCAGGCCTC-3'	pYM6
RAD9 +4781R	5'-GCCTCGTTCAGCACATTTCC-3'	
AFT1 +739F	5'-CCTGATTCCGAAGAGTAC-3'	Check of endogenous untagged
AFT1 +2289R	5'-ATCCTGATCTTAGCACCGAT-3'	Check of

		endogenous untagged
RAD9 disr TRP F S2	5'-AATCGTCCCTTTCTATCAATTATGAGTTTA TATATTTTTATAATTATCGATGAATTCGA GCTCG-3'	*rad9Δ* in pYM6
RAD9 disr TRP R S3	5'-GATATTACGGACAATGATATATACAACA CTATTTCTGAGGTTAGACGTACGCTGCAGG TCGAC-3'	*rad9Δ* in pYM6
CBF1 -171F	5'-ATCCACGTGCTTATCACG-3'	Check for endogenous
CBF1 +1200R	5'-GAGGCTGAGTGATTCTCT-3'	Check for endogenous
CBF1 disr F	5'-AGAGAACGAAAGAAAAAGCACTAGGAGC GATAATCCACATGAGGCTCGGATCCCCGGGT TAATTAA-3'	CBF1 disruption
CBF1 disr R	5'-ATACATAGGGAGACTCGAAATACATTTA GCTATCTATTTTTAACTCGAATTCGAGCT CGTTTAAAC-3'	CBF1 disruption
CTR1 -220R	5'-CCT CTC GAG ATG ACA ATA C-3'	CTR1 promoter
CTR1 -475F	5'-CCC TAC TAT ACT ACA AAC CGA TAC-3'	CTR1 promoter
CTR1 -180F	5'-AGTAAAACAGATACGCAGTGTG-3'	
CTR1 +71R	5'-GATGCTACTGTCTTGGATGCAC-3'	
CTR1 +118F	5'-CGATATTATCGAGCATGTCATC-3'	CTR1 ORF
CTR1 +360R	5'-ATCCAT CCCTGAAGAGCTACTG-3'	CTR1 ORF
CTR1 +360F	5'-TATGGACATGAGTATGGGAATG-3'	CTR1 ORF
CTR1 +597R	5'-GGAGTTTGCTGAAGGTAAAGTG-3'	CTR1 ORF
CTR1 +703F	5'-CTCTTTCATGACATTATAAGGGC-3'	CTR1 ORF
CTR1 +944R	5'-TGTCTACCACATTGGCAGTTAC-3'	CTR1 ORF
PHO5 F	5'-CGATATCCTAAACTTTTTGAC-3'	PHO5 ORF control
PHO5 R	5'-GTTTCAATTGGAACAACAGCA-3'	PHO5 ORF control
HSP30 +267F	5'-AGG TTG GAC TGG TGT TCA AG-3'	Northern probe
HSP30 +717R	5'-ACC ACC ATC ACT TAG ACC C-3'	Northern probe
MF ALPHA 2 +41F	5'-CCG TTT CTG TCA CTG CTA G -3'	Northern probe
MF ALPHA 2 +313R	5'-AGC GTT GGC CTC TCT CTT G -3'	Northern probe

YIR042C +197F	5'-CGGGACCATTCACTAACTTG-3'	RT probe
YIR042C +401R	5'-GTTGCAATAATCGTCTTCTG-3'	RT probe
YJL166W +73F	5'-ACCTCATATGCTGTGTCTCC-3'	RT probe
YJL166W +226R	5'-ACTCGTTACCGTTCTTCCAC-3'	RT probe
YLR102C +97F	5'-AATTTTACCACACCGCTACG-3'	RT probe
YLR102C +315R	5'-ACTTTCCCTTAGCGTATTGC-3'	RT probe
YGL212W +137F	5'-GGAAACTGAAGACACGATTG-3'	RT probe
YGL212W +408R	5'-AGTTTCTAGATGCTGCTGTG-3'	RT probe
YCR089W +2041F	5'-TCGACCAGCAAGTATCCATC-3'	RT probe
YCR089W +2293R	5'-TGTATTCCGTAGCAGCACCG-3'	RT probe
YCL027W +744F	5'-GAGTGAGAAATGGAGTTACG-3'	RT probe
YCL027W +1017R	5'-TGAATCTGGCGTGGTATTAC-3'	RT probe

2.3. CELL TRANSFORMATION

Yeast transformation

Yeast transformation was performed following the acetic lithium method (LiAc TRAFO). It is a highly efficient method based on the creation of competent yeast cells due to alcalic cations described by (Gietz et al., 1995) (http://home.cc.umanitoba.ca/~gietz/).

Transformation of bacterial cells

Competent bacterial cells (DH5a) were produced with the $CaCl_2$ chemical method (Ausubel, 1987-2011). Transformation of bacterial cells was performed by thermal shock (42^0C) as described (Ausubel, 1987-2011).

2.4. DNA MANIPULATION

These included i) cutting of DNA molecules by hydrolysis from DNA endonucleases (Minotech or NEB), ii) creation of blunt ends in molecules with 5' or 3' protruding ends by the use of Klenow fragment of DNA polymerase I and iii) ligation of DNA fragments by the use of T4 ligase. To do the above, the described protocols by Sambrook (1989) were used and also the conditions proposed by the enzyme manufacturers were followed.

2.5. ELECTROPHORETIC ANALYSIS AND DNA EXTRACTION FROM AGAROSE GEL

The electrophoretic analysis from agarose gel was used for DNA molecules' separation, size specification and rough quantitation. DNA extraction was performed by the use of Nucleospin Extract II kit (Macherey-Nagel) according to manufacturer's instructions. The latter kit was also used for PCR purification.

Yeast genomic DNA extraction

Yeast genomic DNA extraction was performed as described by (Ausubel, 1987-2011). Briefly, put an overnight starter culture of the desired strain, the next day spin 1-2ml of the saturated culture and wash with 500μl H_2O once. Add 200μl lysis buffer (2% Triton X100; 1% SDS; 100mM NaCl; 10mM Tris/Cl pH 8.0; 1mM EDTA pH 8.0) and vortex. Add 200μl glass beads, 100μl phenol, 100μl chlorophorm and vortex for 4mins in RT. Add 200μl H_2O, spin 13000rpm in RT and collect supernatant. Precipitate with 1ml 100% ethanol, spin 15mins 13000rpm at 4^0C and dry the pellet. Resuspend in 400μl H_2O and treat with 3μl RNAse (10μg/ml) for 15mins at 37^0C. Spin and collect supernatant in new tube. Add 1/10V CH_3COONa 3M pH 5.2 (12.5μl) and 1ml 100% ethanol. Flick mix and put for 30mins at -80^0C. Spin at 13000rpm for 15mins at 4^0C, discard supernatant and wash the pellet with 500μl 70% ethanol. Spin at 13000rpm for 5mins, discard supernatant, dry pellet and resuspend in proper volume of water (~30μl).

2.6. PLASMID EXTRACTION FROM BACTERIA

Plasmid DNA extraction was performed as described by (Sambrook and Maniatis, 1989). For medium or large scale plasmid production we used a combination of alkaline lysis and DNA precipitation with PEG 8000 (PEG prep). For a greater DNA purity we used the JET QUICK plasmid mini prep spin kit according to the manufacturer's instructions.

2.7. RADIOLABELING AND RNA NORTHERN ANALYSIS

dsDNA molecules were radiolabeled by either a) nick translation, which is based in the creation of random nicks in DNA (by DNAse) and their repair by DNA pol I in the presence of radiolabeled nycleotides or b) random priming, which is based on the

temporary DNA denaturation and subsequent synthesis of complementary strands by Kelow fragment of DNA polymerase I, in the presence of random hexamers and radiolabeled nucleotides. The above methods were executed as described (Ausubel, 1987-2011; Sambrook and Maniatis, 1989).

RNA Northern analysis included RNA samples' electrophoresis in 1.5% agarose gel containing formaldehyde, subsequently transfer to Nylon membrane (Scheischer & Schuell, Bioscience), covalently crosslinking by UV (4min). After that, follows the membrane hybridization with the radiolabeled probes of genes (ORFs derived by PCR), with the Church method. The above methods were executed as described (Ausubel, 1987-2011; Sambrook and Maniatis, 1989).

2.8. RT ANALYSIS

Reverse Transcription (RT) analysis was performed in order to check the fluctuation in expression levels of genes in certain conditions (also to confirm our expression microarray results). Briefly, the RNA sample (~2μg) is first treated by DNAse (as described in Microarray Expression Protocol-Affymetrix) and extracted with phenol/chlorophorm. The reverse transcription reaction follows in order to obtain the cDNA of the RNA after adding random primers, dNTPs, RNAsin and MMLV reverse transcriptase (Invitrogen). The produced cDNA is used in regular PCR reactions as a template (1/25 of the RT reaction), using primers corresponding to genes of interest. The method is described by (Ausubel, 1987-2011).

2.9. PROTEIN TAGGING AND GENE DELETION

The tagging of the proteins was performed following the protocol of Knop et al. (1999). Briefly, the tagging was done at the C-terminus of chromosomal genes in the way illustrated in the figure below (Knop et al., 1999).

S3-SPC42

module

TAG MARKER

PCR S2-SPC42

PCR-product

TAG MARKER

transformation
into yeast

chromosomal
target gen

SPC42

homologous
recombination

chromosomally
tagged gen

SPC42-TAG TAG MARKER
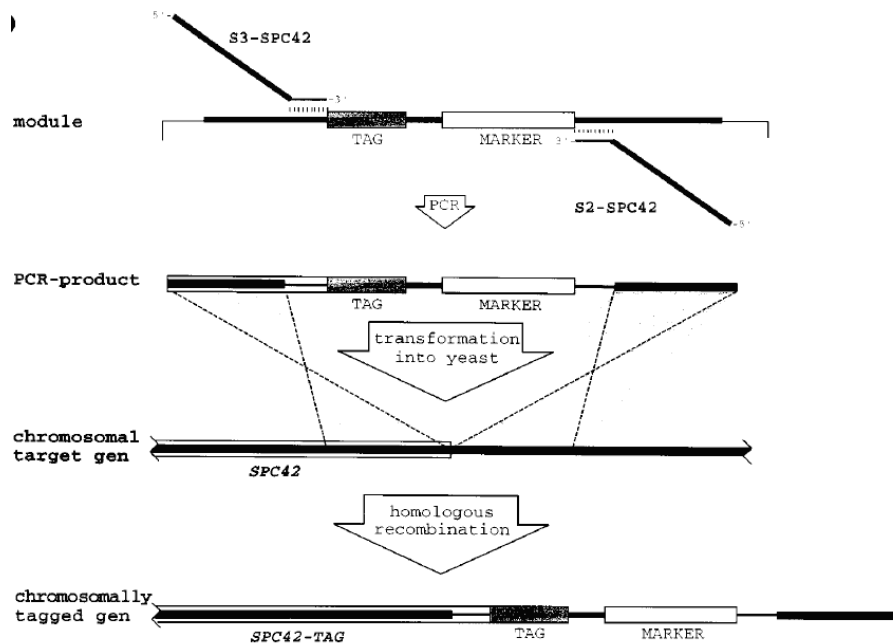
Firstly, we designed primers S2 reverse (15nts) preceded by 45nts exactly after the STOP codon of the gene of interest and S3 forward (15nts) preceded by 45nts exactly before the STOP codon of the gene of interest. In that way the tagging is done in the C-terminus. S2 and S3 primers are hybridized to pYM1 *kanMX6* (3HA) and pYM6 *k1TRP1* (9Myc) on each side of the selection cassette (including the tag). After obtaining the PCR product having the plasmid of preference as a template, we transformed the desired yeast strains with the product and selected the strains in which the tag was inserted by homologous recombination. The deletion was performed based on the same principle by designing the S3 forward primer followed by 45nts exactly before the START of the gene of interest. Tagging with 13Myc was performed by a similar way using the Longtine et al. (1998) protocol using the plasmid pFA6a-13Myc-TRP1 (for the tagging and selection) and R1 and F2 primers with specific sequences (20nts) preceded by the 40nts sequences specific for the gene of interest.

2.10. CHROMATIN IMMUNOPRECIPITATION AND REAL TIME qPCR

The following protocol was adapted from (Kuo and Allis, 1999) and was used for the manual ChIP assays.

MATERIALS

TBS	Proteinase K buffer
20mM Tris/HCl pH 7.5	0.01M Tris/HCl pH 7.8
200mM NaCl	0.005M EDTA pH 8.0
(store at 4^0C)	0.5% SDS
	(store at 4^0C)
FA 150mM NaCl	**FA 500mM NaCl**
50mM Hepes pH 7.5	50mM Hepes pH 7.5
150mM NaCl	500mM NaCl
1mM EDTA pH 8.0	1mM EDTA pH 8.0
1% Triton X100	1% Triton X100
0.1% Sodium desoxycholat	0.1% Sodium desoxycholat
(store at 4^0C)	(store at 4^0C)
Wash III	**Elution buffer**
10mM Tris/HCl pH 8.0	50mM Tris/HCl pH 7.5
1mM EDTA pH 8.0	10mM EDTA pH 8.0
250mM LiCl	1% SDS
0.5% NP-40	
0.5% Sodium desoxycholat	
(store 4^0C)	
TE	
10mM Tris/HCl pH 8.0	
1mM EDTA pH 8.0	

DAY 1

1) Grow an O/N culture (10ml) of your strain.

DAY 2

2) On the next day dilute in 50ml medium in starting OD_{550} ~0.1.

3) Grow cells at 30^0 C and stop incubation when OD_{550}~0.65-0.8 (logarithmic phase).

4) Crosslink by adding 1.35ml **formaldehyde**, shaking for 20mins.

5) Add 0.47gr **glycine** and shake for 5mins to absorb formaldehyde excess.

   * Alternatively you can add 2.5ml 2.5M glycine.

6) Pellet cells by spinning at 2500rpm for 5mins at 4^0C.

7) Wash twice with ice cold **TBS** buffer (1/2V) -25ml here- and spin at 2500rpm for 5mins at 4^0C.

8) After the washes spin again to remove all the remains of TBS buffer so that only pellet will be in the tube. You can freeze the pellets here.

9) Resuspend pellet in 400μl **FA 150mM** buffer and transfer in 1.5ml tubes which already have ~400μl washed glass beads (425-600μm).

10) Add 16μl 25x **protease inhibitor cocktail complete EDTA-free** (Roche, 11 873 580 001).

   * Alternatively you can add 12μl **proteinase inhibitor cocktail** (SIGMA P8215).

11) Adjust tube on vortex machine and vortex for 40mins at 4^0C. From now on and until the elution step, always treat your samples on ice, unless otherwise described.

12) Collect solution with the debris by spinning 1min at 3000rpm at 4^0C (by making a hole with a 0.25μm needle to the tube and placing to another one before spinning).

13) Sonicate samples 5 times for 12secs each at 40% energy and rest on ice 1min between intervals.
   * Sonication time may vary according to the machine used. Check on a control sample in order to get fragmented chromatin with a peak at 300-500 bp.

14) Spin twice for 15mins each at 13000rpm at 4^0C (change tubes) keeping the supernatant in each one.

15) Keep 50μl as IP sample, 50μl as INPUT sample (and 50μl as MOCK sample-optional). Keep the rest of the supernatant at -80^0C. Keep the INPUT samples at -20^0C until the next day.

16) PRECLEARING
   Raise the volume of your IP samples to 200μl by adding 150mM FA buffer. Add 20μl packed beads to your IP samples and rotate for 2hrs at 4^0C. *The beads must be equilibrated to the 150mM FA buffer before using them [see step 18]* (the stock is in 20% ethanol). Centrifuge for 1min at 3000rpm and collect the supernatant in a new tube.

17) In the IP sample add **FA 150mM** buffer until final volume ~210μl, 2μg **antibody** and 2μl **proteinase inhibitor cocktail** (SIGMA P8215) or

equivalent amount of **protease inhibitor cocktail complete EDTA-free (stock is 25X)**. Incubate O/N at 4^0C rotating.

DAY 3

18) Equilibrate 20µl **G** sepharose (or agarose) beads 3 times with 1ml **FA 150mM** buffer (spin at 3-4000 rpm between the washes). Add buffer till final volume 70µl.

19) Add these 70µl of beads to IP sample (and MOCK sample if you have one). Add also 40µg sheared **herring sperm DNA** after you have heated it at 65^0C for 5' and cooled it on ice for 2 mins. Keep rotating at 4^0C for 1.5-2 hrs.

20) Spin at 3000rpm for 1min at RT and keep the beads.

21) Add 1ml **FA 150mM** buffer along with 1mM final concentration fresh **PMSF** and rotate for 5mins at RT.

22) Spin at 3000rpm for 1min at RT and keep the beads.

23) Repeat steps 21-22.

24) Add 1ml **FA 500mM** buffer along with 1mM final concentration fresh **PMSF** and rotate for 5mins at RT.

25) Spin at 3000rpm for 1min at RT and keep the beads.

26) Repeat steps 24-25 two times.

27) Add 1ml **WASH III** buffer and rotate for 5mins at RT.

28) Spin at 3000rpm for 1min at RT and keep the beads.

29) Repeat steps 27-28.

30) Add 1ml **TE** buffer and rotate for 5mins at RT.

31) Spin at 3000rpm for 1min at RT and keep the beads.

32) Repeat step 30.
   While rotating the IP, thaw the INPUT sample (step 15) and prepare a mix of 0.2µg/µl **RNAse** in TE buffer (20µl RNAse 10mg/ml in 1ml TE buffer).

33) Spin at 3000rpm for 1min at RT and keep the beads.

34) Add to each of both IP and INPUT samples (and MOCK if you have) 100µl of RNAse mix and incubate at 37^0C for 20mins.

35) **To INPUTs**: add 350µl **ELUTION** buffer and 40µl **NaCl** 2.5M. Incubate at 65^0C for at least 5hrs or O/N.

36) **To IPs**: add 1ml **TE** buffer, spin at 3000rpm for 1min at RT and keep the beads.

37) Add 250μl **ELUTION** buffer to the beads and rotate for 15mins at RT. Vortex 3 times in between (every 5 mins).

38) Spin at 3000rpm for 1min at RT and KEEP THE SUPERNATANT to a new 1.5ml tube.

39) Repeat steps 37 and 38. Keep all the supernatant in one tube.

40) Add 40μl 2.5M **NaCl** to the eluted sample and incubate at 65^0C for at least 5hrs or O/N.

If you choose not to leave your samples O/N you can proceed to step 41 and leave at -80^0C until the next day.

DAY 4

41) Add 1ml **ethanol 100%** and incubate 2 hrs at -80^0C or O/N at -20^0C.

42) Spin at 13000rpm at 4^0C for 30mins and discard supernatant.

43) Wash the pellet once with 500μl **70% ethanol**.

44) Spin at 13000rpm at RT for 5mins and discard supernatant.

45) Speed vac the pellets so that all ethanol is evaporated.

46) Prepare **PROTEINASE K** MIX (for ~6 samples):

> 700μl **H$_2$O**
>
> 77μl **proteinase K buffer 10X**
>
> 14μl **proteinase K 20μg/μl**

47) Add 112μl from the PROTEINASE K MIX to each of the pellets and incubate at 50^0C (water bath) for 30mins.

48) Add 390μl **H$_2$O** to increase volume at ~500μl.

49) Add 50μl **sodium acetate 3M pH=5.2** (1/10 V).

50) Add 250μl **phenol**.

51) Add 250μl **chloroform**.

52) Vortex and spin at 13000rpm for 10mins at RT.

53) Keep the supernatant in new 1.5ml tubes.

54) Add 500μl chloroform, vortex, spin at 13000rpm for 5mins at RT and keep supernatant in a new 1.5ml tube.

55) Add 1ml **ethanol 100%** and 1μl **glycogen** and incubate O/N at -80^0C.

DAY 5

56) Spin at 13000rpm at 4^0C for 30mins and discard supernatant.

57) Wash the pellet once with 500μl **70% ethanol**.

58) Spin at 13000rpm at RT for 5mins and discard supernatant.

59) Speed vac the pellets so that all ethanol is evaporated.

60) Resuspend the IP pellets in 50μl **H_2O** for injection and in 250μl the pellets of your INPUT samples. Use 5-10μl in each reaction in real time PCR.

A typical PCR reaction (V_f=25μl) is set as follows:

11.8μl H_2O

5μl IP/INPUT sample

1μl forward primer 200ng/μl

1μl reverse primer 200ng/μl

0.5μl dNTPs 10mM

2μl $MgCl_2$ 25mM

2.5μl Taq buffer 5 u/μl

0.2μl Taq polymerase

1μl SYBRE green

The typical programme used in the PCR is set as follows:

1) Incubate at 94^0C for 2'

2) Incubate at 94^0C for 30''

3) Incubate at **56^0C** for 30''

4) Incubate at 72^0C for 30''

5) Incubate at 80^0C for 1''

6) Plate read

7) Go to line 2 for **39** times more

8) Incubate at 72^0C for 2'

9) Perform melting curve from 60^0C to 94^0C, read every 0.5^0C, hold for 1' between reads

10) Incubate at 15^0C for 1''

The annealing temperature depends on the primers used each time. The temperature in which the machine measures the fluorescence in each cycle also depends on where the product for each primer is obtained.

The Real Time PCR that followed was performed in MJResearch or BIORAD PCR machines and analysed with the accompanied software. We obtained our enrichment results by performing two types of normalization, one over the INPUT

sample and one over the enrichment to the ORF of a control gene on which the protein of interest is not bound.

In real-time quantitative PCR (qPCR), the amount of PCR product is measured at each cycle. This ability to monitor the reaction during its exponential phase enables users to determine the initial amount of target with great precision. PCR theoretically amplifies DNA exponentially, doubling the number of molecules present with each amplification cycle. The number of cycles and the amount of PCR end-product can theoretically be used to calculate the initial quantity of genetic material (by comparison with a known standard), but numerous factors complicate this calculation. The ethidium bromide staining typically used to quantify endpoint PCR products prevents further amplification, and is only semiquantitative. PCR may not be exponential for the first several cycles, and the reaction eventually plateaus, so the amount of DNA should be measured while the reaction is still in the exponential amplification phase, which can be difficult to determine in endpoint PCR. To address these factors, the technique of real-time quantitative PCR was developed.

In real-time PCR, the amount of DNA is measured after each cycle by the use of fl uorescent markers that are incorporated into the PCR product. The increase in fluorescent signal is directly proportional to the number of PCR product molecules (amplicons) generated in the exponential phase of the reaction. Fluorescent reporters used include double-stranded DNA (dsDNA)-binding dyes, or dye molecules attached to PCR primers or probes that are incorporated into the product during amplification (here we used SYBR green). The change in fluorescence over the course of the reaction is measured by an instrument that combines thermal cycling with scanning capability. By plotting fluorescence against the cycle number, the real-time PCR instrument generates an amplification plot that represents the accumulation of product over the duration of the entire PCR reaction.

The advantages of real-time PCR include: a) The ability to monitor the progress of the PCR reaction as it occurs in real time, b) The ability to precisely measure the amount of amplicon at each cycle, c) An increased dynamic range of detection, d) The combination of amplification and detection in a single tube, which eliminates post-PCR manipulations.

2.11. CHROMATIN IMMUNOPRECIPITATION ON CHIP (ChIP on chip)

The **array** that was used for our ChIP on chip assays was GeneChip *S.cerevisiae* **Tiling 1.0R Array** manufactured by Affymetrix (900645). The GeneChip *S. cerevisiae* Tiling 1.0R Array is designed for identifying novel transcripts, mapping sites of protein/DNA interaction in chromatin immunoprecipitation (ChIP) experiments, and other whole-genome experiments. The *S. cerevisiae* 1.0R Array is a single array comprised of over 3.2 million perfect match/mismatch probe pairs tiled through the complete *Saccharomyces cerevisiae* genome. Genome sequence information for the design of the *S. cerevisiae* Tiling 1.0R Array was drawn from the October 2003 Stanford Yeast Genome Database files (www.yeastgenome.org). The array also contains probes to interrogate a 2-μm circle plasmid (NCBI Accession J01347). Centromeric regions are not included in the array; for this reason we performed manual ChIPs for these loci.

Probes are tiled at an average of 5 base pair resolution, as measured from the central position of adjacent 25-mer oligos, creating an overlap of approximately 20 base pairs on adjacent probes.

We followed the chromatin immunoprecipitation assay for our genome-wide experiments as proposed and described by Affymetrix http://media.affymetrix.com/support/downloads/manuals/chromatin_immun_ChIP.pdf adapting it in order to fit the needs and specifications of *Saccharomyces cerevisiae*.

The Affymetrix Chromatin Immunoprecipitation (ChIP) Assay is designed to generate double-stranded labeled DNA targets that identify sites of protein-DNA interactions or chromatin modifications on a genome-wide scale. This assay has been designed specifically for use with Affymetrix GeneChip Tiling Arrays for ChIP on chip studies in order to study transcription factor binding sites, histone protein modifications, and other chromatin-protein interactions. ChIP experiments can be used as a powerful tool to complement RNA transcription studies because they enable researchers to study the DNA-protein interactions that regulate gene expression. Following the protocol, cells are first fixed with formaldehyde to crosslink DNA to any associated proteins. The cells are then lysed and DNA is sheared into smaller fragments using sonication. Protein-DNA complexes are then immunoprecipitated with an antibody directed against the specific protein of interest. Following the immunoprecipitation, crosslinking is reversed, samples are protease-treated and the purified DNA sample is amplified using a random-primed PCR method.

Subsequently, targets are fragmented and labeled to hybridize onto GeneChip Tiling Arrays. By comparing the hybridization signals generated by an immunoprecipitated sample versus an antibodynegative or non-specific antibody control, the regions of chromatinprotein interaction can be identified. The procedure outlined in this protocol describes all the necessary steps and reagents for fixing cells, fragmenting chromatin, immunoprecipitating sheared chromatin, amplifying and labelling precipitated DNA.

An optimization must be done before the execution of the protocol because of the variability inherent in the cell type, the protein of interest, the antibody, the DNA fragmentation and the PCR conditions. Our optimizations are mentioned during the description of the protocol. A schematic representation of the protocol is presented below:
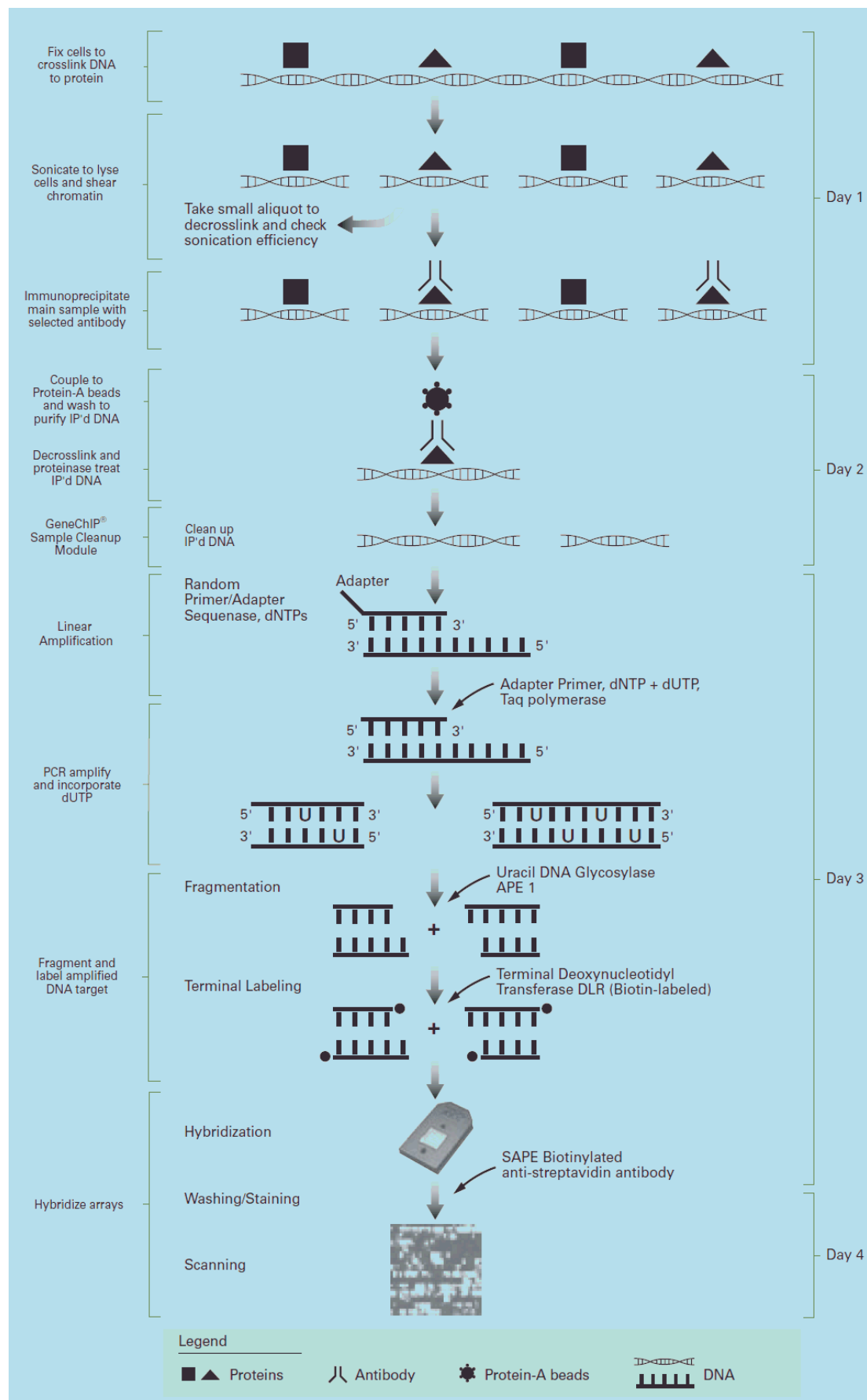
ChIP on chip assay schematic overview

2.11.A. MATERIALS

The materials required for the protocol are presented in the following tables.

Material	Source	Part Number
Formaldehyde Solution (37%), 500 mL	Sigma-Aldrich	F8775
Glycine, 1 kg	Sigma-Aldrich	50046
Phosphate Buffered Saline (PBS) pH 7.4 (1X), liquid	Various	
IGEPAL® CA-630	Sigma-Aldrich	9036-19-5
Phenylmethanesulfonyl Fluoride Solution (PMSF), 250 mL	Sigma-Aldrich	93482
Microccocal Nuclease (MNase) (Optional)	USB	70196Y
EGTA (optional)	Sigma-Aldrich	E3889-100G
Protease Inhibitor Tablet	Roche	11873580001
Decrosslink and check sonication efficiency		
Proteinase K	New England BioLabs	P8102S
LiCl (8M), 500 mL	Sigma-Aldrich	L7026
Glycogen	Roche	10901393001
Immunoprecipitation		
Triton-X100 (non-ionic viscous liquid)	Roche	10789704001
Protein A Sepharose™ CL-4B	Amersham	17-0963-03
Antibody*	Various	

Material	Source	Part Number
PCR Amplification		
Sequenase™ Version 2.0 DNA Polymerase	USB	70775Y
Primer A: 200 µM GTTTCCCAGTCACGGTC(N)$_9$	Various	HPLC purified
Primer B: 100 µM GTTTCCCAGTCACGGTC	Various	HPLC purified
Taq Polymerase 5 U/µL	Various	
10X PCR Buffer	Various	
dATP 100 mM	Various	
dCTP 100 mM	Various	
dGTP 100 mM	Various	
dTTP 100 mM	Various	
dUTP 100 mM	Various	
BSA 20 mg/mL	Various	
DTT 0.1M	Various	
Wash Buffer		
Tris-HCl	Various	
EDTA	Various	
SDS, 100g	Sigma-Aldrich	71725
NaCl	Various	
Deoxycholate (sodium salt), 100 g	Sigma-Aldrich	D6750
MgCl$_2$, 1M	Various	
CaCl$_2$, 1M	Sigma-Aldrich	21115
Fragmentation and Labeling		
GeneChip® WT Double-Stranded DNA Terminal Labeling Kit, 30 Rxn	Affymetrix	900812

DNA Cleanup		
GeneChip® Sample Cleanup Module, 30 Rxn	Affymetrix	900371
ERC Buffer[*], 85 mL	QIAGEN	1018144
Hybridization, Stain and Wash		
GeneChip® Hybridization, Wash, and Stain Kit	Affymetrix	900720
Control Oligonucleotide B2, 3nM	Affymetrix	900301

212

BUFFERS

Lysis Buffer (Store at 4°C)
10 mM Tris-HCl (made from stock 1M Tris-HCl pH 7.5) 10 mM NaCl 3 mM $MgCl_2$ 0.5% IGEPAL 1 mM PMSF (add fresh)
Pre-IP Dilution Buffer (Store at RT)
10 mM Tris-HCl (made from stock 1M Tris-HCl pH 7.5) 10 mM NaCl 3 mM $MgCl_2$ 1 mM $CaCl_2$ 4% IGEPAL 1 mM PMSF (add fresh)
IP Dilution Buffer (Store at RT without protease inhibitors)
20 mM Tris-HCl (made from stock 1M Tris-HCl pH 8) 2 mM EDTA 1% Triton X-100 150 mM NaCl Protease Inhibitor Stock (add fresh)
Protease Inhibitor Stock
Prepare a 25X stock by dissolving 1 protease inhibitor tablet in 2 mL of nuclease-free water
ChIP Wash 1 (Store at RT)
20 mM Tris-HCl (made from stock 1M Tris-HCl pH 8) 2 mM EDTA 1% Triton X-100 150 mM NaCl 1 mM PMSF (add fresh)

ChIP Wash 2 (Store at RT)
20 mM Tris-HCl (made from stock 1M Tris-HCl pH 8) 2 mM EDTA 1% Triton X-100 0.1% SDS 500 mM NaCl 1 mM PMSF (add fresh)
ChIP Wash 3 (Store at RT)
10 mM Tris-HCl (made from stock 1M Tris-HCl pH 8) 1 mM EDTA 0.25M LiCl 0.5% IGEPAL 0.5% Deoxycholate (sodium salt)
Elution Buffer
25 mM Tris-HCl (made from stock 1M Tris-HCl pH 7.5) 10 mM EDTA 0.5% SDS

2.11.B. THE ASSAY

Procedure A: Prepare the cells

We use a freshly streaked plate (from stab) to grow an overnight starter culture of the strain of interest. The next day we dilute the starter culture to an $OD_{550} \sim 0.1$ and leave enough time for the cells to grow for 6-7 hours in order to have enough time for the

induction with BCS (for 3 hours) and BPS (for 6 hours) without exceeding the exponential phase. Depending on the samples needed we grow enough cells to an OD_{550}=0.8-1 in SC or YPD medium. We use the chromatinic extract from ~$7x10^7$ cells per IP sample (equivalent to ~9ml of an exponentially growing culture of OD_{550}=0.8). For each experiment it is vital to grow cells for at least two IP samples, one INPUT sample and one MOCK sample ($28x10^7$ cells). The INPUT sample is used for the normalization in the PCR reaction by which the immunoprecipitation efficiency is evaluated. As a MOCK sample we used an antibody(-) one, to serve as the control group in the downstream two-sample analysis and we treated it exactly as the IP experimental sample.

Procedure B: Fix cells, Lyse and Sonicate the whole cell extract

1. When the cells are ready to harvest, add formaldehyde to the culture flask to a final concentration of 1% and incubate in a fume hood for 20 minutes.

2. Add 1/20 volume of 2.5 M glycine and incubate at room temperature (RT) for 5 minutes with gentle mixing. Alternatively add 0.47gr glycine and shake for 5mins to absorb formaldehyde excess.

3. Wash pellet with 10 mL ice-cold 1X PBS to resuspend cells, and pellet cells at 4°C, (3000 rpm) for 5 minutes, discard supernatant and repeat wash with ice-cold 1X PBS once.

4. Wash the pellet 3 times with 10 mL Lysis Buffer with fresh PMSF and pellet cells at 4^0C, 3000 rpm for 5 minutes between washes.

5. Discard supernatant and proceed to the next step or flash freeze pellet and store at – 80°C.

6. Resuspend the pellet in 240μl pre-IP dilution buffer (with fresh PMSF).

7. Add to the tube:

100mM PMSF	6.4μl
25X protease inhibitor stock	16μl
Pre-IP dilution buffer	73.6μl
20% SDS	16μl
2.5M NaCl	25.6μl
Nuclease free water	22.4μl
Final Sample volume before sonication	400μl

8. Transfer in 1.5ml tubes which already have ~400µl washed glass beads (of 425-600µm diameter). Adjust tube on vortex machine and vortex for 40mins at 4^0C. Collect solution and debris by spinning 1min at 3000rpm at 4^0C (by making a hole with a 0.25µm needle to the tube and placing to another one before spinning).

9. Sonicate samples 5 times for 12secs each at 40% energy and rest on ice 1min between intervals. Sonication time may vary according to the machine used. Under these conditions samples are sheared to fragments of 300-500bp (peak).

10. Spin twice for 15mins each at 13000rpm at 4^0C (change tubes) keeping the supernatant from each one in the same tube. The sonication efficiency can be checked by taking an aliquot of this supernatant, de-crosslinking it (see Procedure C, below), and running the de-crosslinked DNA on a 1-2% agarose gel.

11. If not directly used, freeze the supernatant in -80^0C.

Procedure C: Check sonication efficiency

1. Add 40 µl 10 mM Tris pH 8.0 to a 40 µl aliquot taken from the sonicated samples.

2. Add Proteinase K (20 mg/ml) to a final concentration of 0.2mb/µl and mix well by vortexing.

3. Incubate 42°C for 2 hours, then 65°C for 6 hours to overnight. This step can be performed in a thermocycler.

4. Clean-up using Affymetrix cDNA cleanup columns, from the GeneChip Sample Cleanup Module, eluting with 20 µL Elution Buffer following the manufacturer's instructions.

5. Load 100-500 ng of purified DNA sample on an agarose gel to check sonication efficiency. Typically, sheared DNA size ranges from 100-4000 bp, with the average size fragment between 300-500 bp.

Procedure D: Incubate with specific antibody

1. If the sample (from Procedure B Step 11) was frozen, thaw.

2. Equilibrate an equal volume with the sample of G sepharose (or agarose) packed beads 3 times with IP dilution buffer (spin at 3-4000 rpm between the washes). Add buffer till there is enough for a final volume of 70µl per sample.

3. Preclear the chromatin samples: Transfer desired amount of sample chromatin supernatant to a 0.5 mL tube (~60-70µl/400µl equivalent to ~$7x10^7$ cells' extract per sample) and add the 70µl of the equilibrated G sepharose beads from step 2. If

needed, raise the volume with IP dilution buffer (containing Roche complete EDTA free protease inhibitor cocktail) until enough to mix well while rotating (usually ~250μl final volume).

4. Incubate on a rotating platform at 4°C for 1 hr and 30 minutes.

6. Centrifuge at 2,000 rpm for 2 minutes at 4°C.

7. Transfer supernatant to a new 0.5 μl tube and discard beads. Aliquot the final volume of precleared chromatin so that each sample (IP, INPUT or MOCK) contains volume equivalent to the ~7×10^7 cells' extract.

8. Freeze the INPUT sample at -20^0C. Add 6μg of antibody per IP. MOCK sample contains no antibody but otherwise is treated as the IP sample. Add Roche complete EDTA free protease inhibitor cocktail to an 1X final concentration. Raise the final volume to ~250μl with IP dilution buffer.

9. Incubate on rotating platform at 4°C overnight.

Procedure E: Immunoprecipitate and wash

1. Pre-equilibrate protein G Sepharose beads as in Procedure D Step 2 and transfer an amount of ~60-70μl packed beads to each of the IP or MOCK samples

2. Add PMSF to each tube sample (final concentration 1mM PMSF in final volume).

3. Incubate on rotating platform at RT for 2 hours.

4. Centrifuge at 2,000 rpm at 4°C for 4 minutes, and then discard supernatant.

5. Resuspend the pellet with 700 μL ChIP wash 1 (containing 1 mM PMSF added fresh), mix and transfer to spin-X column.

6. Incubate on rotating platform at RT for 1 minute.

7. Centrifuge at 2,000 rpm at RT for 2 minutes and discard flowthrough.

8. Repeat steps 5–7.

9. Wash the beads with 700 μL ChIP wash 2 (containing 1 mM fresh PMSF).

10. Incubate on rotating platform at RT for 5 minutes.

11. Centrifuge at 2,000 rpm at RT and discard flow-through.

12. Wash the beads with 700 μL ChIP wash 3.

13. Incubate on rotating platform at RT for 5 minutes.

14. Centrifuge at 2,000 rpm at RT and discard flow-through.

15. Wash the beads with 700 μL TE (10 mM Tris-HCl pH 8, 1 mM EDTA).

16. Incubate on rotating platform at RT for 1 minute.

17. Centrifuge at 2,000 rpm at RT and discard flow-through.

18. Repeat steps 15 through 17.

19. Transfer the spin-X column with beads to a dolphin-nose tube.

20. Add 200 µL Elution Buffer to the column.

21. Incubate at 65°C for 30 minutes.

22. Centrifuge at 3,000 rpm at RT for 2 minutes.

23. Add 200 µL Elution Buffer to the column.

24. Centrifuge at 3,000 rpm at RT for 2 minutes. This 400 µL eluted sample is the "enriched" or "IP'd" sample.

Procedure F: Reverse crosslinks

1. Add 5 µL Proteinase K (20mg/mL) per 100 µL of negative control or IP sample, mix well. (20 µL for 400 µL of eluted sample.)

2. Incubate in incubator at 65°C overnight.

Procedure G: Cleanup de-crosslinked samples

i. Clean up samples using Affymetrix cDNA cleanup columns as follows:

1. Add 5X volumes of cDNA Binding Buffer to sample, and vortex for 3 seconds.

2. Apply the sample to a cDNA Spin Column sitting in a 2 mL Collection Tube (max capacity of column = 700 µL; if volume exceeds 700 µL, spin 700 µL at 10000rpm for 1 minute, discard flow-through, and repeat).

3. Spin at 10000rpm for 1 minute. Discard the flow-through.

4. Transfer the cDNA Spin Column to a new 2 mL Collection Tube and add 750 µL of cDNA Wash Buffer to the column. Spin at 10000rpm for 1 minute and discard the flow-through.

5. Open cap of the cDNA Spin Column, and spin at 13000rpm for 5 minutes with the caps open. Discard the flow-through, and place the column in a 1.5 mL collection tube.

6. Pipet 20µl of cDNA Elution Buffer directly to the column membrane and incubate at room temperature for 1 minute. Then, spin at 13000rpm for 1 minute.

7. Repeat step 6 with another 20µl of Elution Buffer. Total elution volume recovered is ~ 38 µL.

ii. IP efficiency can be checked at this stage in the protocol using polymerase chain reaction (PCR) and designing primer sets against regions that are known to be bound

by the protein of interest and immunoprecipitated using the antibody being investigated. A significant (or the expected, if known) increase or enrichment for the specific target should be observed for the IP condition compared to the Ab- control (MOCK).

Procedure H: PCR amplification of the immunoprecipitated DNA targets

1) Use 9µl of IP'd or negative control sample for initial round of linear amplification .

2) Set up first round reaction:

Round A reaction Mix

DNA to be amplified and labeled	9 µl
5X sequenase reaction buffer	2.4 µl
Primer A (40µM)*	1.2 µl

*For smaller amounts of DNA increase Primer A to a concentration up to 200µM. You can test this by performing serial dilutions.

3) Cycle conditions: Random Priming.

A. 95^0C for 4 mins.

B. Snap cool samples on ice.

C. 10^0C hold.

D. Prepare first cocktail

FIRST COCKTAIL	1X (µl)	3X (µl)	5X (µl)
5X sequenase reaction buffer	1	3	5
dNTP mix (3mM each)	1.5	4.5	7.5
DTT	0.75	2.25	3.75
BSA	1.5	4.5	7.5
Sequenase	0.3	0.9	1.5
Total	5.05	15.15	25.25

Round A stocks	
dNTPs	3mM each
DTT	0.1M
BSA	500μg/ml
Sequenase	13U/μl

    E. Add 5μl of the first cocktail mix.

    F. Mix well by pipetting and put the sample back in thermocycler block.

    G. 10^0C for 5 mins.

    H. Ramp from 10^0C to 37^0C over 9 mins.

    I. 37^0C for 8 mins.

    J. 95^0C for 4 mins.

    K. Snap cool on ice.

    L. 10^0C hold.

    M. Add 0.3μl of 13U/μl sequenase to each sample.

    N. 10^0C for 5 mins.

    O. Ramp from 10^0C to 37^0C over 9 mins.

    P. 37^0C for 8 mins.

    Q. Repeat from J) to P) for 1 more cycle (* this step is optional, we have found that only 2 cycles with sequenase are enough for satisfactory amplification)

    R. 4^0C hold.

4) For each IP, purify with Microspin S-300 HR (GE Healthcare) columns (2 columns per reaction) as follows:

A. Add 35 μl of 10 mM TE pH 8.0 to each reaction.

B. Spin 2 columns (A & B) at 3,000 rpm for 1 minute, discard flow-through.

C. Transfer reaction volume (~ 43 μl) to column A, while equilibrating column B with 300 μl of 10 mM Tris pH 8.0.

D. Spin both columns at 3,000 rpm for 1 minute, keep flowthrough from column A (sample) and discard flow-through of column B (Tris buffer).

E. Transfer flow-through of column A to column B with new collection tube.

F. Spin at 3,000 rpm for 2 minutes.

G. Collect ~ 56 μl of first round purified DNA per reaction.

5) Prepare dNTP/dUTP mix

dCTP-25mM

dATP-25mM

dGTP-25mM

dTTP-20mM

dUTP-5mM

6) PCR Mix Setup (Round B)

	1X	4X
First round DNA from step 4	15 μl	
10X Taq buffer	10 μl	40 μl
25mM MgCl$_2$	8 μl	32 μl
dNTP/dUTP mix (step 5)	1 μl	4 μl
Primer B (100mM)	4 μl	16 μl
Taq polymerase (5u/μl)	1 μl	4 μl
Nuclease free water	61 μl	244 μl
Total	100 μl	

Set up 4 reactions of 100μl (aliquoted in 8 low tube strips, 50μl each) to get enough amount of amplified DNA sample for one hybridization.

7) Cycle conditions:

A. 16 cycles

1) 95°C 30 seconds.

2) 45°C 30 seconds.

3) 55°C 30 seconds.

4) 72°C 1 minute.

B. 16 cycles

1) 95°C 30 seconds.

2) 45°C 30 seconds.

3) 55°C 30 seconds.

4) 72°C 1 minute.

For every subsequent cycle add 5 seconds.

E.g., cycle 1: 60 seconds, cycle 2: 65 seconds, etc.

C. 4°C hold.

8) Check amplified DNA on 1% agarose gel.

9) Purify PCR samples with Affymetrix cDNA cleanup columns, provided in the GeneChip Sample Cleanup Module, eluting twice with 20 μL of Elution Buffer (see Procedure G, Part i).

10) Calculate DNA quantity by using a NanoDrop. Normally, greater than 9 μg of amplified DNA is obtained from each reaction.

Procedure I: Fragment amplified targets

1. Fragment the samples using the table below:

Fragmentation Mix for single arrays (e.g., *S. cerevisiae* 1.0R Tiling Array)

Component	Volume/Amount in 1 Rxn
Double-Stranded DNA	7.5 μg
10X cDNA Fragmentation Buffer*	4.8 μL
UDG, 10 U/μL*	1.5 μL
APE 1, 100 U/μL*	2.25 μL
Nuclease-free Water*	up to 48 μL
Total Volume	48.0 μL

* Available in GeneChip® WT Double-Stranded DNA Terminal Labeling Kit (P/N 900812)

2. Set up fragmentation mix according to the above table. Flick-mix and spin down the tubes.

3. Incubate the reactions at:

• 37°C for 1 hour.

• 93°C for 2 minutes.

• 4°C for at least 2 minutes.

4. Flick-mix, spin down the tubes, and transfer 45 μL of the sample to a new tube.

5. The remainder of the sample is to be used for fragmentation analysis using a Bioanalyzer or agarose gel. If not labeling the samples immediately, store the fragmented DNA at –20°C.

Procedure J: Label fragmented dsDNA

1. Prepare the Double-Stranded DNA Labeling Mix as described in the table below:

Component	Volume in 1 Rxn
5x TdT Buffer*	12 µL
TdT*	2 µL
DNA Labeling Reagent, 5 mM*	1 µL
Total Volume	15 µL

* Available in the GeneChip® WT Double-Stranded DNA Terminal Labeling Kit (P/N 900812).

2. Add 15 µl of the Double-Stranded DNA Labeling Mix to the DNA samples (45µl), flick-mix, and spin them down.

3. Incubate the reactions at:

• 37°C for 60 minutes.

• 70°C for 10 minutes.

• 4°C for at least 2 minutes.

Hybridization and Array Processing

Procedure K: Hybridize labeled target on the array

This Procedure requires the use of the GeneChip Hybridization, Wash, and Stain Kit (P/N 900720).

1. Prepare the Hybridization Cocktail in a 1.5 mL RNase-free microfuge tube as shown in the table below.

Component	Volume in 1 Rxn	Final Concentration or Amount
Fragmented and Labeled DNA Target	~ 60.0 µL*	~ 7.5 µg
Control Oligonucleotide B2	3.3 µL	50 pM
2X Hybridization Mix†	100 µL	1X
DMSO	14.0 µL	7%
Nuclease-free Water	up to 200.0 µL	
Total Volume	200.0 µL	

*This volume is 56 µL if a portion of the sample was set aside for gel-shift analysis.

2. Flick-mix, and centrifuge the tube.

3. Heat the Hybridization Cocktail at 99°C for 5 minutes. Cool to 45°C for 5 minutes, and centrifuge at maximum speed for 1 minute.

4. Inject ~ 200 μL of the specific sample into the array through one of the septa (see Figure below). Save the remaining hybridization cocktail in –20°C for future use.

GeneChip® Probe Array
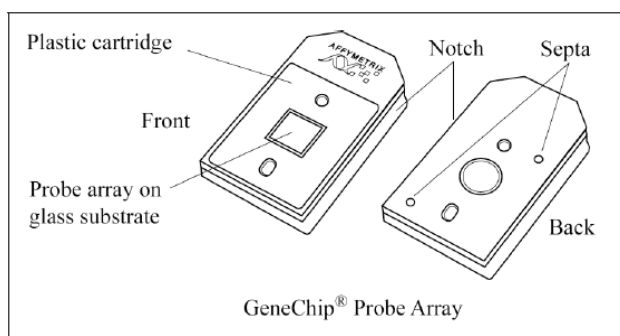
5. Place array in 45°C hybridization oven, at 60 rpm, and incubate for 16 hours.

6. After hybridization, remove the hybridization cocktail for future use.

Array Washing and Staining

This part of the protocol includes preparation and priming of the Fluidics station 450, selection of the appropriate protocol, wash and staining of the probe array and shutting down the station. These procedures are being performed by our technician (G. Papayannakis) according to the Affymetrix proposed protocol. All buffers needed can be found in the extended protocol:

http://media.affymetrix.com/support/downloads/manuals/chromatin_immun_ChIP.pdf

Scanning

Scanning of the probe array is also being performed by our technician (G. Papayannakis) according to the Affymetrix proposed protocol. After the scanning a series of files are obtained, namely

- DAT file, which contains the primary image of the scanning.
- CEL file (Cell Intensity File), which contains processed cell intensities from the primary image in the .DAT file. Intensity data is computed by the

Affymetrix GCOS application and stored in CEL files. Each GeneChip Tiling Array produces a single CEL file.

- RPT (Report) file which stores report results about the quality of the experiment such as intensity threshold, median intensity, number of probes that failed a threshold set, average intensity of bright and dim probes etc.

- GRD (Grid) file, which stores the estimate of the sub-pixel location of the center of every feature in the array.

- JPG file, which provides an illustration-snapshot of the scanned array.

2.11.C. ANALYSIS OF THE RESULTS

The CEL file obtained from the scanning process after the computation by the Affymetrix GCOS application is used as an input in the Tiling Analysis Software (TAS v1.1). Analysis functions provided within the TAS application include:

• Analyzing feature-intensity data stored in CEL files to produce signal and p-values for each interrogated genomic probe position

• Computation of genomic intervals based on computed signal and p-values

• Computation of summary statistics

• Visualizations for assessing the quality of array data

Analyses produced using TAS can be imported into applications such as the Integrated Genome Browser (IGB) for visualization against genomic annotations as we shall see further below.

The workflow that the TAS follows is illustrated below:

```
                    ┌─────────────────────────────┐
                    │ DEFINE ANALYSIS PARAMETERS  │
                    │                             │
                    │      * Data Paths           │
                    │      * Export               │
                    │      * Normalization        │
                    │      * Scale                │
                    │      * Probe Analysis       │
                    │      * Interval Analysis    │
                    └─────────────────────────────┘
                                 │
                                 ▼
CEL Files                ┌──────────────────────┐
BPMAP Files         ────▶│ DEFINE ANALYSIS GROUP│────▶  TAG File
Analysis Options         └──────────────────────┘
                                 │
                                 ▼
TAG Files           ────▶┌────────────────────────────┐────▶ BAR Files
                         │ CALCULATE SIGNAL & P-VALUES │
                         └────────────────────────────┘
                                 │
                                 ▼
CEL Files                                              MVA files
GFF Files           ────▶┌──────────────────────┐────▶ ROC files
BAR Files                │ ASSESS INTENSITY DATA│
BPMAP Files              └──────────────────────┘      RPT files
                                 │
                                 ▼
BAR Files           ────▶┌──────────────────────┐────▶ BED Files
                         │ CALCULATE INTERVALS  │
                         └──────────────────────┘
                                 │
                                 ▼
Ref BED Files       ────▶┌──────────────────────┐────▶ BED Files
Test BED Files           │  PROMOTER ANALYSIS   │
                         └──────────────────────┘
```

Firstly, it is important to specify the analysis settings:

Data paths: Settings on the *Data Paths* tab are used to specify the location of data files and BPMAP files. As data file we used the CEL file obtained from the scanning process. A library file BPMAP (Binary Probe Map) is also needed. BPMAP file contain the genomic probe position map. The BPMAP file maps the X/Y coordinate of a probe on a GeneChip array to a genomic position for an intended function. It designates a probe as either a perfect match (PM) or a mismatch (MM) probe.

Export: Settings on the Export tab are used to specify the type of data saved in the BAR files and whether or not analysis results (signal and p-values) should be exported along with the BAR files as text files. For our analysis we choose to export our results in both BAR and txt files and also to obtain both signal and p-values results.

Normalization options: The setting displayed on the Normalization Options tab is used to specify target intensity when normalizing CEL data. The intensities in the CEL file are linearly scaled so that the median intensity value is equal to the target intensity.

Scale: Settings on the *Scale* tab are used to specify the scale in which the analysis results (signal and p-values) are to be stored in the output files. We choose for the Signal a Log2 scale and for the P-value the -10Log10 scale.

Probe analysis: Settings on the *Probe Analysis* tab (Figure 1.6) are used to determine probe analysis levels for computing signal and p-values. Since bandwidth defines the number of bases to extend from the position being analyzed, these settings ensure that every probe in a region of *2*Bandwidth + 1* is included in the signal and p-value analysis. Bandwidth is a distance (in base pairs) used to locally group positional data and is determined by two main factors: i) Base pair (bp) tiling on the array and ii) Type of experiment. Analysis at a particular position will be based on all data aligning within ± bandwidth of the position, so that the sliding window of the analysis is of size *2*bandwidth+1*. Making bandwidth larger brings more data into each test providing more statistical power and a greater ability to detect signal. However, once the bandwidth exceeds the point where the window is larger than the signal being interrogated, power decreases to include data with no signal. The suggested BW range should be such that the window size (2 x BW +1) roughly corresponds to the median size of an exon (300 for our analysis). Furthermore, for the Test Type we choose "One Sided Upper" which derives p-values to test whether or not the treatment group has a lesser signal than the control group. In addition, we use both PM and MM probe intensities in the analysis.

Interval analysis: Settings on the *Interval Analysis* tab are used to determine how intervals are calculated. Base pair spacing of probes on the array, type of experiment (RNA mapping or ChIP-chip), and stringency of the data set to be created determine which values to use. For a typical ChIP-chip experiment, for p-value interval generation, threshold is set based on the confidence level of p-values in the two sample analysis that users select. We used p-value cutoffs between 10^{-3} and 10^{-5} for interval generation (30 to 50, respectively, on the -10log10, p-value scale). In both RNA mapping and ChIP-chip experiments, max gap and min run parameters are dependent on size of intervals that users want to identify. Calculations are performed by:

• Determining the region where a probe is positive (the signal or p-value is above or below a threshold).

• Selecting a maximum gap between positive probes. This setting is referring to the maximum tolerated gap (in base pairs) between positive positions in the derivation of

detected regions. Decreasing it, results in a more stringent map; increasing it lessens the stringency. We choose a value of 80.

• Selecting a minimum length or run of adjacent probes. This setting is the minimum size (in base pairs) of a detected region. Increasing it, disallows detection of smaller regions which may be appropriate if the expected size of detected regions is large. We choose a value of 40.

After the specification of the above analysis settings (data paths, export, normalization options, scale, probe analysis, interval analysis), the next step involves the definition of the analysis group. In this step we select the appropriate BPMAP file (Sc03b_MR_v04 in our case) and we choose also the type of the analysis that we want to perform. In our case, we selected the *two sample comparison analysis*, in which we defined the Treatment Group (CEL file from our experiment) and the Control Group (CEL file from the INPUT sample grown in the same conditions). In this step we save the group of the two files in a TAG file. The TAG (Tile Analysis Group) file stores a set of CEL files, a BPMAP file, and the normalization option settings of our two sample analysis.

Probe Analysis

Probe analysis uses a combination of CEL files, the BPMAP file, normalization settings specified in the TAG file, and parameters specified in the Default Properties window. Probe analysis results in a signal and a p-value for each genomic position interrogated by the array. These values are then stored in two BAR files (we also chose to obtain the txt format of these BAR files: see *Export* analysis settings).

2.11.D. ALGORITHMS

→Algorithms used for the probe analysis

The BPMAP file is used to associate each perfect match (PM) probe with its position in a genomic sequence. The probe position, whether its target is the forward or the reverse strand, is determined by the location of its 0-based position on the lower coordinate of the probe aligned to the target. Probe position is defined by the positions employed in the genome assembly, which is used for probe selection in the array. Mismatched (MM) probes are always paired with a PM probe and have the same convention.

227

Once the PM and MM pairs have been associated with sequence positions and normalized, the next step is to perform statistical analysis (in a local context for each position) to determine size and significance of the hybridization signal. In the case of PM only analysis, MM is not used. On some arrays, MM is not present. Analysis can be performed in either a one-sample or a two-sample context. A typical one-sample context might consist of using a number of biological or technical replicates for detection of regions of transcription. A typical two-sample context might consist of a treatment versus control comparison to look for regions of enrichment in a chromatin immunoprecipitation (ChIP) experiment. *Probe Analysis* is focused at a single sequence position because the method is the same for all positions. The first step is to define a local data set consisting of all PM probes located within ± bandwidth base pairs of the position of interest. The value of the bandwidth should be driven by the average size in base pairs of the signal to be detected. In the case of transcription monitoring, the bandwidth would typically be on the order of half the average exon length, often about 50bp. In the case of ChIP assays, it would be half the expected fragment length in the step immediately before enrichment, which is assay dependent, but typically on the order of 500bp.

Selection of a bandwidth involves a tradeoff. On one hand, the bandwidth should be as large as possible to provide greatest statistical power for the analysis at each position; on the other hand, if the bandwidth is too large, the analysis tends to dilute signal by including background. The resulting local data set typically consists of a number of PM probes for each array being studied. The next step differs for one-sample and two-sample analysis.

→Algorithms for the two sample comparison analysis used in our experiments

In two-sample analysis, there are two data sets, which are called a treatment and a control group. Each group consists of the subset of data falling within the specified bandwidth as described above, resulting in n_t treatment pairs of probe intensities $\{PM_{t,i}\text{-}MM_{t,i}; i=1,...n_t\}$ and n_c control pairs of probe intensities $\{PM_{c,i}\text{-}MM_{c,i}; i=1,...n_c\}$. The log-transformed quantities $\{S_{g,i}=\log2(\max(PM_{g,i}-MM_{g,l},1)); g=t,c;i=1,...,n_g\}$ are formed and a Wilcoxon signed-rank test is performed on the two samples $\{S_{t,i};i=1,...,n_t\}$ and $\{t_{c,i};i=1,...,n_c\}$. In the case of a PM only analysis, instead of using the log-transformed differences, the log-transformed PM signal intensities $\{S_{g,i}=\log2(PM_{g,i});g=t,c;i=1,...,n_g\}$ are used.

The default test type is a one-sided test, against the alternative that the distribution of the treatment data is shifted up with respect to the distribution of the control data. A two-sided or lower-sided test can be used instead of the one-sided lower. Similar to the one-sample p-values, by default, the $-10\log_{10}$ transform is applied to the output to enable visualization along the sequence.

An estimate of fold enrichment is also computed; the estimator used is the Hodges-Lehmann estimator associated with the Wilcoxon rank-sum test (Hollander and Wolfe, 1999). The estimator is computed by forming all $n_t n_c$ values $\{D_{ij}=(S_{t,i}-S_{c,j}); i=1,...,n_t; j=1,...,n_c\}$. The Hodges-Lehmann estimator is then the median of the D_{ij} and can be interpreted as the $\log_2$ fold change between the treatment and control group signals.

→ Algorithms used for the Normalization

The default workflow assumes that the probe intensity data are normalized using quantile normalization (Bolstad et al., 2003). Quantile normalization makes the assumption that the data being normalized have the same underlying distribution; this should be a reasonable assumption within biological and sample replicates. For the one-sample analysis, the assumption of equal, underlying distributions is usually reasonable. By default, all arrays are quantile-normalized together. For two-sample analysis, it is quite possible that the underlying distributions are different for the two groups; therefore, by default, quantile normalization is performed only within each group.

Normalization, if performed, is full quantile normalization of all probe intensities. We can select the option to normalize TAG files separately for each group or normalize across all groups in an analysis. If the target intensity parameter is set, then the normalized intensities are further scaled to set the median intensity for every array to be the target intensity value. If normalization is not performed, the target intensity parameter is ignored.

2.11.E. POST ANALYSIS OF THE BAR AND TXT FILES

i) Visualization of the intensity values

After obtaining the BAR and TXT files which contain the normalized intensity values of our experiments we use the Integrated Genome Browser (IGB) to visualize

our results and to do a further sorting. The IGB is a free software for distribution and exploration of genome-scale datasets (Nicol et al., 2009) and can be downloaded from the link below:

http://www.affymetrix.com/partners_programs/programs/developer/tools/download_igb.affx

IGB can be used to visualize either p-value.BAR or signal.BAR files. We use the former, in order to be able to set a threshold (see below) above which there are the genomic areas which are significantly enriched according to our settings.

Firstly, we upload the p-value.BAR file to IGB and select the organism (*Saccharomyces cerevisie*) and the genome version used for our array which is from October 2003. We set the Y-axis scale for a minimum of 0 and a maximum of 100 (to keep a consistency between the experiments) and by using the Graph Adjuster tool we set a threshold by value corresponding to a p-value of usually 10^{-3} or 5×10^{-3} (value of 30 and 23 respectively). This is a common analysis step to determine meaningful regions on a sequence based on graph values being above or below a certain threshold. By using the NetAffx tool we can also visualize the ORF of genes according to Saccharomyces Genome Database (SGD). A typical image obtained from IGB is presented in the below figure. This is a visualization of Rad9 binding pattern on the first ~100000 bp of chr1. In the upper part of the plot (A) there is a peak in the locus where Rad9 is significantly enriched. Also visible is the line (B) corresponding to a threshold of a p-value 5×10^{-3}. The genomic areas where Rad9 is bound fitting our threshold criteria are visualized in (C). The coordinates of these loci can be obtained by making and track of them and saving it as a BED file (which can easily be transformed to an XLS file). The ORFs of the Watson (D) and Crick (F) strands are aligned along the chromosome (E).
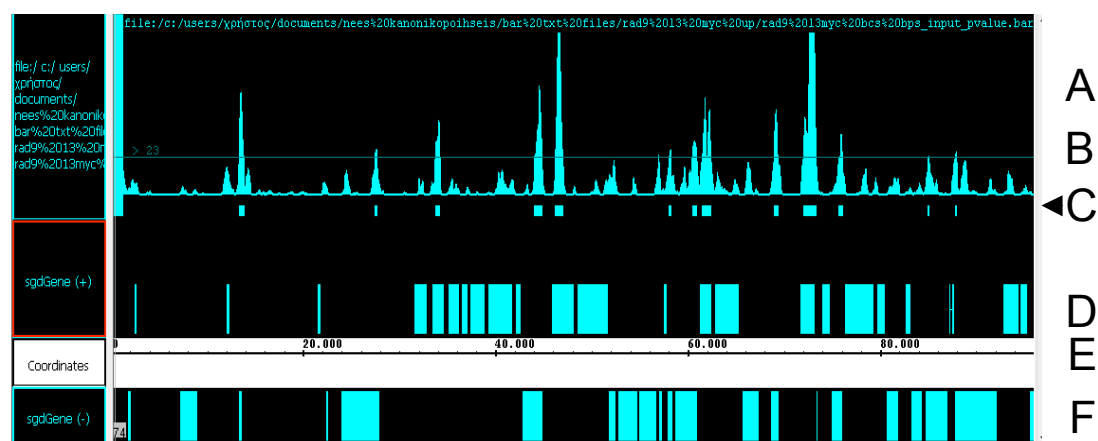
Sorting of the results according to the intensity values and correspondence of the statistically important peaks to the genomic areas

The intensity value of each spot is incorporated in the BAR and TXT files obtained by the TAS. By using an R script (see below about R) written specifically for *S. cerevisie* genome and our data (Georgia Tsiliki) we were able to match each of the statistically important binding loci (obtained from IGB) to the coding (ORF) or non-coding areas. The output file was used in combination with the TAS TXT file in order to match each peak to an intensity value. The latter was done with other specialized scripts for R and Command Promt tools (written by Christophoros Nikolaou).

R is a language and environment for statistical computing and graphics. It is a GNU project which is similar to the S language and environment which was developed at Bell Laboratories (Lucent Technologies) (http://www.r-project.org/). We also used R language to a great extend in order to compare list of genes to find common and uncommon ones (scripts written by Georgia Tsiliki).

ii) Cytoscape Analysis (Functional clustering)

In order to perform a functional clustering on the group of genes on which our proteins were enriched we used the Cytoscape open source software platform for visualizing complex networks (Cline et al., 2007) (http://www.cytoscape.org/). To do that, we used the BiNGO plugin (Maere et al., 2005). The Biological Networks Gene Ontology tool (BiNGO) is an open-source Java tool to determine which Gene Ontology (GO) terms are significantly overrepresented in a set of genes. BiNGO can be used either on a list of genes, pasted as text, or interactively on subgraphs of biological networks visualized in Cytoscape. BiNGO maps the predominant functional themes of the tested gene set on the GO hierarchy, and takes advantage of Cytoscape's versatile visualization environment to produce an intuitive and customizable visual representation of the results (http://www.psb.ugent.be/cbd/papers/BiNGO/Home.html).

BiNGO currently provides two statistical tests for assessing over- or underrepresentation in a set of genes. The basic question answered by these tests is the following : 'When sampling X genes (test set) out of N genes (reference set; graph or annotation), what is the probability that x or more of these genes belong to a functional category C shared by n of the N genes in the reference set.' The hypergeometric test (test without replacement) provides an accurate answer to this

question in the form of a p-value and this is what we used for our analysis. We have also controlled the False Discovery Rate (FDR) i.e. the expected proportion of false positives among the positively identified tests by using the Benjamini & Hochberg correction, which provides strong control over the FDR under positive regression dependency of the null hypotheses. We used a significance level of 0.05.

The goal of the Gene Ontology (GO) project is to provide a structured description of known biological information at different levels of granularity. GO consists of three structured, controlled vocabularies that describe gene products in terms of their associated biological processes, molecular functions and cellular components in a species-independent manner. With BiNGO we used the *Saccharomyces cerevisiae* GO ontologies and annotations.

iii) Average gene analysis

The average gene analysis aimed to visualize the binding pattern results for all the genes of each experiment in one plot as an "average gene" and was performed by Christophoros Nikolaou. We used the raw values included in the signal.BAR files obtained by TAS. Each of the 5769 genes of *S. cerevisiae* (SGD version, sacCer1) was divided in 100 equal bins. For example a 1000bp gene was divided in 100 bins of 10bp, while one of 5000bp was divided in 100 bins of 50bp. The average signal value was calculated for each bin. In this way, every gene was shrunk into 100 entities regardless of size, with the first entity corresponding to TSS and the last to the TTS. Subsequently, an area of +/-500bp from the TSS/TTS respectively was divided into 50 bins of 10bp for every gene. In this way, we finally obtained for each gene 200 entities-bins (50 upstream, 100 genic, 50 downstream). In the occasions where in -500 upstream or +500 downstream there was another gene, the area ended on the spot where the neighbouring gene was met. The plots obtained represent the average value of the 200 entities-bins –for each place- for the 5769 genes. The concept of average gene analysis is also described by other (Li et al., 2007b; Pokholok et al., 2005).

iv) Calculation of the GC content of the genomic areas

To calculate the GC content of the sequences where there was an overrepresentation of the proteins of interest, we first transformed the BED files (obtained by IGB) to XLS files. These files contain the coordinates of the areas where the proteins are bound. We transformed the XLS files to FASTA format files by using

Galaxy (http://main.g2.bx.psu.edu/), an open, web-based platform for data intensive biomedical research. Subsequently, we use Galaxy's EMBOSS GeeCee tool to obtain the percentage of GC content. We compared this to a randomized sample of GC content obtained from random sequences (probes) of the same number and size as the ones from our experiments. The randomization was performed with a specific Perl script (written by Christophoros Nikolaou).

Using R statistical package, we calculated and plotted the median and mean percentage values of experimental and randomized samples after fitting a t-test of values lower than 10^{-5} (ranging from 10^{-5} to 10^{-120}).

12. EXPRESSION MICROARRAY (AFFYMETRIX PLATFORM)

The array that was used for our expression microarray experiments is **GeneChip Yeast Genome 2.0 Array** manufactured by Affymetrix (900554). The GeneChip Yeast Genome 2.0 Array contains probe sets to detect transcripts from both *Saccharomyces cerevisiae* and *Schizosaccharomyces pombe*, which are the two most commonly studied species of yeast. Providing comprehensive coverage of both species, the GeneChip Yeast Genome 2.0 Array includes approximately 5,744 probe sets for 5,841 of the 5,845 genes present in *S. cerevisiae* and 5,021 probe sets for all 5,031 genes present in *S. pombe*. The sequence information for this array was selected from public data sources GenBank (May 2004) and Sanger Center (June 2004) for the *S. cerevisiae* and *S. pombe* genomes, respectively. Probe sets on the array include 11 oligonucleotide pairs to detect each transcript.

We have performed one experiment (*rad9Δ* strain grown in SC BCS BPS and the wild type FT5 in the same conditions) and one biological replicate.

We followed the protocol proposed by Affymetrix.

http://media.affymetrix.com/support/downloads/manuals/expression_analysis_technical_manual.pdf

If any changes were made are presented below.

Briefly, the Expression Analysis includes the steps of i) target preparation, ii) target hybridization, iii) fluidics station setup, iv) probe array washing and staining, v) probe array scan and vi) data analysis. Steps iii, iv and v are performed by our technician (George Papayannakis).

i) RNA isolation from yeast with hot acid phenol protocol

1. Inoculate and grow yeast cultures (10ml) until exponential phase (OD_{550}~0.8).

2. Harvest the cells by centrifugation at 3000rpm (RT) for 5mins.

3. Discard supernatant and resuspend pellet in 0.45ml AE buffer (50mM CH_3COONa pH=6; 10mM EDTA pH=8). Transfer in a 1.5ml tube and add 0.5ml acid phenol prewarmed at 65^0C and 50µl 10% SDS. Vortex for 20sec. Transfer tube to 65^0C waterbath for 1hr, vortexing for 20sec, every 10mins.

4. After the final vortexing coolthe tube on ice for 10mins and add 50µl (1/10V) 3M CH_3COONa pH=5.2

5. Separate the phases by centrifugation at 13000rpm RT for 10mins.

6. Extract the supernatant once with phenol/chlorophorm and once with chlorophorm.

7. Transfer supernatant in new tube and add 1.375ml (2.5V) 100% ethanol. Store at least 2hrs at -80^0C.

8. Cenrifuge at 13000rpm for 30mins at 4^0C, wash the pellet once with 70% ethanol, dry, and resuspend in ~100µl H_2O.

ii) DNAse treatment

We treated 20µg of RNA with DNAse (Promega) for 1 hour at 37^0C

Reaction (20 µl final volume)

17 µl total RNA (15-20 µg in DEPC water)

  2 µl 10x DNase buffer (Promega)

  1 µl DNase (1u/ µl)

    We extracted the reaction volume by phenol/chlorophorm followed by ethanol precipitation. We measured with Nanodrop the A_{260}/A_{280} ratio, ensuring that it was close to 2.0 (1.9-2.1 is acceptable) for pure RNA. We then used 7µg of DNAse treated RNA in the One-Cycle cDNA Synthesis protocol.

iii) One-Cycle cDNA Synthesis protocol

STEP 1: PREPARATION OF POLY-A RNA CONTROLS FOR ONE-CYCLE cDNA SYNTHESIS (SPIKE-IN CONTROLS)

Eukaryotic Poly-A RNA Control Kit is used for this step (Affymetrix 900433).

Designed specifically to provide exogenous positive controls to monitor the entire eukaryotic target labeling process, a set of poly-A RNA controls is supplied in the GeneChip Eukaryotic Poly-A RNA Control Kit. Each eukaryotic GeneChip probe

array contains probe sets for several *B. subtilis* genes that are absent in eukaryotic samples (*lys, phe, thr,* and *dap*). These poly-A RNA controls are *in vitro* synthesized, and the polyadenylated transcripts for the *B. subtilis* genes are pre-mixed at staggered dilutions. The concentrated **Poly-A Control Stock** can be diluted with the **Poly-A Control Dil Buffer** and spiked directly into RNA samples to achieve the final dilutions (referred to as a ratio of copy number) summarized in the table below.

Poly-A RNA Spike	Final Dilution (estimated ratio of copy number)
lys	1:100,000
phe	1:50,000
thr	1:25,000
dap	1:6,667

The controls are then amplified and labeled together with the samples. Examining the hybridization intensities of these controls on GeneChip arrays helps to monitor the labeling process independently from the quality of the starting RNA samples. Anticipated relative signal strength follows the order of *lys < phe < thr< dap*. The **Poly-A RNA Control Stock** and **Poly-A Control Dil Buffer** are provided with the kit to prepare the appropriate serial dilutions based on the table below.

Starting Amount		Serial Dilutions			Spike-in Volume
Total RNA	mRNA	First	Second	Third	
1 µg		1:20	1:50	1:50	2 µL
5 µg		1:20	1:50	1:10	2 µL
10 µg	0.2 µg	1:20	1:50	1:5	2 µL

This is a guideline when 1, 5, or 10 µg of total RNA or 0.2 µg of mRNA is used as starting material. For starting sample amounts other than those listed here, calculations are needed in order to perform the appropriate dilutions to arrive at the same proportionate final dilution of the spike-in controls in the samples.

For example, to prepare the poly-A RNA dilutions for 5 µg of total RNA:

1. Add 2 µL of the **Poly-A Control Stock** to 38 µL of **Poly-A Control Dil Buffer** for the First Dilution (1:20).

2. Mix thoroughly and spin down to collect the liquid at the bottom of the tube.

3. Add 2 µL of the First Dilution to 98 µL of **Poly-A Control Dil Buffer** to prepare the Second Dilution (1:50).

4. Mix thoroughly and spin down to collect the liquid at the bottom of the tube.

5. Add 2 µL of the Second Dilution to 18 µL of **Poly-A Control Dil Buffer** to prepare the Third Dilution (1:10).

6. Mix thoroughly and spin down to collect the liquid at the bottom of the tube.

7. Add 2 µL of this Third Dilution to 5 µg of sample total RNA.

The First Dilution of the poly-A RNA controls can be stored up to six weeks in a non-frost-free freezer at –20°C and frozen-thawed up to eight times.

STEP 2: FIRST-STRAND cDNA SYNTHESIS

One-Cycle cDNA Synthesis Kit (Affymetrxix 900431) is used for this step.

a. Briefly spin down all tubes in the Kit before using the reagents.

b. Perform all of the incubations in thermal cyclers. The following program can be used as a reference to perform the first-strand cDNA synthesis reaction in a thermal cycler; the 4°C holds are for reagent addition steps:

70°C 10 minutes

4°C hold

42°C 2 minutes

42°C 1 hour

4°C hold

1. Mix RNA sample, diluted poly-A RNA controls, and T7-Oligo(dT) Primer.

RNA/T7-Oligo(dT) Primer Mix Preparation for 1 to 8 µg of total RNA, or 0.2 to 1 µg of mRNA is presented in the following table:

Component	Volume
Sample RNA	variable
Diluted poly-A RNA controls	2 µL
T7-Oligo(dT) Primer, 50 µM	2 µL
RNase-free Water	variable
Total Volume	12 µL

A. Place total RNA (1 µg to 15 µg) or mRNA sample (0.2 µg to 2 µg) in a 0.2 mL PCR tube.

B. Add 2 µL of the appropriately diluted poly-A RNA controls

(See *Step 1: Preparation of Poly-A RNA Controls for One-Cycle cDNA Synthesis (Spike-in Controls)*.

C. Add 2 µL of 50 µM T7-Oligo(dT) Primer.

D. Add **RNase-free Water** to a final volume of 12 µL.

E. Gently flick the tube a few times to mix, and then centrifuge briefly (~5 seconds) to collect the reaction at the bottom of the tube.

F. Incubate the reaction for 10 minutes at 70°C.

G. Cool the sample at 4°C for at least 2 minutes.

H. Centrifuge the tube briefly (~5 seconds) to collect the sample at the bottom of the tube.

2. In a separate tube, assemble the First-Strand Master Mix.

A. Prepare sufficient **First-Strand Master Mix** for all of the RNA samples. When there are more than 2 samples, it is prudent to include additional material to compensate for potential pipetting inaccuracy or solution lost during the process. The following recipe, in the Table, is for a single reaction:

Preparation of First-Strand Master Mix

Component	Volume
5X 1st Strand Reaction Mix	4 µL
DTT, 0.1M	2 µL
dNTP, 10 mM	1 µL
Total Volume	7 µL

B. Mix well by flicking the tube a few times. Centrifuge briefly (~5 seconds) to collect the master mix at the bottom of the tube.

3. Transfer 7 µL of **First-Strand Master Mix** to each RNA/T7-Oligo(dT) Primer mix for a final volume of 18 or 19 µL. Mix thoroughly by flicking the tube a few times. Centrifuge briefly (~5 seconds) to collect the reaction at the bottom of the tube, and immediately place the tubes at 42°C.

4. Incubate for 2 minutes at 42°C.

5. Add the appropriate amount of **SuperScript II** to each RNA sample for a final volume of 20 µL.

• For 1 to 8 µg of total RNA: 1 µL **SuperScript II**

• For 8.1 to 15 µg of total RNA: 2 µL **SuperScript II**

• For every µg of mRNA add 1 µL **SuperScript II**.

• For mRNA quantity less than 1 µg, use 1 µL **SuperScript II**.

Mix thoroughly by flicking the tube a few times. Centrifuge briefly (~5 seconds) to collect the reaction at the bottom of the tube, and immediately place the tubes at 42°C.

6. Incubate for 1 hour at 42°C; then cool the sample for at least 2 minutes at 4°C.

After incubation at 4°C, centrifuge the tube briefly (~5 seconds) to collect the reaction at the bottom of the tube and immediately proceed to *Step 3: Second-Strand cDNA Synthesis*.

STEP 3: SECOND-STRAND cDNA SYNTHESIS

One-Cycle cDNA Synthesis Kit (Affymetrxix 900431) is used for this step.

The following program can be used as a reference to perform the second-strand cDNA synthesis reaction in a thermal cycler.

16°C 2 hours

4°C hold

16°C 5 minutes

4°C hold

1. In a separate tube, assemble Second-Strand Master Mix (prepare immediately before use).

A. Prepare sufficient Second-Strand Master Mix for all of the samples. When there are more than 2 samples, it is prudent to include additional material to compensate for potential pipetting inaccuracy or solution lost during the process. The following recipe, in the table, is for a single reaction.

Preparation of Second-Strand Master Mix

Component	Volume
RNase-free Water	91 µL
5X 2nd Strand Reaction Mix	30 µL
dNTP, 10 mM	3 µL
E. coli DNA ligase	1 µL
E. coli DNA Polymerase I	4 µL
RNase H	1 µL
Total Volume	130 µL

B. Mix well by gently flicking the tube a few times. Centrifuge briefly (~5 seconds) to collect the solution at the bottom of the tube.

2. Add 130 µL of Second-Strand Master Mix to each first-strand synthesis sample from *Step 2: First-Strand cDNA Synthesis* for a total volume of 150 µL. Gently flick the tube a few times to mix, and then centrifuge briefly (~5 seconds) to collect the reaction at the bottom of the tube.

3. Incubate for 2 hours at 16°C.

4. Add 2 µL of **T4 DNA Polymerase** to each sample and incubate for 5 minutes at 16°C.

5. After incubation with T4 DNA Polymerase add 10 µL of EDTA, 0.5M and proceed to *Cleanup of Double-Stranded cDNA*. Do not leave the reactions at 4°C for long periods of time.

Cleanup of Double-Stranded cDNA

Sample Cleanup Module (Affymetrix 900371) is used for cleaning up the double-stranded cDNA.

1. Add 600 μL of **cDNA Binding Buffer** to the double-stranded cDNA synthesis preparation. Mix by vortexing for 3 seconds.

2. Check that the color of the mixture is yellow (similar to cDNA Binding Buffer without the cDNA synthesis reaction).

3. Apply 500 μL of the sample to the **cDNA Cleanup Spin Column** sitting in a **2 mL Collection Tube** (supplied), and centrifuge for 1 minute at ≥ 8,000 x g (≥ 10,000 rpm). Discard flow-through.

4. Reload the spin column with the remaining mixture and centrifuge as above. Discard flow-through and Collection Tube.

5. Transfer spin column into a new 2 mL Collection Tube (supplied). Pipet 750 μL of the **cDNA Wash Buffer** onto the spin column. Centrifuge for 1 minute at ≥ 8,000 x g (≥ 10,000 rpm). Discard flow-through.

6. Open the cap of the spin column and centrifuge for 5 minutes at maximum speed (≤ 25,000 x g). Discard flow-through and Collection Tube. Place columns into the centrifuge using every second bucket. Position caps over the adjoining bucket so that they are oriented in the opposite direction to the rotation. Centrifugation with open caps allows complete drying of the membrane.

7. Transfer spin column into a 1.5 mL Collection Tube, and pipet 14 μL of **cDNA Elution Buffer** directly onto the spin column membrane. Incubate for 1 minute at RT and centrifuge 1 minute at maximum speed (≤ 25,000 x g) to elute. Ensure that the cDNA Elution Buffer is dispensed directly onto the membrane. The average volume of eluate is 12 μL recovered from the 14 μL of Elution Buffer.

8. After cleanup, please proceed to *Synthesis of Biotin-Labeled cRNA for One-Cycle Target Labeling Assay*

iv) Synthesis of Biotin-Labeled cRNA for One-Cycle Target Labeling Assay

GeneChip IVT Labeling Kit (Affymetrix 900449) is used for this step.

1. Use the following table to determine the amount of cDNA used for each IVT reaction following the cDNA cleanup step.

IVT Reaction Set Up

Starting Material	Volume of cDNA to use in IVT
Total RNA	
10 to 100 ng	all (~12 μL)
1.0 to 8.0 μg	all (~12 μL)
8.1 to 15 μg	6 μL

2. Transfer the needed amount of template cDNA to RNase-free microfuge tubes and add the following reaction components in the order indicated in the table below. If more than one IVT reaction is to be performed, a master mix can be prepared by multiplying the reagent volumes by the number of reactions. Do not assemble the reaction on ice, since spermidine in the **10X IVT Labeling Buffer** can lead to precipitation of the template cDNA.

Component	Volume
Template cDNA*	variable (see Table 2.17)
RNase-free Water	variable (to give a final reaction volume of 40 μL)
10X IVT Labeling Buffer	4 μL
IVT Labeling NTP Mix	12 μL
IVT Labeling Enzyme Mix	4 μL
Total Volume	40 μL

3. Carefully mix the reagents and collect the mixture at the bottom of the tube by brief (~5 seconds) microcentrifugation.

4. Incubate at 37°C for 16 hours. To prevent condensation that may result from water bath-style incubators, incubations are best performed in oven incubators for even temperature distribution, or in a thermal cycler.

5. Store labeled cRNA at –20°C, or –70°C if not purifying immediately. Alternatively, proceed to *Cleanup and Quantification of Biotin-Labeled cRNA.*

v) Cleanup and Quantification of Biotin-Labeled cRNA
STEP1: CLEANUP OF BIOTIN-LABELED cRNA
Sample Cleanup Module (Affymetrix 900371) is used for cleaning up the biotinlabeled cRNA.

1. Add 60 μL of **RNase-free Water** to the IVT reaction and mix by vortexing for 3 seconds.

2. Add 350 μL **IVT cRNA Binding Buffer** to the sample and mix by vortexing for 3 seconds.

3. Add 250 μL ethanol (96-100%) to the mixture, and mix well by pipetting. Do not centrifuge.

4. Apply sample (700 μL) to the IVT **cRNA Cleanup Spin Column** sitting in a **2 mL Collection Tube**. Centrifuge for 15 seconds at ≥ 8,000 x g (≥ 10,000 rpm). Discard flow-through and Collection Tube.

5. Transfer the spin column into a new **2 mL Collection Tube** (supplied). Pipet 500 μL **IVT cRNA Wash Buffer** onto the spin column. Centrifuge for 15 seconds at ≥ 8,000 x g (≥ 10,000 rpm) to wash. Discard flow-through.

6. Pipet 500 μL 80% (v/v) ethanol onto the spin column and centrifuge for 15 seconds at ≥ 8,000 x g (≥ 10,000 rpm). Discard flow-through.

7. Open the cap of the spin column and centrifuge for 5 minutes at maximum speed (≤ 25,000 x g). Discard flow-through and Collection Tube.

8. Transfer spin column into a new **1.5 mL Collection Tube** (supplied), and pipet 11μL of **RNase-free Water** directly onto the spin column membrane. Ensure that the water is dispensed directly onto the membrane. Centrifuge 1 minute at maximum speed (≤ 25,000 x g) to elute.

9. Pipet 10 μL of **RNase-free Water** directly onto the spin column membrane. Ensure that the water is dispensed directly onto the membrane. Centrifuge 1 minute at maximum speed (≤ 25,000 x g) to elute.

10. For subsequent photometric quantification of the purified cRNA, we recommend dilution of the eluate between 1:100 fold and 1:200 fold.

11. Store cRNA at –20°C, or –70°C if not quantitated immediately. Alternatively, proceed to *Step 2: Quantification of the cRNA*.

STEP 2: QUANTIFICATION OF THE cRNA

Use spectrophotometric analysis to determine the cRNA yield. Apply the convention that 1 absorbance unit at 260 nm equals 40 μg/mL RNA.

• Check the absorbance at 260 nm and 280 nm to determine sample concentration and purity.

• Maintain the A260/A280 ratio close to 2.0 for pure RNA (ratios between 1.9 and 2.1 are acceptable).

For quantification of cRNA when using total RNA as starting material, an adjusted cRNA yield must be calculated to reflect carryover of unlabeled total RNA. Using an

estimate of 100% carryover, use the formula below to determine adjusted cRNA yield:

adjusted cRNA yield = RNAm - (total RNAi) (y)

RNAm = amount of cRNA measured after IVT (µg)

total RNAi = starting amount of total RNA (µg)

y = fraction of cDNA reaction used in IVT

Example: Starting with 10 µg total RNA, 50% of the cDNA reaction is added to the IVT, giving a yield of 50 µg cRNA. Therefore, adjusted cRNA yield = 50 µg cRNA - (10 µg total RNA) (0.5 cDNA reaction) = 45.0 µg.

Use adjusted yield in *Fragmenting the cRNA for Target Preparation.*

vi) Fragmenting the cRNA for Target Preparation

Sample Cleanup Module (Affymetrix 900371) is used for this step.

Fragmentation of cRNA target before hybridization onto GeneChip probe arrays has been shown to be critical in obtaining optimal assay sensitivity. The cRNA used in the fragmentation procedure must be sufficiently concentrated to maintain a small volume during the procedure. This will minimize the amount of magnesium in the final hybridization cocktail. Fragment an appropriate amount of cRNA for hybridization cocktail preparation and gel analysis.

1. The Fragmentation Buffer has been optimized to break down fulllength cRNA to 35 to 200 base fragments by metal-induced hydrolysis. The following table shows suggested fragmentation reaction mix for cRNA samples at a final concentration of 0.5 µg/µL. Use adjusted cRNA concentration, as described in *Step 2: Quantification of the cRNA*. The total volume of the reaction may be scaled up or down dependent on the amount of cRNA to be fragmented.

Component	169 Format
cRNA	7,5µg
5X fragmentation buffer	3µl
RNAse-free water	to 15µl final volume
Total volume	30µl

2. Incubate at 94°C for 35 minutes. Put on ice following the incubation.

3. Store undiluted, fragmented sample cRNA at –20°C (or –70°C for longer-term storage) until ready to perform the hybridization.

vii) Eukaryotic target hybridization

Materials needed are GeneChip Hybridization, Wash and Stain kit (Affymetrix 900720), GeneChip Eukaryotic Hybridization control kit (Affymetrix 900457), control oligo B2 (contained in Affymetrix 900457 or 900301).

Refer to the table below for the necessary amount of cRNA required for the specific probe array format used. These preparations take into account that it is necessary to make extra hybridization cocktail due to a small loss of volume (10-20 µL) during each hybridization.

1. Mix the following for each target, scaling up volumes if necessary for hybridization to multiple probe arrays.

Component	169 Format (Mini) Array /400 Format (Micro) Array	Final Dilution
Fragmented and Labeled cRNA†	5 µg	0.05 µg/µL
Control Oligonucleotide B2 (3 nM)	1.7 µL	50 pM
20X Eukaryotic Hybridization Controls (*bioB, bioC, bioD, cre*)	5 µL	1.5, 5, 25, and 100 pM respectively
2X Hybridization Mix	50 µL	1X
DMSO	10 µL	10%
Nuclease-free Water	to final volume of 100 µL	
Total Volume	100 µL	

2. Equilibrate probe array to room temperature immediately before use.

3. Heat the hybridization cocktail to 99°C for 5 minutes in a heat block.

4. Meanwhile, wet the array with an appropriate volume of Pre- Hybridization Mix (80µl for our array) by filling it through one of the septa.

5. Incubate the probe array filled with Pre-Hybridization Mix at 45°C for 10 minutes with rotation.

6. Transfer the hybridization cocktail that has been heated at 99°C, in step 3, to a 45°C heat block for 5 minutes.

7. Spin the hybridization cocktail at maximum speed in a microcentrifuge for 5 minutes to collect any insoluble material from the hybridization mixture.

8. Remove the array from the hybridization oven. Vent the array with a clean pipette tip and extract the Pre-Hybridization Mix from the array with a micropipettor. Refill the array with the appropriate volume of the clarified hybridization cocktail, avoiding any insoluble matter at the bottom of the tube.

9. Place probe array into the hybridization oven, set to 45°C.

10. To avoid stress to the motor, load probe arrays in a balanced configuration around the axis. Rotate at 60 rpm.

11. Hybridize for 16 hours. During the latter part of the 16-hour hybridization, proceed to wash and staining steps immediately after completion of hybridization.

Washing, Staining and Scanning are being performed by our technician (George Papayannakis. From the scanning, we obtain a CEL file that contains the intensity values of the hybridization of our material to the slide in a raw form.

viii) ANALYSIS OF THE RESULTS

The intensity values were calculated by the use of Affymetrix Expression Console Software as well as other commercial software such as FlexArray using RMA algorithm to normalize our data (Irizarry et al., 2003). For each of the 2 couples of experiments (*rad9Δ* vs FT5 and the biological replicate) we have delogged the values in order to get the raw intensity values of the replicate experiments. We then calculated the average value of the replicates and obtained the exact fold ratios (*rad9Δ*/WT). We performed a t-test analysis (two sample equal variance-homoscedastic) to obtain a p-value for our results. This value determines the possibility of the two samples to have come from the same two underlying populations that have the same mean. We sorted our results depending on the fold change ($-1.2 \leq X \leq 1.2$) and the p-value obtained from the t-test ($X \leq 0.05$). The replicates had over 99% similarity in the intensity values measured. Functional analysis of the results was performed by using BiNGO plugin in Cytoscape platform as described in the ChIP on chip protocol.

2.13. EXPRESSION MICROARRAY (2 DYES)

This type of DNA microarray slides were manufactured by the Genomics Laboratory of Frank Holstege in Utrecht (http://www.microarrays.med.uu.nl/home/index.php). The microarray slide contains 6357 genes of *S. cerevisiae,* in duplicates, as well as 2838 control DNAs used to estimate the quality of the hybridization and to determine the noise level during normalization (http://www.microarrays.med.uu.nl/microarrays/yeast.htm).

244

1. Total RNA isolation from yeast cells

RNA was isolated by following the hot acid phenol RNA extraction protocol (see Expression microarray-Affymetrix Platform protocol)

2. DNase treatment

This step ensures the complete remove of the genomic DNA that might have remained in our sample during total RNA isolation (see Expression microarray-Affymetrix Platform protocol).

3. Reverse Transcription – First strand

Materials

OligoT primer, 5' MC-T7-(dT)24V 3', 65mer (100 ng/µl)

 5X First Strand Buffer (Superscipt)

0.1 M DTT

dNTPs (10 mM each)

Superscript III 200u/µl

- Place on 0.2 ml tube 4 µgr total RNA in final volume 12 µl max
- Add 1/1.5 µl OligoT primer, 5' MC-T7-(dT)24V 3', 65mer (100 ng/µl)
- Adjust volume to 13 µl with DEPC water (if necessary)
- Incubate at $70^{o}C$ for 10 min (denaturizing)
- Place on ice for 1-2 min and do quick spin if there are vapors on the walls of the tube.
- Add 7 µl mix: 4 µl 5x First strand buffer

    1 µl 0.1 M DTT

    1 µl dNTPs (10 mM each)

    1 µl Reverse Transcriptase (Superscript III 200u/µl)
- Incubate: 20 min at $44^{o}C$

  1 h and 45 min at $50^{o}C$

  15 min at $75^{o}C$ (superscript III inactivation)
- Proceed directly to the second strand cDNA synthesis (Step 4)

4. Second strand cDNA synthesis

Reaction (100 µl final volume)

  20 µl reverse transcription reaction (If less than 20, add DEPC-water)

    Reaction mix (prepared on **ice**)

  55 µl DEPC water (on **ice**)

  20 µl 5X second strand buffer

1.5 µl dNTPs (10 mM each)

2 µl DNA pol I (10 u /µl)

1 µl RNase H (2 u/µl)

0.5 µl E.coli DNA ligase (10 u/µl)

- Incubation at 16°C for 2 hours
- Addition of 1.5 µl T4 polymerase (3 u/ µl)
- Incubation at 16°C for 15 min
- Storage at -20°C or cDNA purification

The addition of DNA ligase and T4 polymerase is not necessary, as their absence does not affect either the final quantity, or the quality of amplified RNA that is produced.

5. cDNA purification

- Add DEPC water till volume 200 µl
- Add 200 µl PhOH/CH$_3$Cl, mix, centrifuge at 12.000 rpm for 5 min, transfer aquatic phase to a clean tube
- Add 200 µl CH$_3$Cl, mix, centrifuge at 12.000 rpm for 5 min, transfer aquatic phase to a clean tube
- Centrifuge again at 12.000 rpm for 5 min and remove organic phase (if there is some)
- Add: 100 µl 7,5 M ammonium acetate

    1 µl glycogen (20 µg/µl)

  400 µl isopropanol

- Mix well and incubate for 10 min at room temperature
- Centrifuge at 12.000 rpm for 20 min
- Discard supernatant and wash the pellet with 75% EtOH
- Centrifuge at 13000 rpm for 5 min and remove EtOH
- Dry the pellet on air
- Re-suspend in 7,25 µl DEPC water
- Storage at -20°C or proceed to in vitro transcription

6.1 In vitro transcription

NOT in 1.5ml tubes (significant evaporation for >10h)

Reaction (20 µl final volume)

7,25 µl cDNA

2 µl 10x T7 buffer

1,5 μl ATP (100 mM)

1,5 μl GTP (100 mM)

1,5 μl CTP (100 mM)

0,75 μl UTP (100 mM)

1,5 μl aaUTP (50 mM)

2 μl 0.1 M DTT

2 μl T7 polymerase (not in the mix)

- Resuspend the precipitate obtained after the cDNA purification in 18μl reaction mix, add the 2 μl T7 polymerase.
- Incubation at $42^{o}C$ (or $37^{0}C$) for 6 hours
- Purification of aaRNA with RNeasy mini kit, quantification and electrophoresis in agarose gel.

The quantity of amplified RNA that is produced with this protocol is usually about 15 μgr (initial total RNA is included).

6.2 Cleanup of IVT RNA with RNeasy columns

All steps, including centrifugations, should be performed at RT (room temperature).

1. Take the appropriate volume of buffer **RLT** (**0.35 ml** for each IVT). If a precipitate is formed, redissolve by warming ($37\ ^{o}C$) and place at RT. Add before use **β-mercaptoethanol** (10μl per ml of RLT buffer)

2. Adjust sample to 100μl with DEPC-treated water. Add 350 μl of buffer **RLT** (with β-ME) and mix thoroughly.

3. Prepare the RNeasy column placed in a 2ml collection tube (kit). Mark the top of the column, but not the side, as it may be washed by ethanol. Then add 250 μl absolute **ethanol** to the sample and mix well by pipetting. Do not centrifuge, as the nucleic acids are in a semi-precipitated state.

4. Apply the sample (700 μl), included any formed precipitate, to an RNeasy mini column. Close the tube gently. Centrifuge for 15 sec at full speed. Pass the flow-through through the column one more time and discard the flow-through and the collection tube.

5. Transfer the RNeasy column into a new 2 ml clooection tube (kit). Pipet 500μl buffer **RPE** (with ethanol) onto the RNeasy column. Close the tube and centrifuge for 15 sec full speed. Discard the flow-through, but reuse the collection tube.

6. Add another 500μl buffer **RPE** (with ethanol) onto the RNeasy column. Close the tube and centrifuge for 2min full speed. Discard flow-through and collection tube.

7. Recentrifuge in a 1.5ml tube (not in kit) for 1 min. Discard flow-through and collection tube. Put column in an RNase-free 1.5ml tube (kit). Mark the top of the tube.

8. Apply 40 μl **RNASE-FREE water** (kit) in the column and incubate at RT for 2mins. Elute by spinning at full speed for 1 min. Repeat elution with another 40 μl RNASE-FREE water. Put tube on **ice**. Don't discard the column till after the quantitation.

7. Labeling of mRNA

(We do the whole process in dark, at room temperature)

We use 6μg RNA and we add 15μl SIC RNA (*B.subtilis* spiked-in controls)

Reaction (20 μl final volume)

8 μl aaRNA (6 μg RNA+SIC). If the volume is less than 8 μl we adjust it with DEPC water

2 μl 0,5 M sodium bicarbonate pH 9

10 μl DMSO

We warm the mix at 50^0C for 5'.

- Transfer the above 20 μl of our sample to the dry dye pellet (Alexa 555 or Alexa 647) and re-suspend via pipeting. DO NOT spin.
- Incubate for 2-2,5 hours in dark, at room temperature
- Raise the volume to 25μl with water.
- Clean up labeled RNA with G50 column. Repeat the cleaning and raise volume to 40μl with water.
- Measure absorbance and calculate dye incorporation.

Dye incorporation is usually 1 molecule dye per 40 bases (40 base/dye). For hybridization, 3 μgr of labeled RNA with a ratio base/dye 40 are enough to give a satisfactory signal.

8. Fragmentation and mRNA hybridization

Before the hybridisation, we perform priming of the hybridisation machine for 1hr 30mins with %X SSC, 0.1% SDS.

From the ~40μl of our sample, we collect 2.5μg in final volume of 18μl and we add 2μl fragmentation buffer. Incubate at 70^0C for 15mins. Then add 2μl STOP buffer. For one hybridization we add 1.5μl salmon sperm, 85.5μl hybridization buffer (50%

formamide, 5X SSC, 0.1% SDS) and 25.5μl RNA. After sonic bath, we hybridise the samples on the slides for 16hrs in 42^0C. The scanning of the slides were performed in Scan Array 5000 (GSI Luminomics).

9. ANALYSIS

Arrays were read with a ScanArray 5000 scanner (GSI Lumonics) at 5 nm resolution at three different photomultiplier tube voltage settings (high-S01, medium-S02 and low-S03) to improve the dynamic range of data and also account for low intensity and saturation effects. The fluorescence intensity for each fluorophore and each element on the array was captured using ImaGene 5 (Biodiscovery) and features were manually flagged. A single intensity value was computed from the 3 different settings as described in (Dudley et al., 2002) with the following modifications: The linear regression was performed on the log2-transformed spot values. If more than one setting had values in the linear range of the scanner, then the average of the intensities was computed. Weighted print-tip loess normalization was performed using package limma version "2.10.0" in R version 2.5.0 (www.R-project.org), giving a weight of 2 for the buffer elements. The differentially-expressed genes were computed after fitting a linear model (Smyth, 2005; Smyth et al., 2005) using a statistical cut-off of 5% FDR-adjusted p-value and a 2-fold change. For the significant genes visualization MultiExperiment Viewer software was used. Functional analysis of the results was performed by using BiNGO plugin in Cytoscape platform as described in the ChIP on chip protocol.

PROTEINS

1P. WESTERN BLOT ANALYSIS

i) Protein extraction

We used two protocols for protein extraction:

a) <u>Protein precipitation with TCA</u>: Put an overnight starter culture of the desired strain, the next day dilute in OD_{550}~0.2 and incubate shaking at 30^0C until OD~0.8-1. Harvest 2ml of the cells by centrifugation for 5mins, at 13000rpm, RT, discard supernatant and resuspend in 1ml ice-cool water (repeat twice). Add in the tube 150μl 1.85M NaOH and 7.5% β-mercaptoethanol and leave on ice for 10mins. Add 150μl TCA 55% and leave at least 10mins on ice. Centrifuge for 10mins, 13000rpm in RT, discard supernatant, repeat the centrifugation once until all the supernatant is discarded. Resuspend in ~50μl 5X Protein Loading Buffer.

b) <u>Rapid prep</u>: Put an overnight culture of the desired strain. The next day, quantify the OD_{550} of the culture and pellet ~$4x10^7$ cells. Resuspend the pellet in 100μl H_2O and add 100μl 0.2N NaOH. Incubate for 5mins at RT and centrifuge for 2mins at 13000rpm. Resuspend the pellet in 50μl 1X Loading Buffer, boil for 3mins, spin at 13000rpm for 2mins, RT and load on SDS-PAGE gel.

ii) SDS-PAGE gel electrophoresis

SDS-PAGE electrophoresis is performed for protein analysis (antibody characterization, co-IP, protein characterization and quantification etc). SDS gel is made according to Sambrook et al. (1989) protocol and is of different acrylamide concentration depending on the size of the protein of interest. The gel is discontinuous and consists of two parts: the running gel (where the proteins are analysed according to their size) and the stacking gel (which is used so that all the proteins enter simultaneously in the running gel. The basic difference between the two parts is the pH which is 8.8 in running gel and 6.8 in stacking gel.

	Running (6%) 10ml	Stacking (5%) 5ml
H_2O	5.3ml	3.4ml
30% acrylamide mix	2ml	830μl
1.5M Tris	2.5ml (pH=8.8)	630μl (pH=6.8)
10% SDS	100μl	50μl
10% APS	100μl	50μl
TEMED	8μl	5μl

If you want to analyse phosphorylated forms of proteins, use acrylamide:BIS solution in a ratio 80:1.

<u>Materials</u>

Loading buffer 5X (50% glycerol; 1% SDS; 0.3M Tris pH=6.8; 1% β-mercaptoethanol; 0.002% bromophenol blue)

Loading buffer 1X-rapid prep (5% glycerol; 2% SDS; 0.06M Tris pH=6.8; 4% β-mercaptoethanol; 0.002% bromophenol blue)

Coomassie staining buffer (40% methanol; 10% acetic acid; 0.25% Coomassie Brilliant blue-R250)

Coomassie destaining buffer (10% methanol; 10% acetic acid)

5X Tris/Glycine (0.125M Tris; 0.776M Glycine or 15.1gr Tris, 94gr Glycine for 1l)

Running buffer (20% 5X Tris/Glycine; 0.1% SDS)

Transfer buffer (20% 5X Tris/Glycine; 20% methanol)

Whatman Protran Nitrocellulose Membrane BA83 (0.2μM pore size)

Ponceau Sigma P7767 (0.2% Ponceau S in 3% w/o TCA)

TBS-Tween (0.02M Tris pH 7.5; 0.09M NaCl; 0.05% Tween)

After running the proteins on SDS acrylamide gel in Running buffer, transfer the proteins to the membrane overnight at 110mA, 4^0C constructing a blot with the gel attached to the membrane covered by 3 Whatman papers from each side. The next day, dye the membrane with Ponceau to ensure of the good transfer of the proteins, wash with TBS-Tween twice for 5mins shaking and block the non specific sites for the antibody by incubate the membrane in RT for 1hr with 5% milk. Depending on the experiment, incubate the membrane with the proper antibody concentration in 1% milk (rotating 2-3hrs in RT or overnight at 4^0C). Wash the membrane by TBS-Tween (3 times, 10mins each, RT, shaking). Add in 1% milk the secondary antibody in the proper concentration and incubate shaking for 1hr. Wash the membrane by TBS-Tween (3 times, 10mins each, RT, shaking). Use the SuperSignal West Pico Chemiluminescent Substrate kit (Thermo Scientific; 34077) following the manufacturer's instructions and detect the secondary antibody with LAS-3000 Intelligent Dark Box. The membrane can be probed with another antibody after removing the first one by incubating for 20mins rotating in 50^0C in a buffer containing 2% SDS; 62.5mM Tris pH 6.8; 100mM β-mercaptoethanol.

2P. CO-IMMUNOPRECIPITATION

We used the following co-immunoprecipitation protocol in order to detect *in vivo* interactions between proteins with different tags.

1) Starter cultures of the strains that we want to check for the interaction. Usually there is a strain that has 2 different proteins (A and B) tagged with different epitopes, the interaction of which we want to check. Furthermore, we there are the negative and positive (if available) controls.

2) The next day dilute the starter culture in 200ml medium to an OD_{550}~0.1 and we incubate at 30^0C shaking until OD_{550}~0.8.

3) Collect equal number of cells from each culture by centrifugation (3000rpm, 5mins, 4^0C) and wash twice with water. Pellets can be kept at -80^0C.

4) The next day resuspend the pellets in 1ml Buffer A and transfer sample to a 2ml tube. Spin the tube and remove supernatant. Resuspend the pellet in such volume of Buffer A until the V_f~400μl (cells and buffer). Add proteinase "complete EDTA free" inhibitor cocktail (Roche) in 1X final concentration and PMSF in a finam concentration of 1mM.

5) Add 350μl glass beads (quantity equal to ~80-90% of the final volume).

6) Vortex 8 times, 30secs each, and rest at least 30secs between the repeats. Finally, leave the tubes on ice until glass beads are precipitated due to gravity. Collect supernatant in a new 1.5ml tube.

7) Add 200μl Buffer A in the remaining glass beads along with Proteinase inhibitor cocktail and PMSF, vortex once, leave the beads to precipitate due to gravity, collect the supernatant and combine with the supernatant from step 6.

8) Centrifuge extract at 4^0C for 15mins at 13000rpm and transfer supernatant in new eppendorf.

9) Keep 30μl of every sample to use later as an INPUT for the quantification of the loading on the gel (1/13-1/18 of the volume depending on the abundance of the protein).

10) In the rest of the sample add the first antibody (2μg) which will recognize and bind to one of the proteins. Leave the samples rotating at 4^0C overnight.

11) The next day spin the tubes for 1min at 13000rpm (in case of any precipitant) and collect samples to a new 1.5ml tube. Add 20-30μl packed G sepharose beads which have been equilibrated with Buffer B. Equilibration is done by adding 1ml Buffer B in the beads, spin 1min at 3000rpm and remove supernatant; repeat 3 times; add 20-30μl Buffer B, resuspend and add to the samples. Leave rotating at 4^0C for 2.5hrs. The beads recognize the stable domain of the antibody which is bound to the tagged protein and the proteins which may are also present, will be isolated as a complex.

12) Spin the samples 1min at 3000rpm and discard supernatant.

13) Wash samples 4 times. The first 2 are done by 1ml Wash Buffer I and the second 2 with 1ml Buffer II. More specifically, add to the sample 1ml from the Wash Buffer along with PMSF (C_f=1mM), rotate 5mins in RT, spin 1min at 3000rpm and discard supernatant.

14) Resuspend G sepharose beads in 5X protein Loading Buffer (see Western protocol). Adjust the volume so that it will not exceed 35μl (i.e. leave ~28μl of Wash II and add ~7μl of 5X protein Loading Buffer).

15) Boil the samples for 5 mins, spin and run in SDS gel the whole volume of IPs and INPUTs. A typical Western experiment follows (see Western protocol). We probe the membrane with the antibody which recognizes the other protein to see if there is an interaction.

Materials

Solution 1 (100mM Hepes-KOH pH=7.5; 10mM MgAc; 200mM KAc; 0.2% NP40; 20% glycerol)

Buffer A (1/2V Solution 1; DTT 1mM; BSA 0.5mg/ml; H_2O until 1V)

Buffer B (1/2V Solution 1; DTT 1mM; H_2O until 1V)

Wash I (1/2V Solution 1; DTT 1mM; H_2O until 1V)

Wash II: as Wash I but contains 150mM KAc instead of 100mM

3P. QUANTIFICATION OF β-GALACTOSIDASE ACTIVITY IN TRANSFORMED CELLS

5ml cultures of yeast cells transformed with the proper plasmids (which express Lac-Z) were grown in liquid medium (SC) until OD_{550}~0.8-1. The measurement of the β-galactosidase activity was performed as described by Ausubel (1987-2011). The plasmids transformed in FT yeast cells were the combination of i) pACTII+pGBT9,

ii)   pACTII-Mac1+pGBT9,   iii)   pACTII-Mac1+pGBT9-Mac1   and   iv) pACTII+pGBT9-Mac1. Sequence and information of the plasmids available in the vector database www.lablife.org/.

4P. YEAST ONE-HYBRID ASSAY

One hybrid assay was used to measure the transactivation capability of Mac1 under certain growth conditions (see results). The method was executed as described by Gietz Lab (http://www.umanitoba.ca/faculties/medicine/biochem/gietz/).

5P. 6-AZAURACIL (6-AU) AND ZEOCIN GROWTH ASSAY

Cultures of the certain mutants were grown in rich medium (YPD) until exponential phase (OD_{550}~0.5). All cultures were adjusted to the same optical density and 6-AU (Sigma A1757) was added to a final concentration of 300μg/ml and incubation continued for 30 minutes (or zeocin was added to a final concentration of 150μg/ml and incubation continued for 2hrs). Untreated cells were also kept as control cultures. After that, eight serial dilutions were spotted on YPD plates which also had or not 300μg/ml 6-AU. Plates were incubated for 2 or more days.

BIBLIOGRAPHY

*Al-Moghrabi, N.M., Al-Sharif, I.S., and Aboussekhra, A. (2003). UV-induced de novo protein synthesis enhances nucleotide excision repair efficiency in a transcription-dependent manner in S. cerevisiae. DNA Repair (Amst) *2*, 1185-1197.

*Al-Moghrabi, N.M., Al-Sharif, I.S., and Aboussekhra, A. (2009). The RAD9-dependent gene trans-activation is required for excision repair of active genes but not for repair of non-transcribed DNA. Mutat Res *663*, 60-68.

*Alpha-Bazin, B., Lorphelin, A., Nozerand, N., Charier, G., Marchetti, C., Berenguer, F., Couprie, J., Gilquin, B., Zinn-Justin, S., and Quemeneur, E. (2005). Boundaries and physical characterization of a new domain shared between mammalian 53BP1 and yeast Rad9 checkpoint proteins. Protein Sci *14*, 1827-1839.

*Anindya, R., Aygun, O., and Svejstrup, J.Q. (2007). Damage-induced ubiquitylation of human RNA polymerase II by the ubiquitin ligase Nedd4, but not Cockayne syndrome proteins or BRCA1. Mol Cell *28*, 386-397.

*AS, I.J., and Greider, C.W. (2003). Short telomeres induce a DNA damage response in Saccharomyces cerevisiae. Mol Biol Cell *14*, 987-1001.

*Ataian, Y., and Krebs, J.E. (2006). Five repair pathways in one context: chromatin modification during DNA repair. Biochem Cell Biol *84*, 490-504.

*Ausubel, F.M. (1987-2011). Current Protocols in Molecular Biology (New York, Greene PublishingAssociates and Wiley -Interscience).

*Azvolinsky, A., Giresi, P.G., Lieb, J.D., and Zakian, V.A. (2009). Highly transcribed RNA polymerase II genes are impediments to replication fork progression in Saccharomyces cerevisiae. Mol Cell *34*, 722-734.

*Baudat, F., and Nicolas, A. (1997). Clustering of meiotic double-strand breaks on yeast chromosome III. Proc Natl Acad Sci U S A *94*, 5213-5218.

*Belotserkovskaya, R., Oh, S., Bondarenko, V.A., Orphanides, G., Studitsky, V.M., and Reinberg, D. (2003). FACT facilitates transcription-dependent nucleosome alteration. Science *301*, 1090-1093.

*Bergerat, A., de Massy, B., Gadelle, D., Varoutas, P.C., Nicolas, A., and Forterre, P. (1997). An atypical topoisomerase II from Archaea with implications for meiotic recombination. Nature *386*, 414-417.

*Bermejo, R., Capra, T., Gonzalez-Huici, V., Fachinetti, D., Cocito, A., Natoli, G., *Katou, Y., Mori, H., Kurokawa, K., Shirahige, K.*, et al.* (2009). Genome-organizing factors Top2 and Hmo1 prevent chromosome fragility at sites of S phase transcription. Cell *138*, 870-884.

*Bernstein, B.E., Liu, C.L., Humphrey, E.L., Perlstein, E.O., and Schreiber, S.L. (2004). Global nucleosome occupancy in yeast. Genome Biol *5*, R62.

*Berthelet, S., Usher, J., Shulist, K., Hamza, A., Maltez, N., Johnston, A., Fong, Y., Harris, L.J., and Baetz, K. (2010). Functional genomics analysis of the Saccharomyces cerevisiae iron responsive transcription factor Aft1 reveals iron-independent functions. Genetics *185*, 1111-1128.

*Blaiseau, P.L., Lesuisse, E., and Camadro, J.M. (2001). Aft2p, a novel iron-regulated transcription activator that modulates, with Aft1p, intracellular iron use and resistance to oxidative stress in yeast. J Biol Chem *276*, 34221-34226.

*Blitzblau, H.G., Bell, G.W., Rodriguez, J., Bell, S.P., and Hochwagen, A. (2007). Mapping of meiotic single-stranded DNA reveals double-stranded-break hotspots near centromeres and telomeres. Curr Biol *17*, 2003-2012.

*Bolstad, B.M., Irizarry, R.A., Astrand, M., and Speed, T.P. (2003). A comparison of normalization methods for high density oligonucleotide array data based on variance and bias. Bioinformatics *19*, 185-193.

*Borde, V., Robine, N., Lin, W., Bonfils, S., Geli, V., and Nicolas, A. (2009). Histone H3 lysine 4 trimethylation marks meiotic recombination initiation sites. Embo J *28*, 99-111.

*Bork, P., Hofmann, K., Bucher, P., Neuwald, A.F., Altschul, S.F., and Koonin, E.V. (1997). A superfamily of conserved domains in DNA damage-responsive cell cycle checkpoint proteins. Faseb J *11*, 68-76.

*Bortvin, A., and Winston, F. (1996). Evidence that Spt6p controls chromatin structure by a direct interaction with histones. Science *272*, 1473-1476.

*Botuyan, M.V., Lee, J., Ward, I.M., Kim, J.E., Thompson, J.R., Chen, J., and Mer, G. (2006). Structural basis for the methylation state-specific recognition of histone H4-K20 by 53BP1 and Crb2 in DNA repair. Cell *127*, 1361-1373.

*Bregman, D.B., Halaban, R., van Gool, A.J., Henning, K.A., Friedberg, E.C., and Warren, S.L. (1996). UV-induced ubiquitination of RNA polymerase II: a novel modification deficient in Cockayne syndrome cells. Proc Natl Acad Sci U S A *93*, 11586-11590.

*Brueckner, F., and Cramer, P. (2008). Structural basis of transcription inhibition by alpha-amanitin and implications for RNA polymerase II translocation. Nat Struct Mol Biol *15*, 811-818.

*Buhler, C., Borde, V., and Lichten, M. (2007). Mapping meiotic single-strand DNA reveals a new landscape of DNA double-strand breaks in Saccharomyces cerevisiae. PLoS Biol *5*, e324.

*Buratowski, S. (2009). Progression through the RNA polymerase II CTD cycle. Mol Cell *36*, 541-546.

*Caspari, T., Murray, J.M., and Carr, A.M. (2002). Cdc2-cyclin B kinase activity links Crb2 and Rqh1-topoisomerase III. Genes Dev *16*, 1195-1208.

*Cha, R.S., and Kleckner, N. (2002). ATR homolog Mec1 promotes fork progression, thus averting breaks in replication slow zones. Science *297*, 602-606.

*Chen, Y., and Sanchez, Y. (2004). Chk1 in the DNA damage response: conserved roles from yeasts to mammals. DNA Repair (Amst) *3*, 1025-1032.

*Clapier, C.R., and Cairns, B.R. (2009). The biology of chromatin remodeling complexes. Annu Rev Biochem *78*, 273-304.

Cline, M.S., Smoot, M., Cerami, E., Kuchinsky, A., Landys, N., Workman, C., Christmas, R., Avila-Campilo, I., Creech, M., Gross, B., et al.* (2007). Integration of biological networks and gene expression data using Cytoscape. Nat Protoc *2*, 2366-2382.

Close, P., Hawkes, N., Cornez, I., Creppe, C., Lambert, C.A., Rogister, B., Siebenlist, U., Merville, M.P., Slaugenhaupt, S.A., Bours, V., et al.* (2006). Transcription impairment and cell migration defects in elongator-depleted cells: implication for familial dysautonomia. Mol Cell *22*, 521-531.

*Conde, F., Refolio, E., Cordon-Preciado, V., Cortes-Ledesma, F., Aragon, L., Aguilera, A., and San-Segundo, P.A. (2009). The Dot1 histone methyltransferase and the Rad9 checkpoint adaptor contribute to cohesin-dependent double-strand break repair by sister chromatid recombination in Saccharomyces cerevisiae. Genetics *182*, 437-446.

*Cook, C.E., Hochstrasser, M., and Kerscher, O. (2009). The SUMO-targeted ubiquitin ligase subunit Slx5 resides in nuclear foci and at sites of DNA breaks. Cell Cycle *8*, 1080-1089.

*Courel, M., Lallet, S., Camadro, J.M., and Blaiseau, P.L. (2005). Direct activation of genes involved in intracellular iron use by the yeast iron-responsive transcription factor Aft2 without its paralog Aft1. Mol Cell Biol *25*, 6760-6771.

*Dancis, A., Klausner, R.D., Hinnebusch, A.G., and Barriocanal, J.G. (1990). Genetic evidence that ferric reductase is required for iron uptake in Saccharomyces cerevisiae. Mol Cell Biol *10*, 2294-2301.

*Dancis, A., Roman, D.G., Anderson, G.J., Hinnebusch, A.G., and Klausner, R.D. (1992). Ferric reductase of Saccharomyces cerevisiae: molecular characterization, role in iron uptake, and transcriptional control by iron. Proc Natl Acad Sci U S A *89*, 3869-3873.

*Daniel, J.A., Pray-Grant, M.G., and Grant, P.A. (2005). Effector proteins for methylated histones: an expanding family. Cell Cycle *4*, 919-926.

De Freitas, J.M., Kim, J.H., Poynton, H., Su, T., Wintz, H., Fox, T., Holman, P., Loguinov, A., Keles, S., van der Laan, M., et al.* (2004). Exploratory and confirmatory gene expression profiling of mac1Delta. J Biol Chem *279*, 4450-4458.

*Dekker, J. (2007). GC- and AT-rich chromatin domains differ in conformation and histone modification status and are differentially modulated by Rpd3p. Genome Biol *8*, R116.

*Deshpande, A.M., and Newlon, C.S. (1992). The ARS consensus sequence is required for chromosomal origin function in Saccharomyces cerevisiae. Mol Cell Biol *12*, 4305-4313.

*Dimitrova, P., Yordanov, M., Danova, S., and Ivanovska, N. (2008). Enhanced resistance against systemic Candida albicans infection in mice treated with C. albicans DNA. FEMS Immunol Med Microbiol *53*, 231-236.

*Dix, D.R., Bridgham, J.T., Broderius, M.A., Byersdorfer, C.A., and Eide, D.J. (1994). The FET4 gene encodes the low affinity Fe(II) transport protein of Saccharomyces cerevisiae. J Biol Chem *269*, 26092-26099.

*Dotiwala, F., Harrison, J.C., Jain, S., Sugawara, N., and Haber, J.E. (2010). Mad2 prolongs DNA damage checkpoint arrest caused by a double-strand break via a centromere-dependent mechanism. Curr Biol *20*, 328-332.

*Downs, J.A., Lowndes, N.F., and Jackson, S.P. (2000). A role for Saccharomyces cerevisiae histone H2A in DNA repair. Nature *408*, 1001-1004.

*Du, L.L., Nakamura, T.M., and Russell, P. (2006). Histone modification-dependent and -independent pathways for recruitment of checkpoint protein Crb2 to double-strand breaks. Genes Dev *20*, 1583-1596.

*Dudley, A.M., Aach, J., Steffen, M.A., and Church, G.M. (2002). Measuring absolute expression with microarrays with a calibrated reference sample and an extended signal intensity range. Proc Natl Acad Sci U S A *99*, 7554-7559.

*Durocher, D., Henckel, J., Fersht, A.R., and Jackson, S.P. (1999). The FHA domain is a modular phosphopeptide recognition motif. Mol Cell *4*, 387-394.

*Egly, J.M., and Coin, F. (2011). A history of TFIIH: two decades of molecular biology on a pivotal transcription/repair factor. DNA Repair (Amst) *10*, 714-721.

*Emili, A. (1998). MEC1-dependent phosphorylation of Rad9p in response to DNA damage. Mol Cell *2*, 183-189.

*Enomoto, S., Glowczewski, L., Lew-Smith, J., and Berman, J.G. (2004). Telomere cap components influence the rate of senescence in telomerase-deficient yeast cells. Mol Cell Biol *24*, 837-845.

*Fasullo, M., Bennett, T., AhChing, P., and Koudelik, J. (1998). The Saccharomyces cerevisiae RAD9 checkpoint reduces the DNA damage-associated stimulation of directed translocations. Mol Cell Biol *18*, 1190-1200.

*Fong, Y.W., Inouye, C., Yamaguchi, T., Cattoglio, C., Grubisic, I., and Tjian, R. (2011). A DNA repair complex functions as an Oct4/Sox2 coactivator in embryonic stem cells. Cell *147*, 120-131.

*Fousteri, M., and Mullenders, L.H. (2008). Transcription-coupled nucleotide excision repair in mammalian cells: molecular mechanisms and biological effects. Cell Res *18*, 73-84.

*Fragiadakis, G.S., Tzamarias, D., and Alexandraki, D. (2004). Nhp6 facilitates Aft1 binding and Ssn6 recruitment, both essential for FRE2 transcriptional activation. Embo J *23*, 333-342.

*Friedberg, E.C., Bardwell, A.J., Bardwell, L., Feaver, W.J., Kornberg, R.D., Svejstrup, J.Q., Tomkinson, A.E., and Wang, Z. (1995). Nucleotide excision repair in the yeast Saccharomyces cerevisiae: its relationship to specialized mitotic recombination and RNA polymerase II basal transcription. Philos Trans R Soc Lond B Biol Sci *347*, 63-68.

*Frit, P., Kwon, K., Coin, F., Auriol, J., Dubaele, S., Salles, B., and Egly, J.M. (2002). Transcriptional activators stimulate DNA repair. Mol Cell *10*, 1391-1401.

*Furuya, K., Poitelea, M., Guo, L., Caspari, T., and Carr, A.M. (2004). Chk1 activation requires Rad9 S/TQ-site phosphorylation to promote association with C-terminal BRCT domains of Rad4TOPBP1. Genes Dev *18*, 1154-1164.

*Georgatsou, E., and Alexandraki, D. (1994). Two distinctly regulated genes are required for ferric reduction, the first step of iron uptake in Saccharomyces cerevisiae. Mol Cell Biol *14*, 3065-3073.

*Georgatsou, E., Mavrogiannis, L.A., Fragiadakis, G.S., and Alexandraki, D. (1997). The yeast Fre1p/Fre2p cupric reductases facilitate copper uptake and are regulated by the copper-modulated Mac1p activator. J Biol Chem *272*, 13786-13792.

*Gerton, J.L., DeRisi, J., Shroff, R., Lichten, M., Brown, P.O., and Petes, T.D. (2000). Global mapping of meiotic recombination hotspots and coldspots in the yeast Saccharomyces cerevisiae. Proc Natl Acad Sci U S A *97*, 11383-11390.

*Ghaemmaghami, S., Huh, W.K., Bower, K., Howson, R.W., Belle, A., Dephoure, N., O'Shea, E.K., and Weissman, J.S. (2003). Global analysis of protein expression in yeast. Nature *425*, 737-741.

*Giannattasio, M., Lazzaro, F., Plevani, P., and Muzi-Falconi, M. (2005). The DNA damage checkpoint response requires histone H2B ubiquitination by Rad6-Bre1 and H3 methylation by Dot1. J Biol Chem *280*, 9879-9886.

*Gietz, R.D., Schiestl, R.H., Willems, A.R., and Woods, R.A. (1995). Studies on the transformation of intact yeast cells by the LiAc/SS-DNA/PEG procedure. Yeast *11*, 355-360.

*Gilbert, C.S., Green, C.M., and Lowndes, N.F. (2001). Budding yeast Rad9 is an ATP-dependent Rad53 activating machine. Mol Cell *8*, 129-136.

*Gilbert, J., Gore, S.D., Herman, J.G., and Carducci, M.A. (2004a). The clinical application of targeting cancer through histone acetylation and hypomethylation. Clin Cancer Res *10*, 4589-4596.

*Gilbert, N., Boyle, S., Fiegler, H., Woodfine, K., Carter, N.P., and Bickmore, W.A. (2004b). Chromatin architecture of the human genome: gene-rich domains are enriched in open chromatin fibers. Cell *118*, 555-566.

Goffeau, A., Barrell, B.G., Bussey, H., Davis, R.W., Dujon, B., Feldmann, H., Galibert, F., Hoheisel, J.D., Jacq, C., Johnston, M., et al.* (1996). Life with 6000 genes. Science *274*, 546, 563-547.

*Gottipati, P., Cassel, T.N., Savolainen, L., and Helleday, T. (2008). Transcription-associated recombination is dependent on replication in Mammalian cells. Mol Cell Biol *28*, 154-164.

*Govind, C.K., Zhang, F., Qiu, H., Hofmeyer, K., and Hinnebusch, A.G. (2007). Gcn5 promotes acetylation, eviction, and methylation of nucleosomes in transcribed coding regions. Mol Cell *25*, 31-42.

Granata, M., Lazzaro, F., Novarina, D., Panigada, D., Puddu, F., Abreu, C.M., Kumar, R., Grenon, M., Lowndes, N.F., Plevani, P., et al.* (2010). Dynamics of Rad9 chromatin binding and checkpoint function are mediated by its dimerization and are cell cycle-regulated by CDK1 activity. PLoS Genet *6*.

*Grenon, M., Magill, C.P., Lowndes, N.F., and Jackson, S.P. (2006). Double-strand breaks trigger MRX- and Mec1-dependent, but Tel1-independent, checkpoint activation. FEMS Yeast Res *6*, 836-847.

*Gross, C., Kelleher, M., Iyer, V.R., Brown, P.O., and Winge, D.R. (2000). Identification of the copper regulon in Saccharomyces cerevisiae by DNA microarrays. J Biol Chem *275*, 32310-32316.

*Hammet, A., Magill, C., Heierhorst, J., and Jackson, S.P. (2007). Rad9 BRCT domain interaction with phosphorylated H2AX regulates the G1 checkpoint in budding yeast. EMBO Rep *8*, 851-857.

*Hamza, A., and Baetz, K. (2011). The iron-responsive transcription factor Aft1 interacts with the kinetochore protein Iml3 and promotes pericentromeric cohesin. J Biol Chem.

*Hanawalt, P.C. (2002). Subpathways of nucleotide excision repair and their regulation. Oncogene *21*, 8949-8956.

*Hanawalt, P.C., and Spivak, G. (2008). Transcription-coupled DNA repair: two decades of progress and surprises. Nat Rev Mol Cell Biol *9*, 958-970.

*Harrison, J.C., and Haber, J.E. (2006). Surviving the breakup: the DNA damage checkpoint. Annu Rev Genet *40*, 209-235.

*He, Z., Brinton, B.T., Greenblatt, J., Hassell, J.A., and Ingles, C.J. (1993). The transactivator proteins VP16 and GAL4 bind replication factor A. Cell *73*, 1223-1232.

*Henry, K.W., Wyce, A., Lo, W.S., Duggan, L.J., Emre, N.C., Kao, C.F., Pillus, L., Shilatifard, A., Osley, M.A., and Berger, S.L. (2003). Transcriptional activation via sequential histone H2B ubiquitylation and deubiquitylation, mediated by SAGA-associated Ubp8. Genes Dev *17*, 2648-2663.

*Heredia, J., Crooks, M., and Zhu, Z. (2001). Phosphorylation and Cu+ coordination-dependent DNA binding of the transcription factor Mac1p in the regulation of copper transport. J Biol Chem *276*, 8793-8797.

*Hollander, M., and Wolfe, D.A. (1999). Nonparametric Statistical Methods, 2nd edn (John Wiley and Sons, Inc.).

*Huen, M.S., Grant, R., Manke, I., Minn, K., Yu, X., Yaffe, M.B., and Chen, J. (2007). RNF8 transduces the DNA-damage signal via histone ubiquitylation and checkpoint protein assembly. Cell *131*, 901-914.

*Huyen, Y., Zgheib, O., Ditullio, R.A., Jr., Gorgoulis, V.G., Zacharatos, P., Petty, T.J., Sheston, E.A., Mellert, H.S., Stavridi, E.S., and Halazonetis, T.D. (2004). Methylated lysine 79 of histone H3 targets 53BP1 to DNA double-strand breaks. Nature *432*, 406-411.

*Irizarry, R.A., Bolstad, B.M., Collin, F., Cope, L.M., Hobbs, B., and Speed, T.P. (2003). Summaries of Affymetrix GeneChip probe level data. Nucleic Acids Res *31*, e15.

*Iwabuchi, K., Basu, B.P., Kysela, B., Kurihara, T., Shibata, M., Guan, D., Cao, Y., Hamada, T., Imamura, K., Jeggo, P.A., *et al.* (2003). Potential role for 53BP1 in DNA end-joining repair through direct interaction with DNA. J Biol Chem *278*, 36487-36495.

*Izban, M.G., and Luse, D.S. (1991). Transcription on nucleosomal templates by RNA polymerase II in vitro: inhibition of elongation with enhancement of sequence-specific pausing. Genes Dev *5*, 683-696.

*Jamai, A., Imoberdorf, R.M., and Strubin, M. (2007). Continuous histone H2B and transcription-dependent histone H3 exchange in yeast cells outside of replication. Mol Cell *25*, 345-355.

*Jamison McDaniels, C.P., Jensen, L.T., Srinivasan, C., Winge, D.R., and Tullius, T.D. (1999). The yeast transcription factor Mac1 binds to DNA in a modular fashion. J Biol Chem *274*, 26962-26967.

*Javaheri, A., Wysocki, R., Jobin-Robitaille, O., Altaf, M., Cote, J., and Kron, S.J. (2006). Yeast G1 DNA damage checkpoint regulation by H2A phosphorylation is independent of chromatin remodeling. Proc Natl Acad Sci U S A *103*, 13771-13776.

*Jeon, C., and Agarwal, K. (1996). Fidelity of RNA polymerase II transcription controlled by elongation factor TFIIS. Proc Natl Acad Sci U S A *93*, 13677-13682.

*Joshi, A., Serpe, M., and Kosman, D.J. (1999). Evidence for (Mac1p)2.DNA ternary complex formation in Mac1p-dependent transactivation at the CTR1 promoter. J Biol Chem *274*, 218-226.

*Kaback, D.B., Guacci, V., Barber, D., and Mahon, J.W. (1992). Chromosome size-dependent control of meiotic recombination. Science *256*, 228-232.

*Kao, C.F., Hillyer, C., Tsukuda, T., Henry, K., Berger, S., and Osley, M.A. (2004). Rad6 plays a role in transcriptional activation through ubiquitylation of histone H2B. Genes Dev *18*, 184-195.

*Kaplan, C.D., Laprade, L., and Winston, F. (2003). Transcription elongation factors repress transcription initiation from cryptic sites. Science *301*, 1096-1099.

*Kaplan, C.D., Larsson, K.M., and Kornberg, R.D. (2008). The RNA polymerase II trigger loop functions in substrate selection and is directly targeted by alpha-amanitin. Mol Cell *30*, 547-556.

*Keeney, S. (2001). Mechanism and control of meiotic recombination initiation. Curr Top Dev Biol *52*, 1-53.

*Keeney, S., Giroux, C.N., and Kleckner, N. (1997). Meiosis-specific DNA double-strand breaks are catalyzed by Spo11, a member of a widely conserved protein family. Cell *88*, 375-384.

*Keogh, M.C., Kurdistani, S.K., Morris, S.A., Ahn, S.H., Podolny, V., Collins, S.R., Schuldiner, M., Chin, K., Punna, T., Thompson, N.J., *et al.* (2005). Cotranscriptional set2 methylation of histone H3 lysine 36 recruits a repressive Rpd3 complex. Cell *123*, 593-605.

*Kilkenny, M.L., Dore, A.S., Roe, S.M., Nestoras, K., Ho, J.C., Watts, F.Z., and Pearl, L.H. (2008). Structural and functional analysis of the Crb2-BRCT2 domain reveals distinct roles in checkpoint signaling and DNA damage repair. Genes Dev *22*, 2034-2047.

*Kim, J.M., Vanguri, S., Boeke, J.D., Gabriel, A., and Voytas, D.F. (1998). Transposable elements and genome organization: a comprehensive survey of retrotransposons revealed by the complete Saccharomyces cerevisiae genome sequence. Genome Res *8*, 464-478.

*Kim, N., Abdulovic, A.L., Gealy, R., Lippert, M.J., and Jinks-Robertson, S. (2007). Transcription-associated mutagenesis in yeast is directly proportional to the level of

gene expression and influenced by the direction of DNA replication. DNA Repair (Amst) *6*, 1285-1296.

*Kim, N., and Jinks-Robertson, S. (2009). dUTP incorporation into genomic DNA is linked to transcription in yeast. Nature *459*, 1150-1153.

*Kim, T.K., Ebright, R.H., and Reinberg, D. (2000). Mechanism of ATP-dependent promoter melting by transcription factor IIH. Science *288*, 1418-1422.

*Kimura, H., and Cook, P.R. (2001). Kinetics of core histones in living human cells: little exchange of H3 and H4 and some rapid exchange of H2B. J Cell Biol *153*, 1341-1353.

*Kitanovic, A., Walther, T., Loret, M.O., Holzwarth, J., Kitanovic, I., Bonowski, F., Van Bui, N., Francois, J.M., and Wolfl, S. (2009). Metabolic response to MMS-mediated DNA damage in Saccharomyces cerevisiae is dependent on the glucose concentration in the medium. FEMS Yeast Res *9*, 535-551.

*Knop, M., Siegers, K., Pereira, G., Zachariae, W., Winsor, B., Nasmyth, K., and Schiebel, E. (1999). Epitope tagging of yeast genes using a PCR-based strategy: more tags and improved practical routines. Yeast *15*, 963-972.

Kolas, N.K., Chapman, J.R., Nakada, S., Ylanko, J., Chahwan, R., Sweeney, F.D., Panier, S., Mendez, M., Wildenhain, J., Thomson, T.M., et al.* (2007). Orchestration of the DNA-damage response by the RNF8 ubiquitin ligase. Science *318*, 1637-1640.

*Kristjuhan, A., and Svejstrup, J.Q. (2004). Evidence for distinct mechanisms facilitating transcript elongation through chromatin in vivo. Embo J *23*, 4243-4252.

Krogan, N.J., Kim, M., Tong, A., Golshani, A., Cagney, G., Canadien, V., Richards, D.P., Beattie, B.K., Emili, A., Boone, C., et al.* (2003). Methylation of histone H3 by Set2 in Saccharomyces cerevisiae is linked to transcriptional elongation by RNA polymerase II. Mol Cell Biol *23*, 4207-4218.

*Kuo, M.H., and Allis, C.D. (1999). In vivo cross-linking and immunoprecipitation for studying dynamic Protein:DNA associations in a chromatin environment. Methods *19*, 425-433.

*Kvint, K., Uhler, J.P., Taschner, M.J., Sigurdsson, S., Erdjument-Bromage, H., Tempst, P., and Svejstrup, J.Q. (2008). Reversal of RNA polymerase II ubiquitylation by the ubiquitin protease Ubp3. Mol Cell *30*, 498-506.

*Labbe, S., Zhu, Z., and Thiele, D.J. (1997). Copper-specific transcriptional repression of yeast genes encoding critical components in the copper transport pathway. J Biol Chem *272*, 15951-15958.

Lancelot, N., Charier, G., Couprie, J., Duband-Goulet, I., Alpha-Bazin, B., Quemeneur, E., Ma, E., Marsolier-Kergoat, M.C., Ropars, V., Charbonnier, J.B., et al.* (2007). The checkpoint Saccharomyces cerevisiae Rad9 protein contains a tandem tudor domain that recognizes DNA. Nucleic Acids Res *35*, 5898-5912.

*Lashkari, D.A., DeRisi, J.L., McCusker, J.H., Namath, A.F., Gentile, C., Hwang, S.Y., Brown, P.O., and Davis, R.W. (1997). Yeast microarrays for genome wide parallel genetic and gene expression analysis. Proc Natl Acad Sci U S A *94*, 13057-13062.

*Lazzaro, F., Sapountzi, V., Granata, M., Pellicioli, A., Vaze, M., Haber, J.E., Plevani, P., Lydall, D., and Muzi-Falconi, M. (2008). Histone methyltransferase Dot1 and Rad9 inhibit single-stranded DNA accumulation at DSBs and uncapped telomeres. Embo J *27*, 1502-1512.

*Le May, N., Egly, J.M., and Coin, F. (2010a). True lies: the double life of the nucleotide excision repair factors in transcription and DNA repair. J Nucleic Acids *2010*.

*Le May, N., Mota-Fernandes, D., Velez-Cruz, R., Iltis, I., Biard, D., and Egly, J.M. (2010b). NER factors are recruited to active promoters and facilitate chromatin modification for transcription in the absence of exogenous genotoxic attack. Mol Cell *38*, 54-66.

*Lee, C.K., Shibata, Y., Rao, B., Strahl, B.D., and Lieb, J.D. (2004). Evidence for nucleosome depletion at active regulatory regions genome-wide. Nat Genet *36*, 900-905.

*Lee, P.S., Greenwell, P.W., Dominska, M., Gawel, M., Hamilton, M., and Petes, T.D. (2009). A fine-structure map of spontaneous mitotic crossovers in the yeast Saccharomyces cerevisiae. PLoS Genet *5*, e1000410.

*Lee, S.K., Yu, S.L., Prakash, L., and Prakash, S. (2001). Requirement for yeast RAD26, a homolog of the human CSB gene, in elongation by RNA polymerase II. Mol Cell Biol *21*, 8651-8656.

*Lee, S.K., Yu, S.L., Prakash, L., and Prakash, S. (2002a). Yeast RAD26, a homolog of the human CSB gene, functions independently of nucleotide excision repair and base excision repair in promoting transcription through damaged bases. Mol Cell Biol *22*, 4383-4389.

Lee, T.I., Rinaldi, N.J., Robert, F., Odom, D.T., Bar-Joseph, Z., Gerber, G.K., Hannett, N.M., Harbison, C.T., Thompson, C.M., Simon, I., et al.* (2002b). Transcriptional regulatory networks in Saccharomyces cerevisiae. Science *298*, 799-804.

*Lemoine, F.J., Degtyareva, N.P., Lobachev, K., and Petes, T.D. (2005). Chromosomal translocations in yeast induced by low levels of DNA polymerase a model for chromosome fragile sites. Cell *120*, 587-598.

*Lesage, P., and Todeschini, A.L. (2005). Happy together: the life and times of Ty retrotransposons and their hosts. Cytogenet Genome Res *110*, 70-90.

*Li, B., Gogol, M., Carey, M., Lee, D., Seidel, C., and Workman, J.L. (2007a). Combined action of PHD and chromo domains directs the Rpd3S HDAC to transcribed chromatin. Science *316*, 1050-1054.

*Li, B., Gogol, M., Carey, M., Pattenden, S.G., Seidel, C., and Workman, J.L. (2007b). Infrequently transcribed long genes depend on the Set2/Rpd3S pathway for accurate transcription. Genes Dev *21*, 1422-1430.

*Li, J., Moazed, D., and Gygi, S.P. (2002). Association of the histone methyltransferase Set2 with RNA polymerase II plays a role in transcription elongation. J Biol Chem *277*, 49383-49388.

*Li, R., and Botchan, M.R. (1993). The acidic transcriptional activation domains of VP16 and p53 bind the cellular replication protein A and stimulate in vitro BPV-1 DNA replication. Cell *73*, 1207-1221.

*Lichten, M. (2008). Genomics: Thoroughly modern meiosis. Nature *454*, 421-422.

Liu, P., Barkley, L.R., Day, T., Bi, X., Slater, D.M., Alexandrow, M.G., Nasheuer, H.P., and Vaziri, C. (2006). The Chk1-mediated S-phase checkpoint targets initiation factor Cdc45 via a Cdc25A/Cdk2-independent mechanism. J Biol Chem *281*, 30631-30644.

*Longhese, M.P., Bonetti, D., Guerini, I., Manfrini, N., and Clerici, M. (2009). DNA double-strand breaks in meiosis: checking their formation, processing and repair. DNA Repair (Amst) *8*, 1127-1138.

*Longhese, M.P., Mantiero, D., and Clerici, M. (2006). The cellular response to chromosome breakage. Mol Microbiol *60*, 1099-1108.

*Longtine, M.S., McKenzie, A., 3rd, Demarini, D.J., Shah, N.G., Wach, A., Brachat, A., Philippsen, P., and Pringle, J.R. (1998). Additional modules for versatile and

economical PCR-based gene deletion and modification in Saccharomyces cerevisiae. Yeast *14*, 953-961.

*Louis, E.J. (1995). The chromosome ends of Saccharomyces cerevisiae. Yeast *11*, 1553-1573.

*Louis, E.J., Naumova, E.S., Lee, A., Naumov, G., and Haber, J.E. (1994). The chromosome end in yeast: its mosaic nature and influence on recombinational dynamics. Genetics *136*, 789-802.

*Luse, D.S. (2012). Promoter clearance by RNA polymerase II. Biochim Biophys Acta.

*Lydall, D., and Whitehall, S. (2005). Chromatin and the DNA damage response. DNA Repair (Amst) *4*, 1195-1207.

*MacIsaac, K.D., Wang, T., Gordon, D.B., Gifford, D.K., Stormo, G.D., and Fraenkel, E. (2006). An improved map of conserved regulatory sites for Saccharomyces cerevisiae. BMC Bioinformatics *7*, 113.

*Maere, S., Heymans, K., and Kuiper, M. (2005). BiNGO: a Cytoscape plugin to assess overrepresentation of gene ontology categories in biological networks. Bioinformatics *21*, 3448-3449.

*Mailand, N., Bekker-Jensen, S., Faustrup, H., Melander, F., Bartek, J., Lukas, C., and Lukas, J. (2007). RNF8 ubiquitylates histones at DNA double-strand breaks and promotes assembly of repair proteins. Cell *131*, 887-900.

*Maldonado, E., Shiekhattar, R., Sheldon, M., Cho, H., Drapkin, R., Rickert, P., Lees, E., Anderson, C.W., Linn, S., and Reinberg, D. (1996). A human RNA polymerase II complex associated with SRB and DNA-repair proteins. Nature *381*, 86-89.

*Margaritis, T., and Holstege, F.C. (2008). Poised RNA polymerase II gives pause for thought. Cell *133*, 581-584.

*Maringele, L., and Lydall, D. (2002). EXO1-dependent single-stranded DNA at telomeres activates subsets of DNA damage and spindle checkpoint pathways in budding yeast yku70Delta mutants. Genes Dev *16*, 1919-1933.

*Martini, E., Diaz, R.L., Hunter, N., and Keeney, S. (2006). Crossover homeostasis in yeast meiosis. Cell *126*, 285-295.

*Martins, L.J., Jensen, L.T., Simon, J.R., Keller, G.L., and Winge, D.R. (1998). Metalloregulation of FRE1 and FRE2 homologs in Saccharomyces cerevisiae. J Biol Chem *273*, 23716-23721.

*Mason, P.B., and Struhl, K. (2005). Distinction and relationship between elongation rate and processivity of RNA polymerase II in vivo. Mol Cell *17*, 831-840.

Measday, V., Baetz, K., Guzzo, J., Yuen, K., Kwok, T., Sheikh, B., Ding, H., Ueta, R., Hoac, T., Cheng, B., et al.* (2005). Systematic yeast synthetic lethal and synthetic dosage lethal screens identify genes required for chromosome segregation. Proc Natl Acad Sci U S A *102*, 13956-13961.

*Mellon, I., Spivak, G., and Hanawalt, P.C. (1987). Selective removal of transcription-blocking DNA damage from the transcribed strand of the mammalian DHFR gene. Cell *51*, 241-249.

*Michelson, R.J., Rosenstein, S., and Weinert, T. (2005). A telomeric repeat sequence adjacent to a DNA double-stranded break produces an anticheckpoint. Genes Dev *19*, 2546-2559.

*Mieczkowski, P.A., Dominska, M., Buck, M.J., Lieb, J.D., and Petes, T.D. (2007). Loss of a histone deacetylase dramatically alters the genomic distribution of Spo11p-catalyzed DNA breaks in Saccharomyces cerevisiae. Proc Natl Acad Sci U S A *104*, 3955-3960.

*Morin, I., Ngo, H.P., Greenall, A., Zubko, M.K., Morrice, N., and Lydall, D. (2008). Checkpoint-dependent phosphorylation of Exo1 modulates the DNA damage response. Embo J *27*, 2400-2410.

*Naiki, T., Wakayama, T., Nakada, D., Matsumoto, K., and Sugimoto, K. (2004). Association of Rad9 with double-strand breaks through a Mec1-dependent mechanism. Mol Cell Biol *24*, 3277-3285.

*Nakamura, T.M., Du, L.L., Redon, C., and Russell, P. (2004). Histone H2A phosphorylation controls Crb2 recruitment at DNA breaks, maintains checkpoint arrest, and influences DNA repair in fission yeast. Mol Cell Biol *24*, 6215-6230.

*Natsoulis, G., Thomas, W., Roghmann, M.C., Winston, F., and Boeke, J.D. (1989). Ty1 transposition in Saccharomyces cerevisiae is nonrandom. Genetics *123*, 269-279.

*Nesser, N.K., Peterson, D.O., and Hawley, D.K. (2006). RNA polymerase II subunit Rpb9 is important for transcriptional fidelity in vivo. Proc Natl Acad Sci U S A *103*, 3268-3273.

*Ng, H.H., Ciccone, D.N., Morshead, K.B., Oettinger, M.A., and Struhl, K. (2003). Lysine-79 of histone H3 is hypomethylated at silenced loci in yeast and mammalian cells: a potential mechanism for position-effect variegation. Proc Natl Acad Sci U S A *100*, 1820-1825.

*Nicol, J.W., Helt, G.A., Blanchard, S.G., Jr., Raja, A., and Loraine, A.E. (2009). The Integrated Genome Browser: free software for distribution and exploration of genome-scale datasets. Bioinformatics *25*, 2730-2731.

*Nnakwe, C.C., Altaf, M., Cote, J., and Kron, S.J. (2009). Dissection of Rad9 BRCT domain function in the mitotic checkpoint response to telomere uncapping. DNA Repair (Amst) *8*, 1452-1461.

*O'Sullivan, J.M., Sontam, D.M., Grierson, R., and Jones, B. (2009). Repeated elements coordinate the spatial organization of the yeast genome. Yeast *26*, 125-138.

*Ohkuni, K., and Kitagawa, K. (2011). Endogenous transcription at the centromere facilitates centromere activity in budding yeast. Curr Biol *21*, 1695-1703.

*Orphanides, G., LeRoy, G., Chang, C.H., Luse, D.S., and Reinberg, D. (1998). FACT, a factor that facilitates transcript elongation through nucleosomes. Cell *92*, 105-116.

*Paciotti, V., Clerici, M., Lucchini, G., and Longhese, M.P. (2000). The checkpoint protein Ddc2, functionally related to S. pombe Rad26, interacts with Mec1 and is regulated by Mec1-dependent phosphorylation in budding yeast. Genes Dev *14*, 2046-2059.

*Paciotti, V., Lucchini, G., Plevani, P., and Longhese, M.P. (1998). Mec1p is essential for phosphorylation of the yeast DNA damage checkpoint protein Ddc1p, which physically interacts with Mec3p. Embo J *17*, 4199-4209.

Pan, J., Sasaki, M., Kniewel, R., Murakami, H., Blitzblau, H.G., Tischfield, S.E., Zhu, X., Neale, M.J., Jasin, M., Socci, N.D., et al.* (2011). A hierarchical combination of factors shapes the genome-wide topography of yeast meiotic recombination initiation. Cell *144*, 719-731.

*Panizza, S., Mendoza, M.A., Berlinger, M., Huang, L., Nicolas, A., Shirahige, K., and Klein, F. (2011). Spo11-accessory proteins link double-strand break sites to the chromosome axis in early meiotic recombination. Cell *146*, 372-383.

*Park, Y.J., and Luger, K. (2006). Structure and function of nucleosome assembly proteins. Biochem Cell Biol *84*, 549-558.

*Paulovich, A.G., Margulies, R.U., Garvik, B.M., and Hartwell, L.H. (1997). RAD9, RAD17, and RAD24 are required for S phase regulation in Saccharomyces cerevisiae in response to DNA damage. Genetics *145*, 45-62.

*Philpott, C.C., and Protchenko, O. (2008). Response to iron deprivation in Saccharomyces cerevisiae. Eukaryot Cell *7*, 20-27.

Pokholok, D.K., Harbison, C.T., Levine, S., Cole, M., Hannett, N.M., Lee, T.I., Bell, G.W., Walker, K., Rolfe, P.A., Herbolsheimer, E., et al.* (2005). Genome-wide map of nucleosome acetylation and methylation in yeast. Cell *122*, 517-527.

*Prado, F., and Aguilera, A. (2005). Impairment of replication fork progression mediates RNA polII transcription-associated recombination. Embo J *24*, 1267-1276.

*Pryde, F., Khalili, S., Robertson, K., Selfridge, J., Ritchie, A.M., Melton, D.W., Jullien, D., and Adachi, Y. (2005). 53BP1 exchanges slowly at the sites of DNA damage and appears to require RNA for its association with chromatin. J Cell Sci *118*, 2043-2055.

*Puddu, F., Granata, M., Di Nola, L., Balestrini, A., Piergiovanni, G., Lazzaro, F., Giannattasio, M., Plevani, P., and Muzi-Falconi, M. (2008). Phosphorylation of the budding yeast 9-1-1 complex is required for Dpb11 function in the full activation of the UV-induced DNA damage checkpoint. Mol Cell Biol *28*, 4782-4793.

*Puig, S., Askeland, E., and Thiele, D.J. (2005). Coordinated remodeling of cellular metabolism during iron deficiency through targeted mRNA degradation. Cell *120*, 99-110.

*Putnam, C.D., Jaehnig, E.J., and Kolodner, R.D. (2009). Perspectives on the DNA damage and replication checkpoint responses in Saccharomyces cerevisiae. DNA Repair (Amst) *8*, 974-982.

*Raghuraman, M.K., Winzeler, E.A., Collingwood, D., Hunt, S., Wodicka, L., Conway, A., Lockhart, D.J., Davis, R.W., Brewer, B.J., and Fangman, W.L. (2001). Replication dynamics of the yeast genome. Science *294*, 115-121.

*Ratner, J.N., Balasubramanian, B., Corden, J., Warren, S.L., and Bregman, D.B. (1998). Ultraviolet radiation-induced ubiquitination and proteasomal degradation of the large subunit of RNA polymerase II. Implications for transcription-coupled DNA repair. J Biol Chem *273*, 5184-5189.

*Reed, S.H. (2011). Nucleotide excision repair in chromatin: damage removal at the drop of a HAT. DNA Repair (Amst) *10*, 734-742.

*Robert, F., Douziech, M., Forget, D., Egly, J.M., Greenblatt, J., Burton, Z.F., and Coulombe, B. (1998). Wrapping of promoter DNA around the RNA polymerase II initiation complex induced by TFIIF. Mol Cell *2*, 341-351.

*Robine, N., Uematsu, N., Amiot, F., Gidrol, X., Barillot, E., Nicolas, A., and Borde, V. (2007). Genome-wide redistribution of meiotic double-strand breaks in Saccharomyces cerevisiae. Mol Cell Biol *27*, 1868-1880.

*Rochette-Egly, C., Adam, S., Rossignol, M., Egly, J.M., and Chambon, P. (1997). Stimulation of RAR alpha activation function AF-1 through binding to the general transcription factor TFIIH and phosphorylation by CDK7. Cell *90*, 97-107.

*Rouse, J., and Jackson, S.P. (2000). LCD1: an essential gene involved in checkpoint control and regulation of the MEC1 signalling pathway in Saccharomyces cerevisiae. Embo J *19*, 5801-5812.

*Rutherford, J.C., and Bird, A.J. (2004). Metal-responsive transcription factors that regulate iron, zinc, and copper homeostasis in eukaryotic cells. Eukaryot Cell *3*, 1-13.

*Rutherford, J.C., Jaron, S., Ray, E., Brown, P.O., and Winge, D.R. (2001). A second iron-regulatory system in yeast independent of Aft1p. Proc Natl Acad Sci U S A *98*, 14322-14327.

*Rutherford, J.C., Jaron, S., and Winge, D.R. (2003). Aft1p and Aft2p mediate iron-responsive gene expression in yeast through related promoter elements. J Biol Chem *278*, 27636-27643.

*Sambrook, J.F.J., and Maniatis, T. (1989). Molecular Cloning: A laboratory manual (New York, Cold Spring Harbor Laboratory Press).

*Sanders, S.L., Portoso, M., Mata, J., Bahler, J., Allshire, R.C., and Kouzarides, T. (2004). Methylation of histone H4 lysine 20 controls recruitment of Crb2 to sites of DNA damage. Cell *119*, 603-614.

*Schaft, D., Roguev, A., Kotovic, K.M., Shevchenko, A., Sarov, M., Shevchenko, A., Neugebauer, K.M., and Stewart, A.F. (2003). The histone 3 lysine 36 methyltransferase, SET2, is involved in transcriptional elongation. Nucleic Acids Res *31*, 2475-2482.

*Scholes, D.T., Kenny, A.E., Gamache, E.R., Mou, Z., and Curcio, M.J. (2003). Activation of a LTR-retrotransposon by telomere erosion. Proc Natl Acad Sci U S A *100*, 15736-15741.

*Schotta, G., Ebert, A., and Reuter, G. (2003). SU(VAR)3-9 is a conserved key function in heterochromatic gene silencing. Genetica *117*, 149-158.

Schubeler, D., MacAlpine, D.M., Scalzo, D., Wirbelauer, C., Kooperberg, C., van Leeuwen, F., Gottschling, D.E., O'Neill, L.P., Turner, B.M., Delrow, J., et al.* (2004). The histone modification pattern of active genes revealed through genome-wide chromatin analysis of a higher eukaryote. Genes Dev *18*, 1263-1271.

*Schwabish, M.A., and Struhl, K. (2004). Evidence for eviction and rapid deposition of histones upon transcriptional elongation by RNA polymerase II. Mol Cell Biol *24*, 10111-10117.

*Schwartz, M.F., Duong, J.K., Sun, Z., Morrow, J.S., Pradhan, D., and Stern, D.F. (2002). Rad9 phosphorylation sites couple Rad53 to the Saccharomyces cerevisiae DNA damage checkpoint. Mol Cell *9*, 1055-1065.

*Selth, L.A., Sigurdsson, S., and Svejstrup, J.Q. (2010). Transcript Elongation by RNA Polymerase II. Annu Rev Biochem *79*, 271-293.

*Serpe, M., Joshi, A., and Kosman, D.J. (1999). Structure-function analysis of the protein-binding domains of Mac1p, a copper-dependent transcriptional activator of copper uptake in Saccharomyces cerevisiae. J Biol Chem *274*, 29211-29219.

*Shakoury-Elizeh, M., Tiedeman, J., Rashford, J., Ferea, T., Demeter, J., Garcia, E., Rolfes, R., Brown, P.O., Botstein, D., and Philpott, C.C. (2004). Transcriptional remodeling in response to iron deprivation in Saccharomyces cerevisiae. Mol Biol Cell *15*, 1233-1243.

*Sherman, F. (2002). Getting started with yeast. Methods Enzymol *350*, 3-41.

*Shimada, M., and Komatsu, K. (2009). Emerging connection between centrosome and DNA repair machinery. J Radiat Res (Tokyo) *50*, 295-301.

*Siede, W., Friedberg, A.S., and Friedberg, E.C. (1993). RAD9-dependent G1 arrest defines a second checkpoint for damaged DNA in the cell cycle of Saccharomyces cerevisiae. Proc Natl Acad Sci U S A *90*, 7985-7989.

*Smyth, G.K. (2005). Limma: linear models for microarray data. In: Bioinformatics and Computational Biology Solutions using R and Bioconductor (New York, Springer).

*Smyth, G.K., Michaud, J., and Scott, H.S. (2005). Use of within-array replicate spots for assessing differential expression in microarray experiments. Bioinformatics *21*, 2067-2075.

*Somesh, B.P., Reid, J., Liu, W.F., Sogaard, T.M., Erdjument-Bromage, H., Tempst, P., and Svejstrup, J.Q. (2005). Multiple mechanisms confining RNA polymerase II ubiquitylation to polymerases undergoing transcriptional arrest. Cell *121*, 913-923.

*Somesh, B.P., Sigurdsson, S., Saeki, H., Erdjument-Bromage, H., Tempst, P., and Svejstrup, J.Q. (2007). Communication between distant sites in RNA polymerase II through ubiquitylation factors and the polymerase CTD. Cell *129*, 57-68.

*Soulier, J., and Lowndes, N.F. (1999). The BRCT domain of the S. cerevisiae checkpoint protein Rad9 mediates a Rad9-Rad9 interaction after DNA damage. Curr Biol *9*, 551-554.

*Stearman, R., Yuan, D.S., Yamaguchi-Iwai, Y., Klausner, R.D., and Dancis, A. (1996). A permease-oxidase complex involved in high-affinity iron uptake in yeast. Science *271*, 1552-1557.

*Storici, F., Bebenek, K., Kunkel, T.A., Gordenin, D.A., and Resnick, M.A. (2007). RNA-templated DNA repair. Nature *447*, 338-341.

*Sun, W., Xie, W., Xu, F., Grunstein, M., and Li, K.C. (2009). Dissecting nucleosome free regions by a segmental semi-Markov model. PLoS One *4*, e4721.

*Sun, Z., Hsiao, J., Fay, D.S., and Stern, D.F. (1998). Rad53 FHA domain associated with phosphorylated Rad9 in the DNA damage checkpoint. Science *281*, 272-274.

*Svejstrup, J.Q. (2003). Transcription. Histones face the FACT. Science *301*, 1053-1055.

*Svejstrup, J.Q. (2007). Contending with transcriptional arrest during RNAPII transcript elongation. Trends Biochem Sci *32*, 165-171.

*Sweeney, F.D., Yang, F., Chi, A., Shabanowitz, J., Hunt, D.F., and Durocher, D. (2005). Saccharomyces cerevisiae Rad9 acts as a Mec1 adaptor to allow Rad53 activation. Curr Biol *15*, 1364-1375.

*Tantin, D., Kansal, A., and Carey, M. (1997). Recruitment of the putative transcription-repair coupling factor CSB/ERCC6 to RNA polymerase II elongation complexes. Mol Cell Biol *17*, 6803-6814.

*Thiriet, C., and Hayes, J.J. (2005). Replication-independent core histone dynamics at transcriptionally active loci in vivo. Genes Dev *19*, 677-682.

*Thomas, M.J., Platas, A.A., and Hawley, D.K. (1998). Transcriptional fidelity and proofreading by RNA polymerase II. Cell *93*, 627-637.

*Toh, G.W., and Lowndes, N.F. (2003). Role of the Saccharomyces cerevisiae Rad9 protein in sensing and responding to DNA damage. Biochem Soc Trans *31*, 242-246.

*Toh, G.W., O'Shaughnessy, A.M., Jimeno, S., Dobbie, I.M., Grenon, M., Maffini, S., O'Rorke, A., and Lowndes, N.F. (2006). Histone H2A phosphorylation and H3 methylation are required for a novel Rad9 DSB repair function following checkpoint activation. DNA Repair (Amst) *5*, 693-703.

*Tu, Y., Tornaletti, S., and Pfeifer, G.P. (1996). DNA repair domains within a human gene: selective repair of sequences near the transcription initiation site. Embo J *15*, 675-683.

*Ueta, R., Fukunaka, A., and Yamaguchi-Iwai, Y. (2003). Pse1p mediates the nuclear import of the iron-responsive transcription factor Aft1p in Saccharomyces cerevisiae. J Biol Chem *278*, 50120-50127.

*Usui, T., Foster, S.S., and Petrini, J.H. (2009). Maintenance of the DNA-damage checkpoint requires DNA-damage-induced mediator protein oligomerization. Mol Cell *33*, 147-159.

*van Bakel, H., Strengman, E., Wijmenga, C., and Holstege, F.C. (2005). Gene expression profiling and phenotype analyses of S. cerevisiae in response to changing copper reveals six genes with new roles in copper and iron metabolism. Physiol Genomics *22*, 356-367.

*van den Bosch, M., and Lowndes, N.F. (2004). Remodelling the Rad9 checkpoint complex: preparing Rad53 for action. Cell Cycle *3*, 119-122.

*van Leeuwen, F., Gafken, P.R., and Gottschling, D.E. (2002). Dot1p modulates silencing in yeast by methylation of the nucleosome core. Cell *109*, 745-756.

*Vialard, J.E., Gilbert, C.S., Green, C.M., and Lowndes, N.F. (1998). The budding yeast Rad9 checkpoint protein is subjected to Mec1/Tel1-dependent hyperphosphorylation and interacts with Rad53 after DNA damage. Embo J *17*, 5679-5688.

*Volker, M., Mone, M.J., Karmakar, P., van Hoffen, A., Schul, W., Vermeulen, W., Hoeijmakers, J.H., van Driel, R., van Zeeland, A.A., and Mullenders, L.H. (2001). Sequential assembly of the nucleotide excision repair factors in vivo. Mol Cell *8*, 213-224.

*Voutsina, A., Fragiadakis, G.S., Boutla, A., and Alexandraki, D. (2001). The second cysteine-rich domain of Mac1p is a potent transactivator that modulates DNA binding efficiency and functionality of the protein. FEBS Lett *494*, 38-43.

*Vujcic, M., Miller, C.A., and Kowalski, D. (1999). Activation of silent replication origins at autonomously replicating sequence elements near the HML locus in budding yeast. Mol Cell Biol *19*, 6098-6109.

*Wakayama, T., Kondo, T., Ando, S., Matsumoto, K., and Sugimoto, K. (2001). Pie1, a protein interacting with Mec1, controls cell growth and checkpoint responses in Saccharomyces cerevisiae. Mol Cell Biol *21*, 755-764.

*Walmacq, C., Kireeva, M.L., Irvin, J., Nedialkov, Y., Lubkowska, L., Malagon, F., Strathern, J.N., and Kashlev, M. (2009). Rpb9 subunit controls transcription fidelity by delaying NTP sequestration in RNA polymerase II. J Biol Chem *284*, 19601-19612.

*Wang, A., Kurdistani, S.K., and Grunstein, M. (2002). Requirement of Hos2 histone deacetylase for gene activity in yeast. Science *298*, 1412-1414.

*Wang, D., Bushnell, D.A., Westover, K.D., Kaplan, C.D., and Kornberg, R.D. (2006). Structural basis of transcription: role of the trigger loop in substrate specificity and catalysis. Cell *127*, 941-954.

*Ward, I., Kim, J.E., Minn, K., Chini, C.C., Mer, G., and Chen, J. (2006). The tandem BRCT domain of 53BP1 is not required for its repair function. J Biol Chem *281*, 38472-38477.

*Ward, I.M., Minn, K., Jorda, K.G., and Chen, J. (2003). Accumulation of checkpoint protein 53BP1 at DNA breaks involves its binding to phosphorylated histone H2AX. J Biol Chem *278*, 19579-19582.

*Weinert, T. (1998). DNA damage checkpoints update: getting molecular. Curr Opin Genet Dev *8*, 185-193.

*Weinert, T.A., and Hartwell, L.H. (1988). The RAD9 gene controls the cell cycle response to DNA damage in Saccharomyces cerevisiae. Science *241*, 317-322.

*Weinert, T.A., and Hartwell, L.H. (1990). Characterization of RAD9 of Saccharomyces cerevisiae and evidence that its function acts posttranslationally in cell cycle arrest after DNA damage. Mol Cell Biol *10*, 6554-6564.

*Wellinger, R.E., Prado, F., and Aguilera, A. (2006). Replication fork progression is impaired by transcription in hyperrecombinant yeast cells lacking a functional THO complex. Mol Cell Biol *26*, 3327-3334.

*Willson, J., Wilson, S., Warr, N., and Watts, F.Z. (1997). Isolation and characterization of the Schizosaccharomyces pombe rhp9 gene: a gene required for the DNA damage checkpoint but not the replication checkpoint. Nucleic Acids Res *25*, 2138-2146.

*Woods, R.A., and Gietz, R.D. (2001). High-efficiency transformation of plasmid DNA into yeast. Methods Mol Biol *177*, 85-97.

*Workman, J.L., and Kingston, R.E. (1998). Alteration of nucleosome structure as a mechanism of transcriptional regulation. Annu Rev Biochem *67*, 545-579.

*Woudstra, E.C., Gilbert, C., Fellows, J., Jansen, L., Brouwer, J., Erdjument-Bromage, H., Tempst, P., and Svejstrup, J.Q. (2002). A Rad26-Def1 complex coordinates repair and RNA pol II proteolysis in response to DNA damage. Nature *415*, 929-933.

*Wu, T.C., and Lichten, M. (1995). Factors that affect the location and frequency of meiosis-induced double-strand breaks in Saccharomyces cerevisiae. Genetics *140*, 55-66.

*Wyrick, J.J., Aparicio, J.G., Chen, T., Barnett, J.D., Jennings, E.G., Young, R.A., Bell, S.P., and Aparicio, O.M. (2001). Genome-wide distribution of ORC and MCM proteins in S. cerevisiae: high-resolution mapping of replication origins. Science *294*, 2357-2360.

*Wysocki, R., Javaheri, A., Allard, S., Sha, F., Cote, J., and Kron, S.J. (2005). Role of Dot1-dependent histone H3 methylation in G1 and S phase DNA damage checkpoint functions of Rad9. Mol Cell Biol *25*, 8430-8443.

*Xiao, T., Hall, H., Kizer, K.O., Shibata, Y., Hall, M.C., Borchers, C.H., and Strahl, B.D. (2003). Phosphorylation of RNA polymerase II CTD regulates H3 methylation in yeast. Genes Dev *17*, 654-663.

*Xiao, T., Kao, C.F., Krogan, N.J., Sun, Z.W., Greenblatt, J.F., Osley, M.A., and Strahl, B.D. (2005). Histone H2B ubiquitylation is associated with elongating RNA polymerase II. Mol Cell Biol *25*, 637-651.

*Xie, W., Gai, X., Zhu, Y., Zappulla, D.C., Sternglanz, R., and Voytas, D.F. (2001). Targeting of the yeast Ty5 retrotransposon to silent chromatin is mediated by interactions between integrase and Sir4p. Mol Cell Biol *21*, 6606-6614.

*Xu, L., and Kleckner, N. (1995). Sequence non-specific double-strand breaks and interhomolog interactions prior to double-strand break formation at a meiotic recombination hot spot in yeast. Embo J *14*, 5115-5128.

*Xue-Franzen, Y., Johnsson, A., Brodin, D., Henriksson, J., Burglin, T.R., and Wright, A.P. (2010). Genome-wide characterisation of the Gcn5 histone acetyltransferase in budding yeast during stress adaptation reveals evolutionarily conserved and diverged roles. BMC Genomics *11*, 200.

*Yabuki, N., Terashima, H., and Kitada, K. (2002). Mapping of early firing origins on a replication profile of budding yeast. Genes Cells *7*, 781-789.

*Yamaguchi-Iwai, Y., Serpe, M., Haile, D., Yang, W., Kosman, D.J., Klausner, R.D., and Dancis, A. (1997). Homeostatic regulation of copper uptake in yeast via direct binding of MAC1 protein to upstream regulatory sequences of FRE1 and CTR1. J Biol Chem *272*, 17711-17718.

*Yamaguchi-Iwai, Y., Ueta, R., Fukunaka, A., and Sasaki, R. (2002). Subcellular localization of Aft1 transcription factor responds to iron status in Saccharomyces cerevisiae. J Biol Chem *277*, 18914-18918.

*Yamashita, K., Shinohara, M., and Shinohara, A. (2004). Rad6-Bre1-mediated histone H2B ubiquitylation modulates the formation of double-strand breaks during meiosis. Proc Natl Acad Sci U S A *101*, 11380-11385.

*Yang, C., Theis, J.F., and Newlon, C.S. (1999). Conservation of ARS elements and chromosomal DNA replication origins on chromosomes III of Saccharomyces cerevisiae and S. carlsbergensis. Genetics *152*, 933-941.

*Yokota, H., Singer, M.J., van den Engh, G.J., and Trask, B.J. (1997). Regional differences in the compaction of chromatin in human G0/G1 interphase nuclei. Chromosome Res *5*, 157-166.

*Yonkovich, J., McKenndry, R., Shi, X., and Zhu, Z. (2002). Copper ion-sensing transcription factor Mac1p post-translationally controls the degradation of its target gene product Ctr1p. J Biol Chem *277*, 23981-23984.

*Yun, C.W., Tiedeman, J.S., Moore, R.E., and Philpott, C.C. (2000). Siderophore-iron uptake in saccharomyces cerevisiae. Identification of ferrichrome and fusarinine transporters. J Biol Chem *275*, 16354-16359.

*Zgheib, O., Pataky, K., Brugger, J., and Halazonetis, T.D. (2009). An oligomerized 53BP1 tudor domain suffices for recognition of DNA double-strand breaks. Mol Cell Biol *29*, 1050-1058.

*Zhu, X., and Gustafsson, C.M. (2009). Distinct differences in chromatin structure at subtelomeric X and Y' elements in budding yeast. PLoS One *4*, e6363.

*Zhu, Z., Labbe, S., Pena, M.M., and Thiele, D.J. (1998). Copper differentially regulates the activity and degradation of yeast Mac1 transcription factor. J Biol Chem *273*, 1277-1280.

*Zubko, M.K., Guillard, S., and Lydall, D. (2004). Exo1 and Rad24 differentially regulate generation of ssDNA at telomeres of Saccharomyces cerevisiae cdc13-1 mutants. Genetics *168*, 103-115.